Mechanisms of Osteoarthritis: Interrelationships between Bone and Cartilage

A Thesis submitted to The University of Adelaide in fulfilment of the requirements for the degree of Doctor of Philosophy

By

Geetha Mohan, M.Phil

Discipline of Anatomy and Pathology, School of Medical Sciences

The University of Adelaide

Bone and Joint Research Laboratory, Directorate of Surgical Pathology,

SA Pathology, Adelaide

March 2012

TABLE OF CONTENTS

Abstract i
Declaration iv
Acknowledgments v
Published abstracts vii
Scientific communication viii
Awards xii
Abbreviations xiii

Chapter 1 Literature review and project aims 1

1. Introduction 2

1.1. The knee joint 2

1.2. Aetiopathology of osteoarthritis (OA) 5

1.3. Articular cartilage 5
1.3.1. Structural organisation of normal articular cartilage 6
1.3.2. Composition of articular cartilage 8
1.3.2.1. Chondrocytes 8
1.3.2.2. Collagen 8
1.3.2.3. Proteoglycans 10
1.3.3. Pathological changes in OA cartilage matrix 10
1.3.4. Alteration in OA articular cartilage metabolism 11
1.3.5. Cellular changes in OA cartilage 13

1.4. Subchondral bone 15
1.4.1. Normal structure of the subchondral plate 16
1.4.2. The osteochondral junction 17
1.4.3. Vascularity of the subchondral bone plate 19
1.4.4. Subchondral plate thickness and density distribution 19
1.4.5. Pathological changes in OA subchondral bone 20
1.4.6. Subchondral bone remodelling in OA 21
1.4.7. OA related changes in trabecular microarchitecture 23
1.4.8. Biochemical changes of subchondral bone in OA 24
1.4.9. Hypomineralisaton of bone in OA 25
1.4.10. Biochemical properties of bone 26
1.4.11. Biomechanical adaptation: Osteophyte formation 27
1.4.12. Subchondral bone cyst formation in OA 30
1.4.13. Bone marrow lesion (BMLs) in OA 33

1.5. Bone-cartilage interaction **34**
1.5.1. Molecular cross-talk between bone and cartilage 36
1.5.2. Key regulators of bone remodelling: the RANK/RANKL/OPG System 37
1.5.2.1. OPG 38
1.5.2.2. RANK 38
1.5.2.3. RANKL 39

1.6. Bisphosphonates as disease modifying OA drugs (DMOADs) **40**
1.6.1. Structure of Bisphosphonates 41
1.6.2. Mechanism of action of bisphosphonate 43
1.6.3. Biological activity of nitrogen containing bisphosphonates: with reference to alendronate 43
1.6.4. Bisphosphonate treatment for OA 44

1.7. Animal models of OA **50**
1.7.1. Commonly used animal species 50
1.7.2. Type of OA induction 51
1.7.3. Monosodium iodoacetate-induced experimental OA model 52
1.7.4. Dose response study 53

1.8. *In vivo* micro-CT tomography (micro-CT) assessment of bone in rodent models of OA **55**
1.8.1. *In vivo* micro-CT imaging of cartilage in rodent models of OA 56
1.8.2. Consideration for *in vivo* micro-CT imaging of rodents 57

1.9. Research aims **58**
1.9.1. Project aims 60

2. Chapter 2 Application of *in vivo* micro-computed tomography in the temporal characterisation of subchondral bone architecture in a rat model of low-dose monosodium iodoacetate induced osteoarthritis **61**

2.1. Introduction **66**

2.2. Materials and methods **66**
2.2.1. Animal and OA induction 66
2.2.2. *In vivo* micro-CT imaging 67
2.2.3. Bone histomorphometric analysis 67
2.2.3.1. Subchondral trabecular bone 67
2.2.3.2. Subchondral plate 68
2.2.4. Macroscopic analysis 68
2.2.5. Histological analysis 68
2.2.6. Serum C-reactive protein (CRP) analysis 68
2.2.7. Statistical analysis 68

2.3. Results **68**
2.3.1. Micro-CT 68
2.3.1.1. Bone histomorphometric changes 68
2.3.1.2. Subchondral trabecular bone 69
2.3.1.3. Subchondral plate 69
2.3.1.4. Qualitative subchondral bone changes 69
2.3.2. Macroscopy 69
2.3.3. Histology 72
2.3.4. Serum CRP levels 72

2.4. Discussion **73**

2.5. Conclusions **76**

3. Chapter 3 Pre-emptive, early, and delayed alendronate treatment in a rat model of low-dose monosodium iodoacetate induced osteoarthritis: effect on subchondral trabecular bone microarchitecture, cartilage degradation, bone and cartilage turnover, and joint discomfort **79**

3.1. Introduction **86**

3.2. Materials and methods **88**
3.2.1. Animals and OA induction 88
3.2.2. Alendronate (ALN) treatment 89
3.2.3. *In vivo* micro-CT analysis 90
3.2.4. Hind limb weight-bearing (HLWB) assessment 91
3.2.5. Macroscopic analysis 92
3.2.6. Histological analysis 92
3.2.7. Serum COMP, CTX-I and urine CTX-II analysis 93
3.2.8. Statistical analysis 93

3.3. Results **94**
3.3.1. *In vivo* micro-CT: subchondral trabecular bone Histomorphometry 94
3.3.1.1. Effect of pre-emptive ALN treatment 94
3.3.1.2. Effect of early ALN treatment 95
3.3.1.3. Effect of delayed ALN treatment 96
3.3.2. Effect of ALN on hind limb weight-bearing 98
3.3.3. Effect of ALN on macroscopic cartilage changes 98
3.3.4. Effect of ALN on microscopic cartilage changes 99
3.3.5. Effect of ALN on subchondral trabecular bone mineral apposition rate (MAR) 101
3.3.6. Effect of ALN on serum COMP, CTX-I and urine CTX-II 101

3.4. Discussion **101**

3.5. Conclusions **107**

4. Chapter 4 Alendronate modulates gene expression of osteoprotegerin and receptor activator of nuclear factor κB ligand in subchondral bone in the early phase of experimental osteoarthritis 126

4.1. Introduction 132

4.2. Materials and methods 134
4.2.1. Animals and OA induction 134
4.2.2. Alendronate (ALN) treatment 135
4.2.3. Tissue preparation 135
4.2.4. Total RNA isolation and cDNA synthesis 136
4.2.4.1. Real-time RT-PCR 137
4.2.5. Statistical analysis 138

4.3. Results 138
4.3.1. Target gene expression within the OA group 139
4.3.2. Target gene expression within the ALN treatment group 139
4.3.3. Effect of ALN treatment on RANK, RANKL, and OPG mRNA expression 140
4.3.4. Effect of ALN on tibial subchondral bone histomorphometric parameters 141

4.4. Discussion 141

4.5. Conclusions 147

5. Chapter 5 Discussion 157
5.1. Overview of study findings 159
5.2. Comparison to existing literature 160
5.3. Strengths and limitations 167
5.4. Areas for further research and clinical implications 168
5.5. Conclusion 171

Appendices 172
Appendix I: A dose response study in the monosodium iodoacetate rat model of osteoarthritis: *in vivo* micro-CT, histological and serological evaluation 173

Appendix II: Development of an *in vivo* scanning protocol for tracking temporal changes in tibial subchondral bone in a low-dose MIA-induced OA rat model 201

References 221

ABSTRACT

Osteoarthritis (OA) is a progressive joint disease and a common cause of disability. OA is characterised by loss of articular cartilage, subchondral bone sclerosis, cysts, and osteophyte formation. Increased subchondral bone remodelling plays an important role in the pathophysiology of OA and is associated with disease progression. It is known that Osteoprotegerin (OPG), receptor activator of nuclear factor kappa b (RANK) and its ligand RANKL tightly control bone remodelling. In addition, RANK, RANKL and OPG gene expression has been shown to be dysregulated in human OA subchondral bone.

Commonly OA is diagnosed at advanced stages, which makes it difficult to study the initiating events in the human disease. Animal models of OA are of considerable importance to study the progressive changes in OA, and to evaluate suitable OA drugs. Alendronate (ALN) is a potent bone resorption inhibitor and clinical trials using bisphosphonates to treat OA have yielded mixed results. This suggests that the effects of bisphosphonates may or may not be beneficial depending on the stage of OA progression.

The first aim of this thesis was to characterise the temporal structural changes of tibial articular cartilage and subchondral bone in a low-dose MIA-induced OA rat model. The results from micro-CT analysis showed that the tibiae of the MIA-injected knees had significant bone loss at 2 weeks (early OA), followed by increased bone volume, trabecular thickness and separation at 6 weeks (intermediate OA) and 10 weeks

(advanced OA). Micro-CT images revealed subchondral bone sclerosis, cysts, and osteophyte formation at 6 and 10 weeks. Histology revealed progressive cartilage degradation characteristic of the human disease.

The second aim of this thesis was to study the effect of ALN treatment initiated at day 0 (pre-emptive), week 2 (early treatment), and week 6 (delayed treatment) in a low-dose MIA rat model. To address the second aim the efficacy of ALN was tested on cartilage degradation, subchondral bone remodelling, and joint discomfort observed in this animal model. The study demonstrated that pre-emptive ALN treatment preserved subchondral trabecular bone microarchitecture, decreased bone turnover, prevented joint discomfort, and offered moderate chondroprotection. Early and delayed ALN treatment prevented loss of trabeculae and decreased bone turnover but did not have any identified effect on cartilage.

Finally, the RANK, RANKL, OPG gene expression in OA was characterised in a low-dose MIA rat model. The effect of ALN treatment on subchondral bone RANK, RANKL, and OPG gene expression at 2, 6, and 10 weeks after OA induction was assessed. This study showed that the RANKL and OPG gene expression was dysregulated in this animal model. In addition, the efficacy of ALN on early subchondral bone changes appears to occur through the modulation of RANKL and OPG gene expression.

Collectively, these findings demonstrate that the low-dose MIA rat model closely mimics the pathological features of progressive human OA disease. Moreover, this animal model showed a clear relationship between the cartilage damage and subchondral bone changes. ALN treatment preserved subchondral trabecular bone microarchitecture and decreased bone turnover. In addition, ALN prevented RANKL and OPG gene dysregulation in OA subchondral bone. Normalising subchondral bone remodelling offers an optimal treatment option and future drug intervention studies focusing on subchondral bone would provide improved treatment options for OA.

DECLARATION

I, Geetha Mohan certify that this work contains no material which has been accepted for the award of any other degree or diploma in any university or other tertiary institution and, to the best of my knowledge and belief, this thesis contains no material previously published or written by another person, except where due reference has been made in the text.

I give consent to this copy of my thesis, when deposited in the University Library, being made available for loan and photocopying, subject to the provisions of the Copyright Act 1968. The author acknowledges that copyright of published works contained within this thesis (as listed below) resides with the copyright holder(s) of those works.

Mohan G, Perilli E, Kuliwaba JS, Humphries JM, Parkinson IH, Fazzalari NL (2011) Application of *in vivo* micro-computed tomography in the temporal characterisation of subchondral bone architecture in a rat model of low-dose monosodium iodoacetate-induced osteoarthritis. *Arthritis Res Ther* 13:R210.

I also give permission for the digital version of my thesis to be made available on the web, via the University's digital research repository, the Library catalogue and also through web search engines, unless permission has been granted by the university to restrict access for a period of time.

Geetha Mohan

Date

ACKNOWLEDGEMENTS

I would like to acknowledge the endless support of my supervisors, Professor Nick Fazzalari, Dr Julia Kuliwaba and Dr Ian Parkinson. Their expertise, ideas, enthusiastic encouragement and constructive comments have been invaluable throughout my candidature. I thank them for their mentorship, guidance and all the wonderful opportunities they have provided me to grow as a researcher.

I would like to express my sincere gratitude to Dr Egon Perilli who was instrumental in developing the *in vivo* micro-CT scan protocols. It was a pleasure knowing him and working with him. I will always value his advice, friendship, and optimism. I am grateful to Dr Julia Humphries for helping me with the biomarker analysis. I thank her for her time, friendship, and support. My sincere and heartfelt thanks to Lena Truong for her patience, care, friendship, and continuous encouragement. I thank her for making the late night lab work less cumbersome with all the wonderful conversations and laughs. It was very nice of her to share this lonely journey with me. I am thankful to Mrs Helen Tsangari, Ms Cheryl Ghan and Mrs Yolandi Starzak for their help with histology, wonderful company and support. I am thankful to Duminda Kumarasinghe, Clare Jones, Melissa Cantley, Pranay Sharma, and Balaji Seshadri for their friendship, support, and constant encouragement throughout these years.

I am greatly indebted to Dr Cally Guerin for her support, encouragement and perspectives that greatly helped me to develop an understanding of the academic, linguistic and cultural conventions relating to postgraduate research at The University of

Adelaide. I thank her for including me during happy occasions with her family which was heart-warming and a rewarding cultural experience. I am grateful to Dr Tim Kuchel, Dr Allan Rofe, Dr Dorota Gancarz, Brian Lewis and the staff at the Animal Care Facility for their generous assistance with animal work. I am likewise grateful to Mr John Terlet, Ms Ruth Williams and staff at the Adelaide Microscopy for their generous assistance and advice during *in vivo* micro-CT scans. I acknowledge the Endeavour Postgraduate award, a generous scholarship for my Ph.D provided by the Australian Government, Department of Education, Employment and Workplace Relations. I also acknowledge funding from Bone and Joint Research Laboratory and SA pathology, Adelaide, Australia for my project. I thank the case managers from Austraining International for their support and advice during my Ph.D.

Above all I would like to express my deepest gratitude to my parents for their unconditional love, strong support and encouragement. Their strong belief in me has always motivated me to strive for greater achievements in life. I thank my grandparents, sister Sathyavathi and brother Padmanabhan for understanding me and supporting me in my endeavour. Special thanks to my uncles, aunts, cousins and family friends in India for their well wishes for the successful completion of my Ph.D in Australia.

PUBLISHED ABSTRACTS (reviewed)

Mohan G, Perilli E, Kuliwaba JS, Parkinson IH, Humphries JH, Fazzalari NL (2011) Characterisation of temporal subchondral bone changes in a rat model of low-dose monosodium iodoacetate induced osteoarthritis: An *in vivo* micro-CT study. *Osteoarthritis Cartilage* 19:S61-S62.

Mohan G, Perilli E, Kuliwaba JS, Parkinson IH, Humphries JH, Fazzalari NL (2011) Alendronate treatment reduces tibial subchondral bone damage in early-stage osteoarthritis: An *in vivo* micro-CT study in a rodent model. *Osteoporos Int* 22:S579.

SCIENTIFIC COMMUNICATION

Mohan G, Perilli E, Kuliwaba JS, Parkinson IH, Humphries JM, Fazzalari NL. Positive Effect of Alendronate on Tibial Subchondral Bone loss and Cartilage Repair at early stage experimental osteoarthritis in rats. *2011 Annual Scientific and Clinical Meeting & Annual General Meeting of the Australian Rheumatology Association (ARA) (South Australian Branch)*. Adelaide, Australia, October 28, 2011.

Mohan G, Perilli E, Kuliwaba JS, Parkinson IH, Humphries JM, Fazzalari NL. Characterisation of temporal subchondral bone changes in a rat model of low-dose monosodium iodoacetate induced osteoarthritis: An *in vivo* micro-CT study. *2011 OARSI world congress of Osteoarthritis Research Society International (OARSI).* San Diego, CA, USA, September 15 – 18, 2011.

Mohan G, Perilli E, Kuliwaba JS, **Parkinson IH,** Humphries JM, Fazzalari NL. Alendronate treatment reduces tibial subchondral bone damage at early-stage osteoarthritis: an *in vivo* micro-CT study in a rodent model. *The 21st Annual Scientific Meeting of the Australian and New Zealand Bone and Mineral Society (ANZBMS).* Gold Coast, Australia, September 4 – 8, 2011.

Mohan G, Perilli E, Kuliwaba JS, **Parkinson IH,** Humphries JM, Fazzalari NL. Tibial subchondral bone damage in early-stage osteoarthritis is reduced by Alendronate administration: an *in vivo* micro-CT study in a rodent model. *17th Annual Scientific Meeting of the Australian & New Zealand Orthopaedic Research Society (ANZORS).* Brisbane, Queensland, Australia, September 1 – 2, 2011.

Mohan G, Perilli E, Kuliwaba JS, Parkinson IH, Humphries JM, Fazzalari NL. Alendronate inhibits early subchondral bone loss and joint discomfort by modulating the RANKL/OPG nexus in a rodent model of osteoarthritis. *The University of Adelaide, Faculty of Health Sciences Postgraduate Research Conference.* Adelaide, Australia, August 25, 2011.

Mohan G, Perilli E, Kuliwaba JS, Parkinson IH, Humphries JM, Fazzalari NL. Anti-resorptive efficacy of alendronate treatment on tibial subchondral bone at early-stage osteoarthritis: an *in vivo* micro-CT study in a rodent model. *Annual scientific meeting of the Australian Society for Medical Research SA Scientific Meeting (ASMR) (South Australian Division).* Adelaide, Australia, June 8, 2011.

Mohan G, Perilli E, Kuliwaba JS, Humphries JM, Parkinson IH, Fazzalari NL. Application of *in vivo* micro-computed tomography in the characterisation of a rat model of osteoarthritis. *The 16th Annual Scientific Meeting of the ANZORS*. Melbourne, Australia, November 14 – 18, 2010.

Mohan G, Perilli E, Kuliwaba JS, Humphries JM, Parkinson IH, Fazzalari NL. Characterisation of a non-trauma rat model of iodoacetate induced osteoarthritis. *2010 Annual Scientific meeting of the ARA (South Australian Branch).* Adelaide, Australia, October 22, 2010.

Mohan G, Perilli E, Kuliwaba JS, Humphries JM, Parkinson IH, Fazzalari NL. *In vivo* imaging of subchondral bone using micro-CT in a rodent model of osteoarthritis. *The 20th Annual Scientific Meeting of the ANZBMS*. Adelaide, Australia, September 5 – 8, 2010.

Mohan G, Perilli E, Kuliwaba JS, Humphries JM, Parkinson IH, Fazzalari NL. Characterisation of articular cartilage and subchondral bone changes in a non-trauma rat model of osteoarthritis. *The Annual Scientific Meeting of the Australian Orthopaedic Association (AOA) (South Australian Branch).* Adelaide, Australia, August 13, 2010.

Mohan G, Perilli E, Kuliwaba JS, Humphries JM, Parkinson IH, Fazzalari NL. *In vivo* imaging of subchondral bone using micro computed tomography: A novel method to track longitudinal changes in a rodent model of osteoarthritis. Annual scientific meeting of the ASMR *(South Australian Division).* Adelaide, Australia, June 9, 2010.

Mohan G, Perilli E, Kuliwaba JS, Humphries JM, Parkinson IH, Fazzalari NL. Articular cartilage and subchondral bone changes in the monosodium iodoacetate rat model of osteoarthritis: A dose-response study. *The Sixth Clare Valley Bone Meeting.* Clare, Australia, March 26 – 30, 2010.

Mohan G, Perilli E, Kuliwaba JS, Parkinson IH, Fazzalari NL. Cartilage and subchondral bone changes in osteoarthritis: *In vivo* Micro-CT, Serological, and Histological Evaluation in a Rodent Model. *2009 Annual Scientific meeting of the ARA (South Australian Branch).* Adelaide, Australia, November 6, 2009.

Mohan G, Perilli E, Kuliwaba JS, Parkinson IH, Fazzalari NL. Cartilage and subchondral bone changes in osteoarthritis: *in vivo* micro-CT, serological and histological evaluation in a rodent. *15th Annual Scientific Meeting of the ANZORS.* Adelaide, Australia, October 8 – 10, 2009.

Mohan G, Perilli E, Kuliwaba JS, Parkinson IH, Fazzalari NL. Longitudinal subchondral bone changes in a rodent model of osteoarthritis using *in vivo* micro-computed tomography. *Annual scientific meeting of the ASMR (South Australian Division).* Adelaide, Australia, June 2, 2009.

AWARDS

The following awards were received for original work in this thesis:

Best poster presentation award at The University of Adelaide, Faculty of Health Sciences Postgraduate Research Conference. Adelaide, Australia, August 25, 2011.

ANZORS Travel award at the 16th Annual Scientific Meeting of the Australian & New Zealand Orthopaedic Research Society (ANZORS). Melbourne, Australia, November 14 – 18, 2010.

The Philip Alpers award at the 2009 Annual Scientific and Clinical Meeting & Annual General Meeting of the Australian Rheumatology Association (ARA) (South Australian Branch). Adelaide, Australia, November 6, 2009.

ABBREVIATIONS

2D	Two dimensional
3D	Three dimensional
ACLT	Anterior cruciate ligament transection
ADAMTS	A disintegrin and metalloproteinase with thrombospondin motifs
ALN	Alendronate
BML	Bone marrow lesions
BMP	Bone morphogenetic proteins
BV	Bone volume
BV/TV	Bone volume fraction
COMP	Cartilage oligomeric matrix protein
CRP	C-reactive protein
CT	Cycle threshold
CTX-I	C-terminal telopeptide of collagen type I
CTX-II	C-terminal telopeptide of collagen type II
DEXA	Dual energy x-ray absorptiometry
Dkk-1	Dickkopf-1
FE	Finite element
GAPDH	Glyceraldehyde-3-phosphate dehydrogenase
HLWB	Hind limb weight-bearing
IL-1	Interleukin-1
KVp	Kilovoltage peak
MAPK	Mitogen activated protein kinase

MAR	Mineral apposition rate
MIA	Monosodium iodoacetate
Micro-CT	Micro computed tomography
ml	Millilitres
mm	Millimetre
MMPs	Metalloproteinases
MRI	Magnetic resonance imaging
NFAT	Nuclear factor of activated T cells,
NTX	N-terminal type I collagen telopeptides
OA	Osteoarthritis
OARSI	Osteoarthritis Research Society International
ºC	degrees Celsius
OPG	Osteoprotegerin
OVX	Ovariectomized
Pl.Por	Plate porosity
Pl.Th	Plate thickness
RANK	Receptor activator of nuclear factor κB
RANKL	Receptor activator of nuclear factor κB ligand
ROI	Region of interest
RT	Reverse transcription
SPECT	Single-photon–emission computed tomography
Tb.N	Trabecular number
Tb.Sp	Trabecular separation
Tb.Th	Trabecular thickness

TGF-β	Transforming growth factor-β
TNFα	Tumor necrosis factor alpha
TRAF	TNFR-associated factor proteins
TRAP	Tartrate-resistant acid phosphatase
vBMD	Volumetric bone mineral density
VEGF	Vascular endothelial growth factor
VOI	Volume of interest
Wnt	Wingless-type MMTV integration site
μA	Microampere
μl	Micro litres
μm	Micrometres

CHAPTER 1

Literature review and project aims

1 Introduction

Osteoarthritis (OA) is the most common degenerative joint disease among middle aged and older people throughout the world. The prevalence of OA is very high after the age of 55 and it is more common in women than in men (Fig. 1.1) (Oliveria et al. 1995). The risk factors for OA include age, sex, heredity, joint trauma, and obesity. OA mainly affects the weight-bearing joints of the knee, hip, vertebra, hand and foot. The knee joint is the most commonly affected site and approximately 6% of the adult population 30 years or older is estimated to have symptomatic knee OA (Felson and Zhang 1998). The main symptoms of OA are persistent pain, stiffness, and limitation in movement of the affected joints. Advanced stages could lead to joint contractures, muscle atrophy, joint deformation, and joint dysfunction (Buckwalter et al. 2004). OA is a major socio-economic burden to society due to its high and increasing prevalence. It is a common cause of long-term immobility, psychological distress, and poor quality of life among the aged population (Altman 2010). The etiopathology of OA is poorly understood and currently there is no treatment available to prevent or halt the progression of the disease. Costly joint replacement surgery remains the only option for patients with late or end stage OA.

1.1 The knee joint

The knee joint is the most commonly affected joint by OA. It is a complex organ consisting of three major compartments: the patellofemoral joint, and the medial and lateral tibiofemoral compartments (Fig. 1.2) (Englund 2010). The patella, sesamoid bone that articulates within the femoral groove to form the patellofemoral joint (Clark A. L. 2008). The menisci are fibrocartilaginous structures present between the

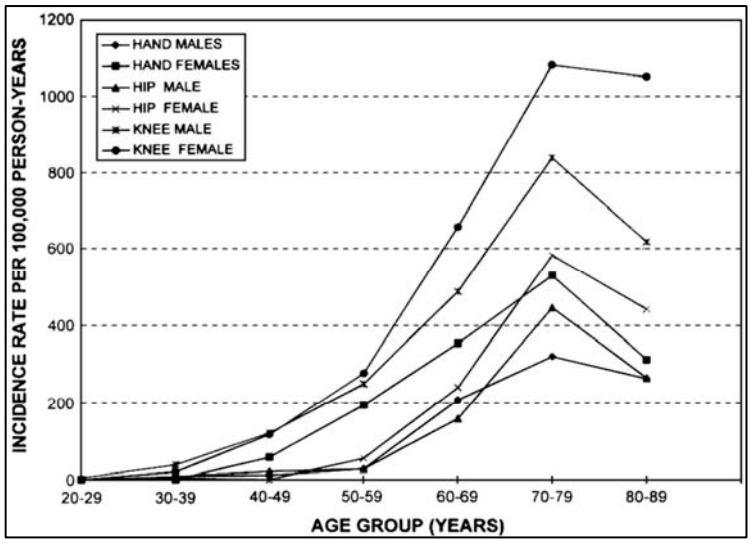

Figure 1.1 Incidence of the hand, hip, and knee OA in members of the Fallon Community Health Plan, 1991–1992, by age and sex (Oliveria et al. 1995, with permission from John Wiley & Sons, Inc.).

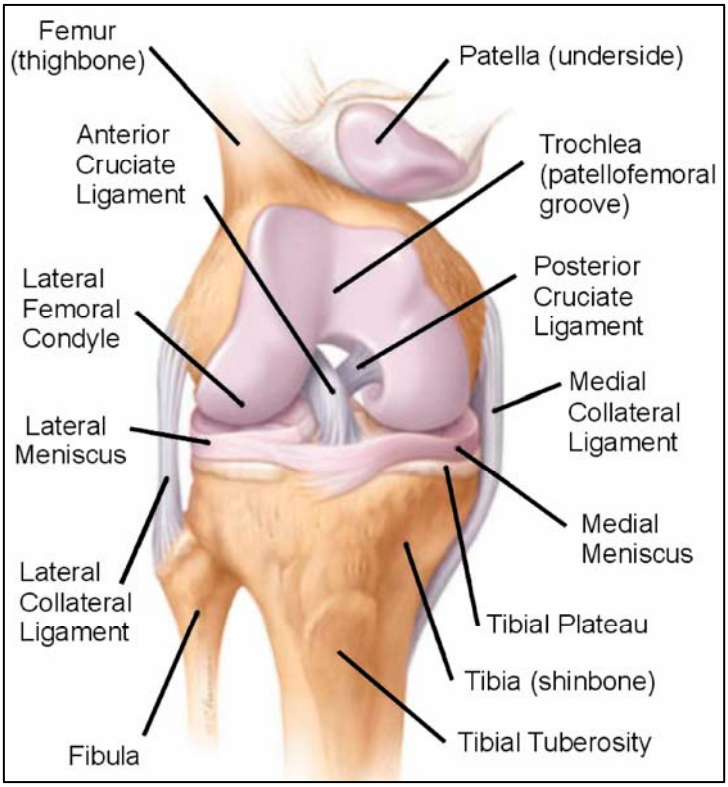

Figure 1.2 Frontal view of the normal knee joint showing tibia, femur, patella, ligaments and meniscus (adapted with permission from http://factotem.org/library/database/Knee-Articles/Knee-anatomy-physiology.shtml).

articulating surfaces of the tibia and femur on the medial and lateral compartments. The tibial and femoral condyles are covered by cartilage and the subchondral bone is present just beneath the cartilage. The knee joint is surrounded by a capsule which consists of the synovial membrane and the whole knee joint is stabilised by both muscles and ligaments. It is now known that all these joint structures are involved in OA (Fig. 1.3) (Martel-Pelletier and Pelletier 2010). Subchondral bone has been shown to be involved in the early stages of OA with dynamic changes during the disease progression which will be the main focus of this thesis.

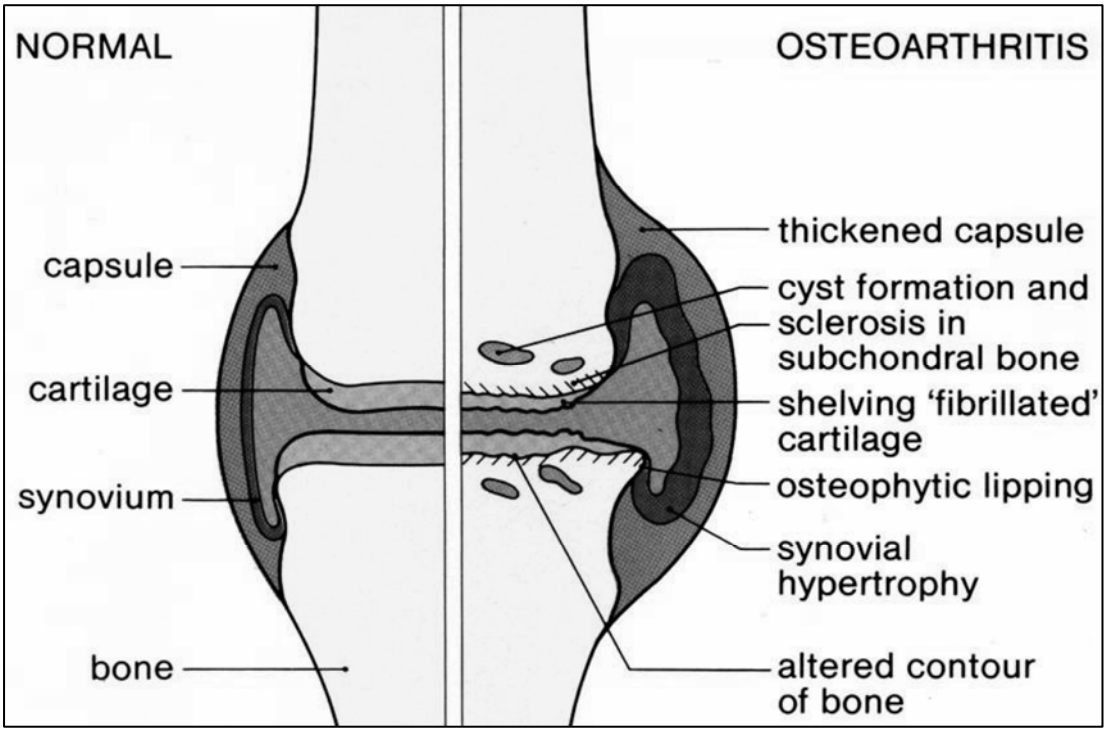

Figure 1.3 Structure of the normal and OA knee joint showing pathological features such as cartilage fibrillation, subchondral bone sclerosis, osteophyte formation and cyst formation (adapted from http://www.hss.edu/conditions_an-in-depth-overview-of-osteoarthritis.asp).

1.2 Aetiopathology of OA

Primary or idiopathic OA develops in the absence of any known underlying predisposing factor while, secondary OA develops due to local or systemic pathogenic factors. Secondary OA may occur due to joint injuries (post-traumatic), joint malformation/malalignment, joint inflammation, metabolic diseases such as rickets and endocrine disorders such as acromegaly, and hyperparathyroidism (Arden and Nevitt 2006, Michael et al. 2010, Moskowitz R.W. et al. 2001). Recently, Herrero-Beaumont et al. has proposed classifying primary OA into three interrelated subsets: genetically determined (type I OA), estrogen hormone dependent (type II OA), and aging related (type III OA) (Herrero-Beaumont et al. 2009). OA is mainly characterised by loss of cartilage, subchondral bone sclerosis, cyst, and osteophyte formation. This disease is associated with morphologic, biochemical, molecular and biomechanical changes of both cells and matrixes in the cartilage and bone which is reviewed in the following sections.

1.3 Articular cartilage

Articular cartilage is an avascular, aneural and alymphatic connective tissue that forms a smooth gliding surface over the subchondral bone of the diarthrodial joints. It is a highly specialised biomaterial with high tensile and compressive properties that absorbs and dissipates load across the entire joint surface, and sustains shearing forces (Heinegard and Saxne 2011). Articular cartilage derives its unique biomechanical properties from a dense network of collagen fibrils and proteoglycans. Both the structure and composition of the cartilage extracellular matrix, synthesised by sparsely populated chondrocytes are important to fulfil its functions (Aigner and McKenna

2002). Any change in the structure and composition of the extracellular matrix, affects the functional integrity of the cartilage.

1.3.1 Structural organisation of normal articular cartilage

Articular cartilage can be divided into four zones: the superficial zone, the middle (transitional) zone, the deep (radial) zone, and the calcified cartilage zone, where the cartilage interfaces with the bone (Fig. 1.4). The superficial zone consists of flattened chondrocytes arranged parallel to the articular surface. They secrete lubricin, which is essential for the smooth, frictionless movement of the joints (Poole A. R. et al. 2001). In the superficial zone the proteoglycan content is low with thin tangentially arranged collagen fibrils. The collagen fibrils are associated with small leucine rich decorin, and biglycan, which are most concentrated in the superficial zone. This zone enables cartilage to resist shear, tensile and compressive forces during movement (Poole A. R. et al. 2001). The middle zone is composed of abundant proteoglycans, with thicker collagen fibrils arranged in radial bundles, which are secreted by round shaped chondrocytes. The deep zone has the largest collagen fibrils arranged radially, and has the highest aggrecan content. The cell density is the lowest and the chondrocytes are aligned perpendicular to the articular surface. The calcified cartilage is demarcated by a tidemark that separates hyaline cartilage from the subchondral bone. It mainly anchors the cartilage to the subchondral bone and consists of a very sparse chondrocyte population, which are hypertrophic (Martel-Pelletier et al. 2008).

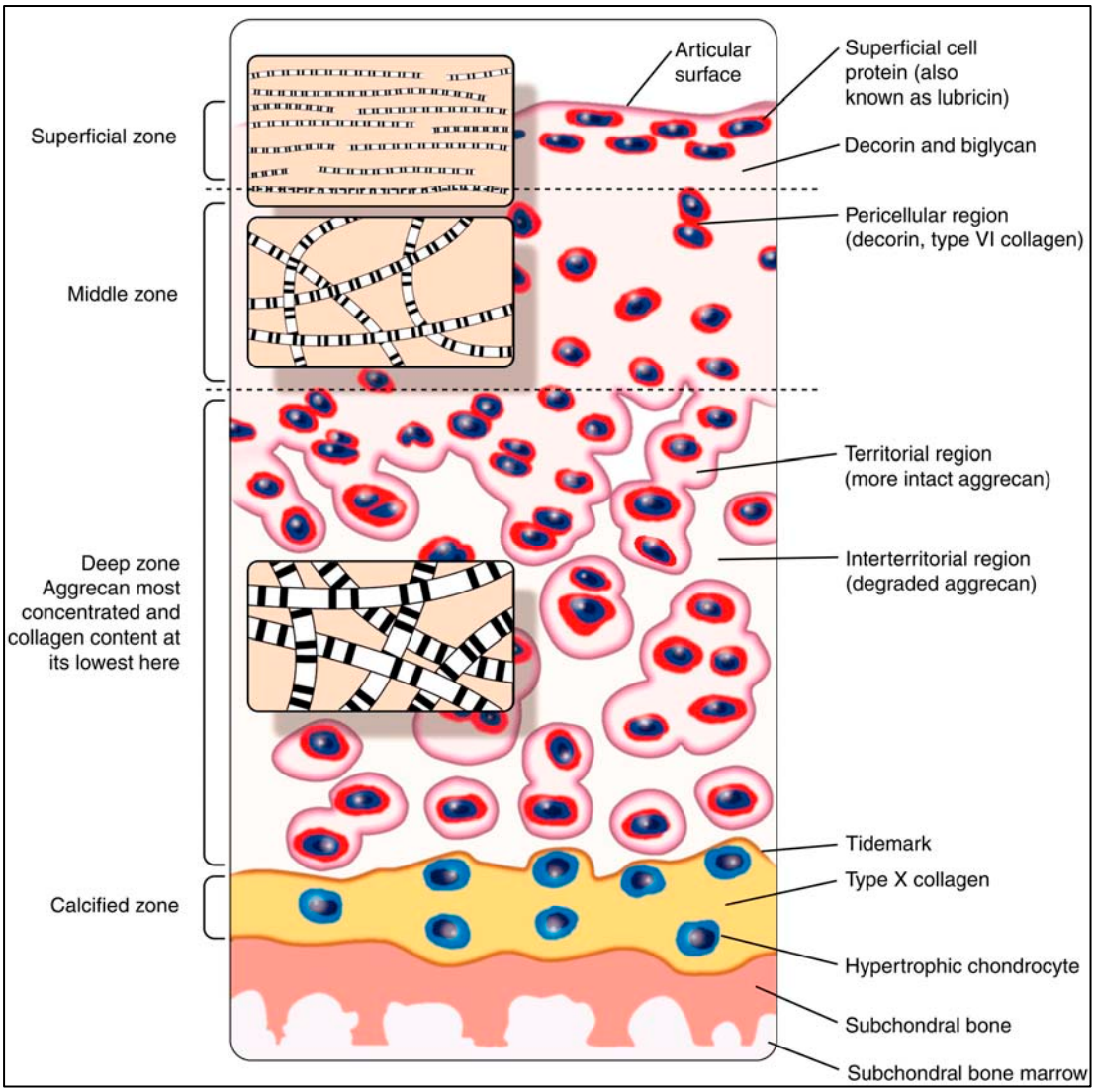

Figure 1.4 Structural organisation of normal articular cartilage showing various zones of the cartilage, the calcified zone and the subchondral bone. Important cartilage matrix components such as chondrocytes, collagen fibrils and associated molecules are shown in this diagram (Poole et al., 2001, with permission from Lippincott Williams & Wilkins).

1.3.2 Composition of articular cartilage

1.3.2.1 Chondrocytes

Chondrocytes are the only cell type found in the cartilage matrix and occupy less than 2 % of the cartilage volume (Hunziker et al. 2002). Chondrocytes are formed from undifferentiated mesenchymal cells and the majority of the epiphyseal chondrocytes undergo secondary ossification and subsequent endochondral ossification. However, the epiphyseal chondrocytes present closer to the synovial cavity become permanent resident articular chondrocytes (Pacifici et al. 2000). Chondrocytes differ in size, shape, and metabolic activity depending on the different cartilage zone in which they reside (Fig. 1.5) (Schumacher et al. 1994). They are highly resilient and are able to survive at low oxygen concentration in the cartilage extracellular matrix (Lafont 2010). Chondrocytes are metabolically active and synthesize collagen and proteoglycan molecules. Moreover, cartilage matrix turnover is regulated by several cytokines such as interleukin-1 (IL-1), insulin-dependent growth factor-I and transforming growth factor-β (TGF-β).

1.3.2.2 Collagen

Collagen constitutes 50 – 60% of the cartilage dry weight. Type II collagen forms a major bulk of collagen fibrils in the healthy articular cartilage. The diameter of collagen fibrils ranges from 20 nm (superficial zone) to 120 nm (deep zone). Type II collagen is a triple helix composed of three identical α_1 (II) chains (Poole A. R. et al. 2001). A number of pyridinoline cross-links stabilize the collagen molecules which serve as a marker for mature collagen (Takahashi et al. 1994). Cartilage oligomeric matrix protein (COMP), a noncollagenous extracellular matrix protein is also involved in binding the

collagen molecules together. Hence COMP plays a major role in fibril assembly to form collagen microfibrils (Poole A. R. et al. 2001). Collagen type XI, type IX, and type VI are also found in normal cartilage. Type XI and IX collagen are found in association with type II collagen. Type VI collagen is found in the pericellular matrix directly surrounding the chondrocyte and anchors the chondrocytes to the matrix. Type X collagen is synthesized only by the deep zone chondrocytes of the articular cartilage and hypertrophic chondrocytes of the growth plate under normal conditions (Buckwalter and Mankin 1998).

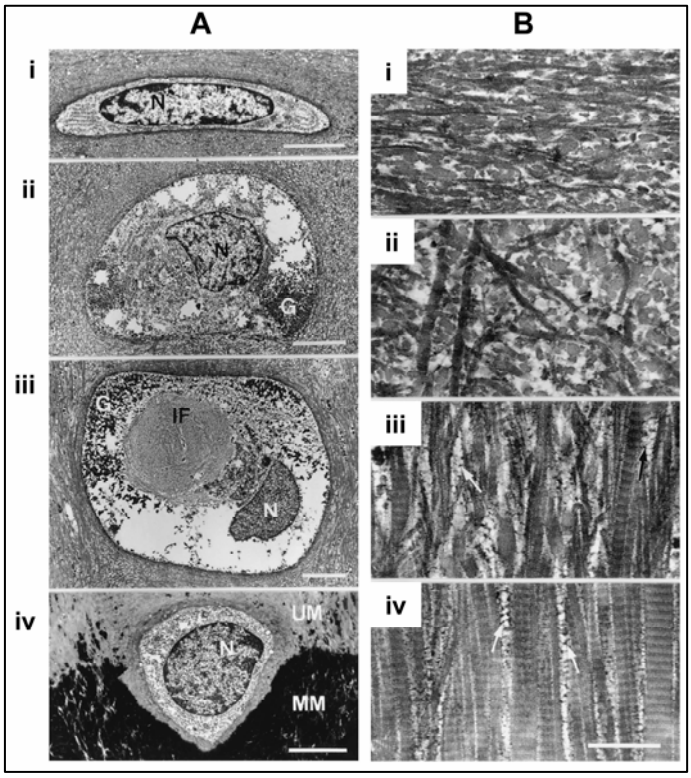

Figure 1.5 Chondrocytes and collagen fibrils from normal articular cartilage.
(A) Chondrocytes from superficial layer (i) to deep cartilage zone (iv) differ in size and shape. (B) Collagen fibrils from different zones of the cartilage differ in size and arrangement (Buckwalter et al. 1998, with permission from Journal of Bone and Joint Surgery).

1.3.2.3 Proteoglycans

Proteoglycans constitute about 5 – 10% of cartilage and aggrecan is the abundant proteoglycan found in the cartilage. The aggrecan monomer consists of a core protein with repeating units of chondroitin sulfate and keratin sulfate. Multiple monomer aggrecan molecules are attached non-covalently to hyaluronic acid to form supramolecular aggregates of proteoglycans (Martel-Pelletier et al. 2008). These aggregates are negatively charged and provide the osmotic properties needed for the articular cartilage to resist compressive loads. Other proteoglycans such as the syndecans, glypican, decorin, biglycan, fibromodulin, lumican, epiphycan, and perlecan are also present in the cartilage matrix (Umlauf et al. 2010).

1.3.3 Pathological changes in OA cartilage matrix

Loss of articular cartilage is an important feature of OA; however, the initiating events that lead to OA pathology are still unclear. Microscopically, cartilage fibrillation is the first sign of OA pathology due to degradation of collagen fibrils. Matrix metalloproteinases (MMPs) play a major role in collagen fibril degradation. This leads to a weakened collagen network, which no longer can resist the swelling properties of the proteoglycan and subsequent swelling of cartilage. Using high-resolution magnetic resonance imaging (MRI), cartilage swelling at the early stages of experimental OA has been shown (Calvo et al. 2001). At the same time, there is loss of proteoglycans and the chondrocytes try to compensate this loss by increasing proteoglycan synthesis (Poole A. R. et al. 2002). However, due to increased activity of both MMPs and aggrecanases, there is increased loss of aggrecan fragments. Moreover, expression of molecules such as tenascin, collagen type IIA and III that are not normally present in the cartilage has also been reported (Aigner and McKenna 2002).

Apart from biochemical changes, biomechanical changes also play a key role in progressive cartilage degradation (Lammi 2004). Using quantitative cartilage loss assessment, Sharma et al. showed that factors that altered mechanical loading such as medial meniscal damage and varus malalignment and lateral meniscal damage independently predicted tibial and femoral cartilage loss (Sharma et al. 2008). Kleeman et al. has demonstrated a relationship between cartilage degradation and stiffness of various grades of OA cartilage (Kleemann et al. 2005). The data from their mechanical tests showed a correlation between increasing cartilage degradation and stiffness reduction. Mechanical loading has been shown to induce increased activity of MMPs that induce catabolic events or increased turnover in cartilage (Blain et al. 2001). Human and animal OA studies have shown increased MMP activity that leads to degradation of collagen fibrils (Reboul et al. 1996, Salminen et al. 2002). In particular, MMP-13 plays the greatest role in degrading the collagen fibrils in the cartilage matrix. MMP-1 is also involved in the degradation of newly synthesised collagen. Cleavage of type II collagen by collagenses leads to chondrocyte hypertrophy and expression of type X collagen (Martel-Pelletier et al. 2008).

1.3.4 Alterations in OA articular cartilage metabolism

During the disease process, chondrocyte metabolism is altered with subsequent cartilage degradation mediated by the activity of proteolytic enzymes, cytokines, chemokines, and inflammatory mediators (van der Kraan et al. 2002). Articular cartilage turnover is regulated mainly by collagenases, which are specifically named as MMPs. The collagen fibrils are cleaved by MMP-1, MMP-8, and MMP-13. MMP-13 favours type II collagen cleavage and the collagen fragments are further cleaved by gelatinases such as MMP-2 and MMP-9. Proteolytic cleavage of aggrecan is brought about by aggrecanase

(Cawston and Wilson 2006). Aggrecanases namely ADAMTS-4 and 5 (a disintegrin and metalloproteinase with thrombospondin motifs) are involved in the normal turnover of aggrecan molecules and their activity is shown to be increased in OA cartilage (Hardingham 2008). Literature also shows that both ADAMTS-4 and ADAMTS-5 are involved in early cartilage degradation that may progress into OA (Heinegard and Saxne 2011). Chondrocyte metabolism is regulated by members of the TGF-β superfamily, which induce chondrogenic differentiation and promote chondrogenesis. TGF-β plays an important role in cartilage formation during embryonic stages and stimulates proteoglycan synthesis and cartilage repair (van der Kraan et al. 2009). Bone morphogenetic proteins (BMPs) are multi-functional growth factors that belong to the TGF-β superfamily. BMP signalling is involved in endochondral bone formation and chondrogenesis. Elevated BMP levels have been reported in OA which stimulates both matrix synthesis and cartilage degeneration by altering chondrocyte metabolism and stimulating MMP-13 expression (van der Kraan et al. 2010). Other proinflammatory cytokines that are critically involved in OA pathogenesis are IL-1β and tumor necrosis factor alpha (TNFα). The levels of both these cytokines are increased in OA cartilage and are known to stimulate MMP and ADAMTS activity (Kapoor et al. 2011). Figure 1.6 shows the involvement of MMPs and other proteases involved in OA cartilage matrix degradation.

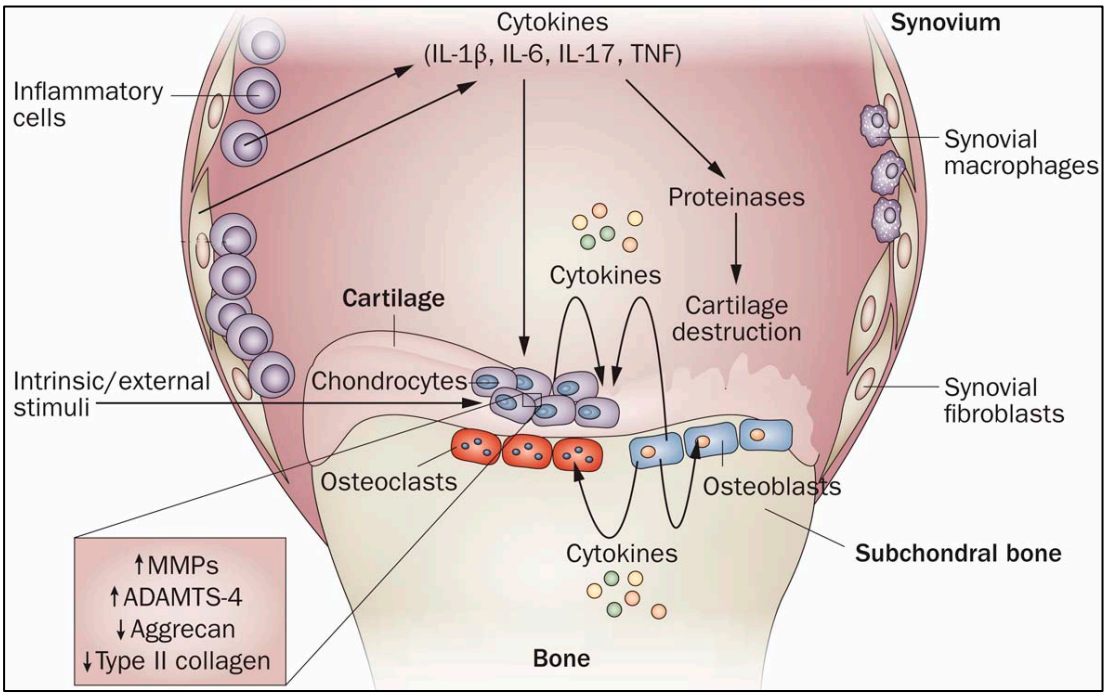

Figure 1.6 Cartilage degradation mediated by proinflammatory cytokines, increased activity of proteases, and external factors such as altered loading of the knee joint (Kapoor et al. 2011, with permission from Nature Pub. Group).

1.3.5 Cellular changes in OA cartilage

A number of cellular-level changes occur in OA cartilage such as phenotypic alterations, activation, redifferentiation, hypertrophy, and chondrocyte death. The altered chondrocytes can no longer maintain the cartilage matrix and this subsequently leads to cartilage degradation. It has been shown that chondrocytes from fibrillated cartilage are clustered (Fig. 1.7), with dissimilar morphological phenotypes that fluctuate between an active secretory phenotype and an osmiophilic contracted apoptotic cell type (Kouri et al. 1996a, Kouri et al. 1996b). The altered OA chondrocytes undergo activation and redifferentiation in OA (Kirsch et al. 2000, Kouri and Lavalle 2006). Recent studies show that chondrocyte hypertrophy could be an initiating event in OA that leads to protease-mediated cartilage degradation (van der

Kraan and van den Berg 2012). Hypertrophic chondrocytes have also been shown to upregulate MMP-13 and aggrecanase activity that leads to cartilage matrix damage (Dreier 2010).

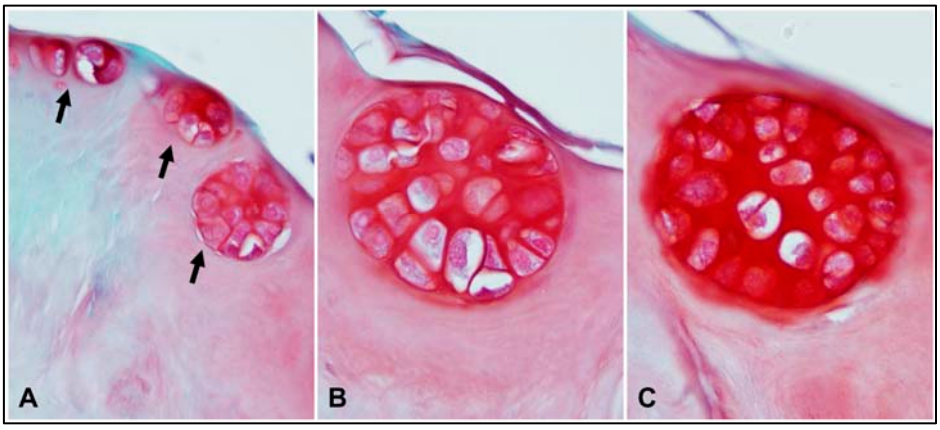

Figure 1.7 Safranin O/Fast green stained sections showing chondrocyte cluster formation in OA. Chondrocyte clusters (A, arrow) from a rat tibial articular cartilage at 10 weeks after OA induction with 0.2 mg monosodium iodoacetate. Magnified image of a chondrocyte cluster (B). Cartilage matrix showed loss of proteoglycans, however increased proteoglycan synthesis is evident in the pericellular matrix surrounding the chondrocytes with altered metabolism (C).

Cell death has long been considered pathological; however, more recently it has been accepted that physiological cell death is essential for normal development and maintenance of adult tissues (Kim and Blanco 2007). In OA, chondrocyte death could occur due to excessive mechanical force, cartilage injury, increased production of reactive oxygen species, and inadequate growth factor production. Chondrocyte loss in OA had also been correlated to disease severity in both animal and human studies (Zamli and Sharif 2011). Cell death in OA is controversial as it is unclear if chondrocytes undergo necrosis or apoptosis. Moreover, occasional identification of markers for both forms of cell death in a single cell makes it difficult to distinguish between the two forms of cell death (Del Carlo and Loeser 2008). A study by Matsuo et

al. supports the occurrence of cell apoptosis in OA, in which they reported significantly increased caspase-3 and caspase-9 positive cells in the superficial and deep zones of OA cartilage (Matsuo et al. 2001).

Based on the above literature, it is clear that cartilage damage in OA is brought about by a multitude of factors. Increased cartilage matrix turnover mediated by the effect of growth factors and cytokines act on the chondrocytes and increase the anabolic activity as a repair mechanism. However, due to altered chondrocyte metabolism the catabolic activity exceeds the anabolic activity, which leads to a net loss of matrix molecules and the chondrocytes can no longer maintain the cartilage matrix. Further loading of the weakened cartilage leads to progressive cartilage loss, which is observed as joint space narrowing in radiographs of OA patients. Recent exciting research focussed on the molecular mechanisms that cause cartilage damage has the potential to advance our understanding of OA pathogenesis.

1.4 Subchondral bone

The subchondral trabecular bone together with the subchondral plate that are present immediately beneath the articular cartilage form the "subchondral bone", which provides support for the overlying articular cartilage (Fig. 1.8). According to Duncan et al. the "subchondral plate" is defined as a zone that separates the articular cartilage from the marrow cavity. It normally consists of the calcified region of the articular cartilage and a layer of lamellar bone that gives rise to the supporting trabeculae (Duncan et al. 1987). The subchondral plate and subchondral trabeculae are different mechanically, physiologically and the anatomy of the subchondral region itself is highly variable (Madry et al. 2010).

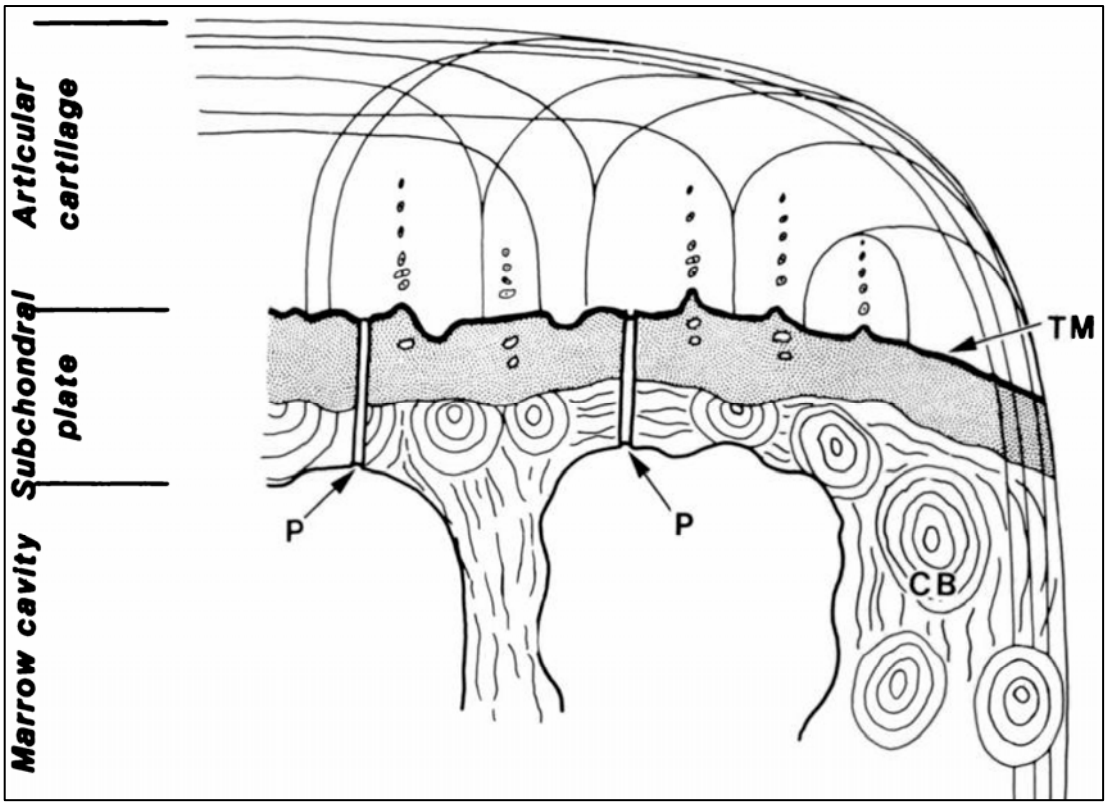

Figure 1.8 Diagram of normal tibial plateau showing subchondral bone made of the subchondral plate and the trabecular bone. TM=tidemark; P=perforation; CB=cortical bone (Duncan et al. 1987, with permission from Journal of Bone and Joint Surgery).

1.4.1 Normal structure of the subchondral plate

The subchondral plate consists of two mineralized layers, together forming a single unit (Fig. 1.9). The calcified cartilage is distinctly separated from the hyaline cartilage by a discrete band of mineralized cartilage called the tidemark, which is denser than the adjacent cartilage and measures up to 10 μm in thickness (Lyons et al. 2005). The tidemark is chemically more complex with a distinct trilaminate appearance and it forms a sharp boundary between the calcified and non-calcified cartilage (Lyons et al. 2007). The calcified cartilage extends towards the marrow cavity and is remodelled and replaced by lamellar bone that supports the subchondral trabeculae, which are

perpendicular to the joint surface. The collagen fibrils of the articular cartilage cross the tidemark and are continuous with those of the calcified cartilage. The articular cartilage or the hyaline cartilage mainly consists of type II collagen, and the calcified zone consists of type X collagen; whereas, the underlying subchondral bone is composed of type I collagen (Madry et al. 2010).

1.4.2 The osteochondral junction

The junction between the cartilage and bone is called the osteochondral junction, the integrity of which is essential for maintaining a healthy joint. The osteochondral junction (Fig. 1.10) consists of the deepest layer of non-calcified cartilage, the tidemark, the calcified cartilage, the cement line that separates the subchondral plate and calcified cartilage, the subchondral plate of lamellar bone, trabecular bone and bone marrow spaces (Lyons et al. 2006). The tidemark clearly delineates the calcified and un-calcified cartilage and is involved in pathological conditions such as OA (Suri and Walsh 2011). Histomorphometric analysis of the adult articular calcified cartilage zone has revealed distinct morphology of the calcified cartilage zone with a ‘‘ravine-engomphosis” shape on the upper interface, and a ‘‘comb-anchor” shape on the lower interface (Wang et al. 2009). This morphology of the calcified cartilage tightly binds the subchondral bone and cartilage.

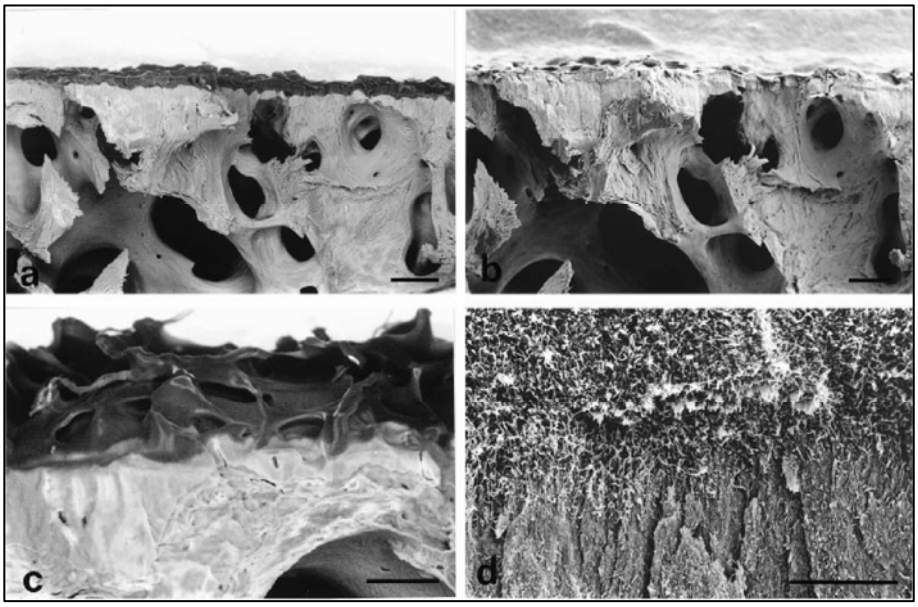

Figure 1.9 Electron microscopic appearance of normal subchondral bone plate from a 76-y-old male. Back-scattered image (a), secondary emission image (b), scale bar 200 μm. Enlarged image showing subchondral bone layers (c) and fibrous nature (d), scale bar 100 μm (from Li et al. 1999, with permission from Blackwell Publishing Ltd.).

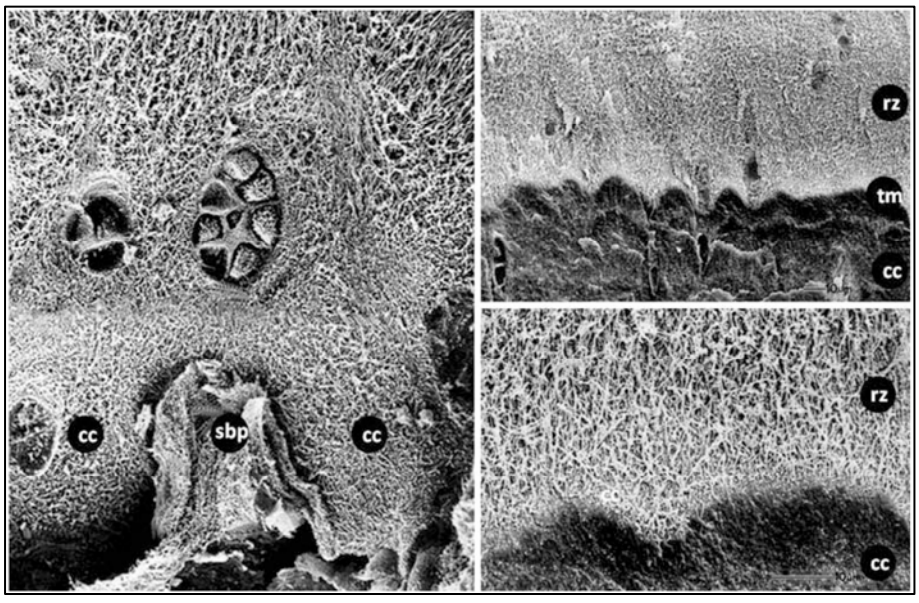

Figure 1.10 Scanning electron micrograph of subchondral plate. cc, calcified cartilage; scp, subchondral plate; rz, radial zone; tm, tidemark between the non-calcified cartilage and calcified cartilage (from Madry et al. 2010, with permission from Springer).

1.4.3 Vascularity of the subchondral bone plate

Subchondral bone is richly supplied with blood vessels and is well innervated. The subchondral plate is invaded by hollow spaces, which provide a direct connection between the uncalcified cartilage and the marrow cavity of the subchondral trabecular bone. The perforations that are canal-like holes are preferentially grouped in the central weight bearing regions of the subchondral plate of the tibial plateau (Berry et al. 1986). Duncan et al reported that the subchondral bone perforations in the medial tibial plateau occurred beneath the area covered by the meniscus. Some of these holes penetrated the subchondral plate and connected with the marrow space. Interestingly, in the medial tibial plateau the larger holes occupied a more peripheral and posterior location; whereas, a large number of holes were found in the central area of the lateral tibial plateau than in its submeniscal region (Duncan et al. 1987). Moreover, the occurrence of perforations varied with the stress within the joint, which were concentrated in the regions with greatest stress (Ahmed and Burke 1983). These perforations supply nutrients and oxygen to the chondrocytes in the deep layers of the calcified cartilage (Imhof et al. 2000).

1.4.4 Subchondral plate thickness and density distribution

The thickness of the subchondral plate varies within the joint and depends on the stress applied to the joint. The subchondral plate in the tibial plateau is thicker at the centre, which is in contact with the femur. Milz et al. reported that a 7 – 12 fold increase in subchondral plate thickness occurs from the periphery to its centre in the tibial plateau (Milz et al. 1995). Similar to the thickness distribution reported by Milz et al. the density of the normal tibial plateau was found to be maximum at the centre of the medial and lateral compartment and the density decreased concentrically towards the

periphery (Noble and Alexander 1985, Odgaard et al. 1989). Thus, the patterns of density distribution correlate with the mechanical situation in each joint and reflect the long-term stress acting. The strength of subchondral plate is greater on the medial condyle than the lateral condyle and the strength decreased rapidly with distance from the surface. Moreover, there was a significant correlation between the strength distribution and mineralization of the subchondral plate (Madry et al. 2010). Subchondral bone is an effective shock absorber in the diarthrodial joints and protects the overlying cartilage against damage due to excessive loading. During load transfer from cartilage to subchondral bone, large shear stresses are created in the subchondral region. The undulations of the tidemark and the osteochondral junction play an important role in transforming these shear stresses into compressive and tensile stresses. Moreover, normal subchondral bone can attenuate about 30% of the load through joints while cartilage can attenuate only up to 3% (Radin et al. 1970).

1.4.5 Pathological changes in OA subchondral bone

Key features of OA include subchondral bone sclerosis, osteophyte formation, development of subchondral bone cysts, and advancement of tidemark with vascular invasion into the calcified cartilage (Walsh et al. 2007). These changes indicate that subchondral bone plays a major role in the pathology of OA (Fig. 1.11). Radin and Rose were the first to propose that changes in the subchondral bone in OA were associated with cartilage damage (Radin et al. 1978a). They also speculated that the changes in subchondral bone preceded the changes in articular cartilage, and that the bone changes adversely affected the load bearing capacity of the overlying cartilage, leading to cartilage damage (Radin and Rose 1986). Moreover, studies using isotope-labelled agents and radiographic techniques strongly suggest that modifications in subchondral

bone occur early in OA and confirm that changes in bone turnover precede the evidence of any bone-related changes detected (Buckland-Wright et al. 1991b, Hutton et al. 1986).

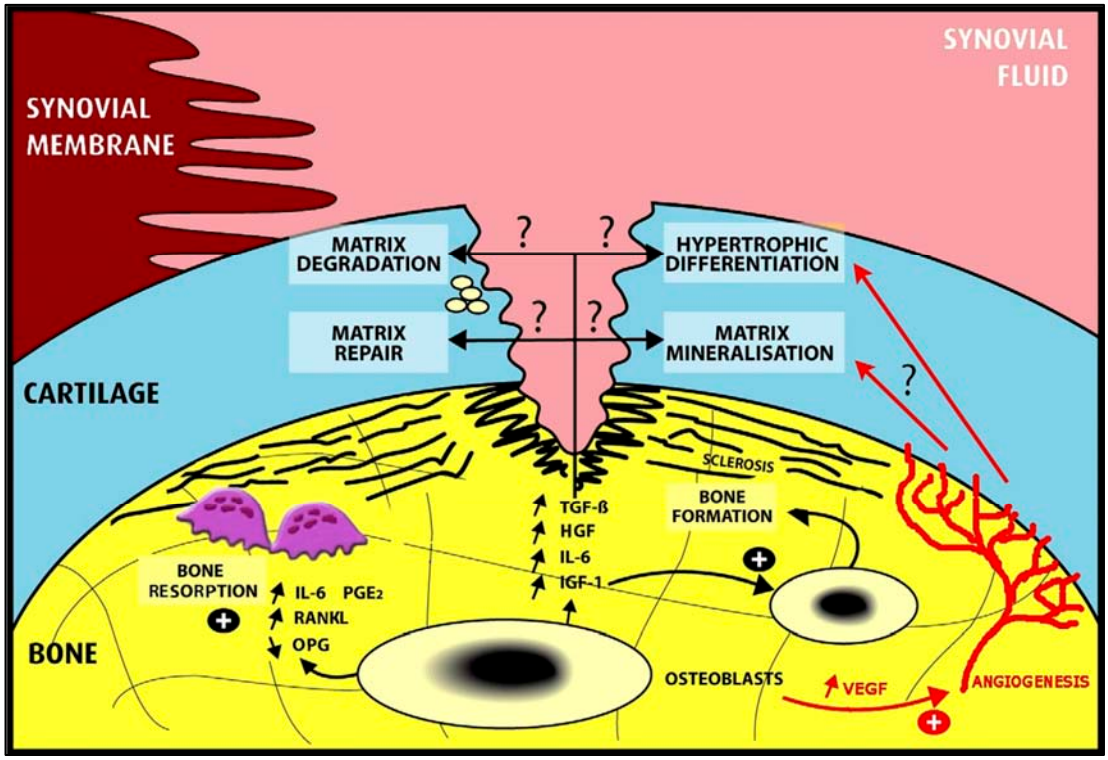

Figure 1.11 Pathological changes in the OA subchondral bone and possible relationship with cartilage damage (Henrotin et al. 2009, with permission from ISO press).

1.4.6 Subchondral bone remodelling in OA

Subchondral bone changes have been proposed as an early event in the pathogenesis of OA and subchondral bone remodelling plays an important role in the disease process (Lajeunesse and Reboul 2003). Pre-clinical and clinical studies clearly indicate that altered subchondral bone remodelling leads to increased bone resorption at the early phase of OA followed by increased bone volume due to subchondral bone sclerosis. Animal models have consistently showed increased subchondral bone remodelling in

OA (Botter et al. 2006, Hayami et al. 2006, Panula et al. 1998, Pastoureau P. C. et al. 1999). Examination of femoral head trabecular bone from a guinea pig model of OA showed a significant increase in bone volume fraction due to the development of thicker trabeculae. Moreover, a microscopic computed axial tomography study revealed that trabecular remodelling is an early event in this animal model of OA (Layton et al. 1988). Another experimental study using young beagle dogs showed that increased subchondral bone remodelling was evident at the early phase of OA (Panula et al. 1998). Using a canine model of OA, Lavigne et al. reported intense subchondral bone remodelling in the knee after anterior cruciate ligament transection (Lavigne et al. 2005).

In human OA, dual energy x-ray absorptiometry (DEXA) analysis of the hip and total body showed that patients with OA had similar or increased bone density compared to controls, suggesting increased bone turnover in OA (Stewart et al. 1999). A study by Hunter et al. showed that both bone turnover and bone resorption was increased in knee OA in female twins (Hunter et al. 2003). In the Chingford study, urinary N-terminal type I collagen telopeptides (NTX) and C-terminal type I collagen telopeptides (CTX) of OA patients were measured at three different time points. Progressive knee OA patients demonstrated significantly increased bone resorption marker level than control. Bone resorption was increased in patients with progressive knee OA due to altered bone turnover (Bettica et al. 2002). Histology and bone morphometry of tibial condyles with OA revealed increased bone volume and higher bone formation activity in the medial condyle in comparison with the lateral condyle. Moreover, cartilage degeneration was found to be influenced by remodelling of subchondral bone (Matsui et al. 1997).

1.4.7 OA related changes in trabecular microarchitecture

The altered bone remodelling in OA leads to microarchitectural changes in the trabecular bone. Fazzalari et al. showed OA related changes in the trabecular bone architecture in femoral head specimens obtained from end stage OA patients. The authors reported increased trabecular thickness, trabecular spacing and a decrease in trabecular number in OA specimens compared to normal controls (Fazzalari and Parkinson 1998). Osteoarthritis may also change the age dependences of both the structural parameters and the mechanical properties usually reported for normal cancellous bone (Perilli et al. 2007a). A radiographic study of patients with OA of the hand over an 18-month period showed greater subchondral cortical thickness at an early stage of OA compared to healthy control subjects which increased with time. However, in one third of the patients cortical plate thickness reduced over time and the authors speculate that it could be due to local inflammation (Buckland-Wright et al. 1991a). Moreover, sclerosis was greatest in joints with progressive joint space narrowing the extent of which is determined by the forces exerted within the hand (Buckland-Wright et al. 1992). Similarly, in the knee joint significant thickening of the subchondral plate was observed in the medial compartment of joints with severe joint space narrowing due to complete loss of articular cartilage (Buckland-Wright et al. 1994). Chappard et al. assessed the subchondral microarchitectural alterations in the femoral head from OA (with and without cartilage) and osteoporosis using micro-computed tomography (micro-CT). They found significantly increased bone volume fraction, trabecular thickness, and trabecular number with decreased trabecular separation in the OA femoral head subchondral bone without cartilage, compared to OA subchondral bone with cartilage and subchondral bone of osteoporosis (Chappard et al. 2006).

In a meniscectomized guinea pig model of OA, evidence of early subchondral bone changes was observed in a densitometric study using DEXA (Pastoureau P. C. et al. 1999). The bone mineral density (BMD) of the medial femoral condyle was significantly lower in the meniscectomized animals compared to sham animals one month after operation. By contrast, 3 months after meniscectomy the BMD was found to be higher in the femur than in the contralateral femur. In another pre-clinical study, Hayami et al. have shown that anterior cruciate ligament transection leads to early bone loss followed by increased bone volume (Hayami et al. 2006).

1.4.8 Biochemical changes of subchondral bone in OA

The pathological changes observed in the subchondral bone are due to altered bone metabolism, which is abnormally increased in OA. Mansell et al. reported highly increased collagen turnover rate in OA bone compared to controls (Mansell et al. 1997). The authors reported a 20-fold increase in the levels of C-terminal pro-peptide of type I collagen, increased alkaline phosphatase activity and a significant increase in MMP-2 activity in the OA femoral head compared to controls. Moreover, the collagen content was significantly increased; however, collagen mineralization was significantly decreased in the OA femoral head (Mansell and Bailey 1998). Earlier studies have reported hypomineralization in the femoral head and the femoral neck of OA patients (Li B. and Aspden 1997a, b). Apart from the presence of normal type I collagen heterotrimer [$(\alpha1(I))_2\alpha2(I)$], the osteoblasts from OA femoral head also synthesised type I collagen homotrimer [$\alpha1(I)_3$] (Bailey et al. 2002). The ratio of type I collagen $\alpha1$ to $\alpha2$ chains in normal bone was found to be 2:1, whereas in OA bone the ratio ranged from 4:1 – 17:1. Moreover, the presence of an excess of $\alpha1$ chain depended on bone

turnover rate and the severity of OA. The pathological changes in the OA subchondral bone have been shown to be directed by changes in the underlying molecular mechanisms that lead to altered bone metabolism (Chan et al. 2011, Hopwood et al. 2005, Kuliwaba et al. 2000, Truong et al. 2006).

1.4.9 Hypomineralizaton of bone in OA

Another important feature of human OA is decreased mineralization of subchondral bone. Couchourel et al. reported that mineralization of OA osteoblasts from tibial plateaus was reduced compared with mineralization of normal osteoblasts in culture. Collagen synthesis, alkaline phosphatase, and osteocalcin levels were found to be elevated, while COL1A1:COL1A2 mRNA ratio was 3-fold higher in OA osteoblasts compared with normal osteoblasts (Couchourel et al. 2009). In studies by both Mansell et al. and Couchourel et al. TGFβ levels were higher in OA compared to normal. TGFβ has been shown to control collagen synthesis and mineralization (Pfeilschifter et al. 1990). Increased levels of TGFβ have been shown to be a pathogenic factor in OA (van den Berg 1995). A significant increase in TGF-β in OA bone has caused the increased collagen synthesis and decreased mineralization. Candidate genes involved in the changes in mineralization in OA have been described in a recent study by Kumarasinghe et al. The authors have shown that the genes that control osteoblast proliferation, differentiation and mineralization such as tensin homolog (PTEN), twist homolog 1 (TWIST1), and S100 calcium binding protein A4 (S100A4) were differentially expressed in bone samples from the intertrochanteric (IT) region of hip OA patients in comparison to control (Kumarasinghe et al. 2010).

1.4.10 Biomechanical properties of bone

Bone strength depends on both the quantity and quality of bone tissue. Bone strength is determined by the shape of bones, the microarchitecture of the trabecular bones, the turnover, the mineral, and collagen content (Cole and van der Meulen 2011). The collagen framework and the hydroxyapatite deposition play a major role in maintaining the strength of bone. Normal bone contains type I collagen ($[\alpha1(I)]_2\alpha2(I)$) which is about 80% of the total proteins present in bone and 95% of total collagen in bone. Type III and type V collagen are present at low levels in bone. The mineral content of bone is mainly composed of hydroxyapatite [$Ca_{10}(PO4)_6(OH)_2$] crystals, measuring approximately 200 Å in their largest dimension (Clarke 2008). The spindle or plate-shaped hydroxyapatite crystals are deposited between or within the collagen fibers, which are oriented in the same direction as the collagen fibers. The bone mineral content provides stiffness and plays a crucial role in bone structural behaviour. High bone remodelling rate is associated with reduced bone mineralization, resulting in loss of stiffness (Seeman 2008). The subchondral bone plate of femoral heads obtained from OA patients was less stiff than normal, was hypomineralised, and had different organic and water fractions suggesting a defect in the matrix (Li B. and Aspden 1997b).

The type I collagen molecules are involved in the mechanical properties of bone and hence the collagenous framework provides the tensile strength to bone. The tensile strength of collagen is derived from its intermolecular cross-links. The collagen fibers are stabilized by the formation of inter- and intramolecular cross-links. The initial head to tail cross-linking occurs in the non-helical telopeptide region by condensation of a hydroxyallysine with a lysyl or hydroxylysyl side chain catalysed by lysyl oxidase. These cross-links are further stabilized by the formation of divalent cross-links

hydroxylysinonorleucine and dihydroxylysinonorleucine. These divalent cross-links correspond to the immature cross-links found in the young bone collagen. The formation of trivalent mature cross-links such as pyrroles and the pyridinolines occurs by spontaneous condensation between two divalent ketoamine cross-links (Viguet-Carrin et al. 2006). Therefore, high bone turnover would reduce the number of cross-links resulting in decreased tensile strength of bone.

Both the matrix properties and microarchitecture influence bone mechanical properties. In OA bone mechanical properties are altered which is associated with the disease process (Day et al. 2004). Day et al. reported an association between decreased tissue elastic modulus of subchondral trabecular bone with pre-arthritic cartilage damage in post-mortem specimen from proximal tibia. The bone tissue modulus was found to be reduced by 60% in the medial condyle with cartilage damage compared to the control specimens. The subchondral trabecular bone volume fraction was found to be higher in the medial compartment compared to the lateral compartment of tibiae with cartilage damage (but not in the controls) (Day et al. 2001).

1.4.11 Biomechanical adaptation: Osteophyte formation

Osteophytes are the major radiographic hallmark feature of OA, which represents fibrocartilaginous and bony outgrowths found at the joint margins. Marginal osteophytes are of variable size and can appear as “spurs” or “lips” of bone around the edges of a joint (Fig. 1.12). Osteophytes are also known to develop in central areas of the joint with remnants of articular cartilage. Much understanding of osteophyte biology has come from experimental animal models of OA. Osteophyte formation in experimental OA has been reported in mice (van Osch et al. 1996), rats (Hayami et al.

2006), dogs (Brandt et al. 1991), rabbits (Hayashi M. et al. 2008) and guinea pigs (Pastoureau P. et al. 2003). Marginal osteophytes are formed by endochondral ossification at the junction of synovium or periosteum and hyaline cartilage. Moreover, it is suggested that the cell source of osteophyte precursors could be the mesenchymal stem cells present in the periosteum at the bone-cartilage junction, from the synovial membrane or the intramembraneous bone formation (van der Kraan and van den Berg 2007). The newly formed osteophyte is integrated with the subchondral bone and it is covered with cartilage expanding the original cartilage surface.

It has been shown that MR detected cartilage defects were highly associated with radiographically diagnosed osteophytes in the tibiofemoral joint in OA patients. Moreover, there was a correlation between the presence of osteophytes at the medial tibial condyle and knee pain (Boegard et al. 1998). Formation of osteophytes in OA is believed to be a mechanical adaption to stabilize the joint (Moskowitz R. W. 1999, van denBerg 1999). Adaptive remodelling plays a major role in OA in which bone adapts to the changing mechanical demands of the joint, which is brought about by altered responses of cells to mechanical loading (Wolff's law) (Goldring 2008, Moskowitz R. W. 1999). A study by Pottenger et al. showed that in patients with medial compartment knee OA, marginal osteophytes appeared to stabilize OA knees, but can cause fixed deformity. Removal of marginal osteophytes from the medial compartment significantly increased the mobility of joints in these patients (Pottenger et al. 1990).

Both TGF-β and BMP-2 have been shown to induce osteophyte formation in experimental model of OA. BMP-2 induced osteophyte formation from the growth plates on the femur and on top of the patella of mice. Whereas, TGF-β induced

osteophyte formation on the bone shaft beneath the collateral ligament on the femur and on top of the patella (Blaney Davidson et al. 2007b). In a murine model of OA, lack of TGF-β3 has been shown to be associated with cartilage damage, which suggests a protective effect of TGF-β3 in OA. Additionally, that study also showed that TGF-β3 is involved in early osteophyte formation, whereas BMP-2 was involved in the later stages of osteophyte formation (Blaney Davidson et al. 2006).

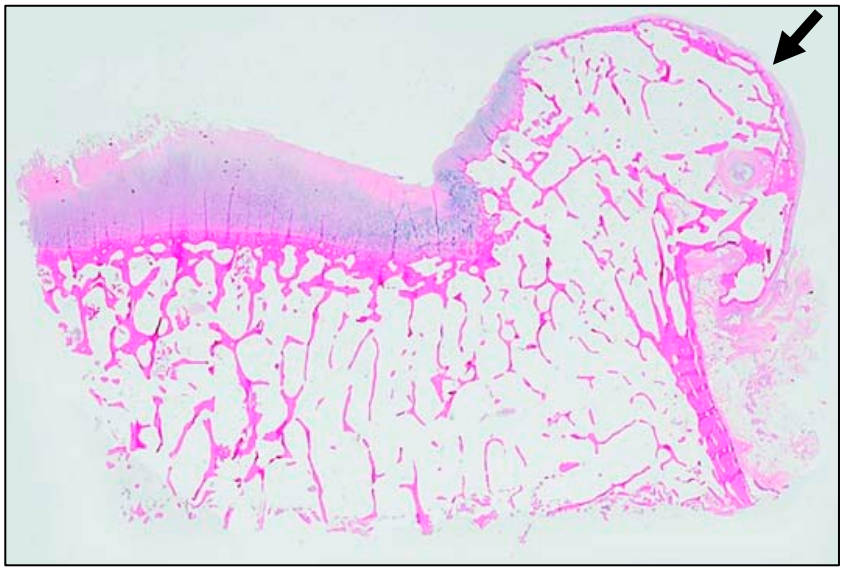

Figure 1.12 Osteophyte formation (arrow) in human OA (from Essentials in Bone and Soft-Tissue Pathology by William R. Reinus, reproduced with permission from Springer).

Repeated, intraarticular injection of TGF-β in the knee joint of normal mice has been shown to induce osteophyte formation at the margins of the cartilage and at insertion sites of ligaments (van den Berg et al. 1993). This suggests a possible role of endogenous TGF-β in osteophyte formation. TGF-β is essential for maintaining healthy cartilage and a lack of TGF-β could result in OA-like cartilage damage (Scharstuhl et al. 2002). However, application of TGF-β supplementation resulted in fibrosis and osteophyte formation, which was blocked by local inhibition of TGF-β or downstream

mediators such as mitogen activated protein kinase (MAPK) signals (Blaney Davidson et al. 2007a). In a murine model of OA, medial meniscectomy induced cartilage degradation and osteophyte formation on the anteromedial aspect of the tibial plateau in wild type mice. However, the MMP-13 knockout mice demonstrated a significant inhibition of cartilage damage with no effect on osteophyte development following medial meniscectomy (Little et al. 2009). This shows that MMP-13 does not have a significant role in osteophyte biology.

1.4.12 Subchondral bone cyst formation in OA

Another typical feature of OA is the formation of subchondral bone cysts in the weight bearing regions of joints (Goldring 2009). Subchondral bone cysts are known to occur in focal areas of bone resorption mainly within areas of sclerotic bone at sites of increased pressure transmission (Pouders et al. 2008). Two theories have been proposed regarding the pathogenesis of subchondral bone cysts in OA. According to the intrusion theory, subchondral bone cysts are formed due to elevated intra-articular pressure, with intrusion of synovial fluid through the damaged cartilage. According to the bone contusion theory, cystic necrosis develops due to fracture and vascular insufficiency of the subchondral bone caused by the impaction of apposing bony surfaces (Bancroft et al. 2004).

Previous human and animal studies have confirmed that subchondral bone cysts occur in advanced stages of OA. Histological examination of acetabulum from hip OA patients showed the presence of acetabular subchondral cysts. The cyst wall was composed of fibrous tissue with mucinous fluid and/or fibromyxoid material in the cyst lumen (Fig. 1.13). Numerous inflammatory cells were found in the cyst wall and the

cyst lumen with macrophages in the fibrotic marrow surrounding the cyst. The surrounding subchondral bone was thickened with the presence of active osteoblasts and osteoclasts suggesting active bone remodelling (Sabokbar et al. 2000). Moreover, macrophages isolated from the wall of subchondral OA cysts have been shown to differentiate into osteoclastic cells in the presence of osteoblasts and $1,25(OH)_2D_3$ (Sabokbar et al. 2000). This shows that the macrophage-osteoclast differentiation may contribute to OA subchondral bone remodelling and enlargement of OA cysts.

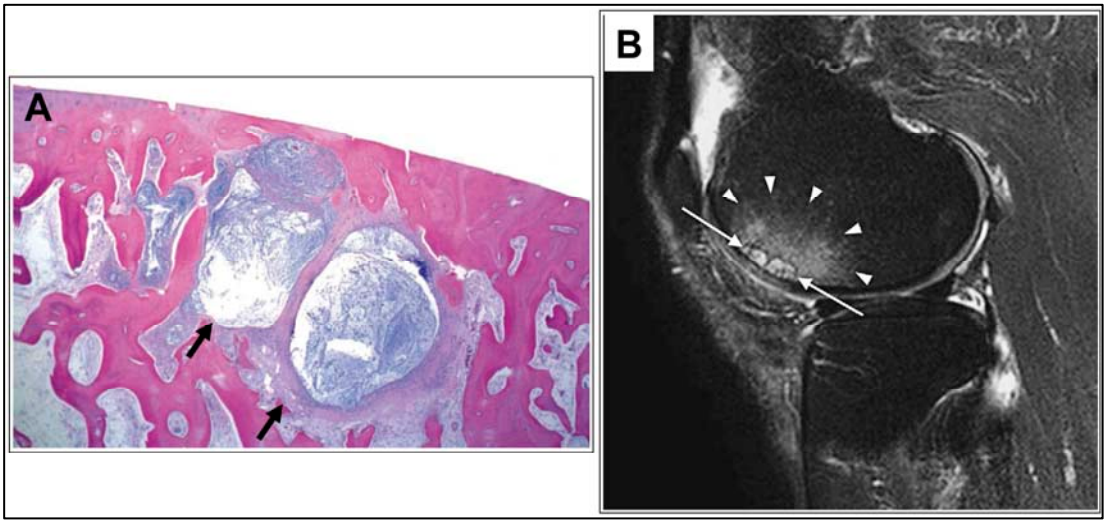

Figure 1.13 A) Histological appearance of subchondral bone cyst formation (arrow) in severe OA (reproduced with permission from Springer). B) MRI of human knee showing subchondral cyst-like signal alterations (arrow) within an ill defined BML (arrowhead) (Crema et al. 2009, with permission from Elsevier).

Radiographic analysis of the tibiofemoral joint of OA patients undergoing arthroplasty revealed that only 10% of the patients with severe OA presented with subchondral bone cysts. Despite low sensitivity, subchondral bone cysts may serve as a reliable indicator of advanced articular cartilage degeneration in the OA joint (Kijowski et al. 2006). MR imaging is more sensitive in detecting small incident subchondral bone cysts as radiographs usually detect cysts with a relative larger area, large enough to produce hyperlucency in the subchondral bone, which usually occurs in advanced disease

(Crema et al. 2009). Subchondral cysts have a characteristic appearance on MRI, demonstrating well defined rounded areas of fluid like signal intensity on unenhanced images (Fig. 1.13).

Finite element (FE) model analysis shows that a subchondral bone cyst in OA develops due to stress-induced bone resorption supporting the bone contusion theory of subchondral bone cyst formation. Thinning of cartilage did not cause a major increase in stress on the femoral head; however, full-thickness cartilage loss significantly increased the stress on the femur just beneath the lesion (Durr et al. 2004). A recent FE analysis of micro-CT scans from early knee OA patients showed that the presence of an intra-osseous defect such as the subchondral bone cyst leads to a two-fold increase in the peri-cystic stress under modest loading. The FE model showed a positive correlation between the diameter of the subchondral bone cyst and the resultant intra-osseous stress under load (McErlain et al. 2011). However, in this study data from early knee OA with a synthetically constructed subchondral bone cyst was used to monitor its effect on OA joints.

In a low-dose MIA induced OA rat model, micro-CT images revealed focal areas of bone resorption in the medial tibia plateau which was consistent with the formation of subchondral bone cysts as confirmed from histology. Formation of subchondral bone cysts was associated with subchondral plate breach in this animal model (Mohan et al. 2011). Other pre-clinical studies have reported the presence of subchondral bone cysts (Nolte-Ernsting et al. 1996, Tessier et al. 2003) and its association with subchondral plate breach (Janusz et al. 2001, McErlain et al. 2008).

1.4.13 Bone marrow lesions (BMLs) in OA

MR imaging, a more advanced imaging technique, has further improved our knowledge regarding subchondral bone marrow lesions/edema and subchondral bone cysts in human OA. The term ‘‘bone marrow lesion’’ is now widely accepted to describe ‘‘bone marrow edema-like lesion’’ as edema appears to be only a minor constituent of bone marrow related abnormalities in OA (Crema et al. 2010a). BMLs are associated with pain and progressive structural deterioration in OA (Felson et al. 2001) however, few studies did not find a significant correlation between pain and BMLs (Bassiouni 2010).

Studies show a strong association between subchondral bone cysts and BMLs in patients with knee OA (Carrino et al. 2006, Tanamas et al. 2010). Presence of cysts identified patients with greater cartilage loss and higher risk of knee replacement than if only BMLs were present. Moreover, their 2-year study period showed that the natural history of subchondral bone cysts varied, including development of new cysts, progression of existing cysts, regression in size, and occurrence of complete resolution (Tanamas et al. 2010). Crema et al. showed that the association between subchondral cysts and prevalent BMLs are much stronger, even though both prevalent BMLs and full-thickness cartilage loss predicted subchondral cyst formation longitudinally (Crema et al. 2010b). The study by Crema et al. strongly supports the bone contusion theory of subchondral cyst formation as prevalent BMLs strongly predicted incident subchondral cysts even after adjustment for full-thickness cartilage loss.

1.5 Bone-cartilage interaction

Mounting evidence suggests increased communication between the subchondral bone and cartilage in the OA disease process (Lories and Luyten 2011, Suri and Walsh 2011). Transport between the articular cartilage and subchondral bone through the calcified cartilage layer has been demonstrated previously (Arkill and Winlove 2008, Pan J. et al. 2009). In a more recent animal study, Pan et al. quantified the diffusivity of a fluorescein marker for small sized signalling molecules, by a new method called fluorescence loss induced by photobleaching. Although that study did not detect significant changes in tissue matrix permeability in OA joints, there was increased vascularity in the calcified cartilage in the aged and OA joints relative to the normal age controls (Pan J. et al. 2011).

As discussed earlier in section 1.4.2 the irregular anatomy of the osteochondral junction and the vascular communication channels allows diffusion of molecules from and into the articular cartilage and the subchondral bone facilitating their communication (Fig. 1.14) (Lyons et al. 2006, Madry et al. 2010). These channels were found to contain blood vessels (Clark J. M. 1990, Clark J. M. and Huber 1990, Duncan et al. 1987). Moreover, it is hypothesised that microcracks in the subchondral bone may provide a pathway for transmission of materials between the marrow cavity and the articular cartilage (Burr and Radin 2003). A study by Fazzalari et al. reported significantly increased accumulation of healing trabecular microfractures in the porotic form of OA femoral head (with widespread cartilage loss and less bone involvement), with decreased bone volume and trabecular thickness compared to the sclerotic form of OA femoral head with localized cartilage loss and more bone formation (Fazzalari et al. 1987).

Angiogenesis of the cartilage, subchondral plate, and synovium is associated with OA (Pesesse et al. 2011, Walsh 2004, Walsh et al. 2007). In OA, increased vascularity is observed as vascular breaching of the tidemark, with invasion of vessels into the noncalcified articular cartilage. Moreover, as discussed earlier in section 1.4.2 loss of tidemark integrity contributes to cartilage degradation and severity of OA (Lyons et al. 2005, 2007). Increased levels of vascular endothelial growth factor (VEGF) that promotes angiogenesis have been reported in the cartilage (Pufe et al. 2001) and subchondral bone in OA (Sanchez et al. 2008).

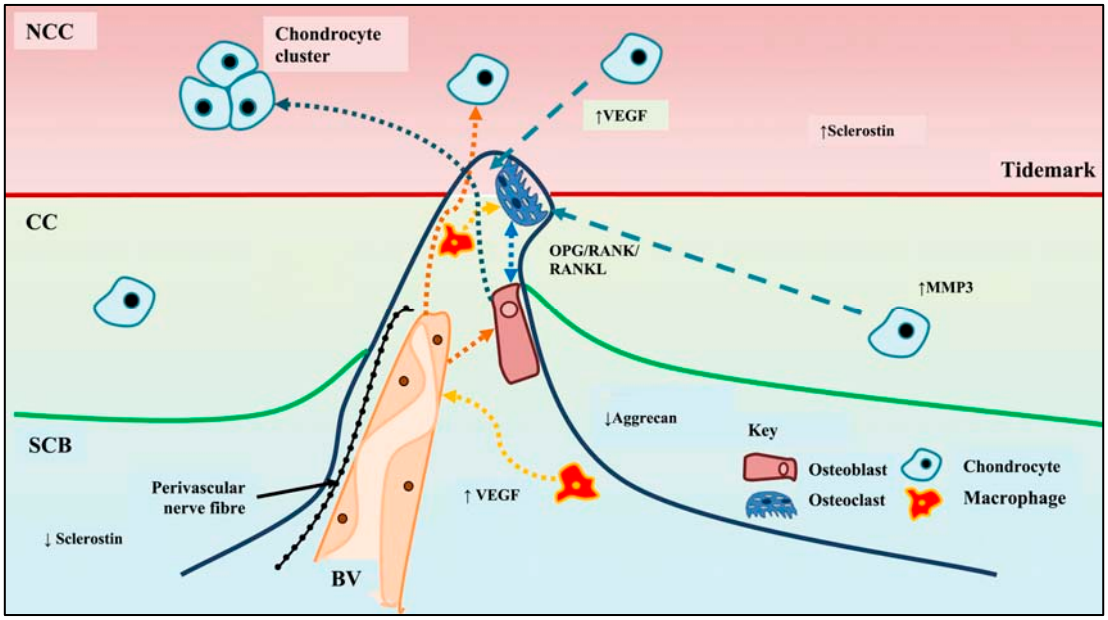

Figure 1.14 Pathological changes in the osteochondral junction. Tidemark breaching due to pathological changes in the osteochondral junction leads to increased communication between cartilage and subchondral bone (from Suri et al. 2011).

1.5.1 Molecular cross-talk between bone and cartilage

In OA, there is increased communication between the subchondral bone osteoblasts and the articular cartilage chondrocytes. The phenotype of subchondral bone osteoblasts is altered in OA and these altered OA osteoblasts have been shown to influence the metabolism of articular cartilage chondrocytes (Bailey et al. 2002, Hilal et al. 1998, Lisignoli et al. 1999, Sanchez et al. 2005b, Sanchez et al. 2008). Sanchez et al. showed that in a co-culture system, osteoblasts isolated from OA sclerotic subchondral bone decrease SOX9, COL2, PTHrP and PTH-R gene expression by OA chondrocytes but increase that of OSF-1. These findings suggest that OA subchondral bone osteoblasts could induce hypertrophic differentiation in chondrocytes and matrix mineralization (Sanchez et al. 2005b). It has also been shown that osteoblasts from OA subchondral bone induce cartilage degradation by stimulating MMP production and inhibiting aggrecan synthesis in chondrocytes isolated from OA cartilage (Sanchez et al. 2005a).

A number of signalling pathways have been identified to be involved in the OA disease process, few of which are discussed here. The wingless-type MMTV integration site (Wnt) signalling pathway and TGF-β/BMP has been shown to be involved in OA (Blom et al. 2009, Kumarasinghe et al. 2011, Luyten et al. 2009). Microarray gene expression profiling of trabecular bone from hip OA patients suggests altered expression of genes belonging to the Wnt and TGF-β/BMP signalling pathways (Hopwood et al. 2007). Both the Wnt and TGF-β/BMP pathways are involved in cell proliferation, differentiation and control of bone mass (Canalis et al. 2003, Krishnan et al. 2006, Wu et al. 2010). In animal models, inhibition of dickkopf-1 (Dkk-1), a Wnt antagonist, has been shown to induce osteophyte formation (Diarra et al. 2007). Over expression of sclerostin, another Wnt antagonist secreted by osteocytes, leads to low bone mass in

transgenic mice (Winkler et al. 2003), while sclerostin knockout mice showed increased bone mass (Li X. et al. 2008).

Recent evidence suggests the involvement of MAPK signalling in OA which plays an important role in osteogenesis and bone homeostasis. MAPKs have important functions as mediators of cellular responses to a variety of extracellular stimuli (Chowdhury et al. 2008, Prasadam et al. 2010a, Prasadam et al. 2010b, Saklatvala 2007). In a more recent study, Prasadam et al. have shown that in human OA, alteration of signals between subchondral bone osteoblasts and articular cartilage chondrocytes occurs via phosphorylation of the MAPK-ERK1/2 signalling pathway (Prasadam et al. 2010b). Another important molecular signalling system involved in OA is the receptor activator of nuclear factor-κB (RANK), RANK ligand (RANKL) and osteoprotegerin (OPG) system that controls bone modelling and remodelling (Boyce and Xing 2008). This molecular triad is known to be involved in OA and has become a potential therapeutic target for OA (Tat et al. 2009). The importance of the RANK/RANKL/OPG system and its involvement in OA is discussed in detail below.

1.5.2 Key regulators of bone remodelling: the RANKL/RANKL/OPG system

Bone remodelling is a tightly coupled process of osteoclast mediated bone resorption and osteoblast mediated bone formation. Bone remodelling is a continuous process, which is essential to repair bone microdamage, and maintain bone mass, architecture and bone strength. Any disruption of the coupled remodelling process leads to increased bone turnover, resulting in excessive bone loss or excess bone formation and consequent skeletal pathology (Eriksen 2010). Discovery of the RANK/RANKL/OPG

system has lead to better understanding of osteoclast biology and the process of bone remodelling (Fig. 1.15). In a more recent study, Tanaka et al. has clearly demonstrated the essential role of RANKL/OPG during bone remodelling *in vivo* (Tanaka et al. 2011).

1.5.2.1 Osteoprotegerin (OPG)

OPG is a natural decoy receptor for RANKL, and competes with RANK to bind with RANKL. OPG belongs to the tumour necrosis factor (TNF) receptor super family and is mainly secreted by osteoblasts and cells of the osteoblast lineage. OPG is secreted as a soluble protein and lacks a transmembrane and cytoplasmic domain (Khosla 2001). The main function of OPG in bone is to inhibit osteoclast differentiation and activity. OPG inhibits the binding of RANKL to RANK, thereby prevents RANK activation and subsequent osteoclastogenesis, and finally inhibits bone resorption. OPG production is modulated by 1α, 25-dihydroxyvitamin D_3, estrogens, IL-1, TNF-α, TGF-β, parathyroid hormone and glucocorticoids (Tat et al. 2009).

1.5.2.2 RANK

RANK also belongs to the TNF receptor superfamily and it is synthesized as a heterotrimer on the surface of osteoclast progenitor cells, mature osteoclasts, and chondrocytes. Ligation of RANK with its ligand RANKL results in osteoclastogenesis and the activation of mature osteoclasts resulting in bone resorption (Jones D. H. et al. 2002). RANK activation by RANKL involves distinct signalling cascades, including TNFR-associated factor proteins (TRAF), nuclear factor of activated T cells (NFAT), the MAPK and nuclear factor κB (NFκB), which are involved in osteoclastogenesis (Edwards and Mundy 2011).

1.5.2.3 RANKL

RANKL belongs to the TNF receptor superfamily. It exists in three isoforms and is secreted as both a membrane-bound form and soluble form (Ikeda et al. 2001). RANKL is highly expressed in osteoblast/stromal cells, primitive mesenchymal cells and hypertrophic chondrocytes (Lacey et al. 1998). In bone, it mainly stimulates osteoclast differentiation, activity, and inhibits osteoclast apoptosis. RANKL expression is influenced by several hormones, growth factors, peptides and cytokines. Recent literature indicates that β-catenin, a member of Wnt signalling pathway, might also be involved in regulation of RANKL. RANKL expression can be upregulated by bone resorbing factors such as glucocorticoids, vitamin D_3, IL-1, IL-6, IL-11, IL-17, TNF-α, PGE_2, and PTH (Yasuda et al. 1998).

The RANK/RANKL/OPG system has been shown to have important clinical implications and is a treatment target in skeletal disease such as osteoporosis (Jabbar et al. 2011), rheumatoid arthritis (Haynes et al. 2001), Paget's disease (Alvarez et al. 2003), multiple myeloma (Giuliani et al. 2002), and bone metastasis (Kearns et al. 2008). Interestingly in OA, altered expression of RANKL and OPG mRNA has been shown to be associated with bone remodelling (Kwan Tat et al. 2008, Logar et al. 2007, Sakao et al. 2008). Altered expression of RANKL and OPG mRNA/protein has also been demonstrated in OA cartilage (Komuro et al. 2001, Moreno-Rubio et al. 2010, Upton et al. 2012), synovial fluid and serum (Pilichou et al. 2008, Skoumal et al. 2005) Despite the importance of the RANK/RANKL/OPG system in OA, very few studies have focussed on this molecular triad. Moreover, the RANK/RANKL/OPG system could be a potential therapeutic target for OA.

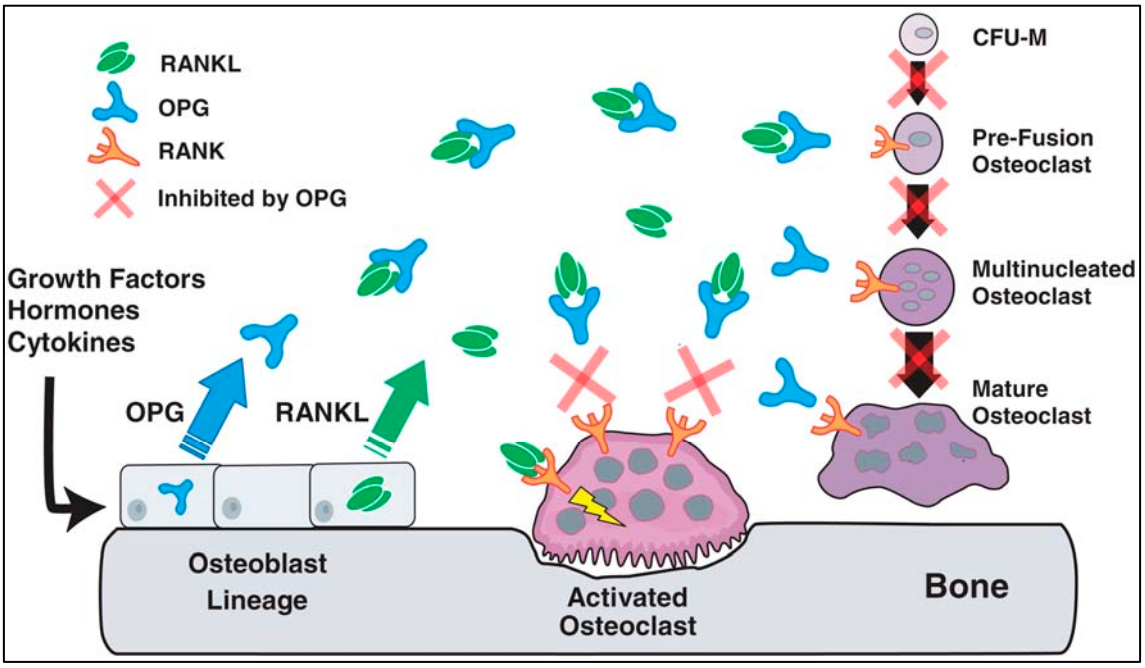

Figure 1.15 Regulatory mechanisms of bone remodelling: role of RANK, RANKL, and OPG in osteoclast activation. (from Kearns et al. 2008).

1.6 Bisphosphonates as disease modifying OA drugs (DMOADs)

In OA, subchondral bone turnover is increased demonstrating decreased trabecular number and decreased integrity, resulting in localized subchondral osteoporosis. Bisphosphonates have the capacity to suppress bone turnover and hence could have the potential to be used as DMOADs. For many decades, bisphosphonates have been mainly used in the treatment of osteoporosis. Besides they are also used to treat other bone pathologies characterised by increased bone resorption, such as Paget's disease, malignant hypocalcaemia during myeloma, metastatic bone disease, and fibrous dysplasia of bone (Devogelaer 2000).

1.6.1 Structure of Bisphosphonates

Bisphosphonates are stable analogues of pyrophosphate with a carbon atom (P-C-P) substituting an oxygen atom (P-O-P) structure (Fig. 1.16). The P-C-P bond of bisphosphonates is completely resistant to enzymatic hydrolysis and is very important for the high affinity of bisphosphonates to attach to the surface of bone. Bisphosphonates bind to hydroxyapatite crystals, and inhibit crystal growth and dissolution similar to pyrophosphate *in vitro*. Their main biological effect is their ability to inhibit osteoclast mediated bone resorption (Russell and Rogers 1999).

In the P-C-P structure both the phosphonate groups are required for both the affinity for bone mineral and biochemical potency of bisphosphonates. The biological activity of bisphosphonates depends on the two side-chains (R1 and R2) attached to the carbon atom. R1 substituents, such as a hydroxyl or amino group, enhance chemisorption to mineral, while R2 substituents are responsible for variations in antiresorptive potency of different bisphosphonates. The antiresorptive potency is attributed to the ability of certain bisphosphonates to interfere with the metabolism of mevalonate, an intermediate compound of the cholesterol biosynthetic pathway and is also thought to be associated with the ability to bind to hydroxyapatite crystals (Russell 2007). According to Nancollas et al. the significant differences in the kinetic binding affinity of several bisphosphonates to hydroxyapatite crystals was in the order as follows: clodronate < etidronate < risedronate < ibandronate < alendronate < pamidronate < zoledronate (Nancollas et al. 2006). Apart from bisphosphonates' most important effect to inhibit osteoclast-mediated bone remodelling, extra-skeletal biological effects have also been reported. It has been shown that bisphosphonates exert ''immunomodulating'' effects on cells of the immune system, by influencing the cells to produce anti-inflammatory

cytokines. They also change the molecular expression involved in the immune processes and anti-inflammatory response (Corrado et al. 2007).

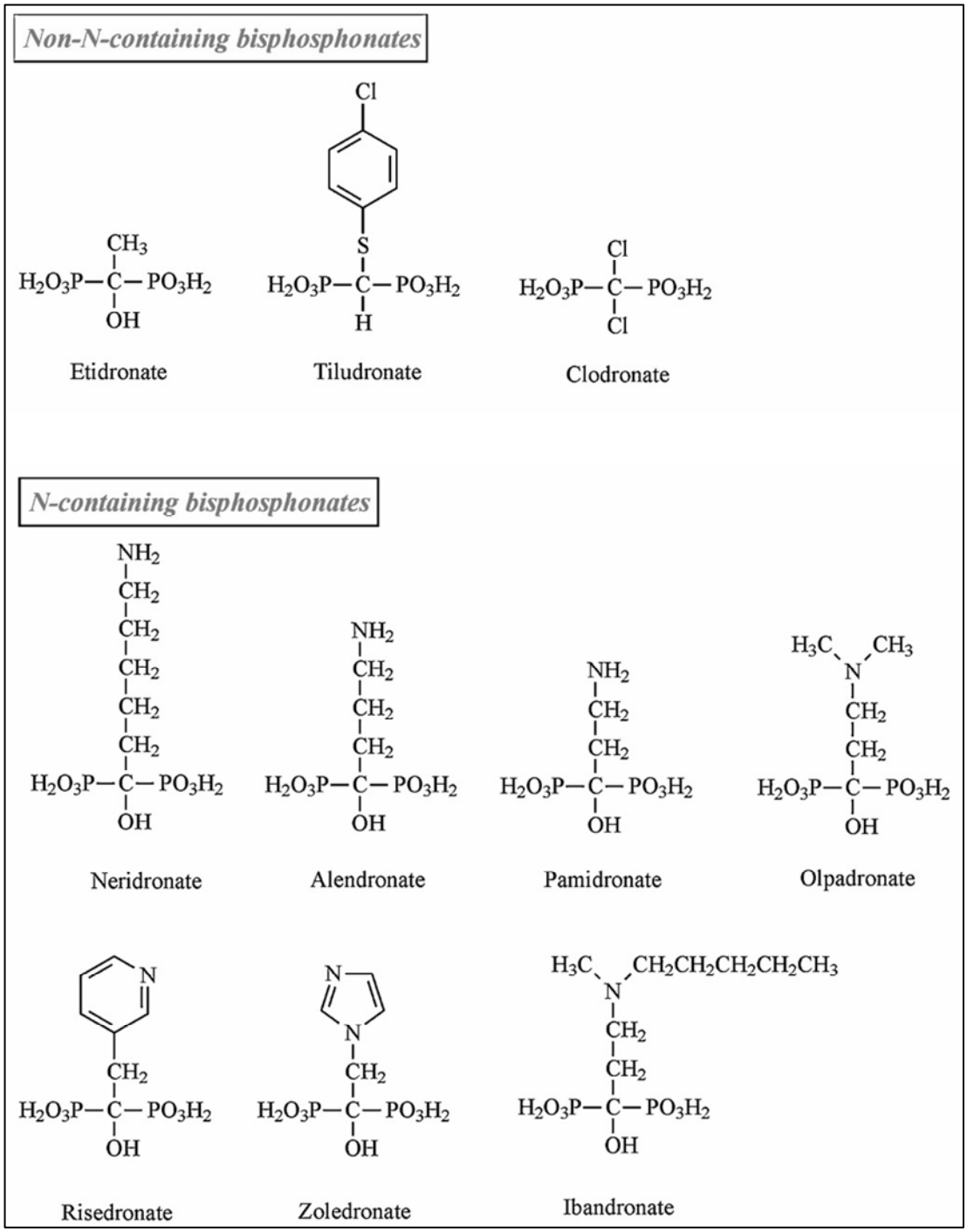

Figure 1.16 Structure of non-nitrogen-containing and nitrogen-containing bisphosphonates (Zacharis 2008, with permission from Elsevier).

1.6.2 Mechanism of action of bisphosphonates

The mechanism of action of bisphosphonates differs based on the presence or absence of a nitrogen group in the R2 side chain. Non-nitrogen-containing bisphosphonates, such as clodronate and etidronate, inhibit the function of osteoclasts and cause osteoclast death by interfering with the mitochondrial ATP translocases (Russell et al. 2008). The nitrogen-containing bisphosphonates such as alendronate, risedronate and zoledronate interfere with specific metabolites and enzymes such as squalene synthase and farnesyl pyrophosphate synthase in the mevalonate biosynthetic pathway that leads to the synthesis of cholesterol and other sterols in the osteoclasts (Fig. 1.17) (Fisher et al. 2000, Kimmel 2007, Reszka and Rodan 2004).

1.6.3 Biological activity of nitrogen containing bisphosphonates: with reference to alendronate

Alendronate, an aminobisphosphonate, is a potent inhibitor of bone turnover and osteoclast-mediated bone loss due to its high affinity for hydroxyapatite crystals in bone (Nancollas et al. 2006), and its high specificity for farnesyl diphosphate synthase (Bergstrom et al. 2000). The mode of action of alendronate is as follows:

1. Binding to bone surfaces: alendronate preferentially binds to areas of high bone resorption and bone turnover. Alendronate binds to hydroxyapatite crystals through its high affinity for Ca^{2+} in the highly acidic spaces under the osteoclasts (Sato et al. 1991).
2. Release of alendronate and internalisation into the osteoclasts: the affinity of alendronate for Ca^{2+} ions reduces due to the high acidity environment created by the osteoclast. As a result, alendronate is released from the bone surface

resulting in increased local concentration of alendronate under the osteoclasts. The released alendronate from the bone surface is internalised by the osteoclasts, probably by endocytosis (Russell and Rogers 1999, Sato et al. 1991).

3. Interference with osteoclast formation and function: The internalised alendronate disrupts the formation of the cytoskeleton or ruffled border of osteoclasts (Russell et al. 1999) by interfering with the mevalonate pathway (Bergstrom et al. 2000, Luckman et al. 1998), resulting in loss of normal osteoclast function. Inhibition of osteoclast formation occurs possibly through the inhibition of IL-6, which is known to stimulate osteoclastogenesis (Sahni et al. 1993). Alendronate also induces apoptosis thereby reducing the number of osteoclasts (Hughes et al. 1995). Collectively, this leads to the inhibition of osteoclast-mediated bone resorption and bone turnover (Breuil et al. 1998, Sato and Grasser 1990, Schenk et al. 1986).

1.6.4 Bisphosphonate treatment for OA

OA is associated with subchondral bone changes including increased subchondral bone remodelling, loss of trabecular architecture and low BMD (Goldring 2009). In postmenopausal osteoporosis, alendronate has been shown to increase bone density in the spine and hip and completely suppressed bone resorption and bone turnover (Watts and Becker 1999). The effect of alendronate on bone turnover suppression has prompted the exploration of the disease-modifying potential of the bisphosphonates.

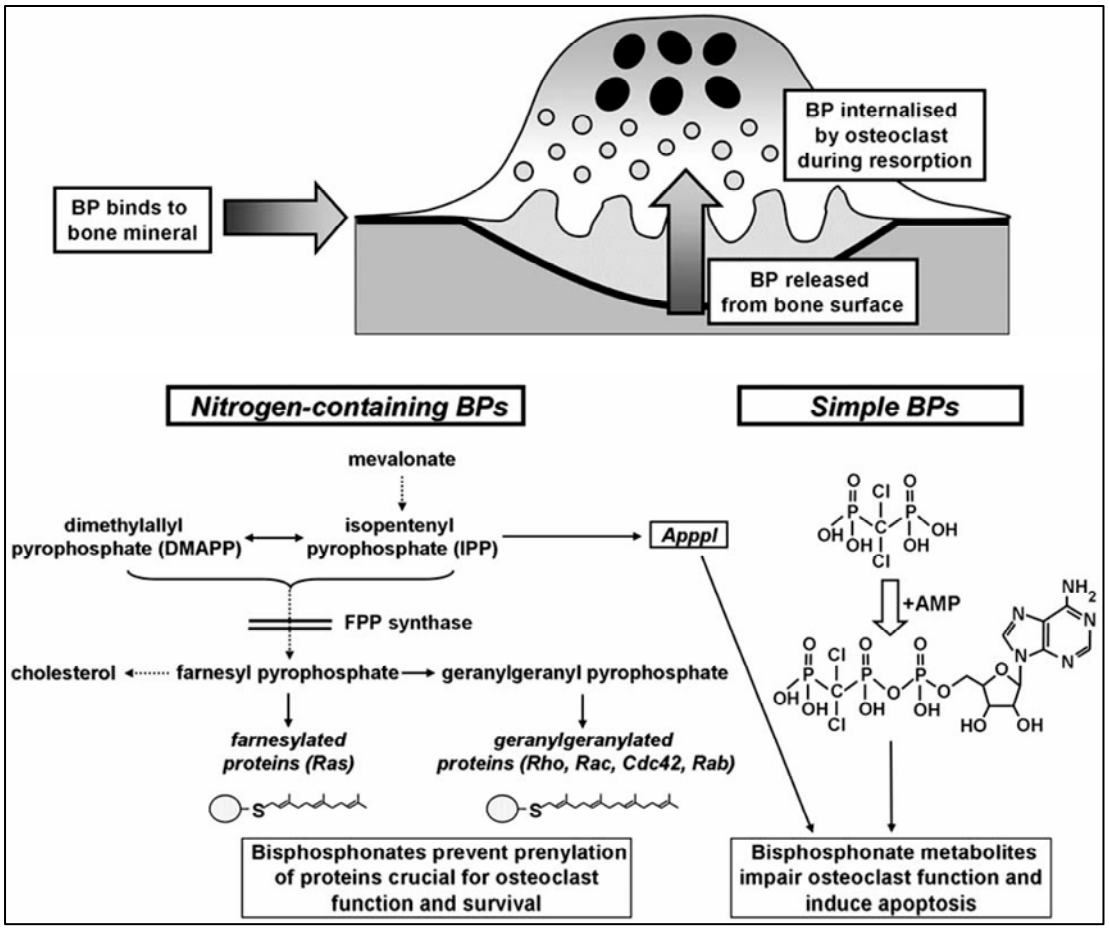

Figure 1.17 Mechanism of action of bisphosphonates. Nitrogen containing bisphosphonates internalised by the osteoclasts during resorption interfere with mevalonate biosynthetic pathway leading to loss of function and apoptosis of osteoclasts (Roelofs et al. 2010, with permission from Bentham Science Publishers).

Clinical trials with bisphosphonate treatment for OA have yielded promising results, while few studies failed to establish a significant association of alendronate treatment and OA disease progression (Saag 2008). Postmenopausal women with knee OA treated with alendronate showed significantly decreased subchondral bone lesions and reduced knee pain compared to those who were not treated (Carbone et al. 2004). However, there was no reduction in the radiographic progression of OA in the elderly women on alendronate treatment. In a secondary analysis of data from a Fracture Intervention Trial, Neogi et al. showed that alendronate was associated with less spinal osteophyte

and disc space narrowing progression compared to placebo (Neogi et al. 2008). However, the authors mentioned that the effect of alendronate on disc space narrowing in the lumbar spine did not persist when the thoracic spine was included in the analysis.

A two-year longitudinal radiographic study showed that risedronate treatment preserved the structural integrity of subchondral bone in knee OA patients. Buckland-Wright et al. found that knee OA patients with marked medial compartment cartilage loss (joint space narrowing ≥0.6 mm) treated with 15 mg/day risedronate retained trabecular structure, and those treated with 50 mg/week risedronate had increased trabecular number (Buckland-Wright et al. 2007). In a much larger study by Bingham et al., although risedronate treatment resulted in a reduction in the level of a cartilage turnover marker, there was no improvement in the signs or symptoms of OA, nor did it alter progression of knee OA (Bingham et al. 2006). After further analysis of data from the same population of OA patients, Garnero et al. reported that risedronate treatment reduced the levels of bone turnover marker, N-terminal telopeptide of type I collagen (NTX-I), and cartilage turnover marker, C-terminal telopeptide of type II collagen (CTX-II), at 6 months, which continued up to 24 months. Moreover, the authors reported that patients with decreased CTX-II levels 6 months after risedronate treatment had a lower risk of radiological progression at 24 months (Garnero et al. 2008). In another clinical trial although risedronate significantly reduced urinary levels of NTX-I and CTX-II there was only a trend towards improvement in joint structure and symptoms in knee OA patients (Spector et al. 2005). Healthy postmenopausal women treated with alendronate showed significantly decreased urinary excretion of CTX-II which suggests that bisphosphonates may have chondroprotective effects in humans (Lehmann et al. 2002).

While clinical trials have been disappointing, pre-clinical studies for bisphosphonate treatment have been promising. An earlier study using the anterior cruciate ligament transection in dogs showed that bisphosphonate treatment (NE-10035) reduced subchondral bone turnover, but did not have a significant effect on osteophyte formation or cartilage degradation (Myers et al. 1999). Risedronate treatment in female New Zealand white rabbits with ACLT altered the short-term progression of subchondral bone changes by slowing early-stage changes in the microarchitecture and preserved mechanical integrity (MacNeil et al. 2008).

In a rat ACLT model of OA, alendronate treatment significantly inhibited subchondral bone remodelling and bone resorption observed at an early stage of OA. Alendronate treatment also decreased the bone and cartilage turnover, prevented osteophyte formation, and suppressed osteoclast formation (Hayami et al. 2004). In a study using male Japanese white rabbit ACLT model of OA, alendronate treatment markedly reduced and delayed cartilage degeneration in OA joints (Zhang et al. 2011). Immunohistochemistry assay indicated that alendronate treatment elevated BMP-2 while inhibited MMP-13 expression in the cartilage. Further, alendronate suppressed subchondral bone resorption, markedly increased bone volume fraction (BV/TV), trabecular thickness (Tb.Th), and trabecular number (Tb.N). However, this study reported higher subchondral plate thickness and porosity in the alendronate treated group compared to the untreated group, while no significant difference was found between the alendronate treated and Sham group. Thus, alendronate treatment protected the cartilage, prevented bone turnover and bone loss in this animal model (Zhang et al. 2011). In another ACLT model using female Japanese White rabbits alendronate treatment prevented subchondral bone loss, protected the cartilage, and suppressed the

expression of MMP-13, IL-1β, type-X collagen, VEGF, and RANKL 12 weeks after OA induction. In this animal model, alendronate had a chondroprotective effect (Shirai et al. 2011).

In chymopapain induced cartilage damage in male New Zealand white rabbits, treatment with zoledronate inhibited bone resorption and decreased biochemical markers for bone and cartilage metabolism (Muehleman et al. 2002). Thus, zoledronate seems to have a chondroprotective effect in this animal model. Zoledronate treatment (either with a low-dose of 10 μg/kg or a high-dose of 25 μg/kg) in dogs with cranial cruciate ligament transection surgery prevented significant BMD decreases in the medial femoral condyle at 1 and 3 months after surgery (Agnello et al. 2005). In that animal model zoledronate reduced subchondral bone loss and bone metabolism markers. In a more recent study using the MIA-induced OA rat model the effects of zoledronate treatment was assessed, with the treatment initiated before OA induction and at various times following OA induction (Strassle et al. 2010). Pre-emptive treatment prevented loss of BMD, cartilage degeneration, resorption of calcified cartilage, subchondral bone resorption, as well as pain. Late treatment resulted in partial restoration of BMD, and had a significant, but limited, effect on pain. This study demonstrated that the bisphosphonate zoledronic acid had a significant effect of bone, cartilage, as well as pain behaviour (Strassle et al. 2010).

In a more recent study, a canine model with ACLT was treated with the non-nitrogen containing bisphosphonate tiludronate. Tiludronate treated dogs showed positive functional outcome in terms of gait and pain behaviour than OA placebo controls.

Tiludronate treatment resulted in decreased synovitis, greater subchondral bone surface lower MMP-13 in cartilage and cathepsin K in subchondral bone (Moreau et al. 2011).

The above literature has discussed the important pathological changes in OA subchondral bone and the potential molecular signalling pathways involved in these changes. Moreover, from the literature, it is evident that subchondral bone changes contribute to the progression of cartilage lesions and subsequent OA disease progression. It is also clear that the health of both the cartilage and the subchondral bone is necessary to maintain joint integrity. The literature on bisphosphonate treatment for OA offers hope as it seems to have a positive effect on both the cartilage as well as bone, at least in animal models. In clinical trials using bisphosphonates for OA, the efficacy was assessed after the treatment was initiated in advanced stages of the disease. In animal models of OA, the efficacy was assessed after the treatment was initiated a few days before OA induction or from the day of OA induction. Therefore, the effect of the bisphosphonate could depend on the time of treatment initiation and explains the mixed results obtained in clinical trials. In this thesis, the effect of a potent nitrogen containing bisphosphonate, alendronate, was assessed at early, intermediate and late stages of the disease using an animal model of OA. Moreover, the efficacy of alendronate was assessed with the treatment initiated at various timepoints after OA induction.

1.7 Animal models of OA

Despite the explosion of information regarding the pathology of OA, the etiopathology of the disease still remains obscure and currently there are no treatment options available to halt the progression of OA. Initiating events in early OA are difficult to study in humans due to difficulty in obtaining suitable tissue samples for research. It is also difficult to track disease progression since human OA progression is very slow and extremely variable. Animal models of OA provide important information regarding the pathological changes in the early stage of OA. Animal models not only shed light on OA pathology but they are also helpful to test suitable therapeutic drugs for OA. Many animal models reproduce the signs and symptoms of human OA; however, they do not completely represent the human disease condition, and the results obtained from any animal model should be interpreted with caution. Careful consideration should also be given to the experimental design, use of suitable controls, and statistical data analysis and interpretation.

1.7.1 Commonly used animal species

The commonly used animals in OA research include mouse, rat, guinea pig, rabbit, and dog. Other animals such as cat, monkey, macaque, sheep, and horse have also been used as OA animal models previously (Table 1.1). When using animal models to study human OA, factors such as species differences, tissue heterogeneity between human and animal tissues, time taken for OA progression, and skeletal maturity of the animals need to be considered. In rats and mice, it is important to note that not all growth plates close completely and even if the animals are skeletally mature, there is still a possibility for long bone growth to exist. When using large animal models, factors such as cost,

management, housing, genetic variability and ethical controversial issues need to be considered.

For drug efficacy studies usually animal models that develop OA more rapidly are preferred as the duration for the experiment is short to determine the effect of drugs. However, it is also important to use an animal model in which OA progression can be monitored. The commonly used animal models of OA include the chemically induced model (monosodium iodoacetate, collagenase), spontaneous model, surgical model (anterior cruciate ligament transection and medial meniscectomy), genetically modified model, and ovariectomy model (postmenopausal OA) (Ameye and Young 2006).

1.7.2 Types of OA induction

Spontaneous OA in the knee joints of mice and guinea pigs occurs naturally, the progression is slow, and the pathological features resemble human disease. However, the period for drug testing is fairly long. Surgical models are instability models of OA and represent traumatic OA in humans. Generally, the greater the instability, the greater the lesion. Therefore, these models may mimic aspects of pathogenesis and pathology of instability-induced OA in human. Surgically induced models of OA often have rapid and severe cartilage degeneration after the instability is created. The use of genetically modified mouse models are useful to examine the role of specific genetic factors in OA. However, there is high variability in the temporal progression of OA in these models and the relationship between disease and activity impairment and OA onset requires to be established. The mouse models could be effective screening models even though they do not accurately represent the effect of joint loading in human OA (Poole R. et al. 2010). OA-like changes in the subchondral bone and calcified cartilage has also been

described in animal models after application of repetitive loading across the surfaces of the joint (Radin et al. 1978b, Thomson et al. 1991).

Table 1.1 Animal models used to study OA and the methods of OA induction

OA induction	Species	Reference
Spontaneous	Mouse Guinea pig Macaque	(Stoop et al. 1999) (Huebner et al. 2002) (Carlson et al. 1994)
Genetic modification	Mouse	
Intraarticular injection (collagenase, iodoacetate, papine)	Mouse, rat, rabbit, horse	(Kalbhen 1987, Muehleman et al. 2002, van der Kraan et al. 1990)
Immobilization	Rat, rabbit, dog	(Brandt 2002)
ACL transection (ACLT)	Rat, guinea pig, rabbit, cat, dog	(Bendele 2001)
Meniscectomy	Rat, guinea pig, rabbit, dog, sheep, monkey	(Moskowitz and Goldberg 1987)
Meniscal destabilisation	Rat, guinea pig, rabbit	
Combination surgery	Mouse, rat, guinea pig, rabbit	(McErlain et al. 2008)
Impact loading	Rabbit, dog	(Radin et al. 1978b, Thomson et al. 1991)
Ovariectomy	Rat, sheep, macaque	(Sniekers et al. 2008a)

1.7.3 Monosodium iodoacetate-induced experimental OA model

The MIA-induced OA model was first described by Kahlben and has been demonstrated in a number of species such as chicken, mice, horses, and rats (Kalbhen 1987). MIA is a potent inhibitor of the enzyme glyceraldehyde-3-phosphate dehydrogenase in chondrocytes, resulting in disruption of glycolysis and eventual cell death (Kalbhen 1984). The MIA model of OA is a highly reproducible non-trauma model in which a

single intra-articular injection of MIA in the rat's knee joint induces OA-like changes in the cartilage and subchondral bone (Guingamp et al. 1997, Guzman et al. 2003). Histological analysis of the MIA-injected knee showed loss of proteoglycan, progressive cartilage degradation, chondrocyte clusters, subchondral bone sclerosis, cyst, and osteophyte formation (Guzman et al. 2003, van der Kraan et al. 1989). These changes were more sever in the medial compartment of the knee. The BMD of the MIA-injected knee was found to be significantly decreased compared to the contralateral knee 7 days after MIA-injection till the end of the study till day 56 (Morenko et al. 2004). The onset, progression, and severity of OA can be easily controlled in this animal model by varying the concentration of MIA (Kobayashi et al. 2003). The MIA-induced OA rat model also represents the effect of weight bearing on OA knee joints and pain (Fernihough et al. 2004, Ferreira-Gomes et al. 2010, Ivanavicius et al. 2007, Pomonis et al. 2005). Bove et al. has showed that the weight bearing of the MIA-injected knee was decreased compared to controls and the changes in weight bearing of the MIA-injected knee were dose-dependent (Bove et al. 2003).

1.7.4 Dose response study

A dose response study by Guingamp et al. clearly showed that the severity of cartilage degradation depends on the dosage of MIA-injected into the knee joint (Table 1.2). Higher doses of MIA (up to 3 mg) caused cartilage erosion, sclerosis and exposure of subchondral bone on day 15 post MIA injection, and on day 30 there was complete loss of articular cartilage, with greatly remodelled subchondral bone (Guingamp et al. 1997). Whereas, a low-dose of MIA (0.25 mg) induced moderate cartilage damage at 3 weeks (Janusz et al. 2001). In a pilot study, I evaluated the dose responsiveness of tibial cartilage and subchondral bone to MIA using a high-dose of 2 mg MIA (n=3) and a

low-dose of 0.2 mg MIA (n=3) in rats. As early as after 2 weeks, high-dose MIA induced characteristic features of end-stage human OA, such as loss of tibial articular cartilage, exposure of subchondral bone, subchondral trabecular bone erosion, cysts and osteophytes. In contrast, these changes were observed only at 10 weeks in the low-dose MIA model. The low-dose MIA model, of relatively slow progressing OA, enables *in vivo* monitoring of tissue-level changes representative of progressive human OA; whereas, in the high-dose model the disease progression is very rapid, which is less suitable for longitudinal monitoring of cartilage and subchondral bone changes. This pilot study has been included in the thesis and discussed in detail in appendix 1.

From the previous literature and the pilot study, it is clear that the low-dose MIA-induced OA rat model is a non-trauma model that reproduces important features of human OA. It is also possible to track the cartilage and subchondral bone changes over time in this animal model. Hence, the low-dose MIA-induced OA rat model was used in this thesis.

Table 1.2 Macroscopic cartilage lesion score on day 30 after injection of saline or various doses of monosodium iodoacetate (MIA) into rat knees (modified from Guingamp et al., 1997)

	Tibial plateaus		Femoral condyles		
Injection	**Medial**	**Lateral**	**Medial**	**Lateral**	**Total**
Saline	0	0	0	0	0.00
MIA (mg)					
0.01	0.44	0.55	0.00	0.00	0.99
0.03	2.11	1.44	1.55	1.33	6.43
0.10	2.67	2.33	2.33	2.67	10.00
0.30	3.56	3.89	4.00	4.00	15.45
3.00	3.89	3.89	3.89	4.00	15.67

1.8 In vivo micro-computed tomography (micro-CT) assessment of bone in rodent models of OA

Small animal models of OA have become invaluable tools in OA related studies. Histological characterisation and quantification of bone and cartilage changes in animal models of OA provides valuable cellular details and dynamic indices of bone remodelling. However, it only gives two-mention (2D) data and it is a destructive technique. On the other hand, micro-CT is an advanced non-destructive imaging technique that provides accurate three-dimension (3D) data and have been used to assess bony changes in small animal models of OA *ex vivo* (Kapadia et al. 1998, Wachsmuth and Engelke 2004).

High-resolution *in vivo* micro-CT (Fig. 1.18) has emerged as a novel non-destructive imaging technique that enables tracking of bone related changes in the same animal over time (Waarsing et al. 2005). Previously *in vivo* micro-CT has been used to track changes in individual bone architecture and trabeculae over time in ovariectomized (OVX) rats (Boyd et al. 2006, Perilli et al. 2010, Waarsing et al. 2004b). The use of *in vivo* micro-CT reduces the number of animals required in an experiment where each animal serves as its own control. Moreover, longitudinal study designs using *in vivo* micro-CT have contributed to pharmacological intervention studies in pre-clinical models. Hence, *in vivo* micro-CT is widely used in imaging small animal models of OA to assess subchondral bone changes (Appleton et al. 2007, Botter et al. 2011, Jones M. D. et al. 2010, McErlain et al. 2008, Morenko et al. 2004).

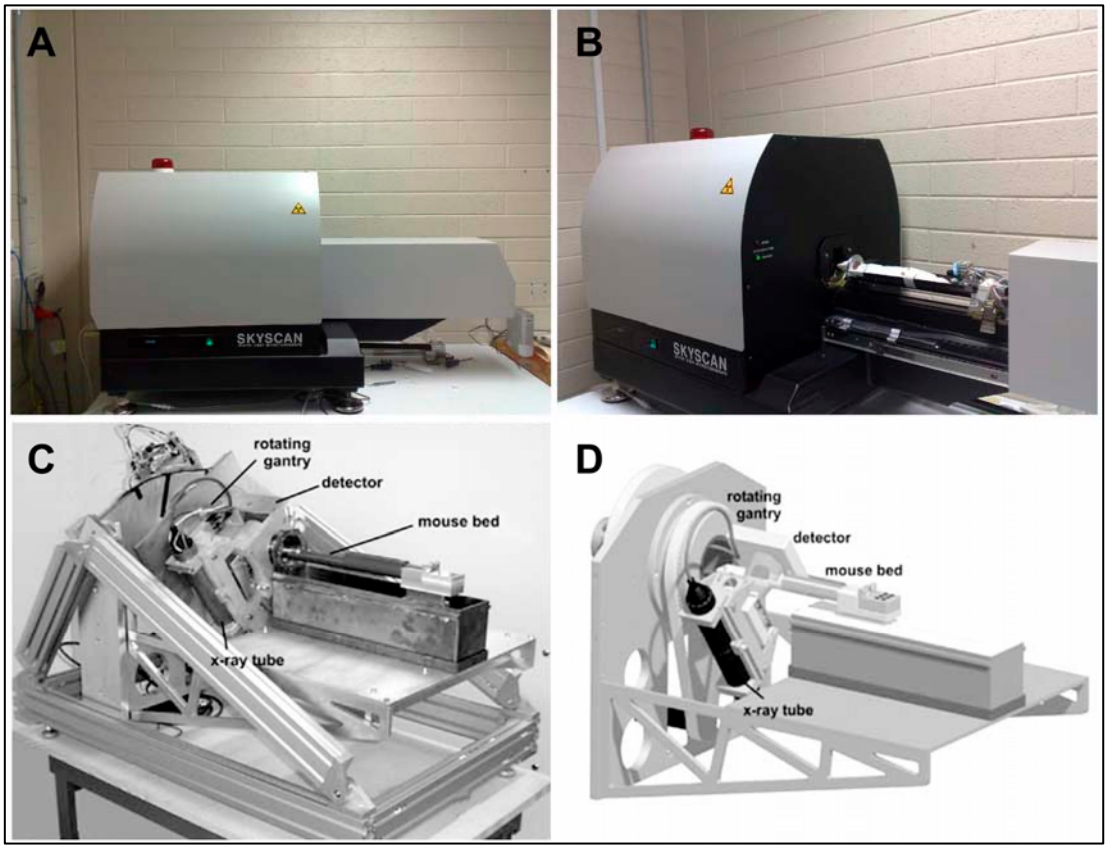

Figure 1.18 High resolution *in vivo* micro-CT scanner for small animal imaging. Skyscan 1076 an *in vivo* scanner for small animal models (A) with a rat in the scanner bed (B). Major components of a typical *in vivo* scanner such as the rotating gantry, detector, x-ray tube and the rodent bed (C, D) (Bartling et al. 2007, with permission from Bentham Science Publishers).

1.8.1 *In vivo* micro-CT imaging of cartilage in rodent models of OA

Apart from detecting bone related changes, *in vivo* micro-CT has also been used to access cartilage changes in small animal models of OA (Piscaer et al. 2008a). *In vivo* micro-CT-arthrography clearly showed glycosaminoglycan depletion and detected cartilage degeneration in the rat OA knee-joints injected with a radio-opaque dye containing ioxaglate complex (Piscaer et al. 2008b, Siebelt et al. 2011a, Siebelt et al. 2011b). However, due to rapid diffusion of the dye out of the joint cavity, the dye did not reach equilibrium state in the cartilage and there was a decrease in attenuation

toward the calcified cartilage. To prevent the rapid diffusion of dye out of the joint cavity, the dye was mixed with epinephrine the effect of which on joint tissues needs to be determined. In a recent study, Piscaer et al. used single-photon–emission computed tomography (SPECT) to indicate macrophage activation. In that study OA was induced in the rat knee joint either using MIA or ACLT followed by an injection with a folate radiotracer for targeting the folate receptor expressed on activated macrophages. SPECT imaging showed peak activity 2 weeks after OA induction, which disappeared after 8 weeks (Piscaer et al. 2011). Thus, recent developments in *in vivo* biomedical imaging including micro-CT and SPECT, show that these imaging modalities have the potential to detect changes in bone, cartilage and cellular activity in small animal models of OA.

1.8.2 Considerations for *in vivo* micro-CT imaging of rodents

Some important factors need to be considered when scanning small animal models using *in vivo* micro-CT scanner such as scan resolution, scan time, radiation exposure, and anaesthesia. Use of inhalation anaesthetics such as isoflurane gives good muscle relaxation, maintains cardiac function and quick recovery from anaesthetic, however prolonged exposure affects normal metabolism of animals (Hildebrandt et al. 2008). Scan resolution, scan time and radiation exposure are related to each other and are the limiting factors in *in vivo* scans. High scan resolution gives high quality images however; it leads to increased scan time and radiation exposure (Wachsmuth and Engelke 2004). A study by Dare et al. showed that a single dose of up to 400 mGy does not induce significant changes in cell growth and differentiation of osteoblast-like cells *in vitro* (Dare et al. 1997). However, effects of sublethal doses due to repeated scanning is very important in longitudinal studies. A study by Klink et al. showed that repeated scanning of mice at 10.5 μm isotropic voxel size lead to a 20% reduction in bone

volume fraction but repeated scanning of aged female Wistar rats at 12.5 μm isotropic voxel size did not induce significant differences between radiated and non-radiated limbs (Klinck et al. 2008). In another study, eight weekly scans of aged female Wistar rats at an isotropic solution of 15 μm for 35 minutes did not have an effect on bone structural parameters and bone marrow cells in tibia (Brouwers et al. 2007). Therefore, scanning protocols should be optimised for small animal imaging to minimise radiation exposure and reduce scan time. The development of *in vivo* micro-CT protocol for the studies included in this thesis has been discussed in detail in appendix 2.

1.9 Research aims

It is estimated that one-third of all adults have radiological signs of OA, the incidence of which increases with age and it the most common cause of knee and hip replacement (Felson et al. 2000). OA mainly affects the knee joint which is mostly associated with chronic pain and it is considered as an organ failure as the whole knee joint is affected. Current treatment options aims at alleviating the pain associated with OA. As outlined in previous sections, a considerable literature exists investigating the molecular and tissue level pathological changes in OA cartilage and subchondral bone. Discovery of early involvement of subchondral bone in the pathology of OA has spurred research activities focussed on subchondral bone adaptations in OA.

Difficulty in obtaining early OA tissue samples has hindered obtaining information regarding early initiating events in OA disease. Moreover, human OA is a slowly progressive disease and it takes a very long time to monitor disease progression from early stage to advanced stages. Although animal models of OA do not completely mimic human OA, they give important clue regarding early pathological changes.

Moreover, recent advancements in micro-CT imaging techniques have enabled researchers to follow OA disease progression in small animal models of OA. Previous studies have characterised changes in subchondral BMD over time in animal models. However, microarchitectural changes in the subchondral have not yet been followed in a suitable animal model that represents progressive human OA.

Human and animal studies have shown increased subchondral bone remodelling in OA. Moreover, bisphosphonates have been shown to slow OA disease progression by inhibiting subchondral bone remodelling while human studies have given mixed results. This is mainly due to the difference in the time of bisphosphonate treatment initiation. The effect of bisphosphonate treatment initiated at different time points on subchondral trabecular microarchitecture needs to be determined.

Several molecular mechanisms have been shown to be differentially regulated in OA. The RANK/RANKL/OPG nexus that controls bone remodelling has recently gained importance as it has been shown to play an important role in OA. Few literature exists regarding RANKL and OPG in OA and very few literature is available on the effect of bisphosphonates on RANKL and OPG in OA. RANK, RANKL and OPG mRNA during the progression of OA and the effects of bisphosphonate treatment on RANK, RANKL and OPG mRNA expression needs to be determined.

1.9.1 Project aims

- Characterise a low-dose MIA-induced OA animal model that represents features of human OA to track the subchondral bone and cartilage changes in the early, intermediate and late stages of OA.
- Investigate the effect of bisphosphonate treatment initiated at different time points on subchondral bone and cartilage in the animal model.
- Characterise the mRNA expression of RANK, RANKL, and OPG at early, intermediate, and late stages of OA in the animal model.
- Investigate the effect of bisphosphonate treatment initiated at different time points on mRNA expression of RANK, RANKL, and OPG.

Chapter 2 is a recently published study which characterised the temporal changes in the subchondral bone architecture in a rat model of low-dose monosodium iodoacetate-induced OA using *in vivo* micro-computed tomography. Chapter 3 includes a study that investigated the pre-emptive, early, and delayed alendronate treatment on subchondral trabecular bone microarchitecture, cartilage and joint discomfort in a rat model of low-dose monosodium iodoacetate induced OA. Chapter 4 includes the study that characterised the mRNA expression of RANK, RANKL, and OPG at early, intermediate, and late stages of OA in a rat model of low-dose monosodium iodoacetate-induced OA. Additionally, that study investigated the effect of bisphosphonate treatment initiated at different time points on mRNA expression of RANK, RANKL, and OPG.

CHAPTER 2

Application of *in vivo* micro-computed tomography in the temporal characterisation of subchondral bone architecture in a rat model of low-dose monosodium iodoacetate induced osteoarthritis

Geetha Mohan, Egon Perilli, Julia S Kuliwaba, Julia M Humphries, Ian H Parkinson and Nicola L Fazzalari

Bone and Joint Research Laboratory, Directorate of Surgical Pathology, SA Pathology and Hanson Institute, Frome Road, Adelaide, SA 5000, Australia

Discipline of Anatomy and Pathology, School of Medical Sciences, The University of Adelaide, Adelaide, SA 5005, Australia

Arthritis Research & Therapy 2011;13(6):R210.

STATEMENT OF AUTHORSHIP

Application of in vivo micro-computed tomography in the temporal characterisation of subchondral bone architecture in a rat model of low-dose monosodium iodoacetate induced osteoarthritis

Arthritis Research & Therapy 2011;13(6):R210.

Geetha Mohan (Candidate)

Performed analysis on all samples, interpreted data, wrote manuscript and acted as corresponding author

Certification that the statement of contribution is accurate

Signed

....Date..21/02/2012..

Egon Perilli

Data interpretation and manuscript evaluation

Certification that the statement of contribution is accurate and permission is given for the inclusion of the paper in the thesis

Signed

....Date.....24/02/2012

Julia S. Kuliwaba

Supervised development of work, helped in data interpretation and manuscript evaluation

I hereby certify that the statement of contribution is accurate and I give permission for the inclusion of the paper in the thesis

Signed

…… ……Date…29/2/12……..

Julia M. Humphries

Data interpretation and manuscript evaluation

Certification that the statement of contribution is accurate and permission is given for the inclusion of the paper in the thesis

Signed

…… ……Date…29.02.12……..

Ian H. Parkinson

Supervised development of work, helped in data interpretation and manuscript evaluation

Certification that the statement of contribution is accurate and permission is given for the inclusion of the paper in the thesis

Signed

…… ……Date…21/3/12……..

Nicola L. Fazzalari

Supervised development of work, helped in data interpretation and manuscript evaluation

I hereby certify that the statement of contribution is accurate and I give permission for the inclusion of the paper in the thesis

Signed

… ……Date…6/3/2012

Mohan et al. Arthritis Research & Therapy 2011, 13:R210
http://arthritis-research.com/content/13/6/R210

arthritis research&therapy

RESEARCH ARTICLE Open Access

Application of *in vivo* micro-computed tomography in the temporal characterisation of subchondral bone architecture in a rat model of low-dose monosodium iodoacetate-induced osteoarthritis

Geetha Mohan[1,2*], Egon Perilli[1,2], Julia S Kuliwaba[1,2], Julia M Humphries[1,2], Ian H Parkinson[1,2] and Nicola L Fazzalari[1,2]

Abstract

Introduction: Osteoarthritis (OA) is a complex, multifactorial joint disease affecting both the cartilage and the subchondral bone. Animal models of OA aid in the understanding of the pathogenesis of OA and testing suitable drugs for OA treatment. In this study we characterized the temporal changes in the tibial subchondral bone architecture in a rat model of low-dose monosodium iodoacetate (MIA)-induced OA using *in vivo* micro-computed tomography (CT).

Methods: Male Wistar rats received a single intra-articular injection of low-dose MIA (0.2 mg) in the right knee joint and sterile saline in the left knee joint. The animals were scanned *in vivo* by micro-CT at two, six, and ten weeks post-injection, analogous to early, intermediate, and advanced stages of OA, to assess architectural changes in the tibial subchondral bone. The articular cartilage changes in the tibiae were assessed macroscopically and histologically at ten weeks post-injection.

Results: Interestingly, tibiae of the MIA-injected knees showed significant bone loss at two weeks, followed by increased trabecular thickness and separation at six and ten weeks. The trabecular number was decreased at all time points compared to control tibiae. The tibial subchondral plate thickness of the MIA-injected knee was increased at two and six weeks and the plate porosity was increased at all time points compared to control. At ten weeks, histology revealed loss of proteoglycans, chondrocyte necrosis, chondrocyte clusters, cartilage fibrillation, and delamination in the MIA-injected tibiae, whereas the control tibiae showed no changes. Micro-CT images and histology showed the presence of subchondral bone sclerosis, cysts, and osteophytes.

Conclusions: These findings demonstrate that the low-dose MIA rat model closely mimics the pathological features of progressive human OA. The low-dose MIA rat model is therefore suitable to study the effect of therapeutic drugs on cartilage and bone in a non-trauma model of OA. *In vivo* micro-CT is a non-destructive imaging technique that can track structural changes in the tibial subchondral bone in this animal model, and could also be used to track changes in bone in preclinical drug intervention studies for OA treatments.

* Correspondence: geetha.mohan@health.sa.gov.au
[1]Bone and Joint Research Laboratory, Directorate of Surgical Pathology, SA Pathology and Hanson Institute, Frome Road, Adelaide, SA 5000, Australia
Full list of author information is available at the end of the article

Introduction

Osteoarthritis (OA) is generally a slow progressive joint disease characterized by loss of articular cartilage, subchondral bone sclerosis, cysts, and osteophyte formation [1]. The etiopathology of OA remains obscure and currently there are no pharmacological interventions available to halt or reverse the progression of OA. Animal models of OA are of considerable importance as they are not only useful to study the pathogenesis and progression of OA, but also to evaluate suitable therapeutic drugs for OA treatment. Moreover, knowledge of early pathological changes is essential for early treatment options and to develop better therapeutic agents to modify the disease progression.

The monosodium iodoacetate (MIA)-induced OA rat model is a minimally invasive animal model that reproduces cartilage and bone pathology similar to human OA [2]. The onset, progression and severity of OA can be easily controlled in this model by changing the dose of MIA, which makes it useful to study disease progression and the effect of disease modifying osteoarthritis drugs (DMOAD). A dose response study by Guingamp *et al.* showed that the severity of cartilage degradation depends on the dosage of MIA injected into the knee joint. Higher doses of MIA (up to 3 mg) caused cartilage erosion, sclerosis and exposure of subchondral bone on day 15 post MIA injection, and on day 30 there was complete loss of articular cartilage, with greatly remodelled subchondral bone [3], whereas, a low-dose of MIA (0.25 mg) induced moderate cartilage damage at 3 weeks [4]. In a pilot study, we evaluated the dose responsiveness of tibial cartilage and subchondral bone to MIA using a high-dose of 2 mg MIA (n = 3) and a low-dose of 0.2 mg MIA (n = 3) in rats. As early as after two weeks, high-dose MIA induced characteristic features of end-stage human OA such as loss of tibial articular cartilage, exposure of subchondral bone, subchondral trabecular bone erosion, cysts and osteophytes. In contrast, these changes were observed only at ten weeks in the low-dose MIA model (Mohan G *et al*: unpublished observations). The low-dose MIA model, of relatively slow progressing OA, enables *in vivo* monitoring of tissue-level changes representative of progressive human OA; whereas, in the high-dose model the disease progression is very rapid, which is less suitable for longitudinal monitoring of cartilage and subchondral bone changes.

The tissue-level characterization of animal models of OA has traditionally been done by histological assessment. Developments in X-ray micro-computed tomography (micro-CT) allow *in vivo* imaging of small animal models, with high spatial resolution and at subsequent time points, to study bone architecture [5-7]. This imaging technique enables non-destructive assessment of the bone both quantitatively and qualitatively. Moreover, the use of a longitudinal study design using *in vivo* micro-CT allows the quantification of subchondral bone in the same animal over time. Recent studies have used micro-CT to quantify structural changes in the tibial subchondral bone in the MIA rat model; however, those studies have utilized high-dose MIA injections, with the rats examined only at the end point of the studies [8-10]. The temporal changes in the structure of subchondral trabecular bone during the progression of OA in the low-dose MIA model have not been previously described.

The purpose of this study was to characterize the structural changes in the tibial subchondral bone using longitudinal *in vivo* micro-CT imaging in an animal model that closely mimics human progressive OA. It is hypothesised that low-dose MIA will induce cartilage changes and measurable, progressive tibial subchondral bone changes at two, six, and ten weeks post-injection.

Materials and methods

Animals and OA induction

Twelve 8-week-old male Wistar rats (Animal Resource Center, Canning Vale, WA, Australia), weighing 200 - 230 g at the start of the experiment, were used. They were kept in a sanitary ventilated animal room with controlled temperature (20 to 24°C), a light-dark cycle (12 hour/12 hour) and were fed standard laboratory rodent chow (Specialty Feeds, Glen Forrest, WA, Australia) with water available *ad libitum*. The rats were acclimatized for one week before the start of the experiment. They were closely monitored and daily clinical record sheets were completed throughout the duration of the study by the animal care facility staff.

On day 0, the rats were anesthetized with an isoflurane/O_2 mixture and both their knees were shaved and disinfected with 70% alcohol. Each rat was given a single intra-articular injection of 0.2 mg MIA through the infrapatellar ligament of the right knee. MIA was dissolved in sterile physiologic saline and administered in a volume of 50 μl using a 26-gauge 0.5-inch needle. The left contralateral control knee was injected with 50 μl of sterile physiologic saline.

The hind limbs of all the rats were imaged with high-resolution *in vivo* micro-CT at two, six, and ten weeks post-MIA injection, which represent early, intermediate, and advanced stages of OA. Double-fluorescent labelling of newly formed bone was achieved by using calcein (5 mg/kg body weight; Sigma-Aldrich, Sydney, NSW, Australia) administered intraperitoneally on day 7 before sacrifice, followed by xylenol orange (90 mg/kg body weight; Sigma-Aldrich, Australia) administered

intraperitoneally 2 days before sacrifice. The animal handling and experimental procedures outlined in this study were carried out in accordance with The University of Adelaide Animal Ethics Committee and The Institute of Medical and Veterinary Science Animal Ethics Committee.

In vivo micro-CT imaging

In vivo micro-CT imaging was performed using a bench-top cone-beam type *in vivo* animal scanner (Skyscan model 1076, Skyscan, Kontich, Belgium) [6]. Each rat was anesthetized with isofluroane/O_2 and placed in the scanner bed in a supine position (Figure 1). The MIA-injected knees and the contralateral control knees were scanned separately. During each scan only the knee for image data acquisition was irradiated, while the contralateral limb and the rest of the body were lead-shielded from radiation. The hind limb of the rat was secured into a customized leg fixative device consisting of a cylindrical plastic holder fitted to a polystyrene tube. This allowed positioning of the hind limb close to the central scanner axis, preventing any movement of the limb during scanning. The total scan time for each limb was 20 minutes during which the rat was under anesthesia. The scans were performed using the following scanner settings: X-ray source voltage 60 kVp, current 100 μA, a 1-mm thick aluminum filter to reduce beam-hardening artefact, 1 frame averaging. The pixel size was 8.7 μm, the exposure time was 4.7 seconds, and the rotation step was 0.8°, with a complete rotation over 197° [6]. The cross-sectional images were reconstructed using a filtered back-projection algorithm (NRecon, V 1.4.4, Skyscan, Kontich, Belgium). For each scan, a stack of 1,800 cross-sections was reconstructed, centered over the knee-joint (total reconstructed height about 16 mm), with an interslice distance of 1 pixel (8.7 μm). The reconstructed images were of 1,500 × 1,500 pixels each, 8.7 μm pixel size, and were stored as 8-bit images (256 grey levels) [6].

Bone histomorphometric analysis

Subchondral trabecular bone

On the stack of the reconstructed micro-CT cross-section images, manual regions of interest (ROI) of an irregular anatomical contour were drawn in the subchondral trabecular bone region for the medial and lateral tibial plateau (Figure 2), for both the MIA-injected knee and the control knee (software CT Analyser, V 1.8.05, Skyscan, Kontich, Belgium). The volume of interest (VOI) consisted of a stack of ROIs drawn over 52 cross-sections, resulting in a height of 0.45 mm. The VOI included the subchondral trabecular bone starting below the subchondral plate, and extending distally towards the growth plate, excluding both the cortical bone and growth plate interface. The VOI used was of the same size and shape for all the three time points (two, six and ten weeks), for both the control and the MIA-injected tibia. For the calculation of the morphometric parameters, the images were segmented using a uniform threshold as described in a previously published paper [6]. The following three-dimensional (3D) morphometric parameters were calculated for the medial VOI, the lateral VOI and the total (= medial + lateral) VOI of subchondral trabecular bone (software CT Analyzer, Skyscan): bone volume (BV, mm^3), bone volume fraction (BV/TV, %), trabecular thickness (Tb.Th, μm),

Figure 1 *In vivo* micro-CT imaging of a rat hind limb; anaesthetized rat on the scanner bed in supine position, with the hind limb secured in a customised leg fixative device (inset). Micro-CT, micro-computed tomography.

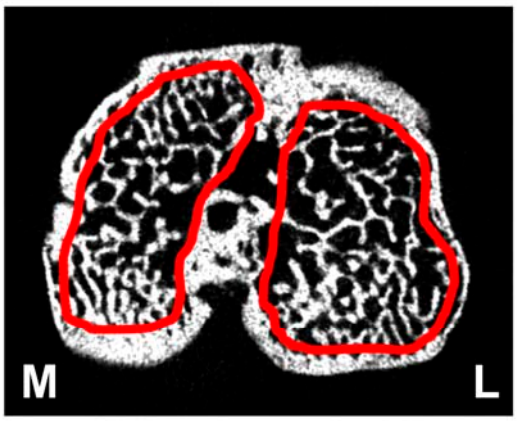

Figure 2 Axial micro-CT image of a rat tibia, with the region of interest (solid red line) in the medial (M) and lateral (L) subchondral bone compartment. Micro-CT, micro-computed tomography.

trabecular separation (Tb.Sp, μm) and trabecular number (Tb.N, 1/mm). BV is the volume in 3D of the structure segmented as bone, and BV/TV is the ratio of the segmented bone volume to the total volume of the region of interest. Tb.Th is the mean thickness of the trabeculae, Tb.Sp is the mean distance between trabeculae, Tb.N is the average number of trabeculae present per unit length. Tb.Th and Tb.Sp were assessed using direct 3D methods, Tb.N was calculated using the formula Tb.N = (BV/TV)/Tb.Th [6,11,12].

Subchondral plate

In the binarized images, the subchondral plate was separated from the trabecular bone of the tibia by using a software kindly provided by Botter *et al.* [13]. The 3D subchondral plate thickness (Pl.Th, μm) and porosity (volume of the pores in the plate over the total volume of the plate, Pl.Por, %) of the medial and lateral compartments of the tibial subchondral plate were calculated on regions measuring 1.5 mm medio-lateral in width, 2.5 mm in length from the posterior side. For both parameters (Pl.Th and Pl.Por), the data from the medial and lateral compartments were averaged to obtain the value of the total compartment [13].

Macroscopic analysis

At ten weeks post-MIA injection the rats were euthanized with a CO_2 overdose and both the right and left tibiae were dissected for macroscopic study. Soft tissues surrounding the tibia were carefully removed to prevent articular cartilage damage. The image of the tibial cartilage was recorded using a fluorescence stereomicroscope (SZX 10, Olympus). With the microscope, the fluorochrome labels calcein and xylenol orange were imaged and recorded. The macroscopic lesions were graded as follows: 0 = normal appearance, 1 = slight yellowish discoloration of the chondral surface, 2 = little cartilage erosions in load-bearing areas, 3 = large erosions extending down to the subchondral bone, and 4 = large erosion with large areas of subchondral bone exposure [3]. Two blinded observers graded the medial and lateral tibial plateaus separately. The scores for the tibiae were combined and the average values were determined for the MIA-injected knee and the control knee.

Histological analysis

After imaging, the tibiae (n = 6 rats; tibiae from the other 6 rats were used in another analysis) were fixed in 4% paraformaldehyde, decalcified and embedded in paraffin. Three coronal sections (5 μm thick) 100 μm apart were obtained and stained with 1.5% Safranin O, and 0.02% fast green counter stain. The sections were observed for OA-like features such as surface discontinuity, loss of proteoglycans, disorientation of chondrocytes, subchondral bone sclerosis and presence of cysts and osteophytes.

The Osteoarthritis Research Society International (OARSI) scoring method [14] was used to grade and stage tibial cartilage in the MIA-injected knee and control knee. For each histological slide, the OA score was obtained by multiplying the grade and stage values. The OA score ranges from 0 (representing no OA activity) to 24 (highest OA degradation).

Serum C-reactive protein (CRP) analysis

Blood samples were obtained by tail venipunture from the MIA-injected rats (n = 6) and a group of age-matched control rats (n = 4, from another non-micro-CT imaging study) under isofluroane anaesthesia. Blood samples were obtained from the rats at pre-injection, two, six, and ten week time points. Serum samples were collected and stored at -80°C until analyzed. Serum levels of CRP, a marker of systemic inflammation, were measured by enzyme-linked immunosorbent assay according to the manufacturer's protocol (Rat CRP ELISA kit, BD Biosciences, San Diego, CA, USA).

Statistical analysis

The morphometric parameters had a normal distribution (Shapiro-Wilk test, $P > 0.05$ for all the examined parameters). For each morphometric parameter it was determined whether there was (a) a 'time effect' and (b) a 'time by group interaction effect'. The 'time effect' indicates if there was any change over time within each group (tibia of control and MIA-injected knee) and the 'time by group interaction effect' indicates if the different groups showed different patterns of changes over time. For each tibia, 3D morphometric parameters and serum CRP data sets were examined using analysis of variance for repeated measures (two-way repeated measures ANOVA). If F-values for a given variable were found to be significant, a paired Student's t-test was applied to assess the changes in the morphometric parameters and CRP between the MIA-injected knee and control knee. The P-values were adjusted for repeated comparisons by Holm's Bonferroni stepdown procedure [15]. Similarly, a paired Student's t-test with P-values adjusted for repeated comparison by Holm's Bonferroni stepdown procedure was done to assess changes in each tibia between time points. The overall type I error rate was set at an alpha level of 0.05.

Results

Micro-CT

Bone histomorphometric changes

The 'time effect' was significant for all the parameters. The 'time by group interaction effect' was significant for

BV, BV/TV, Tb.Th, Pl.Th and Pl.Por. There was a significant increase in total BV, BV/TV, Tb.Th, Tb.N, and Pl.Th. in the tibial subchondral bone of both the MIA-injected knee and the control knee over time ($P < 0.05$, Figure 3). This was due to the natural growth of the animal. The total Tb.Sp of both the control tibia and the tibia of the MIA-injected knee were significantly decreased at ten weeks compared to two weeks ($P < 0.001$, Figure 3).

Subchondral trabecular bone

Table 1 shows the summarized data and comparison of the tibial subchondral trabecular bone microarchitectural parameters of the MIA-injected knee and the control knee at two, six, and ten weeks post-MIA injection. At two weeks there was a significant decrease in BV and BV/TV in the MIA-injected tibia compared to the control tibia, in both the medial and the total compartments (-18% and -14%, respectively, $P < 0.05$ for both parameters). However, at six and at ten weeks post-MIA injection, although not statistically significant, there was an increase in tibial subchondral trabecular BV and BV/TV in the MIA-injected knee compared to the control knee, particularly in the medial compartments (19% for BV and BV/TV at 6 weeks and 26%, 19%, for BV and BV/TV at 10 weeks, respectively).

At two weeks, no statistically significant difference was observed in Tb.Th in all the three tibial compartments between the MIA-injected knee and control. However, at six and ten weeks, there was a significant increase in Tb.Th in the MIA-injected knee compared to the control knee in the medial (25%, $P < 0.001$, and 35%, $P < 0.01$, respectively), lateral (23%, $P < 0.01$, and 22%, $P < 0.05$, respectively) and total (24%, $P < 0.001$, and 29%, $P < 0.01$, respectively) tibial compartments. The Tb.N was significantly lower in the MIA-injected knee compared to the control knee in all the three tibial compartments at two weeks and in the lateral and total compartments at ten weeks post-MIA injection. At 2 weeks, the Tb.N was reduced by 20% ($P < 0.01$), 12% ($P < 0.05$), and 16% ($P < 0.01$) in the medial, lateral and total compartments, respectively. At six weeks, the Tb.N did not differ significantly between the tibia of the MIA-injected knee and control knee. At 10 weeks, the Tb.N was decreased by 14%, 16% ($P < 0.01$) and 15% ($P < 0.05$) in the medial, lateral and total compartments, respectively, when compared to the control knee. The Tb.Sp in the MIA-injected knee was significantly higher than in the control knee at all the three time points, in all the three tibial compartments. At 2 weeks, the Tb.Sp of the MIA-injected knee was increased by 11% ($P < 0.001$), 6% ($P < 0.01$) and 8% ($P < 0.001$) in the medial, lateral and total compartments, compared to control. Similarly, at 6 weeks, in the MIA-injected knee there was an increase of 18%, 13% and 16% ($P < 0.01$ for all compartments), respectively, and at 10 weeks there was an increase of 16% ($P < 0.01$), 16% ($P < 0.001$) and 14% ($P < 0.01$), in the medial, lateral and total compartments, respectively, compared to control.

Subchondral plate

The tibial subchondral plate thickness of the MIA-injected knee increased significantly at two weeks ($P < 0.01$ for medial compartment) and six weeks ($P < 0.01$ for both medial and total compartments) post injection compared to the control knee. At ten weeks there was no significant difference in thickness (medial, lateral or total) between the MIA-injected knee and the control knee (Table 2). The porosity of the tibial subchondral plate was significantly increased in the MIA-injected knee compared to the control knee at all time points in all the three compartments analyzed ($P < 0.01$).

Qualitative subchondral bone changes

All the rats showed pathological subchondral bone changes in the MIA-injected knee, whereas the contralateral control knee showed no OA-like changes in the tibial subchondral bone microarchitecture throughout the study duration (ten weeks). Morphologic evaluation of the MIA-injected knee over time showed sclerosis in the tibial subchondral bone at six and ten weeks after MIA injection, particularly in the medial tibial condyle (Figure 4). At six and ten weeks, the tibial subchondral plate of the MIA-injected knee was breached in focal areas, these breaches were confirmed by histology (Figure 5A, B). From the micro-CT images, in 8 out of 12 rats (67%), empty spaces were observed in the medial tibial subchondral bone of the MIA-injected knee at 6 and 10 weeks. These empty spaces were confirmed as cysts from the histology sections (Figure 5C, D). Marginal osteophytes were observed in all the rats at six and ten weeks from the micro-CT images and these osteophytes were confirmed by histology (Figure 6). Three-dimensional surface rendering of the MIA-injected knee showed erosion and pitting of the tibial subchondral plate, which was more severe in the medial tibial plateau, whereas the control knee maintained the subchondral plate integrity (Figure 7).

Macroscopy

All the rats developed cartilage lesions in the tibia of MIA-injected knees. At ten weeks, the tibial cartilage of the MIA-injected knee showed focal lesions with yellow discoloration indicating cartilage degradation (Figure 8A, D). This was more prominent in the central region of the medial tibial plateau, whereas cartilage degradation remained at a moderate stage on the lateral side, giving a total joint grade of 3.16 ± 0.75 (mean ± SD). Macroscopically, the control tibia showed no cartilage lesions in the medial and lateral tibial plateau (joint grade 0). Significant calcein and xylenol orange labels

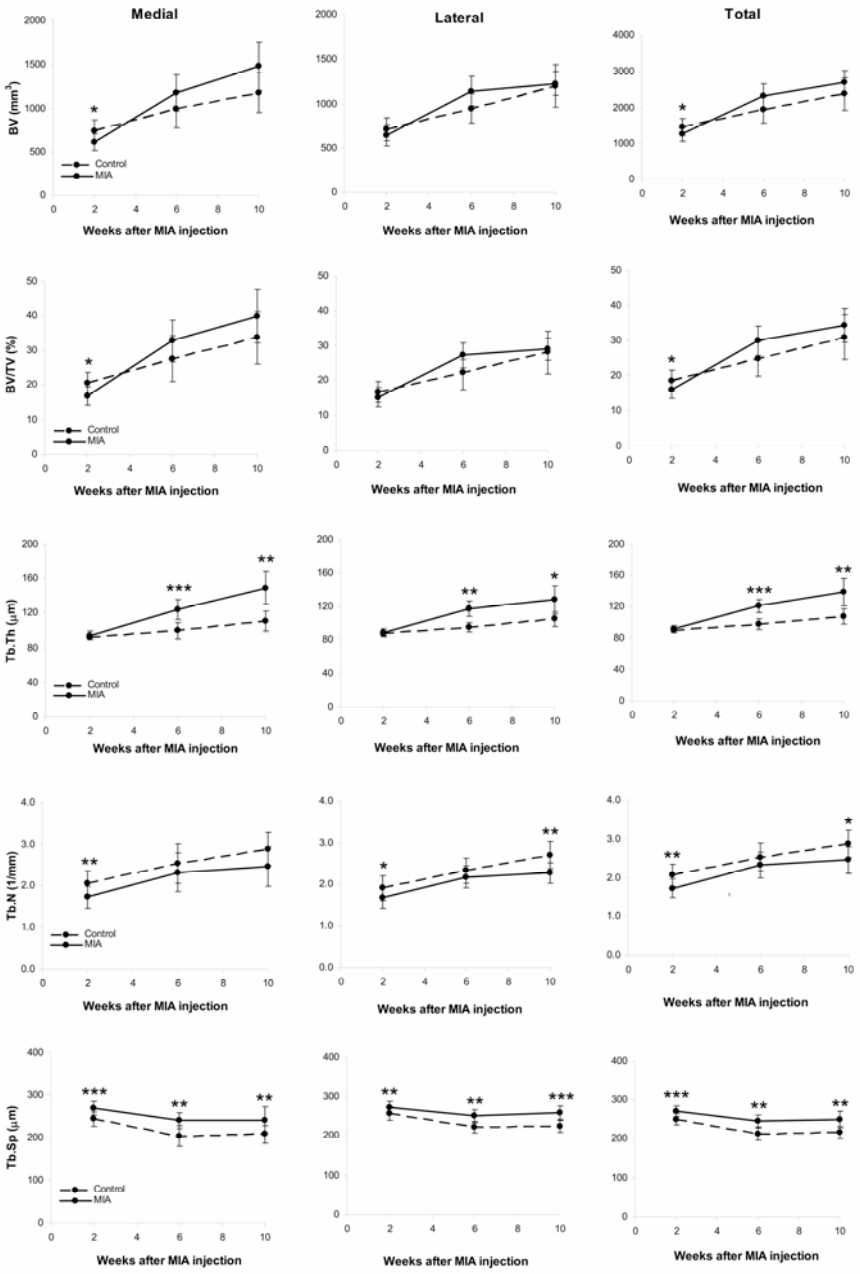

Figure 3 Plots of morphometric parameters of subchondral trabecular bone determined by micro-CT in the control tibiae and in the MIA-injected tibiae, at two, six, and ten weeks post-MIA injection. There was a statistically significant increase over time in BV, BV/TV, Tb.Th, and Tb.N, and a decrease in Tb.Sp, in both the control and MIA-injected tibiae. Error bars = SD. BV, bone volume; BV/TV, bone volume fraction; CT, computed tomography; MIA, monosodium iodoacetate; TB.N, trabecular number; Tb.Sp, trabecular separation; Tb.Th, trabecular thickness. * $P < 0.05$, ** $P < 0.01$, *** $P < 0.001$, between control tibiae and MIA-injected tibiae.

Table 1 Morphometric parameters of tibial subchondral trabecular bone in the MIA-injected tibiae and in the control tibiae, at 2, 6, and 10 weeks post-MIA injection

	2 Weeks				6 Weeks				10 Weeks			
	OA Mean ± SD	Control Mean ± SD	%d OA-CTL	p-value	OA Mean ± SD	Control Mean ± SD	%d OA-CTL	p-value	OA Mean ± SD	Control Mean ± SD	%d OA-CTL	p-value
BV (mm^3)												
Medial	613 ± 97	745 ± 118	-17.8	0.018	1177 ± 211	993 ± 214	18.6	0.102	1481 ± 271	1179 ± 229	25.6	0.102
Lateral	647 ± 120	711 ± 130	-9.0	0.116	1145 ± 168	948 ± 169	20.7	0.116	1229 ± 133	1205 ± 241	2.0	0.709
Total	1260 ± 202	1456 ± 239	-13.5	0.048	2322 ± 341	1941 ± 370	19.7	0.098	2710 ± 326	2384 ± 454	13.7	0.116
BV/TV (%)												
Medial	16.8 ± 2.6	20.4 ± 3.2	-18.0	0.018	32.7 ± 6.5	27.5 ± 6.6	19.1	0.156	39.8 ± 7.7	33.6 ± 7.6	18.5	0.156
Lateral	15.1 ± 2.8	16.7 ± 3.0	-9.1	0.156	27.2 ± 3.6	22.2 ± 3.8	22.5	0.156	29.0 ± 3.2	28.2 ± 6.0	3.0	0.592
Total	15.9 ± 2.5	18.6 ± 3.0	-14.0	0.032	30.0 ± 4.2	24.8 ± 5.0	20.6	0.154	34.4 ± 4.8	30.9 ± 6.4	11.5	0.156
Tb.Th (μm)												
Medial	94 ± 5	92 ± 3	2.1	0.396	124 ± 11	100 ± 9	24.6	p < 0.001	149 ± 19	110 ± 12	34.9	0.001
Lateral	89 ± 4	87 ± 3	1.6	0.360	117 ± 9	95 ± 5	23.1	0.001	128 ± 17	105 ± 8	22.0	0.012
Total	91 ± 4	90 ± 3	1.9	0.396	120 ± 9	97 ± 7	23.9	p < 0.001	138 ± 18	108 ± 10	28.6	0.002
Tb.N (1/mm)												
Medial	1.8 ± 0.3	2.2 ± 0.3	-19.9	0.009	2.5 ± 0.5	2.7 ± 0.5	-9.5	0.405	2.6 ± 0.5	3.1 ± 0.4	-13.7	0.112
Lateral	1.7 ± 0.3	1.9 ± 0.3	-12.2	0.020	2.2 ± 0.3	2.3 ± 0.3	-6.8	0.405	2.3 ± 0.3	2.7 ± 0.3	-16.0	0.009
Total	1.7 ± 0.2	2.1 ± 0.3	-16.3	0.009	2.3 ± 0.3	2.5 ± 0.4	-8.3	0.405	2.5 ± 0.3	2.9 ± 0.4	-14.8	0.012
Tb.Sp (μm)												
Medial	270 ± 16	243 ± 17	10.8	p < 0.001	240 ± 19	203 ± 24	17.9	0.002	241 ± 32	207 ± 20	16.3	0.005
Lateral	272 ± 16	256 ± 17	6.2	0.001	250 ± 16	221 ± 14	13.2	0.001	258 ± 17	223 ± 15	15.7	p < 0.001
Total	271 ± 13	250 ± 14	8.4	p < 0.001	245 ± 15	212 ± 16	15.5	0.001	245 ± 22	215 ± 15	13.8	0.001

Data represented as mean ± SD, % d is the percentage difference in values for tibial subchondral bone between the control and MIA-injected knee. BV, bone volume; BV/TV, bone volume fraction; MIA, monosodium iodoacetate; OA, osteoarthritis; OA-CTL, osteoarthritis control; SD, standard deviation; Tb.N, trabecular number; Tb.Sp, trabecular separation; Tb.Th, trabecular thickness.

Table 2 Tibial subchondral plate thickness and porosity of the MIA-injected knee and control knee, at 2, 6, and 10 weeks post-MIA injection.

	Subchondral Plate Thickness, Pl.Th (μm)									Subchondral Plate Porosity, Pl.Por (%)					
	Medial			Lateral			Total			Medial		Lateral		Total	
	OA	Control	p-value	OA	Control	p-value	OA	Control	p-value	% d OA - CTL	p-value	% d OA - CTL	p-value	% d OA - CTL	p-value
2 weeks	114 ± 7	105 ± 7	0.027	101 ± 6	109 ± 7	0.305	107 ± 4	107 ± 8	0.770	23	0.004	24	0.004	24	0.003
6 weeks	146 ± 32	119 ± 32	0.024	130 ± 17	120 ± 26	0.880	138 ± 23	118 ± 26	0.028	63	0.001	69	p < 0.001	66	p < 0.001
10 weeks	181 ± 27	175 ± 31	0.520	166 ± 18	178 ± 24	0.318	177 ± 19	177 ± 25	0.473	66	0.004	77	0.004	71	0.003

Data represented as mean ± SD for plate thickness, % d is the percentage difference in plate porosity between the control and MIA-injected knee. MIA, monosodium iodoacetate; OA, osteoarthritis; OA-CTL, osteoarthritis control; SD, standard deviation

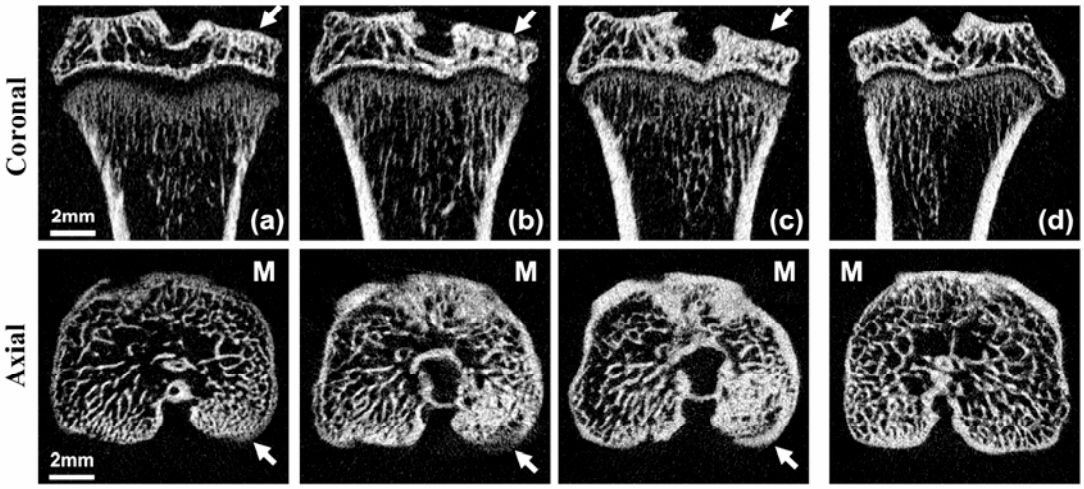

Figure 4 Coronal and axial micro-CT images of an MIA-injected tibia at two weeks (a), six weeks (b) and ten weeks (c) post injection, together with a control tibia at ten weeks (d). The MIA-injected tibia showed altered subchondral bone architecture, with sclerosis on the medial tibial compartment (M) (indicated by arrow) at six and ten weeks after injection, whereas the control tibia showed no sclerosis at ten weeks. Micro-CT, micro-computed tomography; MIA, monosodium iodoacetate.

were detected on the subchondral bone and along the margins of the tibial plateau of the MIA-injected knee (Figure 8E, F), indicating active bone formation, whereas no such accumulation of fluorochrome labels was detected in the control tibial plateau (Figure 8B, C).

Histology

All the rats showed articular cartilage degradation in the tibia of the MIA-injected knee. The contralateral control tibia had a smooth cartilage surface with evenly distributed chondrocytes, well-oriented and arranged in well-ordered zones (Figure 9A). In the MIA-injected knee, the severity of cartilage damage increased from the posterior margin towards the center of the tibial plateau. Proteoglycan loss was observed with Safranin O, and showed greatly reduced cartilage staining in the center of the tibial plateau. In the areas less affected by cartilage degradation there was partial cartilage damage. The superficial layer was devoid of viable chondrocytes, and disorganized chondrocyte clusters (chondrone) of variable size were observed. There appeared to be proliferation of chondrocytes at the mid and deep cartilage zones that extended into the subchondral bone area (Figure 9B). Vertical fissures were observed at the superficial cartilage zone that extended into the cartilage mid and deep zone (Figure 9C). Coronal sections of the tibial plateau showed cartilage fibrillation and delamination (Figure 9D). These osteoarthritic changes were observed in the medial tibial plateau, whereas the lateral tibial plateau showed relatively mild cartilage changes. The OARSI score of the medial tibial plateau in the MIA-injected knee at 10 weeks was 17 ± 3 (mean ± SD). The control tibia showed no OA activity (OARSI score 0).

In the MIA-injected knee, the subchondral bone was sclerosed and exposed in the medial tibial plateau beneath the areas of cartilage damage. Focally extensive areas of subchondral bone marrow were replaced by loosely arranged spindle cells (fibrotic bone marrow) (Figure 9D). At six and ten weeks, the subchondral plate was breached in focal areas, with cartilage damage and proliferating chondrocytes at ten weeks suggesting fibrocartilage repair (Figure 5B). In four out of six rats, subchondral bone cysts were observed below the articular surface. These cysts were present in the sites of severe bone resorption causing bone marrow lesions. The subchondral bone cysts were surrounded by sclerotic bone with fibrous tissue often containing debris of necrotic bone trabeculae. Some trabeculae adjacent to the sites of bone resorption were lined by a row of large reactive osteoblasts (Figure 5D). Marginal tibial osteophytes were observed in all the rats at ten weeks post-MIA injection of the knee. Bone marrow spaces filled with fibrous cells were observed in these osteophytes (Figure 6D).

Serum CRP levels

The serum CRP levels were not significantly different between the MIA-injected rats and control rats at any time-point. In addition, there was no significant difference between time points for each of the two groups. In the MIA-injected rats, the mean ± SD concentrations

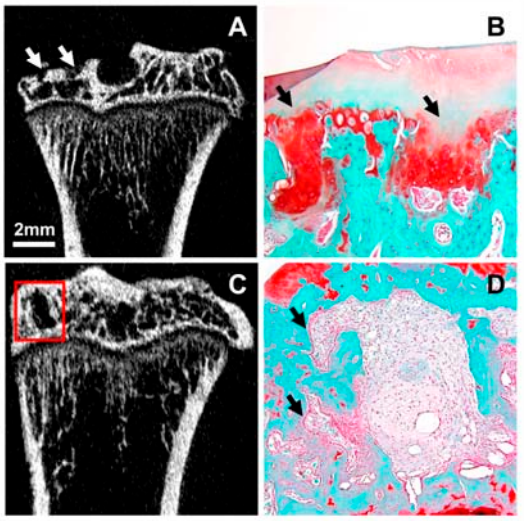

Figure 5 Coronal micro-CT image (A) and histology section (B) of tibia from an MIA-injected knee, showing subchondral plate breach by the activated chondrocytes as a result of abnormal repair, as indicated by arrows (A, B). Micro-CT image revealed the presence of focal subchondral bone lesions in the medial tibial plateau **(C)** at ten weeks post injection (rectangle). The safranin O and fast green stained section of the MIA-injected knee at ten weeks post injection **(D)** confirmed the presence of subchondral bone cyst in the areas of bone lesions as predicted by micro-CT image. The cysts were found to be surrounded by sclerotic bone with fibrous tissue containing debris of necrotic bone. Note the presence of large active osteoblasts (arrow) lining the trabeculae adjacent to the sites of bone resorption. Original magnification × 100. Micro-CT, micro-computed tomography; MIA, monosodium iodoacetate.

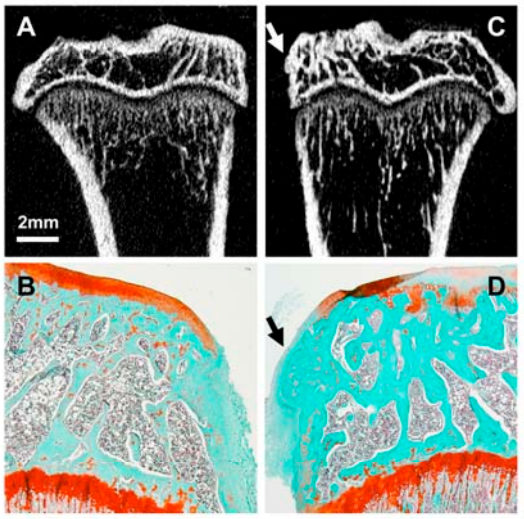

Figure 6 Micro-CT coronal images of tibia from a control knee (A) and a MIA-injected knee (C) at ten weeks post injection. Micro-CT images revealed the presence of marginal tibial osteophytes in all the rats in the MIA-injected knee (C, arrow), whereas the control knee injected with saline showed no osteophyte-like structure formation (A). The normal control tibia **(B)** and the marginal tibial osteophytes in the MIA-injected knee (**D**, arrow) were confirmed by histology at ten weeks post injection. The osteophytes contained marrow spaces filled with fibrous bone marrow cells. Original magnification × 40. Micro-CT, micro-computed tomography; MIA, monosodium iodoacetate.

were as follows: 204 ± 32 μg/ml, 201 ± 44 μg/ml, 190 ± 50 μg/ml, and 202 ± 7 μg/ml at pre-injection, 2, 6 and 10 weeks, respectively. For the control group the mean ± SD concentrations were as follows: 172 ± 42 μg/ml, 186 ± 24 μg/ml, 181 ± 34 μg/ml, and 212 ± 9 μg/ml at pre-injection, 2, 6 and 10 weeks, respectively.

Discussion

This study characterized the temporal changes in the tibial subchondral bone architecture in a low-dose MIA-induced OA rat model using *in vivo* micro-CT. The strength of this study is the use of a longitudinal study design, which enabled the quantitative and qualitative assessment of OA-related changes in the tibial subchondral trabecular bone within the same animal over time. This is the first *in vivo* study to examine subchondral trabecular bone changes over time revealing a significantly lower bone volume fraction at two weeks, followed by subchondral bone sclerosis at six and ten weeks, in the low-dose MIA-induced OA rat model.

The initial bone loss observed at two weeks, followed by sclerosis during the progression of OA is consistent with findings in other animal models of OA, such as the anterior cruciate ligament transection (ACLT) in rats [16], the canine model [17] and the collagenase-induced murine model, and to human OA [18]. This initial bone loss observed at two weeks in the low-dose MIA rat model could have been due to transient unloading of the MIA-injected knee. Previously, it had been shown that MIA injection in the rat knee joint leads to concentration related transient changes in hind paw weight distribution [3,19]. In the MIA-injected knee, Tb.N was decreased and Tb.Sp was increased relative to the control tibia at all time points, which suggests an active process of subchondral trabecular bone erosion. Together with the increases in Tb.Th found at weeks six and ten, these findings indicate that subsequent increased bone formation in the MIA-injected knee resulted from subchondral trabecular bone thickening. This strongly suggests a mechanism for bone remodelling/modelling in the subchondral trabecular bone in OA [20].

It should also be noted that over time the tibial subchondral BV, BV/TV, Tb.Th, Tb.N and Pl.Th increased,

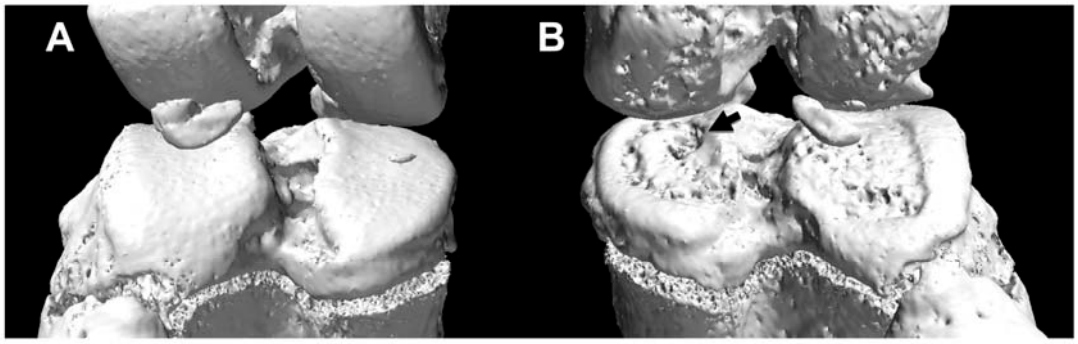

Figure 7 Three-dimensional surface rendering obtained from micro-CT images of a control knee (A) and of a MIA-injected knee (B) at ten weeks after injection. The control knee maintained the subchondral plate integrity with a smooth contour (A). The MIA-injected knee showed erosion and pitting of the tibial subchondral plate, which was more severe in the medial tibial plateau, as indicated by arrow (B). Micro-CT, micro-computed tomography; MIA, monosodium iodoacetate.

whereas the Tb.Sp decreased, in both the MIA-injected knee and the control knee (Figure 3). This is in part due to the normal growth of the rats at baseline, reaching skeletal maturity. Similar age-related changes (increases) in volumetric bone mineral density (vBMD) due to the effect of normal animal growth have been reported in the high-dose MIA rat model [21] and ACLT model [22]. However, in our study the use of the contralateral tibia as an internal control eliminates inter-animal variability for age-related changes and weight.

Pathologic subchondral plate changes are recognized as a characteristic feature of OA. Previous studies have looked at the subchondral plate changes in animal models of OA such as dogs, mice, cynomolgus macaques, guinea pigs, and rabbits but not in rat models of OA.

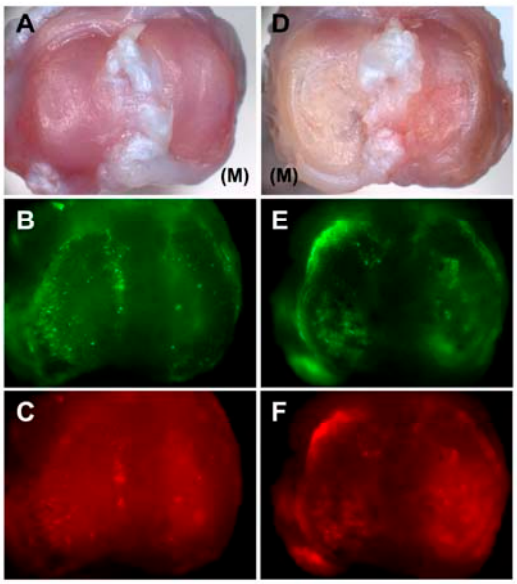

Figure 8 Macroscopic images of a control tibia (A-C) and of a MIA-injected tibia (D-F), at ten weeks post injection. The control tibia (A) had no cartilage lesions on the medial compartment (M) and lateral compartment of the tibial plateau, whereas the MIA-injected tibia (D) had severe cartilage lesions on the medial tibial plateau (M). Fluorochrome images of the MIA-injected tibia showed accumulation of calcein and xylenol orange along the margins of the tibial plateau (E, F), suggesting osteophyte formation whereas there was no accumulation of fluorochrome labels along the margins of control tibia (B, C). MIA, monosodium iodoacetate.

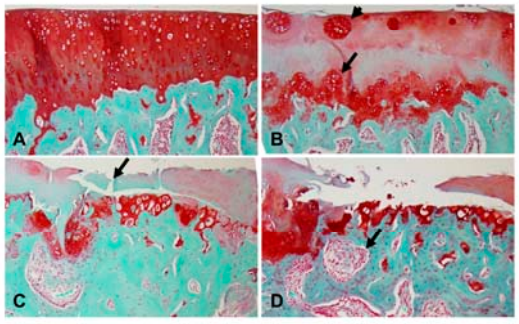

Figure 9 Coronal sections stained with Safranin O and fast green of a control tibia (A) and of a MIA-injected tibia (B-D) showing the cartilage on the medial tibial plateau, at ten weeks post injection. The control tibia (A) showed normal healthy cartilage with normally distributed chondrocytes. The MIA-injected tibia (B) showed loss of proteoglycans, loss of viable chondrocytes, chondrocyte proliferation (arrow), and chondrocyte cluster formation of variable sizes (arrowhead). The cartilage showed fibrillation, vertical fissures (C, arrow) and delamination (D). The subchondral trabecular bone architecture was altered with sclerosed bone (C) and the cellular bone marrow was replaced by loosely arranged spindle cells in a fine fibrous stroma (D, arrow). Original magnification ×100. MIA, monosodium iodoacetate.

Early subchondral plate thinning of the OA knee followed by an increase in thickness has been reported in the ACLT animal models of OA [17,23,24] and collagen induced OA in mice [13,18]. However, in the low-dose MIA-injected OA animal model, we found an increase in the subchondral plate thickness in the medial tibial plateau at two and six weeks post injection. Such an early increase in the subchondral plate thickness has been previously reported in other animal models of OA such as rabbits [25] and guinea pigs [26], and in studies of hand and knee OA patients [27]. This early increase in subchondral plate thickness observed in the MIA-injected knee could be due to altered loading of the affected knee joint. The thickened subchondral bone could also be associated with progression of cartilage degeneration. In our study, at ten weeks we did not observe the expected increase in the tibial subchondral plate thickness in the MIA-injected knee compared to the control. This could be due to the tibial subchondral plate breach observed in the MIA-injected knee. The increased porosity of the tibial subchondral plate in the MIA-injected knee compared to the control is in line with previous literature [23,24]. This increase in porosity is believed to play an important role in the communication between bone and cartilage during the pathogenesis of OA.

In the present study, the involvement of the subchondral trabecular bone structure after induction of OA using low-dose MIA is clearly shown in a temporal sequence. The two, six and ten week time points were chosen to characterize early, intermediate and advanced OA-related changes in the bone. Because previous studies using the high-dose MIA rat model have reported the involvement of subchondral bone as early as two weeks after injection [21], two weeks was chosen as the early time point in this study. A minimum of four weeks interval is recommended between scans [22], hence, six and ten weeks were chosen as subsequent time points. Given the paired study design, where the contralateral knee was used as an internal control, we prioritized the capture of early subchondral bone changes at two weeks over acquiring baseline data.

Qualitative analysis of micro-CT images revealed subchondral trabecular bone sclerosis at six and ten weeks post-MIA injection in the medial tibial plateau (Figure 4). This thickening of the subchondral trabecular bone was detected by the significant increases in trabecular thickness at six and ten weeks. Subchondral trabecular bone loss together with subchondral bone sclerosis suggests increased osteoclastic and osteoblastic activity that leads to altered subchondral bone remodelling [28].

In our study, micro-CT imaging revealed subchondral plate breach at six and ten weeks post-MIA injection. This was observed in areas of cartilage damage in all the rats (Figure 5A, B). In the weight bearing regions of the medial tibial plateau where the cartilage damage was severe, microfractures were observed in the subchondral plate that exposed the subchondral bone marrow to the joint cavity. This could potentially allow synovial fluid to enter the subchondral bone that triggers cystic cavity formation [29]. Another study suggests that the increased pressure between the delaminated joint surface leads to joint erosion, with synovial breach as a secondary event [30]. A recent study of human OA suggests that cysts may develop in pre-existing bone marrow lesions [31]. The subchondral plate breach also suggests fibrocartilage repair, which could be seen as a discontinuity of the articular bony plate [14]. Januz *et al.* have previously reported subchondral plate breach and its association with subchondral bone sclerosis and cyst formation in the MIA rat model [4]. In our study, 67% of the rats showed subchondral bone cysts in areas of bone resorption (Figure 5C, D).

Another hallmark feature of OA is the presence of osteophytes. In our study, marginal osteophytes were observed from micro-CT images in all the rats at six and ten weeks post-MIA injection. The neochondrogenesis of mesenchymal stem cells in the periosteum and synovial lining has been suggested to be the precursor for osteophyte formation [32]. It is still unclear if osteophytes are simply a pathological phenomenon or a functional adaptation in OA. Macroscopic UV illumination of the MIA-injected knee indicated accumulation of fluorochrome labels along the tibial joint margins and beneath the articular cartilage, demonstrating active osteophyte and subchondral bone formation in all the rats (Figure 8). Such calcein label accumulation was reported previously in an ACLT model for OA in rats [16]. Further histomorphometric analysis of fluorochrome double labels is required to elucidate the rate of bone turnover in tibial subchondral trabecular bone in the MIA-injected knee and control knee.

In the present study, we documented histological changes in the cartilage of the medial tibial plateau at ten weeks post-MIA injection, including loss of proteoglycans, chondrocyte necrosis, chondrocyte proliferation, chondrone formation, cartilage fibrillation and delamination (Figure 9). Similar cartilage changes have been reported in other animal models of OA [33,34]. In this study, articular cartilage damage was analyzed only at the end of the study (ten weeks). Analysis of cartilage changes at two and six weeks would have provided a longitudinal correlation between cartilage loss and subchondral bone changes. However, the main aim of this study was to track the changes in subchondral trabecular bone architecture over time. Moreover, we used a longitudinal study design that allows monitoring of bone changes over time in the same animal, and thus

minimizes the number of rats required compared to a cross-sectional study design [5,6].

To our knowledge, this is the first study to show serum levels of CRP in the low-dose MIA induced OA in rats. CRP is an acute phase protein and is a useful non-specific marker of inflammatory diseases [35]. In our study, we have shown that the serum CRP levels of MIA-injected rats do not differ significantly between the baseline and subsequent time points. In addition, there was no significant difference in CRP levels between the low-dose (0.2 mg) MIA-injected rats and control rats at any time point. This demonstrates that a single intra-articular injection of low-dose MIA does not induce marked systemic inflammation in this animal model of OA. Some studies indicated that in human OA the extent and severity of OA is associated with low-grade systemic inflammation with elevated serum CRP levels [36]. However, more recently, the Rotterdam Study-I, the largest cohort study to date, concluded that acute systemic inflammation is not present in OA and future studies should focus on the local inflammation process involved in OA [37].

It is hypothesized that in OA, cartilage matrix breakdown causes synovial inflammation and subsequent changes in the knee joint [38]. In the low-dose MIA rat model, the cartilage breakdown products could lead to mild local inflammation and synovitis in the knee joint that promotes subchondral bone changes. In our study, we were unable to observe for the presence of infiltrated local inflammatory cells as histology was performed only on the tibia and not the whole knee joint. Previous studies using the high-dose MIA rat model have reported the presence of acute inflammation characterized by expansion of the synovial membrane with infiltrating macrophages, neutrophils and plasma cells in the rat's knee joint one day after injection which resolved by day seven [19,28]. In a more recent study, increased activation of macrophages in the knee joint was reported in a high-dose MIA (1 mg) rat model up to four weeks after injection [39].

Although the low-dose MIA model mimics articular cartilage and subchondral bone pathology of human OA, like any other animal model of OA it does not fully mirror human OA. Barve *et al.* (2007) reported that 0.2 mg MIA induced a consistent matrix loss of approximately 35%, similar to the observed range of human OA samples. However, they found that the transcriptional similarity between the MIA rat and human OA cartilage was modest [40]. This modest similarity between rat and human cartilage could have been due to a difference in sampling site, sampling of lesion and non-lesion containing cartilage, stages of OA, and contamination of cartilage by underlying bone. Moreover, this study did not look at the protein expression or post translational modification that may demonstrate greater similarity between MIA rat and human OA cartilage. Other factors such as species variability, tissue heterogeneity and differences in underlying molecular mechanisms need to be considered. The choice of an animal model of OA mainly depends on the purpose of a study. The main purpose of our study was to characterize a non-trauma animal model that mimics tissue-level features of human OA, which could be used to study the effect of disease modifying OA drugs on cartilage and subchondral bone.

Conclusions

In summary, the changes in cartilage and subchondral trabecular bone structure observed in the low-dose MIA rat model reveal important pathologic features of human OA and the temporal progression of the disease in the tibial subchondral bone. The low-dose MIA induced OA rat model mimics the human disease condition and clearly demonstrates disease progression in the tibial subchondral bone in a timely manner. This animal model is suitable to study the effect of suitable therapeutic drugs on cartilage and subchondral bone. *In vivo* micro-CT enabled the temporal characterization of the changes in subchondral bone architecture both quantitatively and qualitatively in 3D. The changes in subchondral trabecular bone structure were found to be consistent with disease progression, as confirmed by end-stage histology. *In vivo* micro-CT is a non-destructive imaging technique that can be used in future studies to track changes in subchondral bone structure in drug intervention studies designed to slow the progression of OA in a non-trauma low-dose MIA induced OA rat model.

Abbreviations

ACLT: anterior cruciate ligament transection; ANOVA: analysis of variance; BV: bone volume; BV/TV: bone volume fraction; CRP: C-reactive protein; DMOAD: disease modifying osteoarthritis drugs; MIA: monosodium iodoacetate; Micro-CT: micro computed tomography; OA: osteoarthritis; OARSI: Osteoarthritis Research Society International; Pl.Por: plate porosity; Pl.Th: plate thickness; ROI: region of interest; Tb.N: trabecular number; Tb.Sp: trabecular separation; Tb.Th: trabecular thickness; vBMD: volumetric bone mineral density; VOI: volume of interest; 3D: three dimensional.

Acknowledgements

The authors wish to thank Dr Sander M. Botter (Erasmus Medical Centre, Rotterdam, The Netherlands) for kindly providing the software for the automatic segmentation of subchondral plate and trabecular bone. The authors thank Ms Cheryl Gan for preparation of the histology slides, Ms Lena Truong for assistance with animal dissection, Dr Dorota Gancarz for assistance with the animal model, Dr Allan Rofe for kindly providing the MIA, the IMVS animal care facility staff, and Adelaide Microscopy staff. The authors also wish to acknowledge the support of the Bone and Joint Research Laboratory staff and funding from Endeavour postgraduate scholarship from the Australian Government, Department of Education, Employment, and Workplace Relations (DEEWR).

Author details

[1]Bone and Joint Research Laboratory, Directorate of Surgical Pathology, SA Pathology and Hanson Institute, Frome Road, Adelaide, SA 5000, Australia.

[2]Discipline of Anatomy and Pathology, School of Medical Sciences, The University of Adelaide, Adelaide, SA 5005, Australia.

Authors' contributions

GM undertook all data acquisition and had full access to all the data in the study; GM, EP, JSK, IHP, and NLF participated in the study design and had final responsibility for the decision to submit for publication; GM and EP participated in the data analysis; GM and JMH carried out immunoassay and CRP data analysis; GM, EP, JSK, JMH, IHP, and NLF participated in the interpretation of the study data. All authors have participated in the preparation of the manuscript and have seen and approved the final version.

Competing interests

The authors declare that they have no competing interests.

Received: 23 February 2011 Revised: 8 November 2011
Accepted: 21 December 2011 Published: 21 December 2011

References

1. Bailey AJ, Mansell JP, Sims TJ, Banse X: **Biochemical and mechanical properties of subchondral bone in osteoarthritis.** *Biorheology* 2004, **41**:349-358.
2. Kalbhen DA: **Chemical model of osteoarthritis–a pharmacological evaluation.** *J Rheumatol* 1987, **14(Spec No)**:130-131.
3. Guingamp C, Gegout-Pottie P, Philippe L, Terlain B, Netter P, Gillet P: **Mono-iodoacetate-induced experimental osteoarthritis: a dose-response study of loss of mobility, morphology, and biochemistry.** *Arthritis Rheum* 1997, **40**:1670-1679.
4. Janusz MJ, Hookfin EB, Heitmeyer SA, Woessner JF, Freemont AJ, Hoyland JA, Brown KK, Hsieh LC, Almstead NG, De B, Natchus MG, Pikul S, Taiwo YO: **Moderation of iodoacetate-induced experimental osteoarthritis in rats by matrix metalloproteinase inhibitors.** *Osteoarthritis Cartilage* 2001, **9**:751-760.
5. Boyd SK, Davison P, Muller R, Gasser JA: **Monitoring individual morphological changes over time in ovariectomized rats by in vivo micro-computed tomography.** *Bone* 2006, **39**:854-862.
6. Perilli E, Le V, Ma B, Salmon P, Reynolds K, Fazzalari NL: **Detecting early bone changes using in vivo micro-CT in ovariectomized, zoledronic acid-treated, and sham-operated rats.** *Osteoporos Int* 2010, **21**:1371-1382.
7. Waarsing JH, Day JS, van der Linden JC, Ederveen AG, Spanjers C, De Clerck N, Sasov A, Verhaar JA, Weinans H: **Detecting and tracking local changes in the tibiae of individual rats: a novel method to analyse longitudinal in vivo micro-CT data.** *Bone* 2004, **34**:163-169.
8. Koh YH, Hong SH, Kang HS, Chung CY, Koo KH, Chung HW, Cha JH, Son KR: **The effects of bone turnover rate on subchondral trabecular bone structure and cartilage damage in the osteoarthritis rat model.** *Rheumatol Int* 2010, **30**:1165-1171.
9. Kalff KM, El Mouedden M, van Egmond J, Veening J, Joosten L, Scheffer GJ, Meert T, Vissers K: **Pre-treatment with capsaicin in a rat osteoarthritis model reduces the symptoms of pain and bone damage induced by monosodium iodoacetate.** *Eurn J Pharmacol* 2010, **641**:108-113.
10. Vermeirsch H, Biermans R, Salmon PL, Meert TF: **Evaluation of pain behavior and bone destruction in two arthritic models in guinea pig and rat.** *Pharmacol Biochem Behav* 2007, **87**:349-359.
11. Bouxsein ML, Boyd SK, Christiansen BA, Guldberg RE, Jepsen KJ, Muller R: **Guidelines for assessment of bone microstructure in rodents using micro-computed tomography.** *J Bone Miner Res* 2010, **25**:1468-1486.
12. Parfitt AM, Drezner MK, Glorieux FH, Kanis JA, Malluche H, Meunier PJ, Ott SM, Recker RR: **Bone histomorphometry: standardization of nomenclature, symbols, and units. Report of the ASBMR Histomorphometry Nomenclature Committee.** *J Bone Miner Res* 1987, **2**:595-610.
13. Botter SM, van Osch GJ, Clockaerts S, Waarsing JH, Weinans H, van Leeuwen JP: **Osteoarthritis induction leads to early and temporal subchondral plate porosity in the tibial plateau of mice: an in vivo microfocal computed tomography study.** *Arthritis Rheum* 2011, **63**:2690-2699.
14. Pritzker KP, Gay S, Jimenez SA, Ostergaard K, Pelletier JP, Revell PA, Salter D, van den Berg WB: **Osteoarthritis cartilage histopathology: grading and staging.** *Osteoarthritis Cartilage* 2006, **14**:13-29.
15. Holm S: **A Simple Sequentially Rejective Multiple Test Procedure.** *Scand J Statistics* 1979, **6**:65-70.
16. Hayami T, Pickarski M, Wesolowski GA, McLane J, Bone A, Destefano J, Rodan GA, Duong le T: **The role of subchondral bone remodeling in osteoarthritis: reduction of cartilage degeneration and prevention of osteophyte formation by alendronate in the rat anterior cruciate ligament transection model.** *Arthritis Rheum* 2004, **50**:1193-1206.
17. Dedrick DK, Goldstein SA, Brandt KD, O'Connor BL, Goulet RW, Albrecht M: **A longitudinal study of subchondral plate and trabecular bone in cruciate-deficient dogs with osteoarthritis followed up for 54 months.** *Arthritis Rheum* 1993, **36**:1460-1467.
18. Botter SM, van Osch GJ, Waarsing JH, Day JS, Verhaar JA, Pols HA, van Leeuwen JP, Weinans H: **Quantification of subchondral bone changes in a murine osteoarthritis model using micro-CT.** *Biorheology* 2006, **43**:379-388.
19. Bove SE, Calcaterra SL, Brooker RM, Huber CM, Guzman RE, Juneau PL, Schrier DJ, Kilgore KS: **Weight bearing as a measure of disease progression and efficacy of anti-inflammatory compounds in a model of monosodium iodoacetate-induced osteoarthritis.** *Osteoarthritis Cartilage* 2003, **11**:821-830.
20. Burr DB: **The importance of subchondral bone in osteoarthrosis.** *Curr Opin Rheumatol* 1998, **10**:256-262.
21. Morenko BJ, Bove SE, Chen L, Guzman RE, Juneau P, Bocan TM, Peter GK, Arora R, Kilgore KS: **In vivo micro computed tomography of subchondral bone in the rat after intra-articular administration of monosodium iodoacetate.** *Contemp Top Lab Anim Sci* 2004, **43**:39-43.
22. McErlain DD, Appleton CT, Litchfield RB, Pitelka V, Henry JL, Bernier SM, Beier F, Holdsworth DW: **Study of subchondral bone adaptations in a rodent surgical model of OA using in vivo micro-computed tomography.** *Osteoarthritis Cartilage* 2008, **16**:458-469.
23. Intema F, Hazewinkel HA, Gouwens D, Bijlsma JW, Weinans H, Lafeber FP, Mastbergen SC: **In early OA, thinning of the subchondral plate is directly related to cartilage damage: results from a canine ACLT-meniscectomy model.** *Osteoarthritis Cartilage* 2010, **18**:691-698.
24. Sniekers YH, Intema F, Lafeber FP, van Osch GJ, van Leeuwen JP, Weinans H, Mastbergen SC: **A role for subchondral bone changes in the process of osteoarthritis; a micro-CT study of two canine models.** *BMC Musculoskelet Disord* 2008, **9**:20.
25. Fahlgren A, Messner K, Aspenberg P: **Meniscectomy leads to an early increase in subchondral bone plate thickness in the rabbit knee.** *Acta Orthop Scand* 2003, **74**:437-441.
26. Layton MW, Goldstein SA, Goulet RW, Feldkamp LA, Kubinski DJ, Bole GG: **Examination of subchondral bone architecture in experimental osteoarthritis by microscopic computed axial tomography.** *Arthritis Rheum* 1988, **31**:1400-1405.
27. Buckland-Wright C: **Subchondral bone changes in hand and knee osteoarthritis detected by radiography.** *Osteoarthritis Cartilage* 2004, **12(Suppl A)**:S10-19.
28. Guzman RE, Evans MG, Bove S, Morenko B, Kilgore K: **Mono-iodoacetate-induced histologic changes in subchondral bone and articular cartilage of rat femorotibial joints: an animal model of osteoarthritis.** *Toxicol Pathol* 2003, **31**:619-624.
29. Ondrouch AS: **Cyst formation in osteoarthritis.** *J Bone Joint Surg Br* 1963, **45**:755-760.
30. Bancroft LW, Peterson JJ, Kransdorf MJ: **Cysts, geodes, and erosions.** *Radiol Clin North Am* 2004, **42**:73-87.
31. Tanamas SK, Wluka AE, Pelletier JP, Martel-Pelletier J, Abram F, Wang Y, Cicuttini FM: **The association between subchondral bone cysts and tibial cartilage volume and risk of joint replacement in people with knee osteoarthritis: a longitudinal study.** *Arthritis Res Ther* 2010, **12**:R58.
32. van der Kraan PM, van den Berg WB: **Osteophytes: relevance and biology.** *Osteoarthritis Cartilage* 2007, **15**:237-244.
33. Bendele AM: **Animal models of osteoarthritis.** *J Musculoskelet Neuronal Interact* 2001, **1**:363-376.
34. Hayami T, Pickarski M, Zhuo Y, Wesolowski GA, Rodan GA, Duong le T: **Characterization of articular cartilage and subchondral bone changes in the rat anterior cruciate ligament transection and meniscectomized models of osteoarthritis.** *Bone* 2006, **38**:234-243.
35. Pepys MB, Hirschfield GM: **C-reactive protein: a critical update.** *J Clin Invest* 2003, **111**:1805-1812.

36. Sturmer T, Brenner H, Koenig W, Gunther KP: **Severity and extent of osteoarthritis and low grade systemic inflammation as assessed by high sensitivity C reactive protein.** *Ann Rheum Dis* 2004, **63**:200-205.
37. Kerkhof HJ, Bierma-Zeinstra SM, Castano-Betancourt MC, de Maat MP, Hofman A, Pols HA, Rivadeneira F, Witteman JC, Uitterlinden AG, van Meurs JB: **Serum C reactive protein levels and genetic variation in the CRP gene are not associated with the prevalence, incidence or progression of osteoarthritis independent of body mass index.** *Ann Rheum Dis* 2010, **69**:1976-1982.
38. Martel-Pelletier J: **Pathophysiology of osteoarthritis.** *Osteoarthritis Cartilage* 2004, **12(Suppl A)**:S31-33.
39. Piscaer TM, Muller C, Mindt TL, Lubberts E, Verhaar JA, Krenning EP, Schibli R, De Jong M, Weinans H: **Imaging of activated macrophages in experimental osteoarthritis using folate-targeted animal single-photon-emission computed tomography/computed tomography.** *Arthritis Rheum* 2011, **63**:1898-1907.
40. Barve RA, Minnerly JC, Weiss DJ, Meyer DM, Aguiar DJ, Sullivan PM, Weinrich SL, Head RD: **Transcriptional profiling and pathway analysis of monosodium iodoacetate-induced experimental osteoarthritis in rats: relevance to human disease.** *Osteoarthritis Cartilage* 2007, **15**:1190-1198.

doi:10.1186/ar3543
Cite this article as: Mohan *et al.*: Application of *in vivo* micro-computed tomography in the temporal characterisation of subchondral bone architecture in a rat model of low-dose monosodium iodoacetate-induced osteoarthritis. *Arthritis Research & Therapy* 2011 **13**:R210.

CHAPTER 3

Pre-emptive, early, and delayed alendronate treatment in a rat model of low-dose monosodium iodoacetate induced osteoarthritis: effect on subchondral trabecular bone microarchitecture, cartilage degradation, bone and cartilage turnover, and joint discomfort

Geetha Mohan, Egon Perilli, Ian H Parkinson, Julia M Humphries, Nicola L Fazzalari and Julia S Kuliwaba

Bone and Joint Research Laboratory, Directorate of Surgical Pathology, SA Pathology and Hanson Institute, Frome Road, Adelaide, SA 5000, Australia

Discipline of Anatomy and Pathology, School of Medical Sciences, The University of Adelaide, Adelaide, SA 5005, Australia

Bone 2012; submitted paper

STATEMENT OF AUTHORSHIP

Pre-emptive, early, and delayed alendronate treatment in a rat model of low-dose monosodium iodoacetate induced osteoarthritis: effect on subchondral trabecular bone microarchitecture, cartilage degradation, bone and cartilage turnover, and joint discomfort

Bone 2012: submitted paper

Geetha Mohan (Candidate)

Performed analysis on all samples, interpreted data, wrote manuscript and acted as corresponding author

I hereby certify that the statement of contribution is accurate

Signed

....Date..21/02/2012

Egon Perilli

Contributed to planning of article, helped in data interpretation and provided critical evaluation

Certification that the statement of contribution is accurate and permission is given for the inclusion of the paper in the thesis

Signed

....Date..26/02/2012

Ian H. Parkinson

Contributed to planning of article and provided critical evaluation

I hereby certify that the statement of contribution is accurate and I give permission for the inclusion of the paper in the thesis

Signed

.....Date.....24/2/12.....

Julia M. Humphries

Data interpretation and manuscript evaluation

Certification that the statement of contribution is accurate and permission is given for the inclusion of the paper in the thesis

Signed

.....Date.....29.02.12.....

Nicola L. Fazzalari

Supervised development of work, helped in data interpretation and manuscript evaluation

I hereby certify that the statement of contribution is accurate and I give permission for the inclusion of the paper in the thesis

Signed

.....Date.....6/3/2012.....

Julia S. Kuliwaba

Supervised development of work, helped in data interpretation and manuscript evaluation

I hereby certify that the statement of contribution is accurate and I give permission for the inclusion of the paper in the thesis

Signed

… ……Date…29/2/12…..

Pre-emptive, early, and delayed alendronate treatment in a rat model of low-dose monosodium iodoacetate induced osteoarthritis: effect on subchondral trabecular bone microarchitecture, cartilage degradation, bone and cartilage turnover, and joint discomfort

Geetha Mohan[1,2*], Egon Perilli[1,2], Ian H Parkinson[1,2], Julia M Humphries[1,2], Nicola L Fazzalari[1,2] and Julia S Kuliwaba[1,2]

[1]Bone and Joint Research Laboratory, Directorate of Surgical Pathology, SA Pathology and Hanson Institute, Frome Road, Adelaide, SA 5000, Australia

[2]Discipline of Anatomy and Pathology, School of Medical Sciences, The University of Adelaide, Adelaide, SA 5005, Australia

Author's e-mail addresses:

geetha.mohan@adelaide.edu.au; egon.perilli@adelaide.edu.au

ian.parkinson@health.sa.gov.au; julia.humphries@health.sa.gov.au

nick.fazzalari@health.sa.gov.au; julia.kuliwaba@health.sa.gov.au

***Corresponding author:** Geetha Mohan (geetha.mohan@adelaide.edu.au)

Bone and Joint Research Laboratory, Directorate of Surgical Pathology,

SA Pathology, Frome Road, Adelaide, SA 5000, Australia

ABSTRACT

Introduction: To investigate the efficacy of pre-emptive, early, and delayed alendronate (ALN) treatment initiation on subchondral trabecular bone and cartilage in low-dose monosodium iodoacetate (MIA)-induced osteoarthritis (OA) in rats.

Methods: Male Wistar rats were randomly divided into three groups: OA (n=36), ALN (n=36) and control (n=12). Rats from the OA and the ALN group were injected with a low-dose of 0.2 mg MIA in the right knee and sterile saline in the left knee joint. Rats in the ALN group received pre-emptive (n=12, day 0 – end of week 2), early (n=12, end of week 2 – end of week 6), or delayed (n=12, end of week 6 – end of week 10) ALN treatment (30 μg/kg/week). The control rats received a single sterile saline injection in the right knee joint and no ALN treatment. The first subgroup of rats (OA, pre-emptive ALN and control) were scanned *in vivo* after 2 weeks and then sacrificed, the second subgroup of rats (OA, early ALN and control) were scanned after 2 and 6 weeks and sacrificed, and the third subgroup of rats (OA, delayed ALN and control) were scanned after 2, 6, and 10 weeks of OA induction and sacrificed. At each time point, bone histomorphometric, histological and biomarker analysis were undertaken. Changes in hind limb weight bearing were assessed from day -1 until day 14.

Results: In the OA group, there was progressive cartilage degradation, increased subchondral bone turnover, early subchondral bone loss followed by sclerosis, cysts, and osteophyte formation. Pre-emptive ALN treatment preserved subchondral trabecular bone microarchitecture, prevented increased bone resorption, decreased bone turnover and joint discomfort. Pre-emptive ALN treatment had a moderate effect on

cartilage. Both early and delayed ALN treatment prevented loss of trabeculae and decreased bone turnover, but did not have a significant effect on cartilage degradation.

Conclusion: Our study indicates that the time point of initiating bisphosphonate treatment for OA is crucial. Pre-emptive ALN treatment preserved subchondral trabecular bone microarchitecture, had a moderate effect on the cartilage and prevented increased bone turnover associated with the onset of OA. Further research into the role of subchondral bone in the pathophysiology of early to late stage OA is necessary to develop new therapeutic strategies for the treatment of OA.

Keywords

Osteoarthritis

Subchondral bone

In vivo micro-CT

OA animal model

Monosodium iodoacetate

Alendronate

1. Introduction

Osteoarthritis (OA) is a slowly progressive degenerative joint disease associated with impaired quality of life as well as high economic costs [1]. OA is characterised by breakdown of articular cartilage, altered subchondral bone remodelling, sclerosis, cysts and osteophyte formation. OA was primarily considered as a cartilage disorder but Radin and Rose first proposed the important role of subchondral bone and its link to cartilage degradation [2]. Numerous important transformations occur in the subchondral bone during the initiation and progression of OA [3]. Most importantly, in OA subchondral bone remodelling is increased and the newly formed bone is less mineralised with greater amounts of osteoid, and reduced mechanical properties [4]. Repeated loading of the subchondral bone with altered chemical and mechanical properties results in the progression of OA [5]. Despite the explosion of information regarding OA pathology, the mechanism of OA initiation and progression remains incompletely understood and currently there is no cure for OA.

Bisphosphonates are potent inhibitors of osteoclast mediated bone resorption and bone turnover. Clinically, bisphosphonates are used in the treatment of osteoporosis, Paget's disease, hypercalcemia, and metastatic cancer [6]. Bisphosphonates also possess anti-inflammatory effects influencing the production of anti-inflammatory cytokines [7]. Recent pre-clinical studies and clinical trials have shown that bisphosphonates could be used as potential disease modifying OA drugs due to their ability to suppress increased bone turnover. However, these clinical studies have yielded mixed results [8-10]. In clinical trials, alendronate (ALN), which is one of the most potent bisphosphonates, has been shown to prevent subchondral bone lesions and reduce knee pain; however, it did not prevent progression of OA [11]. In another study, ALN decreased spinal osteophyte

progression in women with vertebral fractures, despite it not showing a significant improvement in spinal disc space narrowing [12]. In these human OA studies, efficacy of ALN was assessed with the treatment mostly initiated at advanced stages of OA. On the other hand, in pre-clinical studies, ALN treatment initiated either from a few days before OA induction or from the day of OA induction has been shown to protect cartilage, and inhibit altered bone remodelling [13-15].

The potential beneficial effect of ALN (and of bisphosphonates in general) in OA could depend on the timing of treatment initiation, as OA is associated with increased bone turnover and bone resorption in the early phase, followed by subchondral bone sclerosis at the late phase of OA [16]. In a recent study, Strassle et al. showed that pre-emptive zoledronate treatment (day 0 – week 3) prevented decrease of subchondral bone mineral density (BMD), whereas delayed treatment (up to 5 weeks) reduced its efficacy in a high-dose (1 mg) MIA-induced OA rat model [17]. That study assessed BMD by using dual energy X-ray absorptiometry, which gives bone quantity measures from planar projections of the underlying three-dimensional bone structure. However, the effect of bisphosphonate on OA subchondral trabecular bone microarchitecture with the treatment initiated at early, intermediate, and late stages of the disease, has not yet been investigated using three-dimensional methods (3D), such as high resolution *in vivo* micro-computed tomography (micro-CT). As such, it is important to investigate the effect of bisphosphonate treatment initiation time points (pre-emptive, early, and delayed) on subchondral trabecular bone microarchitecture in 3D, in a suitable animal model that mimics human OA disease progression.

Previously, we have demonstrated that a low-dose (0.2 mg) MIA-induced OA rat model mimics in a timely manner important pathologic features of human OA [18]. Using *in vivo* micro-CT and confirmed by histology, we have demonstrated disease progression in the tibial subchondral trabecular bone over time, with an initial increased bone resorption followed by sclerosis, cyst and osteophyte formation representative of progressive human OA [18]. In the present study, we used the low-dose MIA-induced OA rat model to study the effect of pre-emptive, early and delayed ALN treatment initiated at various stages of the disease. We assessed the efficacy of ALN on cartilage degradation, subchondral trabecular bone microarchitecture, and joint discomfort observed in this animal model.

2. Materials and Methods

2.1. Animals and OA induction

Eighty-four 8-week-old young adult male Wistar rats ≈ 230 g (Animal Resource Centre, Canning Vale, WA, Australia), were kept in a sanitary ventilated animal room (12-h light-dark cycle) with food and water available *ad libitum*. The rats were divided into three groups: OA group (n=36), ALN treatment group (n=36), and control group (n=12), and were acclimatised for one week before the start of the experiment. On day 0, all the rats were anaesthetized with isofluroane and OA was induced (OA and ALN group) by injecting 0.2 mg MIA in the rat's right knee joint as described previously [18]. The left contralateral control knee was injected with sterile saline. The control rats received a single sterile saline injection in the right knee while the left knee was un-injected.

2.2. Alendronate treatment

Thirty-six rats were treated with ALN administered as twice-weekly subcutaneous injections at a dosage of 15 μg/kg. The ALN solution was made by dissolving one tablet of alendronate sodium (Fosamax 40 mg, MSD, South Granville, NSW, Australia) in 100 ml of sterile water. The solution was stirred for 2 hours and then diluted with sterile physiologic saline to appropriate concentrations to obtain the required dose as above.

The ALN treatment regime used in this study is as follows:

1. Pre-emptive ALN treatment group – treatment started from day 0 to end of week 2.
2. Early ALN treatment group – treatment started from end of week 2 (day 14) to end of week 6.
3. Delayed ALN treatment group – treatment started from end of week 6 (day 42) to end of week 10.

The hind limbs of all the rats were imaged with high-resolution *in vivo* micro-CT. The first subgroup of rats from the OA (n=12), pre-emptive ALN treatment (n=12) and control group (n=4) were scanned after 2 weeks and sacrificed. The second subgroup of rats from the OA (n=12), early ALN treatment (n=12) and control group (n=4) were scanned after 2 and 6 weeks, and sacrificed. The third subgroup of rats from the OA (n=12), delayed ALN treatment (n=12) and control group (n=4) were scanned after 2, 6, and 10 weeks, and sacrificed.

Double-fluorescent labelling of newly formed bone was achieved by intraperitonial injections of calcein (5 mg/kg body weight; Sigma-Aldrich, Sydney, NSW, Australia)

and xylenol orange (90 mg/kg body weight; Sigma-Aldrich, Sydney, NSW, Australia), 7 and 2 days before sacrifice respectively. The animal handling and experimental procedures outlined in this study were carried out in accordance with The University of Adelaide Animal Ethics Committee and The Institute of Medical and Veterinary Science Animal Ethics Committee.

2.3. *In vivo* micro-CT analysis

In vivo micro-CT imaging was performed using a Skyscan 1076 (Skyscan, Kontich, Belgium) as described previously [18, 19]. Briefly, each rat was anaesthetized with isofluroane and the right and left knees were scanned separately. During each scan only the knee for image data acquisition was irradiated, while the other limb and the rest of the body were lead-shielded from radiation. The scans were performed using the following scanner settings: X-ray source voltage 60 kVp, current 100 μA, a 1-mm thick aluminum filter to reduce beam-hardening artefact, 1 frame averaging. The pixel size was 8.7 μm, the exposure time was 4.7 s, and the rotation step was 0.8°, with a complete rotation over 197° [18, 19]. Each scan lasted 20 minutes during which the rat was under anaesthesia. The cross-sectional images were reconstructed using a filtered back-projection algorithm (NRecon, V 1.4.4, Skyscan, Kontich, Belgium). The reconstructed images were of 1,500×1,500 pixels each, 8.7 μm pixel size, and were stored as 8-bit images (256 gray levels).

On the stack of reconstructed micro-CT cross-section images, manual regions of interest (ROI) of an irregular anatomical contour were drawn in the subchondral trabecular bone region for the medial and lateral tibial plateau, for both the right and left knee (software CT Analyser, V 1.8.05, Skyscan, Kontich, Belgium). The VOI included the subchondral

trabecular bone starting below the subchondral plate, and extending distally towards the growth plate, excluding both the cortical bone and growth plate interface. For the calculation of the morphometric parameters, the images were segmented using a uniform threshold method as done previously [18, 19]. The value for segmentation was based on comparisons with thickness measurements in 3D, by scanning a specially designed physical micro-CT phantom composed of aluminium inserts (foils) with calibrated thicknesses (20, 50, 100, 250 μm), embedded in PMMA [19, 20]. The following 3D morphometric parameters were calculated for the medial, lateral, and total (=medial + lateral) VOI of subchondral trabecular bone (software CT Analyser, Skyscan): bone volume (BV, mm^3), bone volume fraction (BV/TV, %), trabecular thickness (Tb.Th, μm), trabecular separation (Tb.Sp, μm) and trabecular number (Tb.N, 1/mm).

2.4. Hind limb weight-bearing (HLWB) assessment

Hind limb weight-bearing of the rats was measured on days -1, 1, 3, 5, 7, 9, 12, and 14 using an incapacitance tester (Bioseb, Chaville, France). The percent weight borne on the MIA-injected limb was used as an index of joint discomfort in OA [21, 22]. The rats were trained by acclimating them to the incapacitance tester by placing them in the apparatus for 2 – 3 minutes for 5 days before the actual readings were taken. Briefly, the rats were positioned to stand on their hind paws in an angled (65 º from horizontal) plexiglass box placed above the incapacitance tester so that each hind paw rested on a separate force plate. The force (g) exerted by each limb was measured. Three consecutive 5-second readings were taken and averaged to obtain the mean score [21, 22]. The percent weight borne on the MIA-injected limb was determined as described by Pomonis et al [22].

2.5. Macroscopic analysis

The rats were sacrificed after 2, 6, and 10 weeks of OA induction and the tibiae were dissected for macroscopic study. The tibial cartilage was imaged using a fluorescence stereomicroscope (SZX 10, Olympus) and the macroscopic lesions were graded as described previously [18]. Briefly, the macroscopic lesions were graded as follows: 0 = normal appearance, 1 = slight yellowish discoloration of the chondral surface, 2 = little cartilage erosions in load-bearing areas, 3 = large erosions extending down to the subchondral bone, and 4 = large erosion with large areas of subchondral bone exposure [23]. The medial and lateral tibial plateaus were graded separately and the scores were averaged to determine the total grade for the MIA-injected knee and the contralateral control knee.

2.6. Histological analysis

The tibiae of six rats from each subgroup within the OA and the ALN treatment group and two rats from each subgroup within the control group were fixed in 4% paraformaldehyde, decalcified, and embedded in paraffin. Three coronal sections (5 μm thick) 100 μm apart were obtained and stained with 1.5% Safranin O, and 0.02% fast green counter stain. The sections were observed for OA-like features and the Osteoarthritis Research Society International (OARSI) scoring method was used to grade and stage tibial cartilage [24].

The tibiae of the remaining rats (n=6 for each subgroup within the OA and the ALN treatment group and n=2 for each subgroup within the control group) were fixed with 70% ethanol, dehydrated through a graded series of ethanol and embedded in methyl methacrylate. For each sample, two coronal sections were cut at 5μm thickness, spaced

100 μm apart. The amount of label incorporation in the tibial subchondral trabecular bone was measured under epi-fluorescence and the MAR was calculated as described by Frost et al. [25].Mineral apposition rate (MAR) was quantified for each sample at a magnification of 200X from unstained sections. Three areas from both the medial and the lateral tibial plateau were assessed and then combined to obtain the total value.

2.7. Serum COMP, CTX-I and urine CTX-II analysis

Fasting blood specimens were obtained from all the rats at baseline, 2, 6 and 10 weeks after OA induction for repeated measurement of serum cartilage oligomeric matrix protein (COMP, a cartilage turnover marker), and C-terminal telopeptide of collagen type I (CTX-I, a bone turnover marker). The serum samples were collected and frozen in aliquots at -80°C. Assays for serum COMP (Animal COMP ELISA, MD Bioproducts, St. Paul, MN, USA), and CTX-I (IDS RatLaps ELISA, Fountain Hills, AZ, USA) were performed according to the manufacturers' instructions. A morning spot urine sample was collected from all the rats after 2, 6 and 10 weeks of OA induction for urine C-terminal telopeptide of collagen type II (CTX-II, a cartilage turnover marker) analysis. The urine samples were centrifuged and frozen in aliquots at -80°C. Urinary CTX-II levels were determined by IDS Urine pre-clinical Cartilaps ELISA kit (Fountain Hills, AZ, USA). Each measurement for urinary CTX-II was normalized to urinary creatinine.

2.8. Statistical analysis

For bone histomorphometric parameters repeated measures two-way ANOVA was applied to determine the "time effect" and "time by group interaction effect". The "time effect" indicates if there was any change over time within each group (tibia of control

and MIA-injected knee), and the "time by group interaction effect" indicates if the different groups showed different patterns of changes over time. If F-values for a given variable were found to be significant, a paired Student's t-test was applied, to assess the changes in the morphometric parameters in each tibia over time and between the MIA-injected knee and contralateral control knee. The p-values were adjusted for repeated comparisons by Holm's Bonferroni stepdown procedure [26]. The effect of treatment between OA, ALN, and control groups at each time point was studied using a one-way ANOVA with Tukey's post hoc test (SPSS for Windows, Rel. 19.0.0. 2010. Chicago: SPSS Inc., USA). Hind limb weight-bearing and biomarker data sets were examined using Kruskal-Wallis test with Dunn's multiple comparison test (GraphPad Prism version 5.03 for Windows, San Diego, California, USA). Differences were considered significant for $p < 0.05$.

For OARSI score and MAR, the control group was not included since statistical analysis could not be performed with n=2. The OARSI and MAR datasets were analysed with a two way ANOVA to determine whether the effect of treatment or time point was significant. If F-values were found to be significant, a paired Student's t-test was applied and the p-values were adjusted for repeated comparisons by Holm's Bonferroni stepdown procedure.

3. Results

3.1. *In vivo* micro-CT: subchondral trabecular bone histomorphometry

3.1.1 Effect of pre-emptive ALN treatment (treatment started on day 0)

In the MIA-injected knee of the OA group, there was a significant decrease in BV, BV/TV, and Tb.N, and a significant increase in Tb.Sp, relative to the control group

(Fig. 1). After two weeks of OA-induction, pre-emptive ALN treatment effectively prevented the early subchondral bone loss observed in the MIA-injected knee of the OA group. There was a non-significant increase in Tb.N in the pre-emptive ALN group compared to the OA group. BV, BV/TV and Tb.N did not differ significantly between the MIA-injected knee of the pre-emptive ALN treatment group and the control group. The Tb.Sp in the ALN group was significantly lower relative to the OA group, and significantly higher relative to the control group.

At the same time point, the comparison in subchondral trabecular bone histomorphometric parameters between the MIA-injected knee and the contralateral control knee within the pre-emptive ALN treatment group, showed no statistically significant differences (Table 1).

3.1.2 Effect of early ALN treatment (treatment started after 2 weeks of OA induction)

Two weeks after OA induction, in the MIA-injected knee of the OA group, the histomorphometric parameters BV and Tb.N were significantly decreased (medial and total compartment), whereas Tb.Th (all compartments) and Tb.Sp (medial and total) were significantly increased relative to the control group (Fig. 2). At the same time point, the MIA-injected knee of the early ALN treatment group showed no significant differences compared to the OA group in any of the subchondral trabecular bone histomorphometric parameters.

After 6 weeks of OA induction, there was no significant difference in BV and BV/TV in the MIA-injected knee of the OA group relative to the control group. However, Tb.Th

and Tb.Sp were significantly increased, whereas Tb.N was significantly decreased relative to the control group (all compartments). After 6 weeks of OA induction, (4 weeks after ALN treatment initiation), the MIA-injected knee of the early ALN treatment group compared to the OA group did not show significant differences in BV/TV and Tb.Th. However, BV was significantly increased (medial compartment), Tb.N was significantly increased (all the compartments), and Tb.Sp was significantly decreased (all the compartments). Compared to the control group, Tb.N and Tb.Sp from the MIA-injected knee in the early ALN treatment group were not significantly different (Fig. 2); however, BV, BV/TV, and Tb.Th were significantly increased.

The comparison in subchondral trabecular bone histomorphometric parameters between the MIA-injected knee and the contralateral control knee within the early ALN treatment group is summarised in Table 2. After 2 weeks of MIA-injection, BV, BV/TV, Tb.N were significantly decreased and Tb.Sp was significantly increased relative to the contralateral control knee (all the compartments). After 6 weeks of OA induction (4 weeks after ALN treatment initiation), BV, BV/TV, Tb.Th and Tb.Sp were significantly increased. There was no significant difference in Tb.N relative to the contralateral control knee (all the compartments).

3.1.3 Effect of delayed ALN treatment (treatment started after 6 weeks of OA induction)

After 2 weeks of OA induction, the histomorphometric parameters BV, BV/TV and Tb.N in the MIA-injected knee of the OA group were significantly decreased and Tb.Sp was significantly increased relative to the control group (in all the compartments). After 6 weeks, there was no significant difference in BV and BV/TV in the MIA-injected

knee of the OA group relative to the control group. Tb.Th and Tb.Sp in the MIA-injected knee of the OA group were significantly increased compared to the control group, whereas Tb.N was significantly decreased (lateral compartment) of the OA group relative to the control group. After 2 and 6 weeks of OA induction (before ALN treatment initiation), there was no significant difference in the histomorphometric parameters from the MIA-injected knee between the OA group and the ALN treatment group (in all compartments) (Fig. 3). After 6 weeks, BV, BV/TV, Tb.Th and Tb.Sp in the MIA-injected knee of the delayed ALN treatment group were increased compared to the control group (medial and total compartment). At the same time point, Tb.Th and Tb.Sp in the OA group were significantly increased compared to the control group (medial and total compartment).

After 10 weeks (4 weeks after ALN treatment initiation), there was no significant difference in the histomorphometric parameters from the MIA-injected knee between the OA group and the ALN treatment group (all the compartments) (Fig. 3). In the OA group relative to control group, Tb.N was significantly decreased, whereas Tb.Th and Tb.Sp were significantly increased (all the compartments). In the delayed ALN treatment group compared to the control group, BV (medial compartment), Tb.Th, and Tb.Sp (all the compartments) was significantly increased. Tb.N was significantly decreased compared to the control group only in the lateral compartment.

A summary of the comparison in subchondral trabecular bone histomorphometric parameters between the MIA-injected tibia and the contralateral control tibia within the delayed ALN treatment group is given in Table 3. There was a significant increase in subchondral trabecular BV, BV/TV, Tb.Th and Tb.N, and a significant decrease in

Tb.Sp in both the knees over time ($p<0.05$, total compartment). As expected, after 2 weeks, in the MIA-injected tibia compared to the contralateral control, BV, BV/TV, Tb.N were significantly decreased and Tb.Sp was significantly increased. After 6 weeks (before ALN treatment initiation) and 10 weeks (after 4 weeks of ALN treatment initiation), there were significant increases in BV, BV/TV, Tb.Th, and Tb.Sp, relative to the contralateral control knee. There were no significant differences in subchondral Tb.N between the two limbs after 6 weeks and 10 weeks.

3.2 Effect of ALN on hind limb weight-bearing

In the OA group, the HLWB of the MIA-injected limb was significantly decreased on day 1, 3, ($p<0.001$ for both) 5 and 7 ($p<0.05$ for both) compared to its baseline value on day -1 (Fig. 4A). Compared to the control group, the OA group showed a trend towards decreased weight-bearing on the MIA-injected limb from day 1 to day 7, with significant difference in HLWB between the OA and control group observed on day 3 ($p<0.05$). Pre-emptive ALN treatment significantly prevented the decrease in weight-bearing of the MIA-injected knee on day 1, 3, and 5 ($p<0.05$, $p<0.001$ and $p<0.05$, respectively, compared to the OA group) (Fig. 4A). There was no difference in HLWB between the ALN and the control group at any time point. There was no change in HLWB of rats in the ALN group over time, similar to the control group.

3.3 Effect of ALN on macroscopic cartilage changes

There were no detectable macroscopic cartilage changes in both the left and right tibia of the control group. Also, there were no detectable macroscopic cartilage changes in the contralateral control tibia of the OA group, and the contralateral control tibia of the ALN group, compared to the tibiae of the control group, at any time point (Fig. 4B).

After 2 weeks, the tibia from the OA group showed mild cartilage damage. The tibia from the pre-emptive ALN treatment showed discoloration in weight-bearing regions of the medial tibial plateau (Fig. 4B). At 6 weeks, yellow discoloration and mild cartilage lesions were observed in the tibia from both the OA and the early ALN treatment group. At 10 weeks, tibia from both the OA and the delayed ALN treatment group showed focal lesions with yellow discoloration, and a few large lesions exposing the subchondral bone on the medial weight-bearing regions. The joint scores (mean ± SEM) were as follows: 2 ± 0.37, 3 ± 0.26, 3.17 ± 0.31 at 2, 6 and 10 weeks, respectively, for the OA group; 1.17 ± 0.17, 2.33 ± 0.33, 2.5 ± 0.43 for pre emptive, early and delayed ALN treatment groups, respectively. The joint score increased from week 2 to week 10 in both the OA and the ALN treatment groups. The differences in joint score between the OA and the ALN groups and between time points were not statistically significant.

3.4 Effect of ALN on microscopic cartilage changes

Figure 5 shows microscopic cartilage images in the OA, the ALN treatment and control group at 2, 6, and 10 weeks after injection. There were no OA-like cartilage changes in both the left and right tibia of the control group. There were no OA-like changes in the contralateral control tibia of the OA group, and the contralateral control tibia of the ALN group, compared to the tibiae of the control group, at any time points. In the MIA-injected knee of the OA group, after 2 weeks there was loss of proteoglycan, mild chondrocyte degeneration, and cartilage fibrillation in the tibial articular cartilage. Formation of small osteophytes was evident in all the six rats. In the MIA-injected knee of the pre-emptive ALN treatment group the proteoglycan loss and chondrocyte degeneration was less severe compared to the OA group and the cartilage was intact. Small osteophytes were present in 5 out of 6 rats.

After 6 weeks, the cartilage matrix in the MIA-injected knee from both the OA and the early ALN treatment group showed loss of proteoglycans, branched vertical fissures with chondrocyte necrosis and chondrocyte cluster formation. In the MIA-injected knee of both the OA groups and the early ALN treatment group, all the rats showed subchondral bone sclerosis with osteophyte formation. However, in the early ALN treatment group the osteophyte was in the form of cartilaginous outgrowths without bony transformation (Fig. 5). After 10 weeks both the OA and the delayed ALN treatment group showed severe proteoglycans loss, chondrocyte necrosis, chondrocyte clusters, extensive cartilage matrix loss with delamination, and exposure of subchondral bone. The subchondral bone was sclerosed and mineralised osteophytes were visible in both OA and delayed ALN treatment group (Fig. 5). At 6 and 10 weeks, cysts were observed in 4 out of 6 rats in the OA group and in 3 out of 6 rats in the delayed ALN treatment group. In both the OA and ALN group subchondral bone, normal haematopoietic bone marrow was replaced by fine fibrous stroma containing spindle cells. The subchondral plate was breached in focal areas with reparative tissue including fibrocartilage.

The OARSI scores of the OA group were significantly higher at 6 weeks ($p<0.001$) and 10 weeks ($p<0.01$) compared to 2 weeks after MIA injection. Similarly, the OARSI scores of the early ALN treatment and the delayed ALN treatment group were significantly higher compared to the pre-emptive ALN treatment group ($p<0.001$ and $p<0.05$ respectively). The OARSI scores did not differ between the OA group and the ALN treatment group at any time point (Fig. 6A).

3.5 Effect of ALN on subchondral trabecular bone mineral apposition rate (MAR)

The MAR of the OA group was significantly increased at 2 weeks compared to 6 and 10 weeks in the medial ($p<0.0001$, $p<0.01$), lateral ($p=0.001$, $p<0.01$) and total ($p<0.0001$, $p<0.001$) compartments. The MAR of the pre-emptive ALN treatment group was significantly increased compared to the early ALN treatment and the delayed ALN treatment group in all the three compartments ($p<0.001$ for all). Pre-emptive ALN treatment significantly decreased the MAR which was increased in the OA group at 2 weeks in the medial ($p<0.01$), lateral ($p<0.01$) and total ($p<0.0001$) compartments (Fig. 6B).

3.6 Effect of ALN on serum COMP, CTX-I and urine CTX-II

Figure 7 shows the levels of serum COMP, serum CTX-I and urine CTX-II of the OA group, the ALN treatment group and the control group, after 2, 6 and 10 weeks of OA induction. In all the three groups there was statistically significant decrease in the serum COMP, CTX-I and urine CTX-II levels over time ($p<0.05$). In the OA group compared to the control group, there was a non-significant increase in serum COMP, CTX-I and CTX-II levels after 2, 6, and 10 weeks of OA induction. Pre-emptive ALN treatment, early ALN treatment and delayed ALN treatment significantly decreased the serum CTX-I levels similar to the levels in the control group. In contrast, ALN treatment (pre-emptive, early, and delayed) did not have a significant effect on serum COMP and urine CTX-II levels.

4. Discussion

Subchondral bone remodelling plays an important role in the pathophysiology of OA and bisphosphonates are potent inhibitors of bone turnover. Clinical trials using

bisphosphonate treatment for OA have yielded mixed results suggesting that the therapeutic effect of ALN may depend on the time of treatment initiation. Assessing the effects of ALN on early pathological changes in human OA is difficult. Hence, an animal model that mimics OA progression is essential to assess the effects of ALN on cartilage and subchondral bone at various stages of the disease. Using a low-dose MIA rat model, we have previously demonstrated OA progression in a timely manner [18]. In order to assess the efficacy of ALN treatment at early, intermediate, and late stages of OA, we initiated ALN treatment at different stages of OA in a low-dose MIA rat model. The experimental design of the present study enabled us to determine the efficacy of time course ALN treatment on tibial subchondral trabecular bone architecture, cartilage changes, bone and cartilage turnover markers, and joint discomfort in this animal model.

Trabecular bone microarchitecture is an important determinant of bone quality [27], and changes in microarchitectural properties have been reported previously in human OA [28-30] and animal studies [31-33]. In the present study, changes in the tibial subchondral trabecular bone microarchitecture were observed in the OA group, such as decreased BV, and BV/TV after 2 weeks, followed by increased BV, BV/TV, Tb.Th, Tb.Sp and reduced Tb.N at 6 and 10 weeks after OA induction. Pre-emptive ALN treatment prevented subchondral trabecular bone loss and preserved subchondral trabecular microarchitecture (Table 1). Early ALN treatment maintained subchondral Tb.N and Tb.Sp (Fig 2, Table 2), and delayed ALN treatment maintained Tb.N (Table 3). This suggests that pre-emptive ALN treatment has the most beneficial effect on subchondral trabecular bone microarchitecture, and the efficacy gradually decreases with later treatments (early and delayed ALN treatment). A recent OA-study reported

that zoledronic acid increased BMD in the high-dose MIA (1 mg) model in a time-dependent manner, and the longest treatment (from week 2 – week 5) produced the largest beneficial effect on BMD [17]. The present OA-study, using *in vivo* micro-CT in a low-dose MIA rat model, demonstrates the time-dependency of the beneficial effects of ALN on the subchondral bone microarchitecture. A similar dependence on time point of bisphosphonate-treatment initiation on bone microarchitecture was observed in osteoporosis studies, in an animal model of ovariectomized rats treated with zoledronic acid [19, 34].

In the present study, we did not observe significant improvement in cartilage degradation after 2 weeks of ALN treatment in the pre-emptive ALN group. This could be due to the fact that not enough time has elapsed to actually observe a beneficial effect of ALN on cartilage degradation. In our study, although ALN treatment did not have a significant effect on OARSI score, we observed less severe loss of proteoglycans and chondrocytes in the pre-emptive ALN group. This suggests that pre-emptive ALN treatment has a moderate effect on cartilage degradation in this animal model. Hayami et al. reported similar observations in a rat anterior cruciate ligament transection (ACLT) model of OA in which a clinically relevant dose of 30μg/kg/week ALN completely inhibited the early bone loss at 2 weeks but did not have a significant effect on cartilage degradation. However, they found that a high-dose of 240 μg/kg/week ALN prevented bone loss and had partial chondroprotective properties [13]. In another pre-clinical study using rabbit ACLT model, Zhang et al. showed that 70μg/kg/week ALN treatment protected the cartilage and improved subchondral bone architecture by preventing increased subchondral bone resorption at the early phase of OA [15].

In the present study, 30μg/kg/week of alendronate was used. A dosage of 30 μg/kg/week ALN has been shown to completely prevent bone resorption in ovariectomized rats and is suggested to be close to the clinical dose of ALN used to treat human osteoporosis [13]. Higher doses of bisphosphonates may be beneficial to both cartilage and bone; however, the effect of continuous suppression of bone turnover after long-term use needs to be determined. Supra physiological doses of ALN and risedronate have shown to suppress bone turnover by 90 – 95% in the vertebrae and increase microdamage accumulation in beagles [35].

Prevention of bone loss by ALN treatment is mainly attributed to the direct effect of ALN on osteoclasts. During bone resorption, osteoclasts release and internalise ALN from bone, which interferes with the normal mevalonate pathway essential for osteoclast function, ruffled border formation, and survival of osteoclasts. This translates into inhibition of bone resorption and decreased activation frequency of bone remodelling [37]. Apart from a direct effect on osteoclasts ALN has also been shown to inhibit osteoclastic bone resorption through its action on osteoblasts [38, 39]. Osteoblasts have been shown to control osteoclast mediated bone resorption by secreting osteoclast inhibitors [40]. Further, bisphosphonates have been shown to alter bone remodelling in osteoporosis and Paget's disease by modulating osteoprotegerin (OPG) and receptor activator of nuclear factor kappa b ligand (RANKL) [41, 42]. In our study, we observed significant reduction of MAR by pre-emptive ALN treatment, which shows ALN has an effect on osteoblastic activity. It is probable that in our study, ALN treatment inhibited bone resorption by modulating OPG and RANKL secreted by osteoblasts, which have been shown to play a major role in OA pathology [43].

In the present study, ALN did not have a significant effect on osteophyte formation, even though early ALN treatment seemed to slow down osteophyte formation, which were not fully mineralised (Fig. 5). Another pre-clinical study reported that ALN did not have a statistically significant effect on osteophyte score [14]. A few pre-clinical studies have shown that ALN can inhibit osteophyte formation however, in these studies ALN treatment was initiated a few days before OA induction or from the day of OA induction [13, 15, 44]. In a clinical trial, Neogi et al. showed that ALN reduced the progression of spinal osteophytes in OA. However, the spinal radiographic changes in that study were subtle and may not have a major clinical relevance [45].

OA is characterised by painful joints. In our study the rats injected with low-dose MIA showed significant decrease in HLWB up to day 7, and pre-emptive ALN treatment significantly prevented the decrease in HLWB. Increased bone turnover and subchondral bone pathology observed at 2 weeks in the OA group rats coincides with decreased HLWB. In the MIA rat model, the iodoacetate injection causes early phase neuropathy, which could be the cause of pain [46]. Moreover, subchondral bone structural pathology has been shown to be associated with knee pain in OA [11, 47]. Carbone et al. reported that ALN treatment decreased subchondral bone attrition and reduced knee joint pain in postmenopausal women with OA [11]. Risedronate has also been shown to non-significantly improve OA joint pain score from baseline [9].

In the present study, the prevention of subchondral bone pathology by ALN treatment could have resulted in alleviation of weight-bearing deficits in the rats. It is also possible that the direct analgesic property of ALN could have caused the alleviation of weight-bearing deficits found in the low-dose MIA induced OA in rats. Our observation

for HLWB in the pre-emptive ALN group is consistent with a recent study in which pre-emptive treatment with zoledronic acid significantly and dose-dependently reversed weight-bearing deficits in the high-dose MIA rat model [17]. Strassle et al. speculate that apart from direct analgesic action, zoledronate (pre-emptive and delayed treatment) may have reduced joint pain by directly inhibiting chondrocyte cell death induced by MIA or by preventing osteoclast mediated chondrocyte death. A limitation of our study is that we were able to follow HLWB only until day 14 as it became increasingly difficult to fit the growing rats in the incapacitance tester after 2 weeks. Moreover, early and delayed ALN treatment effects on HLWB would have given additional information regarding ALN efficacy on chronic pain.

In the present study, there was an age-related decline in serum COMP, CTX-I and urine CTX-II in the OA group, ALN treatment group and control group due to decreased cartilage and bone turnover. Two weeks after OA induction the serum CTX-I level was significantly increased while the serum COMP and urine CTX-II levels showed a trend towards increased levels compared to the control group. This shows increased cartilage and bone turnover at early stage OA. The difference in cartilage turnover marker levels between the OA group and the control group after 2, 6 and 10 weeks did not reach statistical significance in our study. This may be because only one knee was induced with OA and the levels of biomarker released from a single OA knee are likely to be low. In addition, we had only four rats in the control group, which might be insufficient to reach statistically significant differences.

Pre-emptive ALN, early ALN and delayed ALN treatment significantly decreased bone turnover rate; however, ALN treatment did not have any effect on cartilage turnover.

Human OA has been shown to be associated with increased levels of serum COMP, CTX-I and CTX-II [48, 49]. Hayami et al. reported similar effects of ALN (30μg/kg/week) on COMP, CTX-I and urine CTX-II in OA rats [13]. As mentioned earlier, high doses of ALN may be required to see a significant effect on cartilage as shown by Hayami et al using 240 μg/kg/week ALN [13].

A limitation of our study is that the follow up of pre-emptive and early ALN treatment until the advanced stages of OA is missing. Longer-term follow up could have revealed a significant effect of ALN on cartilage and osteophyte formation as observed in other studies [13, 14]. However, our study design allowed us to determine the effect of ALN treatment on histological changes in the cartilage at early, intermediate, and advanced stages of OA.

5. Conclusions

In conclusion, we have used a low-dose MIA-induced OA rat model that results in progressive pathological changes in the cartilage and subchondral bone. We have demonstrated that pre-emptive ALN treatment preserved subchondral trabecular bone microarchitecture, decreased bone turnover, joint discomfort, and offered moderate cartilage protection. Both early and delayed ALN treatment were less effective on subchondral bone microarchitecture, preventing mainly decrease of trabecular number (loss of trabeculae) and decreased bone turnover, but did not prevent changes in bone volume or trabecular thickness, and did not have any significant effect on the cartilage. Our study indicates that the time point of initiating bisphosphonate treatment for OA is crucial. Targeting subchondral bone remodelling could offer a potential treatment option for the management of OA. However, further research into the role of

subchondral bone in the pathophysiology of early to late stage OA is necessary to develop new therapeutic strategies for the treatment of OA.

Abbreviations

OA: osteoarthritis; MIA: monosodium iodoacetate; ALN: alendronate; Micro-CT: micro computed tomography; BMD: bone mineral density; 3D: three-dimension; COMP: cartilage oligomeric matrix protein; CTX-I: C-terminal telopeptide of collagen type I; CTX-II: C-terminal telopeptide of collagen type II; ROI: region of interest; VOI: volume of interest; BV: bone volume; BV/TV: bone volume fraction; Tb.Th: trabecular thickness; Tb.Sp: trabecular separation; Tb.N: trabecular number; HLWB: hind limb weight-bearing; OARSI: osteoarthritis research society international; MAR: mineral apposition rate; OPG: osteoprotegerin; RANKL: receptor activator of nuclear factor kappa b ligand; ACLT: anterior cruciate ligament transection

Conflicts of interest

The authors declare that they have no conflicts of interest.

Authors' contributions

GM had a major input in the experimental design, conducted all experimental procedures, performed data collection, statistical analysis, graphical presentation of the data collected, and prepared the manuscript for submission. EP, IHP, NLF, and JSK was involved in the experimental design, contributed to the interpretation of the data collected and preparation of the manuscript; JMH was involved in serum COMP, CTX-I and CTX-II analysis and data interpretation; All authors have participated in the preparation of the manuscript and have approved the final version.

Funding source

GM is the recipient of Endeavour postgraduate scholarship from the Australian Government, Department of Education, Employment, and Workplace Relations (DEEWR). This study was supported in part by funding from SA Pathology, Adelaide, Australia.

Acknowledgement

The authors thank Dr Allan Rofe for kindly providing the MIA, Dr Dorota Gancarz for assistance with the animal model, Ms Lena Truong for assistance with animal dissection, Mrs Helen Tsangari for preparing the resin sections (histology), the Institute of Medical and Veterinary Science (IMVS) animal care facility staff, and Adelaide microscopy staff.

Figures

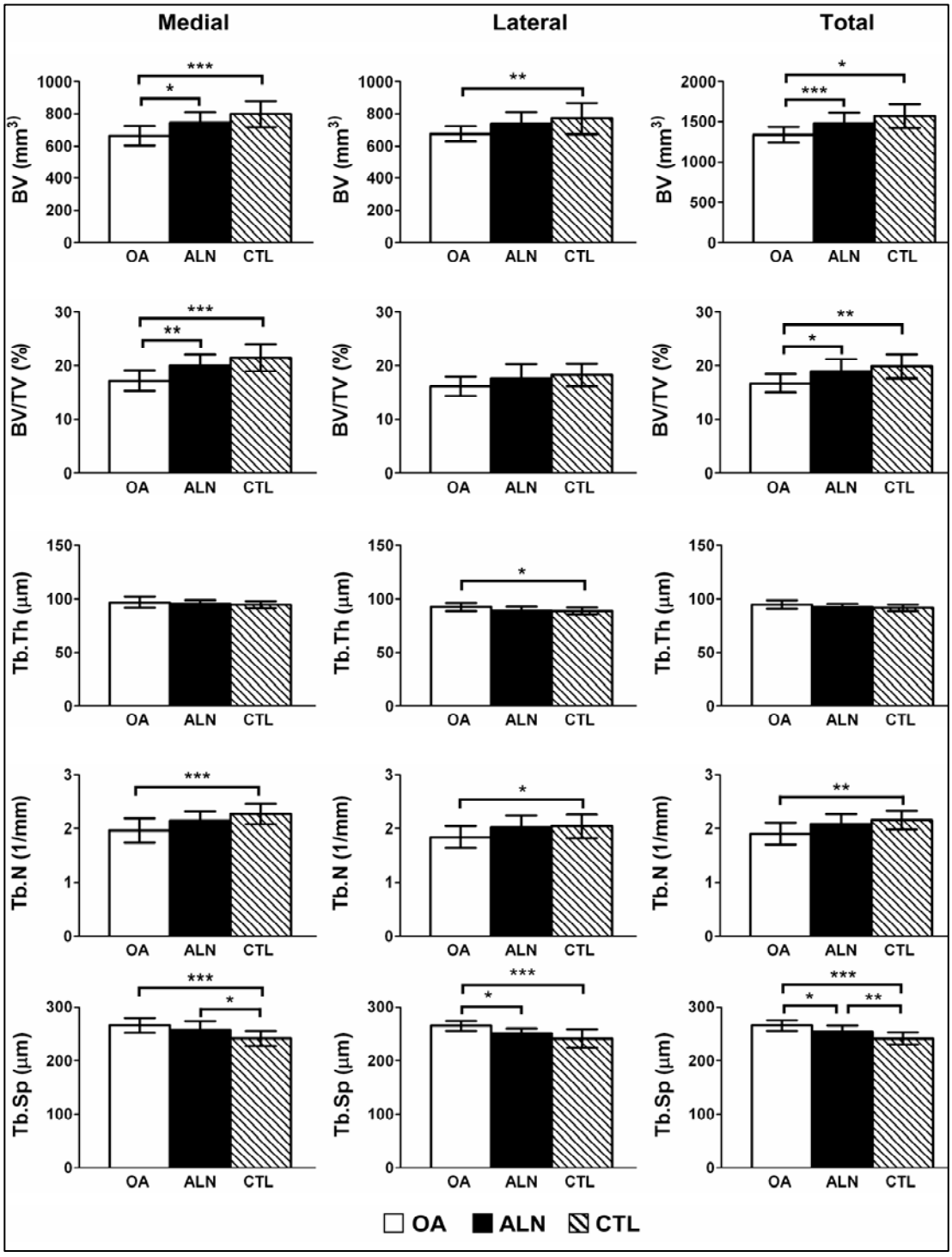

Figure 1. Effect of pre-emptive ALN treatment on tibial subchondral trabecular bone after 2 weeks of ALN treatment initiation. Histomorphometric parameters of the MIA-injected knee from the OA and the ALN group and the right knee of the control group are shown. Data shown as mean ± SD. * p<0.05, ** p<0.001, and *** p< 0.0001.

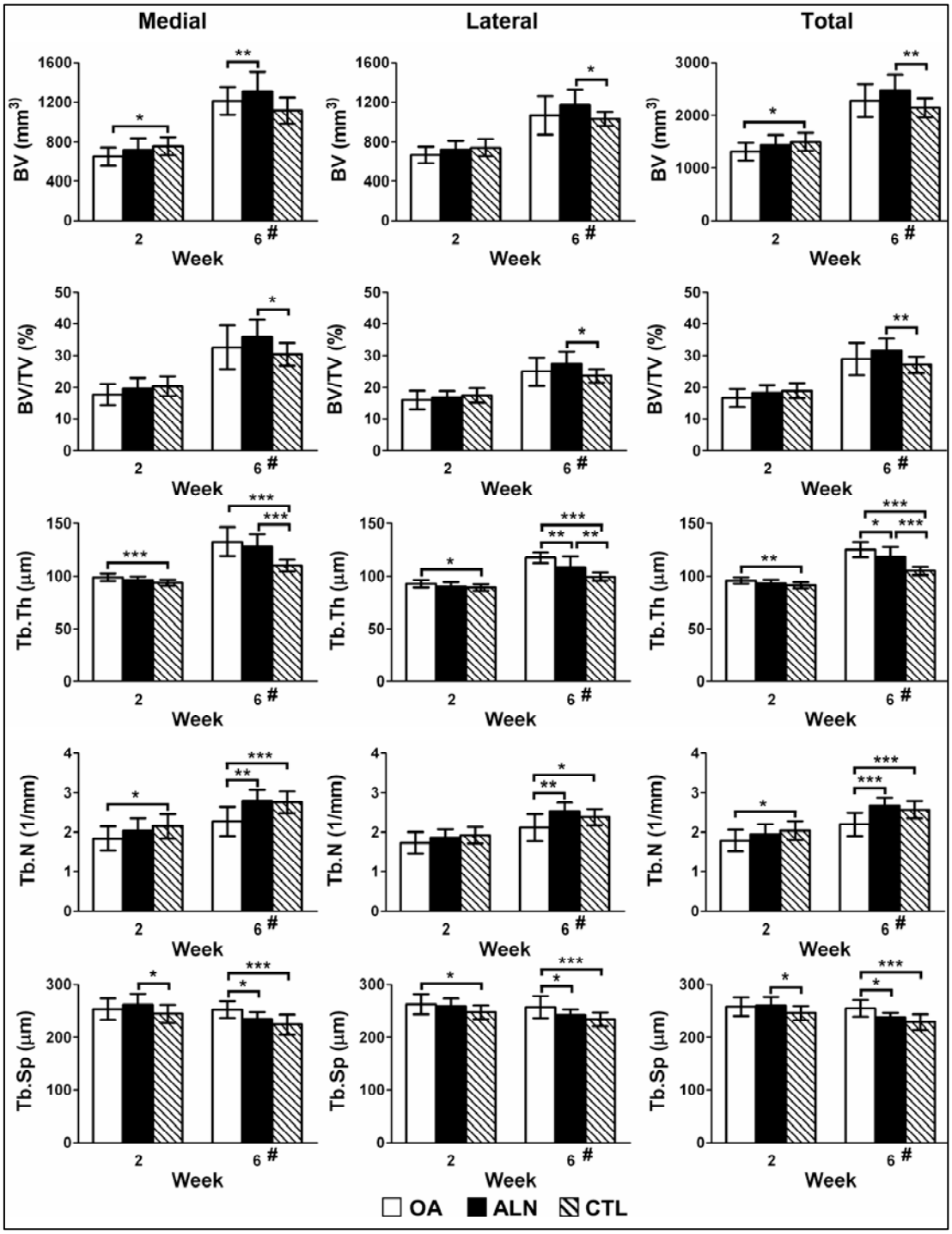

Figure 2. Effect of early ALN treatment (started 2 weeks after OA induction) on tibial subchondral trabecular bone. Histomorphometric parameters of the MIA-injected knee from the OA and the ALN group and the right knee of the control group are shown. Data shown as mean ± SD. # measurement after ALN treatment initiation. * p<0.05, ** p<0.001, and *** p< 0.0001.

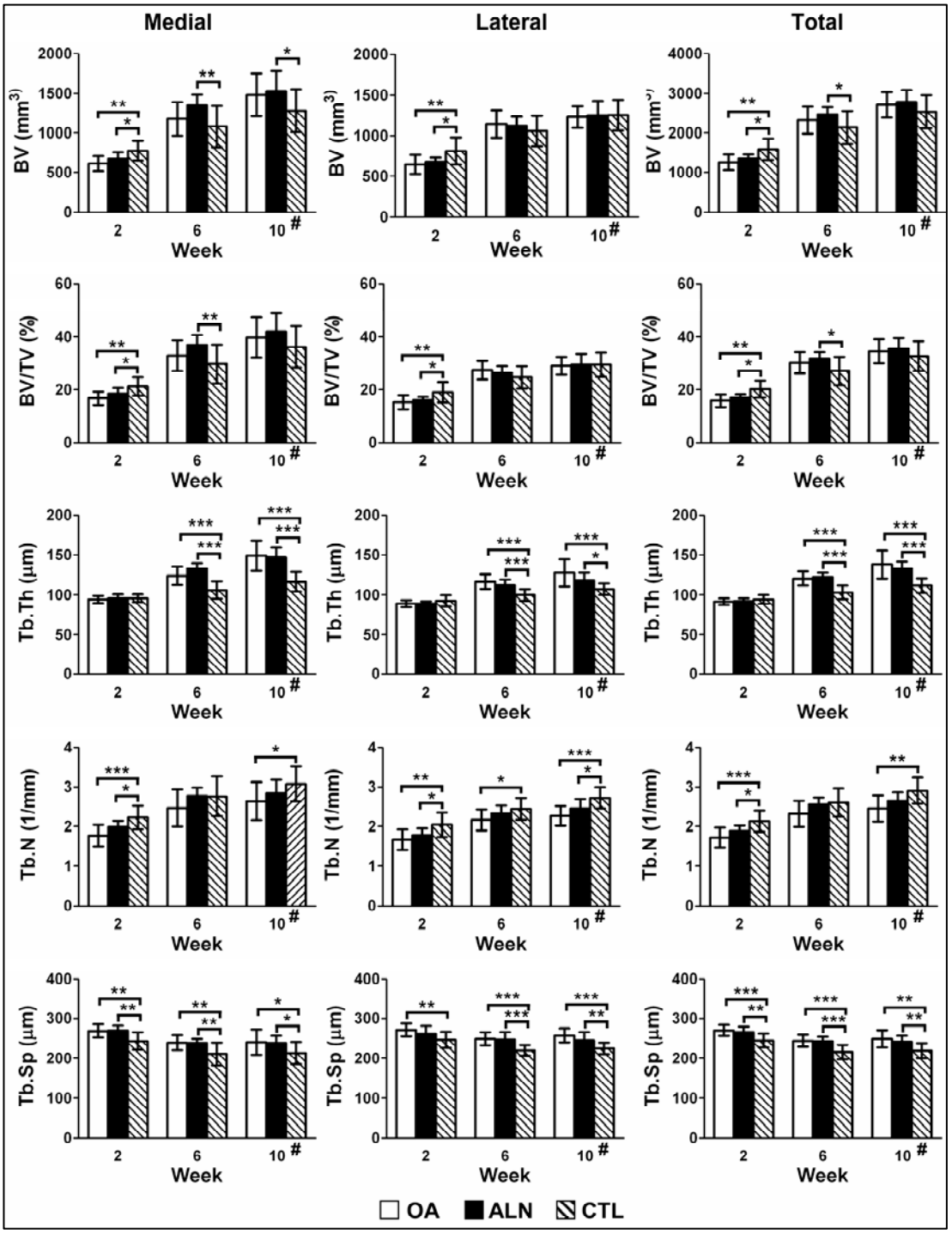

Figure 3. Effect of delayed ALN treatment (started 6 weeks after OA induction) on tibial subchondral trabecular bone. Histomorphometric parameters of the MIA-injected knee from the OA and the ALN group and the right knee of the control group are shown. Data shown as mean ± SD. # measurement after ALN treatment initiation. * p<0.05, ** p<0.001, and *** p< 0.0001.

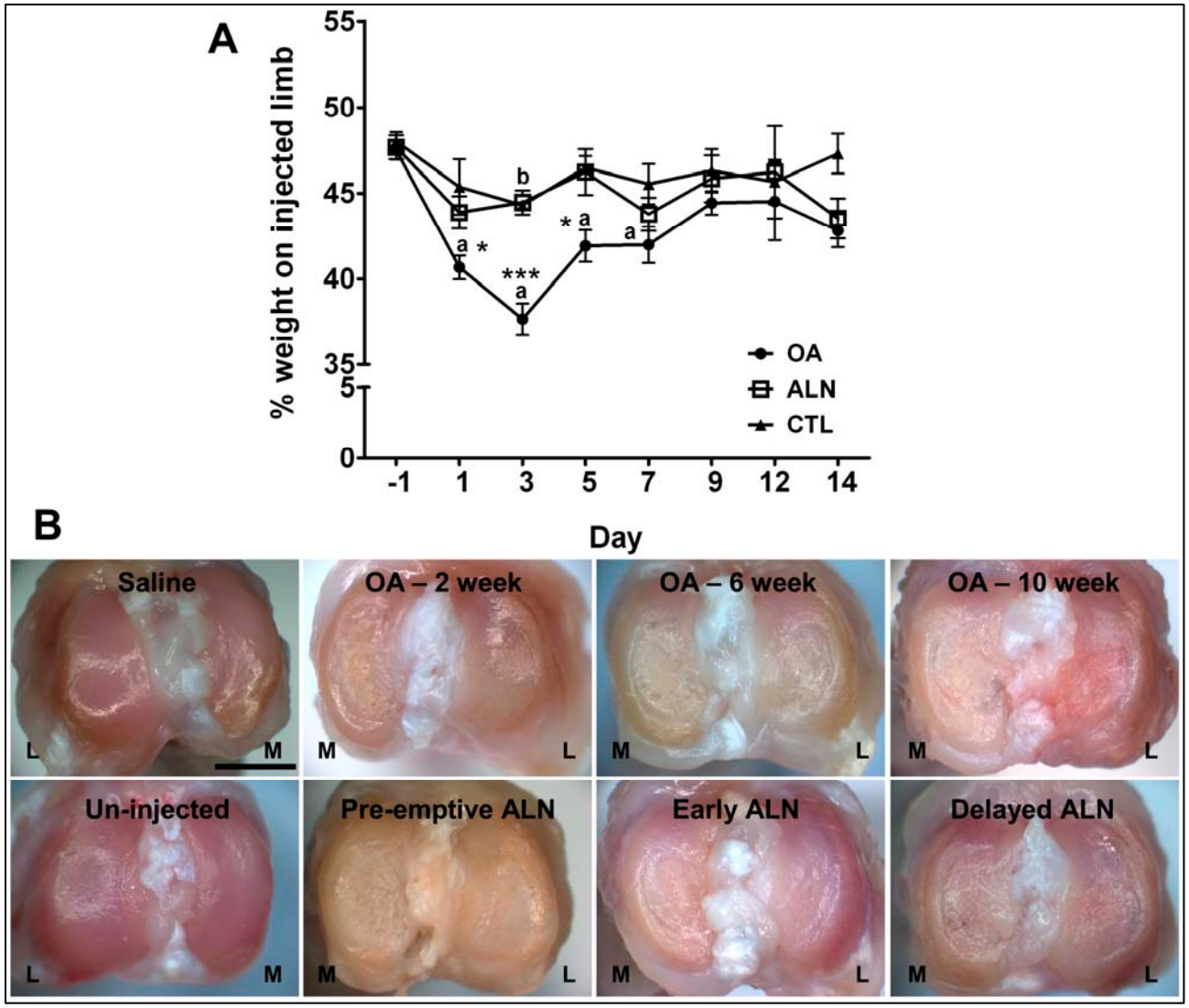
A
% weight on injected limb
55
50
45
40
35
5
0
-1
1
3
5
7
9
12
14
Day
OA
ALN
CTL
B
Saline
OA – 2 week
OA – 6 week
OA – 10 week
Un-injected
Pre-emptive ALN
Early ALN
Delayed ALN
L
M

Figure 4A. Effect of pre-emptive ALN treatment on rat hind limb weight-bearing. Pre-emptive ALN effectively prevented decreased weight-bearing of the OA knee on day 1, 3 and 5 after MIA injection. Results are reported as mean ± SEM.
a = Hind limb weight-bearing difference over time compared to baseline value of the OA group ($p<0.001$ for day 1 and 3 and $p< 0.05$ for day 5 and 7 respectively)
b = OA vs. control ($p<0.05$). * $p<0.05$ OA vs. ALN, *** $p<0.001$ OA vs. ALN

Figure 4B. Rat tibial plateau of saline, un-injected, OA and ALN treated knees. Tibia of saline-injected knee and un-injected control knee showed no macroscopic changes in the cartilage. Tibia of OA knee showed progressive cartilage lesions after 2, 6, and 10 weeks of OA induction. Tibia from pre-emptive ALN treatment showed very mild cartilage changes after 2 weeks whereas, tibia from the early ALN treatment and delayed ALN treatment group showed cartilage changes similar to the respective OA group. Scale bar = 1.5 mm.

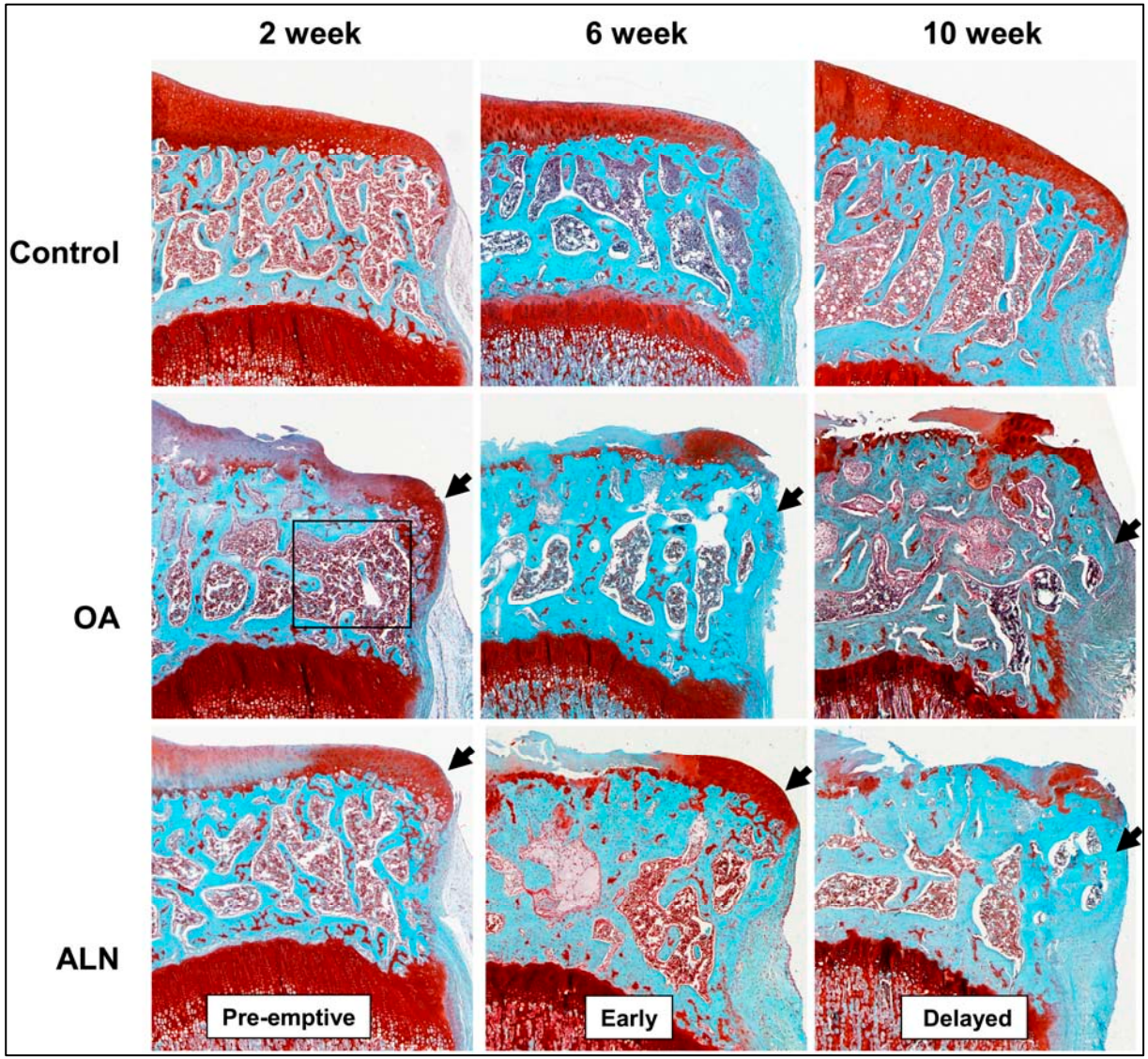
2 week
6 week
10 week
Control
OA
ALN
Pre-emptive
Early
Delayed

Figure 5. Articular cartilage and subchondral bone of medial tibial plateau from control, OA, and ALN treatment group after 2, 6, and 10 weeks. Progressive cartilage degradation was evident in the OA group. Loss of trabeculae was observed after 2 weeks (square) followed by subchondral bone sclerosis after 6, and 10 weeks. Progressive osteophyte formation (arrow) was evident at 2, 6, and 10 weeks after OA induction. In the pre-emptive ALN treatment group there was less severe proteoglycan loss and less chondrocyte necrosis compared to the OA group. Pre-emptive treatment did not have a significant effect on the cartilage or osteophyte formation; however it prevented loss of subchondral trabeculae. Early ALN treatment (treatment started 2 weeks after OA induction) and delayed ALN treatment (treatment started 6 weeks after OA induction) did not prevent cartilage degradation or subchondral bone sclerosis. However, in the early ALN treatment group the osteophytes were in the form of cartilaginous outgrowths without bony transformation. Original magnification x 40.

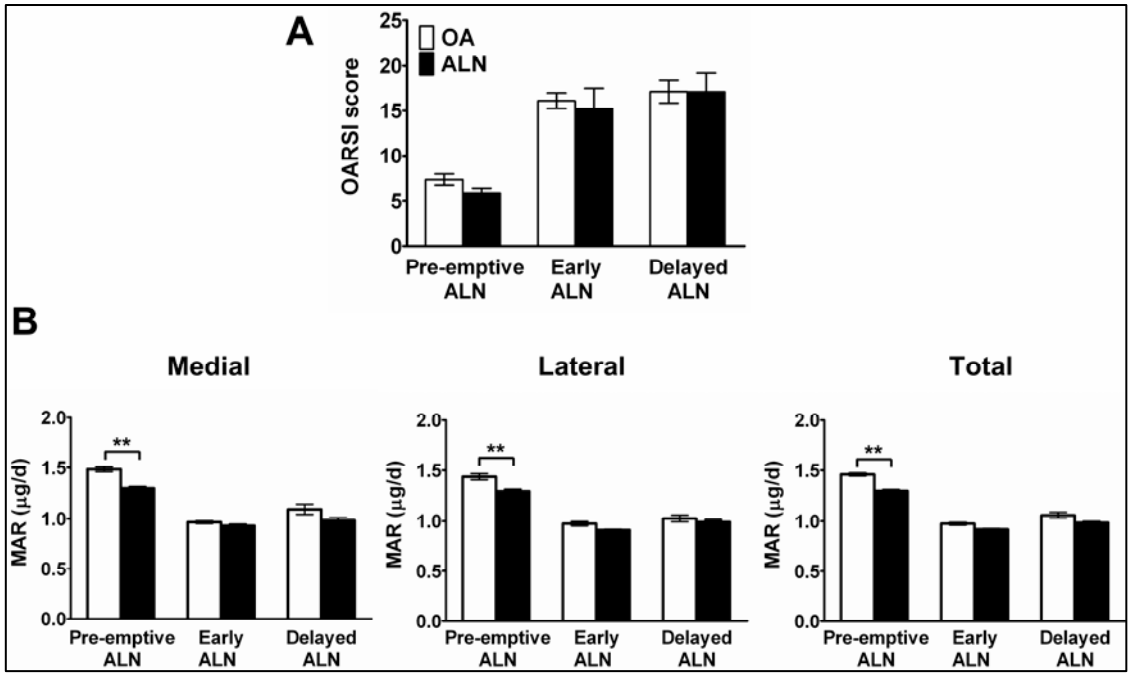

Figure 6A. OARSI scores of OA, pre-emptive ALN, early ALN, and delayed ALN groups. ALN treatment did not have a significant effect on OARSI score. Results are reported as mean ± SEM. * p<0.05 and ** p<0.01.

Figure 6B. Tibial subchondral trabecular bone mineral apposition rate (MAR) of OA, pre-emptive, early ALN, and delayed ALN groups. In the OA group, MAR was significantly increased at 2 weeks compared to, 6, and 10 weeks after OA induction. Pre-emptive ALN treatment significantly decreased MAR whereas, early ALN and delayed ALN treatment did not have a significant effect on MAR. Results are reported as mean ± SEM. * p<0.05 and ** p<0.01.

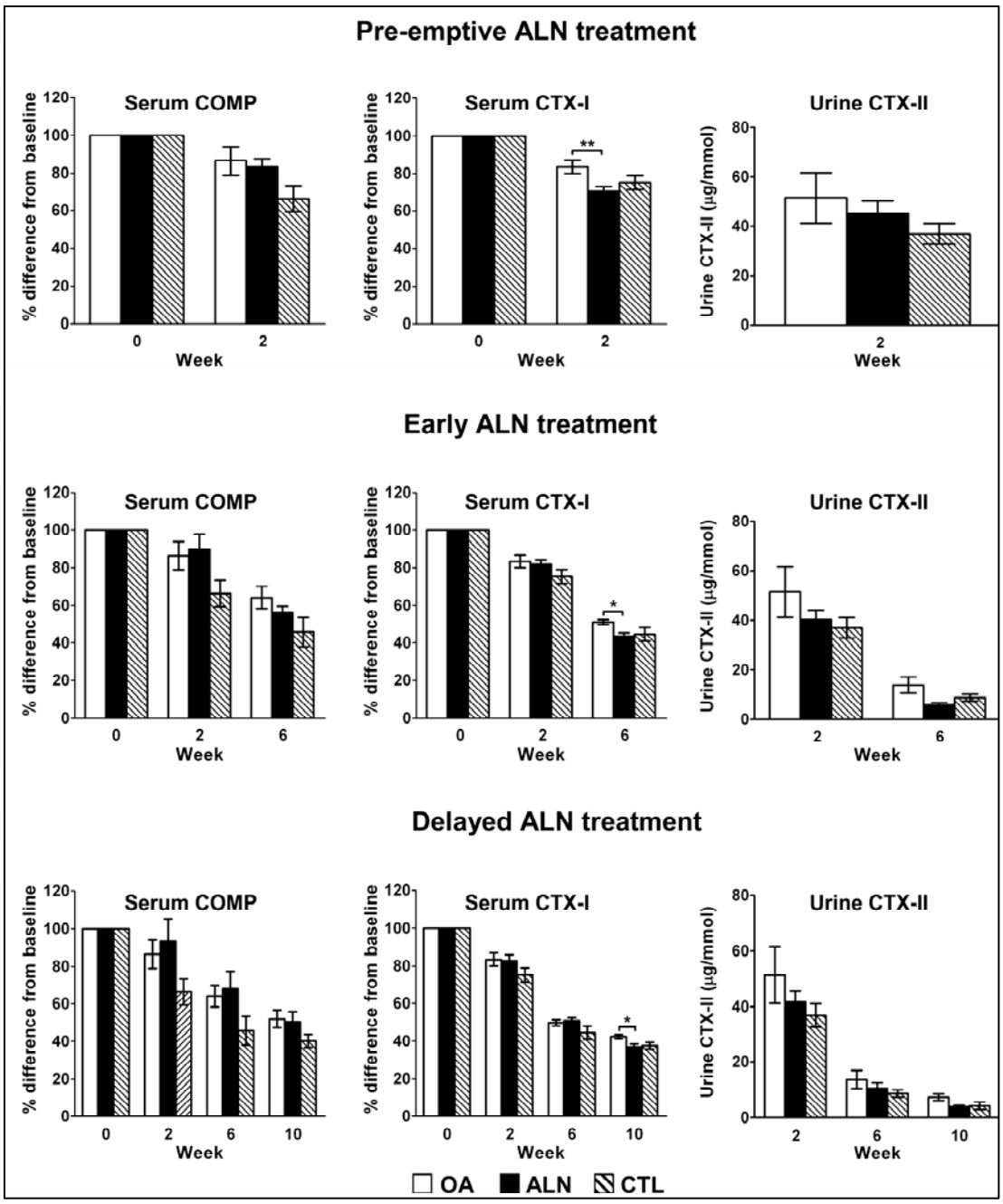

Figure 7. Serum COMP, CTX-I, and urine CTX-II levels of the OA group, pre-emptive ALN, early ALN, delayed ALN treatment groups and the control group. The pre-emptive, early, and delayed ALN treatment did not have a significant effect on serum COMP and urine CTX-II levels. However, they significantly suppressed serum CTX-I levels observed in the OA group. Results are reported as mean ± SEM. * $p<0.05$ and ** $p<0.01$.

Table 1 Tibial subchondral trabecular bone histomorphometric parameters in the pre-emptive ALN treatment group, at 2 weeks after ALN treatment initiation.

	2 Weeks (after ALN treatment)			
	OA	Contralateral control	%d OA-contralateral control	p-value
	mean ± SD	mean ± SD		
BV (mm^3)				
Medial	743 ± 68	785 ± 63	-5.3	0.570
Lateral	738 ± 74	771 ± 53	-4.3	0.234
Total	1480 ± 137	1555 ± 97	-4.8	0.360
BV/TV (%)				
Medial	20 ± 2	21 ± 2	-6.2	0.331
Lateral	18 ± 3	18 ± 1	-2.0	0.646
Total	19 ± 2	20 ± 1	-4.3	0.441
Tb.Th (μm)				
Medial	96 ± 3	93 ± 3	2.5	0.123
Lateral	89 ± 4	87 ± 2	2.6	0.108
Total	92 ± 3	90 ± 2	2.5	0.074
Tb.N (1/mm)				
Medial	2.1 ± 0.2	2.2 ± 0.1	-4.4	0.333
Lateral	2.0 ± 0.2	2.1 ± 0.1	-2.5	0.410
Total	2.1 ± 0.2	2.2 ± 0.1	-3.5	0.331
Tb.Sp (μm)				
Medial	257 ± 16	250 ± 9	2.7	0.381
Lateral	250 ± 9	247 ± 10	1.5	0.224
Total	254 ± 11	249 ± 8	2.1	0.299

Data reported as mean ± SD, % d is the percentage difference in values for tibial subchondral bone between the OA and contralateral control knee.

Table 2 Tibial subchondral trabecular bone histomorphometric parameters in the early ALN treatment group (treatment started 2 weeks after OA induction).

	2 Weeks				6 Weeks (after ALN treatment)			
	OA	Contralateral control	%d OA-contralateral control	p-value	OA	Contralateral control	%d OA-contralateral control	p-value
	mean ± SD	mean ± SD			mean ± SD	mean ± SD		
BV (mm^3)								
Medial	719 ± 118	868 ± 97	-17.2	0.001	1313 ± 195	1165 ± 132	12.7	0.011
Lateral	723 ± 89	818 ± 86	-11.6	0.002	1171 ± 162	1025 ± 126	14.2	0.003
Total	1442 ± 186	1686 ± 158	-14.5	0.001	2484 ± 297	2190 ± 237	13.4	0.003
BV/TV (%)								
Medial	20 ± 3	24 ± 3	-16.9	0.001	36 ± 5	32 ± 4	13.0	0.010
Lateral	17 ± 2	19 ± 2	-11.5	0.002	27 ± 4	24 ± 3	14.3	0.003
Total	18 ± 2	21 ± 2	-14.5	0.001	32 ± 4	28 ± 3	13.5	0.003
Tb.Th (μm)								
Medial	96 ± 3	94 ± 3	2.2	0.064	128 ± 12	104 ± 7	23.0	0.000
Lateral	90 ± 4	88 ± 2	2.1	0.089	108 ± 11	95 ± 3	13.9	0.003
Total	93 ± 3	91 ± 2	2.2	0.053	118 ± 10	99 ± 4	18.7	0.000
Tb.N (1/mm)								
Medial	2.0 ± 0.3	2.5 ± 0.2	-18.8	0.000	2.8 ± 0.2	2.9 ± 0.2	-3.3	0.152
Lateral	1.9 ± 0.2	2.2 ± 0.2	-13.5	0.001	2.5 ± 0.2	2.5 ± 0.3	0.5	0.857
Total	2.0 ± 0.2	2.3 ± 0.2	-16.3	0.000	2.7 ± 0.2	2.7 ± 0.2	-1.5	0.474
Tb.Sp (μm)								
Medial	262 ± 21	239 ± 8	9.7	0.004	234 ± 13	215 ± 13	8.8	0.013
Lateral	259 ± 15	242 ± 13	6.8	0.012	241 ± 11	228 ± 17	5.9	0.025
Total	260 ± 16	240 ± 9	8.2	0.004	237 ± 8	221 ± 13	7.3	0.015

Data reported as mean ± SD, % d is the percentage difference in values between the OA and contralateral control knee.

Table 3. Tibial subchondral trabecular bone histomorphometric parameters in the delayed ALN treatment group (treatment started 6 weeks after OA induction).

	2 Weeks				6 Weeks				10 Weeks (after ALN treatment)			
	OA	Contralateral control	%d		OA	Contralateral control	%d		OA	Contralateral control	%d	
	mean ± SD	mean ± SD		p-value	mean ± SD	mean ± SD		p-value	mean ± SD	mean ± SD		p-value
BV (mm^3)												
Medial	674 ± 85	791 ± 90	-14.7	0.004	1350 ± 136	1102 ± 105	22.5	0.003	1531 ± 251	1159 ± 156	32.1	0.005
Lateral	680 ± 52	767 ± 71	-11.4	0.006	1120 ± 112	1026 ± 70	9.2	0.018	1251 ± 176	1053 ± 88	18.8	0.006
Total	1354 ± 108	1558 ± 156	-13.1	0.004	2470 ± 182	2128 ± 137	16.1	0.001	2782 ± 307	2212 ± 195	25.8	0.000
BV/TV (%)												
Medial	19 ± 2	21 ± 2	-13.0	0.006	37 ± 4	30 ± 3	22.9	0.016	42 ± 7	32 ± 4	32.7	0.004
Lateral	16 ± 1	18 ± 2	-11.3	0.006	26 ± 3	24 ± 2	9.4	0.016	29 ± 4	25 ± 2	19.0	0.005
Total	17 ± 1	20 ± 2	-13.0	0.003	32 ± 2	27 ± 2	16.9	0.001	36 ± 4	28 ± 3	26.7	0.000
Tb.Th (μm)												
Medial	95 ± 5	95 ± 4	0.3	0.824	133 ± 7	107 ± 6	24.6	0.000	147 ± 13	107 ± 7	36.7	0.000
Lateral	89 ± 3	88 ± 3	0.9	0.347	112 ± 7	97 ± 4	15.4	0.000	119 ± 9	98 ± 4	21.0	0.000
Total	92 ± 4	92 ± 3	0.6	0.474	123 ± 5	102 ± 5	20.2	0.000	133 ± 9	103 ± 5	29.2	0.000
Tb.N (1/mm)												
Medial	2.0 ± 0.2	2.3 ± 0.2	-13.3	0.016	2.8 ± 0.2	2.8 ± 0.2	-1.5	0.675	2.8 ± 0.3	2.9 ± 0.3	-3.1	0.412
Lateral	1.8 ± 0.2	2.0 ± 0.2	-12.1	0.010	2.3 ± 0.2	2.5 ± 0.2	-5.2	0.239	2.5 ± 0.2	2.5 ± 0.2	-1.8	0.435
Total	1.9 ± 0.1	2.2 ± 0.2	-12.7	0.007	2.6 ± 0.2	2.6 ± 0.2	-3.2	0.244	2.7 ± 0.2	2.7 ± 0.2	-2.5	0.269
Tb.Sp (μm)												
Medial	271 ± 11	248 ± 12	9.4	0.000	239 ± 10	231 ± 13	3.5	0.062	239 ± 18	217 ± 18	10.3	0.006
Lateral	263 ± 19	247 ± 12	6.4	0.004	248 ± 19	233 ± 11	6.5	0.003	246 ± 21	229 ± 12	7.4	0.010
Total	267 ± 13	247 ± 12	7.9	0.000	244 ± 11	232 ± 11	5.0	0.002	243 ± 15	223 ± 13	8.8	0.001

Data reported as mean ± SD, % d is the percentage difference in values between the OA and contralateral control knee.

References

1. Buckwalter JA, Saltzman C, Brown T: **The impact of osteoarthritis: implications for research.** *Clin Orthop Relat Res* 2004**:**S6-15.
2. Radin EL, Rose RM: **Role of subchondral bone in the initiation and progression of cartilage damage.** *Clin Orthop Relat Res* 1986**:**34-40.
3. Lajeunesse D, Reboul P: **Subchondral bone in osteoarthritis: a biologic link with articular cartilage leading to abnormal remodeling.** *Curr Opin Rheumatol* 2003, **15:**628-633.
4. Bailey AJ, Mansell JP, Sims TJ, Banse X: **Biochemical and mechanical properties of subchondral bone in osteoarthritis.** *Biorheology* 2004, **41:**349-358.
5. Burr DB: **Anatomy and physiology of the mineralized tissues: role in the pathogenesis of osteoarthrosis.** *Osteoarthritis Cartilage* 2004, **12 Suppl A:**S20-30.
6. Cohen SB: **An update on bisphosphonates.** *Curr Rheumatol Rep* 2004, **6:**59-65.
7. Corrado A, Santoro N, Cantatore FP: **Extra-skeletal effects of bisphosphonates.** *Joint Bone Spine* 2007, **74:**32-38.
8. Buckland-Wright JC, Messent EA, Bingham CO, 3rd, Ward RJ, Tonkin C: **A 2 yr longitudinal radiographic study examining the effect of a bisphosphonate (risedronate) upon subchondral bone loss in osteoarthritic knee patients.** *Rheumatology (Oxford)* 2007, **46:**257-264.
9. Spector TD, Conaghan PG, Buckland-Wright JC, Garnero P, Cline GA, Beary JF, Valent DJ, Meyer JM: **Effect of risedronate on joint structure and symptoms of knee osteoarthritis: results of the BRISK randomized, controlled trial [ISRCTN01928173].** *Arthritis Res Ther* 2005, **7:**R625-633.
10. Bingham CO, 3rd, Buckland-Wright JC, Garnero P, Cohen SB, Dougados M, Adami S, Clauw DJ, Spector TD, Pelletier JP, Raynauld JP, et al: **Risedronate decreases biochemical markers of cartilage degradation but does not decrease symptoms or slow radiographic progression in patients with medial compartment osteoarthritis of the knee: results of the two-year multinational knee osteoarthritis structural arthritis study.** *Arthritis Rheum* 2006, **54:**3494-3507.
11. Carbone LD, Nevitt MC, Wildy K, Barrow KD, Harris F, Felson D, Peterfy C, Visser M, Harris TB, Wang BW, Kritchevsky SB: **The relationship of antiresorptive drug use to structural findings and symptoms of knee osteoarthritis.** *Arthritis Rheum* 2004, **50:**3516-3525.
12. Neogi T, Nevitt MC, Ensrud KE, Bauer D, Felson DT: **The effect of alendronate on progression of spinal osteophytes and disc space narrowing.** *Ann Rheum Dis* 2008.
13. Hayami T, Pickarski M, Wesolowski GA, McLane J, Bone A, Destefano J, Rodan GA, Duong le T: **The role of subchondral bone remodeling in osteoarthritis: reduction of cartilage degeneration and prevention of osteophyte formation by alendronate in the rat anterior cruciate ligament transection model.** *Arthritis Rheum* 2004, **50:**1193-1206.
14. Shirai T, Kobayashi M, Nishitani K, Satake T, Kuroki H, Nakagawa Y, Nakamura T: **Chondroprotective effect of alendronate in a rabbit model of osteoarthritis.** *J Orthop Res* 2011, **29:**1572-1577.

15. Zhang L, Hu H, Tian F, Song H, Zhang Y: **Enhancement of subchondral bone quality by alendronate administration for the reduction of cartilage degeneration in the early phase of experimental osteoarthritis.** *Clin Exp Med* 2011, **11:**235-243.
16. Kwan Tat S, Lajeunesse D, Pelletier JP, Martel-Pelletier J: **Targeting subchondral bone for treating osteoarthritis: what is the evidence?** *Best Pract Res Clin Rheumatol* 2010, **24:**51-70.
17. Strassle BW, Mark L, Leventhal L, Piesla MJ, Jian Li X, Kennedy JD, Glasson SS, Whiteside GT: **Inhibition of osteoclasts prevents cartilage loss and pain in a rat model of degenerative joint disease.** *Osteoarthritis Cartilage* 2010, **18:**1319-1328.
18. Mohan G, Perilli E, Kuliwaba JS, Humphries JM, Parkinson IH, Fazzalari NL: **Application of in vivo micro-computed tomography in the temporal characterisation of subchondral bone architecture in a rat model of low-dose monosodium iodoacetate-induced osteoarthritis.** *Arthritis Res Ther* 2011, **13:**R210.
19. Perilli E, Le V, Ma B, Salmon P, Reynolds K, Fazzalari NL: **Detecting early bone changes using in vivo micro-CT in ovariectomized, zoledronic acid-treated, and sham-operated rats.** *Osteoporos Int* 2010, **21:**1371-1382.
20. Perilli E, Baruffaldi F, Bisi MC, Cristofolini L, Cappello A: **A physical phantom for the calibration of three-dimensional X-ray microtomography examination.** *Journal of Microscopy* 2006, **222:**124-134.
21. Bove SE, Calcaterra SL, Brooker RM, Huber CM, Guzman RE, Juneau PL, Schrier DJ, Kilgore KS: **Weight bearing as a measure of disease progression and efficacy of anti-inflammatory compounds in a model of monosodium iodoacetate-induced osteoarthritis.** *Osteoarthritis Cartilage* 2003, **11:**821-830.
22. Pomonis JD, Boulet JM, Gottshall SL, Phillips S, Sellers R, Bunton T, Walker K: **Development and pharmacological characterization of a rat model of osteoarthritis pain.** *Pain* 2005, **114:**339-346.
23. Guingamp C, Gegout-Pottie P, Philippe L, Terlain B, Netter P, Gillet P: **Mono-iodoacetate-induced experimental osteoarthritis: a dose-response study of loss of mobility, morphology, and biochemistry.** *Arthritis Rheum* 1997, **40:**1670-1679.
24. Pritzker KP, Gay S, Jimenez SA, Ostergaard K, Pelletier JP, Revell PA, Salter D, van den Berg WB: **Osteoarthritis cartilage histopathology: grading and staging.** *Osteoarthritis Cartilage* 2006, **14:**13-29.
25. Frost HM (Ed.). **Bone histomorphometry: Analysis of trabecular bone dynamics**. Florida: CRC Press, Inc.; 1983.
26. Holm S: **A Simple Sequentially Rejective Multiple Test Procedure.** *Scandinavian Journal of Statistics* 1979, **6:**65-70.
27. Dempster DW: **The contribution of trabecular architecture to cancellous bone quality.** *J Bone Miner Res* 2000, **15:**20-23.
28. Bobinac D, Spanjol J, Zoricic S, Maric I: **Changes in articular cartilage and subchondral bone histomorphometry in osteoarthritic knee joints in humans.** *Bone* 2003, **32:**284-290.
29. Chappard C, Peyrin F, Bonnassie A, Lemineur G, Brunet-Imbault B, Lespessailles E, Benhamou CL: **Subchondral bone micro-architectural alterations in osteoarthritis: a synchrotron micro-computed tomography study.** *Osteoarthritis Cartilage* 2006, **14:**215-223.

30. Fazzalari NL, Parkinson IH: **Femoral trabecular bone of osteoarthritic and normal subjects in an age and sex matched group.** *Osteoarthritis Cartilage* 1998, **6:**377-382.
31. Botter SM, van Osch GJ, Waarsing JH, Day JS, Verhaar JA, Pols HA, van Leeuwen JP, Weinans H: **Quantification of subchondral bone changes in a murine osteoarthritis model using micro-CT.** *Biorheology* 2006, **43:**379-388.
32. Ding M, Danielsen CC, Hvid I: **Age-related three-dimensional microarchitectural adaptations of subchondral bone tissues in guinea pig primary osteoarthrosis.** *Calcif Tissue Int* 2006, **78:**113-122.
33. Lahm A, Kreuz PC, Oberst M, Haberstroh J, Uhl M, Maier D: **Subchondral and trabecular bone remodeling in canine experimental osteoarthritis.** *Arch Orthop Trauma Surg* 2006, **126:**582-587.
34. Brouwers JE, Lambers FM, Gasser JA, van Rietbergen B, Huiskes R: **Bone degeneration and recovery after early and late bisphosphonate treatment of ovariectomized wistar rats assessed by in vivo micro-computed tomography.** *Calcif Tissue Int* 2008, **82:**202-211.
35. Mashiba T, Turner CH, Hirano T, Forwood MR, Johnston CC, Burr DB: **Effects of suppressed bone turnover by bisphosphonates on microdamage accumulation and biomechanical properties in clinically relevant skeletal sites in beagles.** *Bone* 2001, **28:**524-531.
36. Compston J: **Pathophysiology of atypical femoral fractures and osteonecrosis of the jaw.** *Osteoporos Int* 2011, **22:**2951-2961.
37. Rodan GA, Seedor JG, Balena R: **Preclinical pharmacology of alendronate.** *Osteoporos Int* 1993, **3 Suppl 3:**S7-12.
38. Sahni M, Guenther HL, Fleisch H, Collin P, Martin TJ: **Bisphosphonates act on rat bone resorption through the mediation of osteoblasts.** *J Clin Invest* 1993, **91:**2004-2011.
39. Vitte C, Fleisch H, Guenther HL: **Bisphosphonates induce osteoblasts to secrete an inhibitor of osteoclast-mediated resorption.** *Endocrinology* 1996, **137:**2324-2333.
40. Rodan GA, Martin TJ: **Role of osteoblasts in hormonal control of bone resorption--a hypothesis.** *Calcif Tissue Int* 1981, **33:**349-351.
41. Alvarez L, Peris P, Guanabens N, Vidal S, Ros I, Pons F, Filella X, Monegal A, Munoz-Gomez J, Ballesta AM: **Serum osteoprotegerin and its ligand in Paget's disease of bone: relationship to disease activity and effect of treatment with bisphosphonates.** *Arthritis Rheum* 2003, **48:**824-828.
42. Dobnig H, Hofbauer LC, Viereck V, Obermayer-Pietsch B, Fahrleitner-Pammer A: **Changes in the RANK ligand/osteoprotegerin system are correlated to changes in bone mineral density in bisphosphonate-treated osteoporotic patients.** *Osteoporos Int* 2006, **17:**693-703.
43. Kwan Tat S, Pelletier JP, Lajeunesse D, Fahmi H, Lavigne M, Martel-Pelletier J: **The differential expression of osteoprotegerin (OPG) and receptor activator of nuclear factor kappaB ligand (RANKL) in human osteoarthritic subchondral bone osteoblasts is an indicator of the metabolic state of these disease cells.** *Clinical and experimental rheumatology* 2008, **26:**295-304.
44. Jones MD, Tran CW, Li G, Maksymowych WP, Zernicke RF, Doschak MR: **In vivo microfocal computed tomography and micro-magnetic resonance imaging evaluation of antiresorptive and antiinflammatory drugs as preventive treatments of osteoarthritis in the rat.** *Arthritis Rheum* 2010, **62:**2726-2735.

45. Saag KG: **Bisphosphonates for osteoarthritis prevention: "Holy Grail" or not?** *Ann Rheum Dis* 2008, **67:**1358-1359.
46. Ivanavicius SP, Ball AD, Heapy CG, Westwood FR, Murray F, Read SJ: **Structural pathology in a rodent model of osteoarthritis is associated with neuropathic pain: increased expression of ATF-3 and pharmacological characterisation.** *Pain* 2007, **128:**272-282.
47. Felson DT, Chaisson CE, Hill CL, Totterman SM, Gale ME, Skinner KM, Kazis L, Gale DR: **The association of bone marrow lesions with pain in knee osteoarthritis.** *Annals of internal medicine* 2001, **134:**541-549.
48. Abramson S, Krasnokutsky S: **Biomarkers in osteoarthritis.** *Bull NYU Hosp Jt Dis* 2006, **64:**77-81.
49. Bettica P, Cline G, Hart DJ, Meyer J, Spector TD: **Evidence for increased bone resorption in patients with progressive knee osteoarthritis: longitudinal results from the Chingford study.** *Arthritis Rheum* 2002, **46:**3178-3184.

CHAPTER 4

Alendronate modulates gene expression of osteoprotegerin and receptor activator of nuclear factor κB ligand in subchondral bone in the early phase of experimental osteoarthritis

Geetha Mohan, Le-Hoa Truong, Ian H Parkinson, Egon Perilli, Nicola L Fazzalari and Julia S Kuliwaba

Bone and Joint Research Laboratory, Directorate of Surgical Pathology, SA Pathology and Hanson Institute, Frome Road, Adelaide, SA 5000, Australia

Discipline of Anatomy and Pathology, School of Medical Sciences, The University of Adelaide, Adelaide, SA 5005, Australia

Experimental Biology and Medicine 2012; submitted paper

STATEMENT OF AUTHORSHIP

Alendronate modulates gene expression of osteoprotegerin and receptor activator of nuclear factor κB ligand in subchondral bone in the early phase of experimental osteoarthritis

Experimental Biology and Medicine 2012: submitted paper

Geetha Mohan (Candidate)

Performed analysis on all samples, interpreted data, wrote manuscript and acted as corresponding author

I hereby certify that the statement of contribution is accurate

Signed

....Date...16/02/2012

Le-Hoa Truong

Data interpretation and manuscript evaluation

Certification that the statement of contribution is accurate and permission is given for the inclusion of the paper in the thesis

Signed

....Date...16/2/12

Ian H. Parkinson

Contributed to planning of article and provided critical evaluation

I hereby certify that the statement of contribution is accurate and I give permission for the inclusion of the paper in the thesis

Signed

....Date...21/2/12

Egon Perilli

Contributed to planning of article, and provided critical evaluation

Certification that the statement of contribution is accurate and permission is given for the inclusion of the paper in the thesis

Signed

....Date...24/02/2012

Nicola L. Fazzalari

Supervised development of work and manuscript evaluation

I hereby certify that the statement of contribution is accurate and I give permission for the inclusion of the paper in the thesis

Signed

....Date...6/3/2012

Julia S. Kuliwaba

Supervised development of work, helped in data interpretation and manuscript evaluation

I hereby certify that the statement of contribution is accurate and I give permission for the inclusion of the paper in the thesis

Signed

…… ……Date.29/2/12

Alendronate modulates gene expression of osteoprotegerin and receptor activator of nuclear factor κB ligand in subchondral bone in the early phase of experimental osteoarthritis

Geetha Mohan[1,2], Le-Hoa Truong[1], Ian H Parkinson[1,2], Egon Perilli[1,2], Nicola L Fazzalari[1,2] and Julia S Kuliwaba[1,2]

[1]Bone and Joint Research Laboratory, Directorate of Surgical Pathology, SA Pathology and Hanson Institute, Frome Road, Adelaide, SA 5000, Australia; [2]Discipline of Anatomy and Pathology, School of Medical Sciences, The University of Adelaide, Adelaide, SA 5005, Australia

Running title: Alendronate on RANKL/OPG in OA

Key words: Osteoarthritis; OA animal model; alendronate; subchondral bone; OPG; RANKL

E-mail addresses: geetha.mohan@adelaide.edu.au; lena.truong@health.sa.gov.au; ian.parkinson@health.sa.gov.au; egon.perilli@adelaide.edu.au; nick.fazzalari@health.sa.gov.au; julia.kuliwaba@health.sa.gov.au

Corresponding author:

Geetha Mohan (geetha.mohan@adelaide.edu.au)

Bone and Joint Research Laboratory, Directorate of Surgical Pathology,

SA Pathology, Frome Road, Adelaide, SA 5000, Australia

ABSTRACT

Subchondral bone remodelling plays a critical role in the pathophysiology of osteoarthritis (OA). The RANK/RANKL/OPG nexus that tightly controls bone remodelling is known to be differentially regulated in OA. Bisphosphonates are potent inhibitors of bone resorption/remodelling and are used for the treatment of human osteoporosis. In this study, the effect of alendronate (ALN) on distal femoral subchondral bone RANK, RANKL and OPG mRNA expression was determined in a low-dose monosodium iodoacetate (MIA)-induced OA rat model. Male Wistar rats were randomly divided into three groups: OA, ALN, and control group. Rats (OA and the ALN group) were injected with 0.2 mg MIA in the right knee and sterile saline in the left knee joint (contralateral control). Rats in the ALN group received pre-emptive (day 0 – end of week 2), early (end of week 2 – end of week 6), or delayed (end of week 6 – end of week 10) ALN treatment (30 μg/kg/week). The control rats received a single sterile saline injection in the right knee joint and no ALN treatment. The rats were sacrificed at 2, 6 and 10 weeks and total RNA was extracted from the distal femoral subchondral bone. RANK, RANKL, and OPG mRNA expression was determined by real-time RT-PCR analyses. RANK mRNA expression did not differ significantly between the three groups. Pre-emptive ALN treatment significantly reduced RANKL mRNA expression and the RANKL/OPG mRNA ratio, which was significantly increased in the OA group at 2 weeks compared to the control group. Early ALN treatment significantly decreased RANKL mRNA expression at 6 weeks compared to the OA group. In conclusion, alendronate treatment decreases the RANKL/OPG mRNA ratio and thereby inhibits subchondral bone resorption in the early stage of OA. Targeting subchondral bone offers a potential treatment option for OA and warrants further investigation.

Introduction

Osteoarthritis (OA) is the most common joint disease and a major cause of disability with high socioeconomic costs in Western society. It is a complex disease affecting the whole joint, involving the cartilage, subchondral bone, synovial membrane, and meniscus.[1] OA is characterised by altered subchondral bone remodelling. Altered bone remodelling leads to new bone formation, subchondral bone sclerosis, which is hypomineralized and osteophyte formation.[2] These bone related changes are driven by altered osteoblastic and osteoclastic activity which are closely associated with cartilage degeneration,[3] leading to disease progression. Hence, subchondral bone remodelling has become an important target for OA treatment in recent years.[4, 5]

It is known that bone remodelling is tightly controlled by the molecular triad consisting of osteoprotegerin (OPG), receptor activator of nuclear factor κB (RANK) and its ligand RANKL.[6] RANKL is synthesised primarily by the osteoblasts and activates its receptor, RANK, expressed on osteoclasts to stimulate osteoclastogenesis. Thus, the RANK-RANKL binding is essential for osteoclast formation, activation, survival and promotes bone resorption. In the bone microenvironment, OPG is secreted as a soluble protein by the cells of the osteoblast lineage. It is a decoy receptor for RANKL that inhibits osteoclast differentiation, activation, induces osteoclast apoptosis, and thus modulates bone resorption.[7] The RANK/RANKL/OPG nexus has been shown to play a major role in bone pathologies such as osteoporosis, rheumatoid arthritis, metastatic bone tumours, and Paget's disease.[8] Altered levels of RANKL and OPG are also known to be involved in human OA.[9] Increased serum RANKL/OPG ratio was found to be correlated with disease severity in human OA,[10] and enhanced expression of RANKL mRNA was reported in human OA subchondral bone osteoblasts.[11] Logar et al. reported a

significantly higher expression of cathepsin K, MMP-9, osteocalcin, and TRAP relative to RANKL in the proximal femur of an osteoarthritic group compared to a fracture group, which pointed towards increased bone turnover in OA.[12] Thus, the RANK/RANKL/OPG nexus has important clinical implications in the pathology of OA, and is a potential therapeutic target in the development of treatment for OA.

Alendronate (ALN) is a nitrogen containing bisphosphonate and one of the most potent inhibitors of osteoclast mediated bone resorption.[13] Bisphosphonates have been shown to alter bone remodelling in osteoporosis and Paget's disease by modulating the RANK/RANKL/OPG nexus.[14, 15] Clinical trials[16, 17] and pre-clinical studies[18, 19] have shown that ALN treatment decreases subchondral bone remodelling and protects the cartilage in OA. We have previously shown that pre-emptive ALN prevented early tibial subchondral bone loss and suppressed increased bone turnover in a low-dose monosodium iodoacetate (MIA)-induced OA rat model.[20] However, the effect of ALN treatment on the RANK/RANKL/OPG nexus in OA is not clear. In the present study, we hypothesised that ALN can prevents an increase of subchondral bone remodelling by modulating the RANK/RANKL/OPG nexus in a low-dose MIA-induced OA rat model. Moreover, differential mRNA expression of RANK, RANKL, and OPG has not yet been characterised at different stages of OA progression. This is the first study to look at the differential gene expression of RANK, RANKL, and OPG in a low-dose MIA-induced OA rat model. In addition, we determined the effect of pre-emptive, early, and delayed ALN treatment on OA subchondral bone RANK, RANKL, and OPG gene expression in this rat model.

Materials and Methods

Animals and OA induction

The distal femoral subchondral bone used for target gene expression analysis in this study was collected from male Wistar rats used in our previous study.[a] Eight-week old young adult male Wistar rats ≈ 230g (Animal Resource Centre, Canning Vale, WA, Australia) were kept in a sanitary ventilated animal room with controlled temperature (20 - 24°C), a light-dark cycle (12h/12h) with food and water available ad libitum. They were closely monitored and daily clinical record sheets were completed throughout the duration of the study by the animal care facility staff.

The rats were divided into three groups: OA (n=36), ALN treatment (n=36) and control (n=12). On day 0, all the rats were anaesthetized with isofluroane and were given a single intra-articular injection of 0.2 mg MIA through the infrapatellar ligament of the right knee. MIA was dissolved in sterile physiologic saline and administered in a volume of 50µl using a 26-gauge 0.5-inch needle. The left contralateral control knee was injected with 50µl of sterile physiologic saline. The control rats were given a single sterile saline injection on the right knee while the left knee was un-injected. The control rats did not receive ALN treatment. The animal handling and experimental procedures were carried out in accordance with The University of Adelaide Animal Ethics Committee and The Institute of Medical and Veterinary Science Animal Ethics Committee.

[a] Geetha Mohan, Egon Perilli, Ian H Parkinson, Julia M Humphries, Nicola L Fazzalari and Julia S Kuliwaba. *Pre-emptive, early, and delayed alendronate treatment in a rat model of low-dose monosodium iodoacetate induced osteoarthritis: effect on subchondral trabecular bone microarchitecture, cartilage degradation, bone and cartilage turnover, and joint discomfort*. 2012. Manuscript submitted for publication

Alendronate treatment

Thirty-six rats were treated with ALN administered as twice-weekly subcutaneous injections at a dosage of 15μg/kg. The ALN solution was made by dissolving one tablet of Alendronate (Fosamax 40 mg, MSD, South Granville, NSW, Australia) in 100 ml of sterile water. The solution was stirred for 2 hours and then diluted with sterile physiologic saline to appropriate concentrations to obtain the required dose as above.

The ALN treatment regime used in this study is as follows:

4. Pre-emptive ALN treatment group (n=12) – treatment started from day 0 to end of week 2.
5. Early ALN treatment group (n=12) – treatment started from end of week 2 (day 14) to end of week 6.
6. Delayed ALN treatment group (n=12) – treatment started from end of week 6 (day 42) to end of week 10.

Tissue preparation

As part of a previous study[a] by our group, the left and right hind limbs of all the rats were imaged with high-resolution in vivo micro-CT, with scanning details explained elsewhere.[21] The first subgroup of rats from the OA group, pre-emptive ALN treatment group, and control group, was scanned at week 2. The second subgroup of rats from the OA group, early ALN treatment group, and control group, was scanned after 2 weeks and 6 weeks. The third subgroup of rats from the OA group, delayed ALN treatment group, and control group, were scanned after week 2, 6, and 10. Histomorphometric parameters such as bone volume (BV), bone volume fraction (BV/TV) and trabecular number (Tb.N) were determined for the proximal tibial subchondral bone, as described

previously.[21] The rats of the first subgroup, second subgroup and third subgroup were then sacrificed at 2, 6, and 10 weeks post-MIA injection, respectively, with CO2 overdose. Both the right and left femur from all the rats were dissected using sterile instruments. The articular cartilage was carefully dissected away from the distal femur and incisions were made along the epiphyseal line of the distal femur to remove the subchondral bone using a sterile scalpel. The subchondral bone sampled for total RNA isolation consisted of the subchondral plate and subchondral trabecular bone.

Total RNA isolation and cDNA synthesis

The isolated distal femoral subchondral bone was crushed in liquid nitrogen using a sterile RNase-free mortar and pestle. The crushed bone specimens were mixed with 1 ml of Trizol (Invitrogen, Carlsbad, CA, USA) and stored at -80ºC until RNA was extracted. Total RNA was isolated from the distal femoral subchondral bone using a modified phenol/chloroform extraction method.[22, 23] The homogenized bone samples in Trizol were thawed at room temperature for 5 minutes, and then centrifuged at 12,000g for 10 min at 4ºC. The supernatant was removed and mixed with chloroform and centrifuged at 12,000g for 15 min at 4ºC. Following centrifugation, the aqueous phase containing RNA was transferred to sterile RNase-free eppendorf tubes and mixed with 5µl of glycogen/ml of Trizol to improve the yield of RNA. Then isopropanol was added to this mixture and stored at -20ºC overnight to precipitate the RNA. The following day, the specimens were thawed at room temperature for 10 minutes and centrifuged at 12,000g for 20 min at 4ºC. The supernatant was removed and the pellet containing the RNA was washed with 75% ethanol and centrifuged at 12,000g for 10 min at 4ºC. The supernatant was removed and the pellet was dried on a heating block at 37º for 2 – 3 minutes. The RNA was redissolved in DEPC water and stored at -80ºC. The RNA

specimens were quantified and checked for purity with a Nanodrop 1000 spectrophotometer (Thermo Fisher Scientific, Wilmington, DE, USA). The samples with a 260/280 ratio of 1.9 - 2.0 were used for reverse transcription (RT). RNA was reverse transcribed from 1 μg of total RNA from each sample, using a first-strand cDNA synthesis kit with Superscript III, (Invitrogen, Carlsbad, CA, USA, Cat No. 18080085) and 250 ng random hexamer primer (Geneworks, Adelaide, SA, Australia, Cat No. RP-6), according to the manufacturer's instructions.

Real-time RT-PCR

RANK, RANKL, OPG and glyceraldehyde-3-phosphate dehydrogenase (GAPDH) mRNA expression were analysed by real-time RT-PCR using the SYBR Green incorporation technique.[24] The cDNA was amplified using iQ SYBR Green Supermix (BioRad, Hercules, CA, USA) on a Rotor-Gene 6000 (Corbett Life Science, Sydney, NSW, Australia). The PCR reaction settings were as follows: 94ºC for 15 min, followed by 40 cycles at 94ºC (30 s), at 60ºC (30 s), and at 72ºC (30 s). This was followed by an additional extension step at 72ºC for 4 min. All PCR reactions were validated by the presence of a single peak in the melt curve analysis and confirmation of a single amplified specific product by agarose gel electrophoresis. Relative expression between samples was calculated using the comparative cycle threshold (CT) method (ΔCT).[25] All the PCR reactions were performed in triplicates. The housekeeping gene GAPDH was used as the reference gene and the target gene expression CT values were normalised to the expression of GAPDH. The primer sequences used are listed in Table 1.

Statistical Analysis

Analysis of variance (ANOVA) of multiple groups was performed to compare gene expression levels using a one-way ANOVA followed by Tukey's post hoc test. Non-parametric data were analysed with the Kruskal-Wallis test with Dunn's multiple comparison test (GraphPad Prism version 5.03 for Windows, San Diego, CA, USA). For all statistical tests, a P value less than 0.05 was considered statistically significant.

Results

The mRNA corresponding to each of the target genes was expressed in the distal femoral subchondral bone of the OA, the ALN treatment and the control groups. First, the difference in target gene mRNA expression within each group (OA, ALN treatment and control group) was assessed between time points (2, 6, and 10 weeks). Then, the difference in target gene mRNA expression between the groups at each time point was assessed. The target gene expression between the right saline injected knee and left un-injected knee in the control group did not differ significantly ($p>0.05$ for all genes, data not shown). Moreover, we did not find any statistically significant difference in target gene expression between the right or left knee of the control group and the contralateral control knee from the OA and the ALN treatment groups ($p>0.05$ for all genes, data not shown). Therefore, for the control group, gene expression data of the right and left knee at each time point was combined for comparison with the MIA-injected knee of the OA group and the ALN treatment groups.

Target gene expression within the OA group

The RANK mRNA expression did not differ statistically between the MIA-injected knee and the contralateral control knee, and over time (Fig. 1A). The RANK mRNA expression levels were significantly lower, compared to RANKL at 2 and 6 weeks ($p<0.001$ and $p<0.01$ respectively) and compared to OPG mRNA expression levels, at 2, 6, and 10 weeks ($p<0.05$, $p<0.001$ and $p<0.001$ respectively). At 2 weeks, there was a non-significant increase in RANKL mRNA expression in the MIA-injected knee compared to contralateral control knee. The RANKL mRNA expression significantly decreased over time for both the MIA-injected and the contralateral control knee (Fig. 1B). The OPG mRNA expression of the MIA-injected knee was significantly decreased compared to the contralateral control knee at 2 and 6 weeks post-MIA injection. There was no statistically significant difference in the OPG mRNA expression over time in the MIA-injected knee. In the contralateral control knee, the OPG mRNA expression was significantly increased at 6 weeks compared to 10 week (Fig. 1C). The RANKL/OPG mRNA ratio of the MIA-injected knee was significantly increased compared to the contralateral control knee at 2 weeks. The RANKL/OPG mRNA ratio significantly decreased over time in both the MIA-injected and the contralateral control knee (Fig. 1D).

Target gene expression within the ALN treatment group

The RANK mRNA expression did not differ statistically between the MIA-injected knee and the contralateral control knee in any of the ALN treatment groups. However, the RANK mRNA expression of the contralateral control knee was significantly decreased in the delayed ALN treatment group, compared to the pre-emptive ALN treatment group (Fig. 1E). The RANKL, OPG mRNA expression, and the

RANKL/OPG mRNA ratio did not differ significantly between the MIA-injected knee and the contralateral control knee in any of the ALN treatment groups (Fig. 1F – H). The RANKL mRNA of the MIA-injected knee was significantly increased in the pre-emptive ALN treatment group compared to the early ALN treatment group. In the early ALN treatment group, the OPG mRNA expression of the MIA-injected knee was significantly increased whereas; the RANKL/OPG mRNA ratio was significantly decreased compared to the pre-emptive and the delayed ALN treatment group.

Effect of ALN treatment on RANK, RANKL, and OPG mRNA expression

Pre-emptive ALN, early ALN, or delayed ALN treatment did not alter the RANK mRNA expression levels significantly (Fig. 2A). In addition, there was no statistically significant difference in the RANK mRNA expression between the OA, the ALN treatment, and the control groups over time. At 2 weeks, pre-emptive treatment significantly decreased the RANKL mRNA expression relative to the OA group (Fig. 2B). Early ALN treatment significantly decreased the RANKL mRNA expression relative to the control group whereas; at 10 weeks the RANKL mRNA expression of the delayed ALN treatment group was significantly increased compared to the OA and the control group (Fig. 2B). The OPG mRNA levels were non-significantly increased in the pre-emptive ALN and the early ALN treatment group relative to the OA group (Fig. 2C). Delayed ALN treatment did not have a significant effect on OPG mRNA expression. When we looked at the effect of ALN on the RANKL/OPG mRNA ratio, it was found to be significantly decreased by pre-emptive ALN treatment. At 6 weeks although not statistically significant, the RANKL/OPG mRNA ratio of the early ALN treatment group was decreased; whereas, the ratio of the delayed ALN treatment group was non-significantly increased compared to the OA and the control group (Fig 2D).

Effect of ALN on tibial subchondral bone histomorphometric parameters

Bone histomorphometric analysis (micro-CT) from previous study[a] showed that in the pre-emptive ALN group, BV, BV/TV and Tb.N did not differ significantly while Tb.Sp was significantly increased relative to the control group. BV and BV/TV was significantly increased whereas, Tb.N was non-significantly increased and Tb.Sp was significantly lower relative to the OA group. In the early ALN group, at 6 weeks (4 weeks after ALN treatment initiation), BV, BV/TV, and Tb.Th were significantly increased whereas, Tb.N and Tb.Sp did not differ significantly relative to the control group. Compared to the OA group, there was no significant difference in BV and BV/TV and Tb.Th whereas, Tb.N was significantly increased and Tb.Th and Tb.Sp was significantly decreased in the early ALN treatment group. In the delayed treatment group, at 10 weeks (4 weeks after ALN treatment initiation), Tb.Th and Tb.Sp was significantly increased relative to the control group. There was no significant difference in the histomorphometric parameters between the OA group and the delayed ALN treatment group.

Discussion

Bisphosphonates inhibit bone resorption and are used in the treatment of bone pathologies with increased osteoclast mediated bone resorption [13]. Studies using animal models have shown that OA is associated with increased bone resorption in the early stage followed by sclerosis.[21, 26] In a low-dose MIA-induced OA rat model, we observed increased subchondral bone resorption 2 weeks after MIA injection followed by subchondral bone sclerosis 6 and 10 weeks after MIA-injection (Fig. 3).[21] In the present study, we have characterised RANK, RANKL and OPG mRNA expression at early, intermediate, and late stages of OA disease progression in a low-dose MIA-induced OA

rat model. We assessed the effect of ALN treatment on distal femoral subchondral bone in this animal model. This is the first study to report the effect of time-course ALN on differential gene expression of RANK, RANKL, and OPG in different stages of OA in a low-dose MIA-induced OA rat model.

The structural data reported for the MIA-injected knee at 2, 6 and 10 weeks after OA induction in our previous study [21] coincides with gene expression data reported for the MIA-injected knee in the present study. The significantly increased RANKL mRNA expression and RANKL/OPG mRNA ratio in the subchondral bone of distal femur at 2 weeks in the MIA-injected knee reflects the significantly decreased subchondral BV and BV/TV observed in the tibia of the MIA-injected knee. Similarly at 10 weeks after OA induction, the RANKL mRNA expression and the RANKL/OPG mRNA ratio was significantly decreased compared to 2 weeks which suggested decreased osteoclastic activity that reflects the significantly increased bone tibial subchondral BV and BV/TV in the MIA-injected knee reported in our previous study.

Target gene expression analysis in this animal model revealed increased RANKL mRNA expression, decreased OPG mRNA expression and increased RANKL/OPG mRNA ratio, in the OA group at 2 weeks compared to the control group. The RANKL/OPG ratio is an indicator of bone resorptive status[27] and the increased RANKL/OPG ratio at 2 weeks in this animal model is indicative of increased bone resorption (Fig. 3). This finding strongly supports our previous findings of significantly decreased BV, BV/TV and Tb.N at 2 weeks after MIA injection in the tibial subchondral bone of this animal model.[21] At 10 weeks corresponding to advanced stage OA, we found a non-significant increase in the tibial subchondral bone volume and

bone volume fraction compared to control.[21] However, in the gene expression analysis we did not find a significant difference in RANK, RANKL or OPG mRNA expression in the distal femoral subchondral bone between the OA and control group at 10 weeks. This suggests that other molecular signalling systems such as the canonical β-catenin Wnt pathway, Cathepsin K, and hedgehog pathway could be involved in addition to the RANK, RANKL, and OPG system at advanced stages of the disease.[28, 29] Recently, the Wnt signalling pathway has been identified to contribute to the pathogenesis of OA.[30] Altered Wnt signalling has been shown in human and experimental OA.[24, 31]

The increase in RANKL expression observed in the present study is in line with previous literature. Increased RANKL expression was reported in human osteoblasts isolated from knee OA subchondral bone,[11] and Tat et al. reported increased RANKL mRNA expression in human OA subchondral bone osteoblasts secreting low prostaglandin E_2 (PGE_2).[32] This suggests a strong role for RANKL and OPG in altered bone remodelling in OA. We have previously shown that in end-stage human hip OA, RANK, RANKL and OPG expression is disrupted and there is an increase in osteocalcin gene expression indicating increased osteoblastic activity.[23, 33] This shows altered bone remodelling with an imbalance in osteoclastic and osteoblastic activity in OA.

Bisphosphonates exert their direct effect on osteoclasts by inhibiting the osteoclast mevalonate pathway that leads to abnormal osteoclast morphology and function resulting in impaired bone resorption.[34] The proposed mechanism of ALN action is as follows: ALN binds to hydroxyapatite crystals in the bone matrix, and then is ingested by osteoclasts during bone resorption. The ingested ALN becomes cytotoxic to

osteoclasts, which interferes with ruffled border formation necessary for bone resorption.[35, 36] Later, Sahni et al. showed that part of the inhibitory action of bisphosphonates on osteoclasts is mediated through osteoblasts. They showed that osteoclast-resorbing activity was inhibited when osteoclasts isolated from rat femur were cocultured with bisphosphonate-treated CRP 10/ 30 cells (rat osteoblast cell line). However, the inhibitory effect was not evident when the osteoclasts were treated with bisphosphonate for 5 min and subsequently cocultured with untreated CRP 10/30 cells.[37] In the present study, we did not observe a significant change in RANK mRNA expression in the OA, ALN, and control group. Moreover, pre-emptive ALN treatment significantly decreased the RANKL mRNA expression and the OPG mRNA expression was non-significantly increased in the pre-emptive ALN and early ALN treatment groups. These data suggests that ALN may have an effect on osteoblast activity in addition to its direct effects on osteoclasts.

In a rat anterior cruciate ligament transection (ACLT) model of OA, ALN treatment lead to reduced the number of osteoclasts and suppressed bone loss. In that animal model, ALN treatment not only prevented bone loss by reducing the number of osteoclasts but also affected the normal morphology and function of the osteoclasts.[18] In a rabbit ACLT model of OA, bone loss with an increased number of osteoclasts was observed at 12 weeks. In that animal model, ALN treatment significantly prevented the bone loss by reducing the osteoclast number in the tibia however, a small number of osteoclasts were still present in the femur.[38] In the high-dose MIA (1 mg) rat model, increased osteoclastic activity at the bone-cartilage interface and subchondral bone was observed. Pre-emptive zoledronic acid treatment prevented bone and cartilage erosion and early zoledronic acid treatment significantly reduced bone and cartilage erosion,

thereby improving joint integrity.[39] In the present study, we were unable to look at the osteoclastic activity by TRAP staining due to technical difficulties. However, close observation of the Safranin O/Fast green stained sections showed the presence of increased osteoclastic activity in the tibial subchondral bone in the MIA-injected tibia. Focal areas of resorbed bone were lined by active osteoblasts (Fig. 4).

In our previous study, we have shown that ALN treatment decreased tibial subchondral bone loss, bone turnover rate, mineral apposition rate, and preserved subchondral bone microarchitecture.[a] The cellular mechanism of the therapeutic benefit of ALN in this animal model appears to be via modulation of osteoblast activity. We found that pre-emptive ALN treatment effectively suppressed increased RANKL mRNA expression, and the RANKL/OPG mRNA ratio. Pre-emptive ALN treatment also non-significantly increased OPG mRNA expression, when compared to the OA group. Early ALN treatment decreased the RANKL mRNA expression but the delayed ALN treatment did not have an effect (Fig. 2). However, there was no change in RANK mRNA expression in any of the groups. This is in line with a previous study by Pan et al. which showed that human osteoblast-like cells from human OA specimens exposed to zoledronic acid treatment markedly increased OPG secretion and reduced transmembrane RANKL protein expression even though the gene expression was not significantly altered.[40] Similarly, Eslami et al. reported that the RANKL/OPG mRNA ratio was significantly reduced in bone marrow cell cultures from hip OA patients who were receiving ALN treatment at the time of surgery compared to controls. Moreover, there was a 50% decrease in RANKL/OPG ratio measured in marrow stromal cells from control subjects treated with ALN for 3 days in cell culture.[41] The authors also showed that *in vivo* ALN treatment decreased *in vitro* differentiation of bone marrow cells to develop into

osteoclasts. Another study reported that primary cultures of human osteoblasts from hip OA patients treated with ALN for 24 hours did not show significant change in OPG or RANKL mRNA expression from baseline.[42] Such discrepancies in the reported efficacy of ALN treatment on RANKL and OPG mRNA expression could be due to use of different cell culture techniques in different studies.

In the delayed ALN treatment group we found significantly increased RANKL mRNA expression compared to the OA and control groups which was unexpected. A study by Enjuanes et al. reported that human primary osteoblast cultures from hip OA patients treated with ALN and vitamin D for 72 hours did not have an effect on OPG gene expression but increased RANKL gene expression.[43] The authors speculate that the increase in RANKL mRNA expression could be due to the addition of endogenous vitamin D. Increased number of osteoclasts and formation of giant osteoclasts have been reported previously in osteoporotic women on bisphosphonate therapy.[44] In the present study, although we do not have an explanation for the unexpected increase in RANKL mRNA expression of delayed ALN treatment group, presence of giant osteoclasts with impaired resorptive activity that could have contributed to the increased RANKL mRNA expression in the distal femur needs to be confirmed with TRAP staining.

A main limitation of the present study is that we only looked at the RANK, RANKL, and OPG mRNA expression in the subchondral bone. Immunohistochemical localisation of these cytokines in this animal model would have given more information about the expression of these cytokines at the protein level. Moreover, human OA chondrocytes have also been shown to express RANK, RANKL and OPG.[45, 46] This shows that the RANK, RANKL, and OPG cytokine system intricately controls bone and

cartilage metabolism. Further studies are needed to investigate the effect of ALN on chondrocyte RANK, RANKL, and OPG expression.

Conclusion

In summary, we have demonstrated that RANKL and OPG mRNA are differentially expressed in OA. The increased RANKL mRNA expression and increased RANKL/OPG mRNA ratio that favour bone resorption is likely to contribute to the increased subchondral bone loss observed at 2 weeks (early OA) in the low-dose MIA-induced OA rat model. In addition, this study suggests that the action of ALN on subchondral bone resorption in OA could be by decreasing the RANKL and OPG mRNA expression by osteoblasts. Bisphosphonates may therefore be a promising therapeutic alternative to inhibit bone resorption and thereby preserve the structural integrity of subchondral bone in early stage OA. This study has demonstrated that targeting subchondral bone remodelling is a potential treatment option for the management of OA and warrants further investigation.

Abbreviations

OA: osteoarthritis; RANK: receptor activator of nuclear factor κB; RANKL: receptor activator of nuclear factor κB ligand; OPG: osteoprotegerin; GAPDH: glyceraldehyde-3-phosphate dehydrogenase; MIA: monosodium iodoacetate; ALN: alendronate; MMP: matrix metalloproteinase; TRAP: tartrate-resistant acid phosphatase; Micro-CT: micro computed tomography; RT: reverse transcription; CT: cycle threshold; BV: bone volume; BV/TV: bone volume fraction; Tb.N: trabecular number

Competing interests

The authors declare that they have no competing interests.

Authors' contributions

GM had a major input in the experimental design, conducted all experimental procedures, performed data collection, statistical analysis, graphical presentation of the data collected, and prepared the manuscript for submission. JSK, IHP, and NLF were involved in the experimental design, contributed to the interpretation of the data collected and preparation of the manuscript; LHT was involved in designing the primers, RNA isolation and data interpretation; EP was involved in data analysis and interpretation; all authors have participated in the preparation of the manuscript, and have approved the final version.

Funding source

GM is the recipient of Endeavour postgraduate scholarship from the Australian Government, Department of Education, Employment, and Workplace Relations (DEEWR). This study was supported in part by funding from SA Pathology, Adelaide, SA, Australia.

Acknowledgement

The authors thank Dr Allan Rofe for kindly providing the MIA, Dr Dorota Gancarz for assistance with the animal model, Mrs Yolandi Starzak for help with histology, Mr Andrew Bert (Division of Human Immunology, Centre for Cancer Biology, SA Pathology, Adelaide) for his assistance in validating PCR products on gel and for his advice on RT-PCR analysis, and the Institute of Medical and Veterinary Science (IMVS) animal care facility staff.

Figures

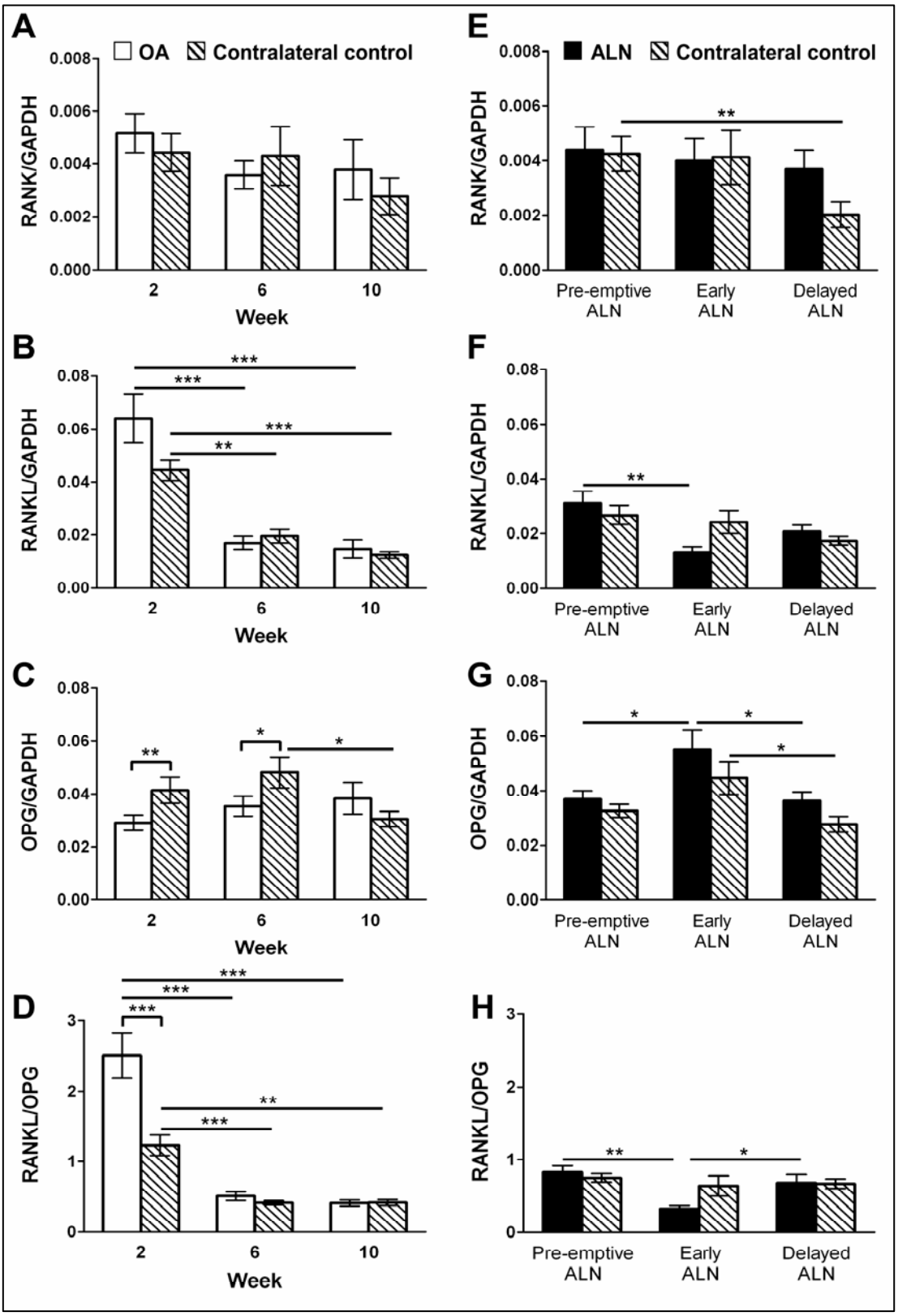

Figure 1. RANK, RANKL, and OPG mRNA expression within the OA group and ALN treatment group. Data are shown as mean ±SEM. ** p<0.01, *** p<0.001

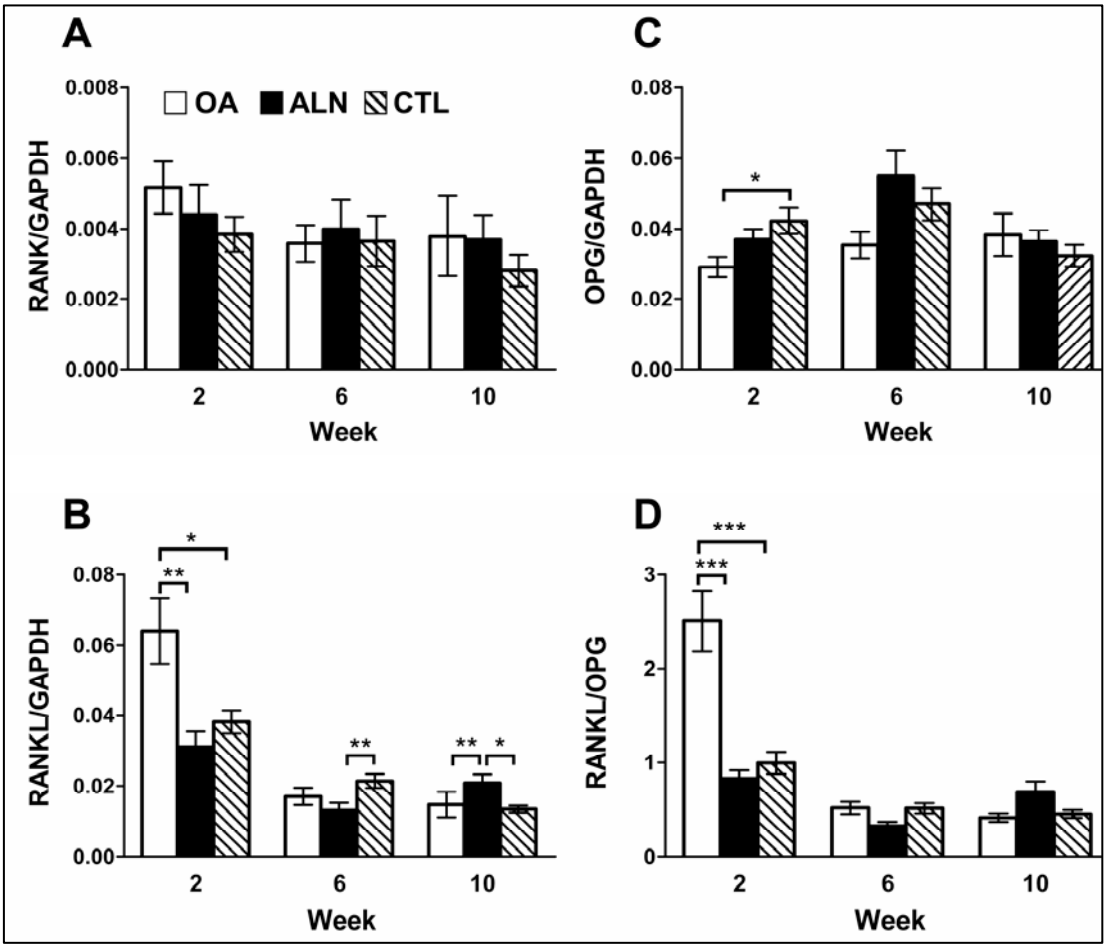

Figure 2. RANK, RANKL, and OPG mRNA expression between the OA group, ALN treatment group and control group. Black bar at 2, 6 and 10 weeks represents pre-emptive ALN, early ALN and delayed ALN treatment group respectively. Data are shown as mean ±SEM. ** p<0.01, *** p<0.001

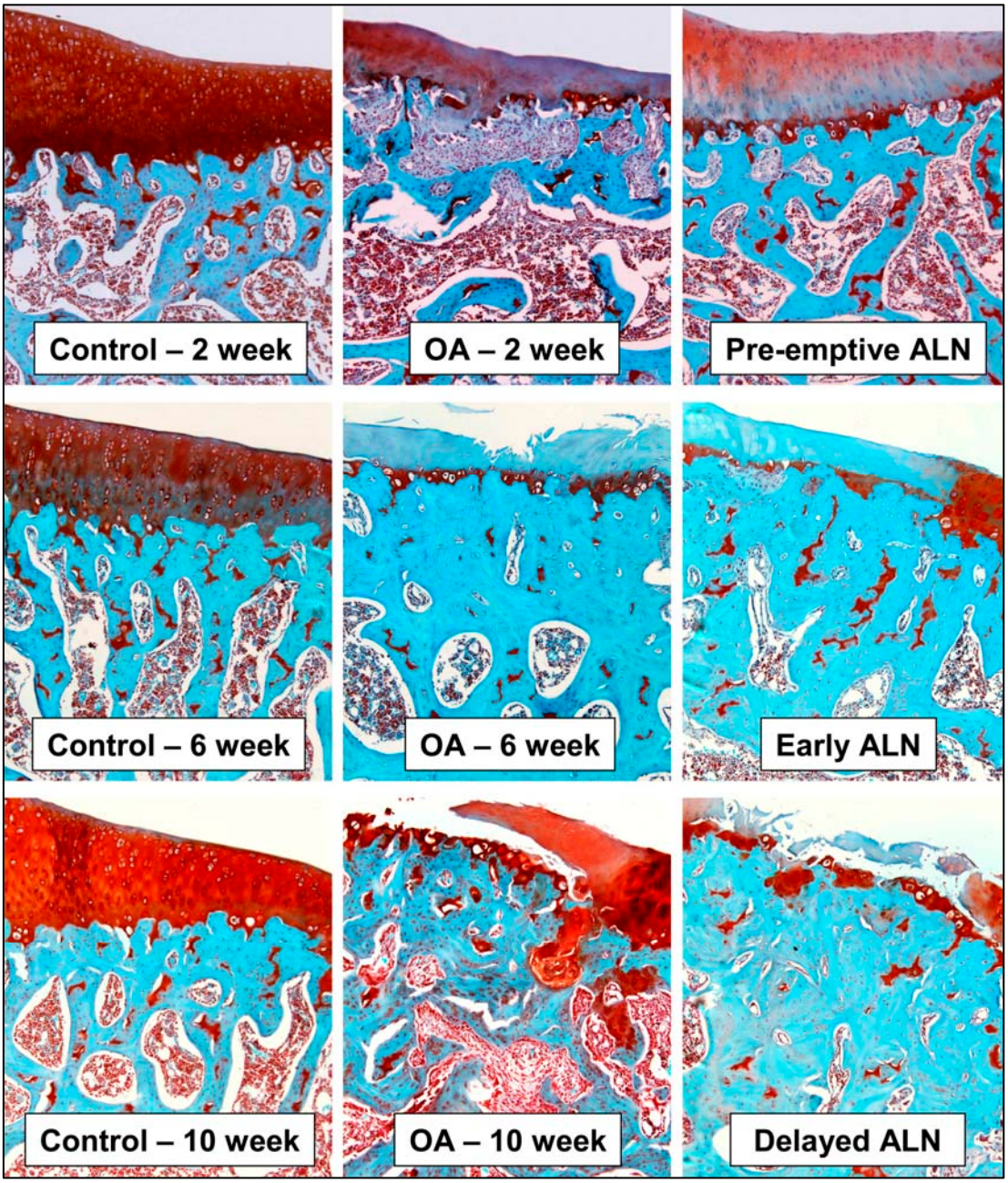

Figure 3. Safranin O/Fast green stained sections showing articular cartilage and subchondral bone of proximal tibia (medial plateau) from control, OA, and ALN treatment group after 2, 6, and 10 weeks of injection. In the OA group, there was progressive cartilage degeneration with increased subchondral bone resorption after 2 weeks followed by sclerosis after 6 and 10 weeks of MIA injection. Pre-emptive ALN treatment partially prevented proteoglycan loss and cartilage degradation and prevented subchondral bone resorption after 2 weeks of treatment. In both the early ALN and delayed ALN treatment group, cartilage degradation and subchondral bone sclerosis was evident after 6 and 10 weeks of MIA injection. Original magnification x 40.

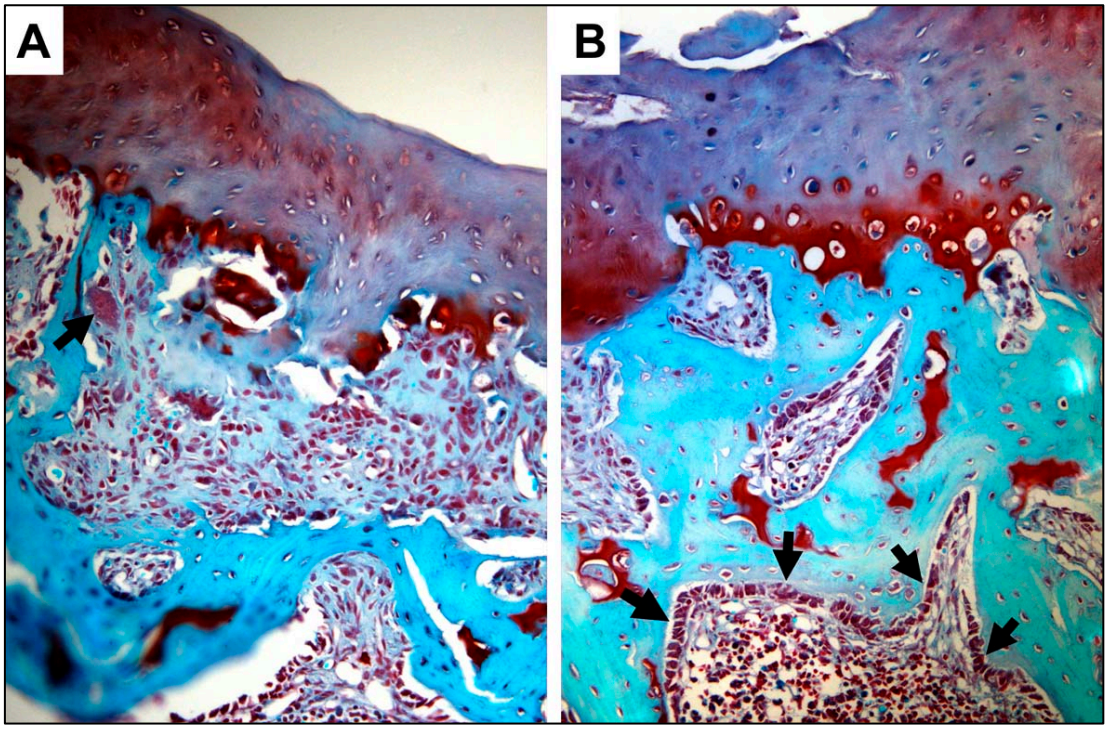

Figure 4. Safranin O/Fast green stained sections articular cartilage and subchondral bone of proximal tibia (medial plateau) from OA group, 2 weeks after MIA injection. Tibia from MIA-injected knee showed increased osteoclastic and osteoblast activity suggesting increased subchondral bone turnover. Note the presence of large osteoclast-like cell (A, arrow) in the large resorptive areas filled with fibrotic bone marrow and reactive osteoblasts (B, arrow) lining the focal areas of subchondral bone resorption. Original magnification x 100.

Table 1 Primers of targeted genes

Targeted genes	Sequence (5′ → 3′)*	Amplicon length (bp)	Accession number
OPG	F: ATTGGCTGAGTGTTCTGGT	142	NM012870
	R: CTGGTCTCTGTTTTGATGC		
RANK	F: CAGCCTGGAAGCAGATCGACA	121	XM573424
	R: AAGTCGCAGCCTTCGGAATC		
RANKL	F: TCGCTCTGTTCCTGTACT	147	NM057149
	R: AGTGCTTCTGTGTCTTCG		
GAPDH	F: CTCTTGTGACAAAGTGGAC	103	NM017008
	R: TGAACTTGCCGTGGGTGA		

OPG, osteoprotegerin; RANK, receptor activator of nuclear factor κB; RANKL, receptor activator of nuclear factor κB ligand; GAPDH, glyceraldehyde-3-phosphate dehydrogenase.

*F = forward; R = reverse.

References

1. Martel-Pelletier J, Pelletier JP. Is osteoarthritis a disease involving only cartilage or other articular tissues? *Eklem Hastalik Cerrahisi* 2010;**21**:2-14.
2. Bailey AJ, Mansell JP, Sims TJ, Banse X. Biochemical and mechanical properties of subchondral bone in osteoarthritis. *Biorheology* 2004;**41**:349-58.
3. Lajeunesse D, Reboul P. Subchondral bone in osteoarthritis: a biologic link with articular cartilage leading to abnormal remodeling. *Curr Opin Rheumatol* 2003;**15**:628-33.
4. Kwan Tat S, Lajeunesse D, Pelletier JP, Martel-Pelletier J. Targeting subchondral bone for treating osteoarthritis: what is the evidence? *Best Pract Res Clin Rheumatol* 2010;**24**:51-70.
5. Lajeunesse D. The role of bone in the treatment of osteoarthritis. *Osteoarthritis Cartilage* 2004;**12 Suppl A**:S34-8.
6. Boyce BF, Xing L. Functions of RANKL/RANK/OPG in bone modeling and remodeling. *Arch Biochem Biophys* 2008;**473**:139-46.
7. Khosla S. Minireview: the OPG/RANKL/RANK system. *Endocrinology* 2001;**142**:5050-5.
8. Kearns AE, Khosla S, Kostenuik PJ. Receptor activator of nuclear factor kappaB ligand and osteoprotegerin regulation of bone remodeling in health and disease. *Endocr Rev* 2008;**29**:155-92.
9. Tat SK, Pelletier JP, Velasco CR, Padrines M, Martel-Pelletier J. New perspective in osteoarthritis: the OPG and RANKL system as a potential therapeutic target? *Keio J Med* 2009;**58**:29-40.
10. Pilichou A, Papassotiriou I, Michalakakou K, Fessatou S, Fandridis E, Papachristou G, et al. High levels of synovial fluid osteoprotegerin (OPG) and increased serum ratio of receptor activator of nuclear factor-kappaB ligand (RANKL) to OPG correlate with disease severity in patients with primary knee osteoarthritis. *Clin Biochem* 2008;**8**:8.
11. Sakao K, Takahashi KA, Mazda O, Arai Y, Tonomura H, Inoue A, et al. Enhanced expression of interleukin-6, matrix metalloproteinase-13, and receptor activator of NF-kappaB ligand in cells derived from osteoarthritic subchondral bone. *J Orthop Sci* 2008;**13**:202-10.
12. Logar DB, Komadina R, Prezelj J, Ostanek B, Trost Z, Marc J. Expression of bone resorption genes in osteoarthritis and in osteoporosis. *J Bone Miner Metab* 2007;**25**:219-25.
13. Vasikaran SD. Bisphosphonates: an overview with special reference to alendronate. *Ann Clin Biochem* 2001;**38**:608-23.
14. Alvarez L, Peris P, Guanabens N, Vidal S, Ros I, Pons F, et al. Serum osteoprotegerin and its ligand in Paget's disease of bone: relationship to disease activity and effect of treatment with bisphosphonates. *Arthritis Rheum* 2003;**48**:824-8.
15. Dobnig H, Hofbauer LC, Viereck V, Obermayer-Pietsch B, Fahrleitner-Pammer A. Changes in the RANK ligand/osteoprotegerin system are correlated to changes in bone mineral density in bisphosphonate-treated osteoporotic patients. *Osteoporos Int* 2006;**17**:693-703.
16. Carbone LD, Nevitt MC, Wildy K, Barrow KD, Harris F, Felson D, et al. The relationship of antiresorptive drug use to structural findings and symptoms of knee osteoarthritis. *Arthritis Rheum* 2004;**50**:3516-25.

17. Lehmann HJ, Mouritzen U, Christgau S, Cloos PA, Christiansen C. Effect of bisphosphonates on cartilage turnover assessed with a newly developed assay for collagen type II degradation products. *Ann Rheum Dis* 2002;**61**:530-3.
18. Hayami T, Pickarski M, Wesolowski GA, McLane J, Bone A, Destefano J, et al. The role of subchondral bone remodeling in osteoarthritis: reduction of cartilage degeneration and prevention of osteophyte formation by alendronate in the rat anterior cruciate ligament transection model. *Arthritis Rheum* 2004;**50**:1193-206.
19. Zhang L, Hu H, Tian F, Song H, Zhang Y. Enhancement of subchondral bone quality by alendronate administration for the reduction of cartilage degeneration in the early phase of experimental osteoarthritis. *Clin Exp Med* 2011;**11**:235-43.
20. Mohan G, Perilli E, Kuliwaba JS, Parkinson IH, Humphries JH, Fazzalari NL. Alendronate treatment reduces tibial subchondral bone damage in early-stage osteoarthritis: An in vivo micro-CT study in a rodent model. *Osteoporos Int*. [Meeting Abstract] 2011;**22**:S579.
21. Mohan G, Perilli E, Kuliwaba JS, Humphries JM, Parkinson IH, Fazzalari NL. Application of in vivo micro-computed tomography in the temporal characterisation of subchondral bone architecture in a rat model of low-dose monosodium iodoacetate-induced osteoarthritis. *Arthritis Res Ther* 2011;**13**:R210.
22. Chomczynski P, Sacchi N. Single-step method of RNA isolation by acid guanidinium thiocyanate-phenol-chloroform extraction. *Anal Biochem* 1987;**162**:156-9.
23. Kuliwaba JS, Findlay DM, Atkins GJ, Forwood MR, Fazzalari NL. Enhanced expression of osteocalcin mRNA in human osteoarthritic trabecular bone of the proximal femur is associated with decreased expression of interleukin-6 and interleukin-11 mRNA. *J Bone Miner Res* 2000;**15**:332-41.
24. Hopwood B, Tsykin A, Findlay DM, Fazzalari NL. Microarray gene expression profiling of osteoarthritic bone suggests altered bone remodelling, WNT and transforming growth factor-beta/bone morphogenic protein signalling. *Arthritis Res Ther* 2007;**9**:R100.
25. Pfaffl MW. A new mathematical model for relative quantification in real-time RT-PCR. *Nucleic Acids Res* 2001;**29**:e45.
26. Hayami T, Pickarski M, Zhuo Y, Wesolowski GA, Rodan GA, Duong le T. Characterization of articular cartilage and subchondral bone changes in the rat anterior cruciate ligament transection and meniscectomized models of osteoarthritis. *Bone* 2006;**38**:234-43.
27. Hofbauer LC, Kuhne CA, Viereck V. The OPG/RANKL/RANK system in metabolic bone diseases. *J Musculoskelet Neuronal Interact* 2004;**4**:268-75.
28. Beyer C, Schett G. Pharmacotherapy: concepts of pathogenesis and emerging treatments. Novel targets in bone and cartilage. *Best Pract Res Clin Rheumatol* 2010;**24**:489-96.
29. Funck-Brentano T, Cohen-Solal M. Crosstalk between cartilage and bone: when bone cytokines matter. *Cytokine Growth Factor Rev* 2011;**22**:91-7.
30. Luyten FP, Tylzanowski P, Lories RJ. Wnt signaling and osteoarthritis. *Bone* 2009;**44**:522-7.
31. Blom AB, Brockbank SM, van Lent PL, van Beuningen HM, Geurts J, Takahashi N, et al. Involvement of the Wnt signaling pathway in experimental and human osteoarthritis: prominent role of Wnt-induced signaling protein 1. *Arthritis Rheum* 2009;**60**:501-12.
32. Kwan Tat S, Pelletier JP, Lajeunesse D, Fahmi H, Lavigne M, Martel-Pelletier J. The differential expression of osteoprotegerin (OPG) and receptor activator of

nuclear factor kappaB ligand (RANKL) in human osteoarthritic subchondral bone osteoblasts is an indicator of the metabolic state of these disease cells. *Clin Exp Rheumatol* 2008;**26**:295-304.
33. Fazzalari NL, Kuliwaba JS, Atkins GJ, Forwood MR, Findlay DM. The ratio of messenger RNA levels of receptor activator of nuclear factor kappaB ligand to osteoprotegerin correlates with bone remodeling indices in normal human cancellous bone but not in osteoarthritis. *J Bone Miner Res* 2001;**16**:1015-27.
34. Fisher JE, Rodan GA, Reszka AA. In vivo effects of bisphosphonates on the osteoclast mevalonate pathway. *Endocrinology* 2000;**141**:4793-6.
35. Rodan GA, Seedor JG, Balena R. Preclinical pharmacology of alendronate. *Osteoporos Int* 1993;**3 Suppl 3**:S7-12.
36. Sato M, Grasser W, Endo N, Akins R, Simmons H, Thompson DD, et al. Bisphosphonate action. Alendronate localization in rat bone and effects on osteoclast ultrastructure. *J Clin Invest* 1991;**88**:2095-105.
37. Sahni M, Guenther HL, Fleisch H, Collin P, Martin TJ. Bisphosphonates act on rat bone resorption through the mediation of osteoblasts. *J Clin Invest* 1993;**91**:2004-11.
38. Shirai T, Kobayashi M, Nishitani K, Satake T, Kuroki H, Nakagawa Y, et al. Chondroprotective effect of alendronate in a rabbit model of osteoarthritis. *J Orthop Res* 2011;**29**:1572-7.
39. Strassle BW, Mark L, Leventhal L, Piesla MJ, Jian Li X, Kennedy JD, et al. Inhibition of osteoclasts prevents cartilage loss and pain in a rat model of degenerative joint disease. *Osteoarthritis Cartilage* 2010;**18**:1319-28.
40. Pan B, Farrugia AN, To LB, Findlay DM, Green J, Lynch K, et al. The nitrogen-containing bisphosphonate, zoledronic acid, influences RANKL expression in human osteoblast-like cells by activating TNF-alpha converting enzyme (TACE). *J Bone Miner Res* 2004;**19**:147-54.
41. Eslami B, Zhou S, Van Eekeren I, LeBoff MS, Glowacki J. Reduced osteoclastogenesis and RANKL expression in marrow from women taking alendronate. *Calcif Tissue Int* 2011;**88**:272-80.
42. Giner M, Rios MJ, Montoya MJ, Vazquez MA, Miranda C, Perez-Cano R. Alendronate and raloxifene affect the osteoprotegerin/RANKL system in human osteoblast primary cultures from patients with osteoporosis and osteoarthritis. *Eur J Pharmacol* 2011;**650**:682-7.
43. Enjuanes A, Ruiz-Gaspa S, Peris P, Ozalla D, Alvarez L, Combalia A, et al. The effect of the alendronate on OPG/RANKL system in differentiated primary human osteoblasts. *Endocrine* 2010;**37**:180-6.
44. Weinstein RS, Roberson PK, Manolagas SC. Giant osteoclast formation and long-term oral bisphosphonate therapy. *N Engl J Med* 2009;**360**:53-62.
45. Kwan Tat S, Amiable N, Pelletier JP, Boileau C, Lajeunesse D, Duval N, et al. Modulation of OPG, RANK and RANKL by human chondrocytes and their implication during osteoarthritis. *Rheumatology (Oxford)* 2009;**48**:1482-90.
46. Upton AR, Holding CA, Dharmapatni AA, Haynes DR. The expression of RANKL and OPG in the various grades of osteoarthritic cartilage. *Rheumatol Int* 2011.

CHAPTER 5

General Discussion

5 Discussion

OA is a complex multifactorial disease affecting the whole joint and the etiopathology of this disease is poorly understood. Currently there is no cure for OA and the treatment available is limited to patients who present with symptomatic disease. OA treatment aims at alleviating symptoms of OA and joint replacement is the only option for patients with advanced OA. So far, cartilage has been the main focus of OA research as OA was considered primarily as a cartilage disorder. However, remarkable research findings from the last three decades have clearly shown a strong role for subchondral bone in the pathogenesis of OA and have opened new avenues for OA drug development (Burr and Radin 2003, Day et al. 2004, Dieppe 1999, Kwan Tat et al. 2010, Radin and Rose 1986).

Image analysis using micro-CT in human OA studies and animal models has advanced our knowledge of subchondral bone changes and its contribution to the progression of cartilage degradation in OA. In pre-clinical studies, *in vivo* micro-CT has been instrumental to accurately detect and quantify bony changes in three dimensions (3D). Despite progress in OA research, there is a lack of understanding regarding early initiating events in OA and the underlying molecular mechanisms. This is because obtaining tissue samples from early OA patients is very difficult and human OA is mostly diagnosed in its advanced stages.

5.1 Overview of study findings

In the first part of this thesis (**Chapter 2**) the tissue level changes in the subchondral bone and cartilage during the early, intermediate and advanced stages of OA were studied in a low-dose (0.2 mg) MIA-induced OA rat model. I*n vivo* micro-CT analysis showed increased bone loss at the early stage of OA (2 weeks after OA induction) followed by increased subchondral bone thickness, decreased trabecular number and increased trabecular separation at the intermediate and advanced stages of OA (6 and 10 weeks after OA induction). Subchondral plate thickness was increased at 2 and 6 weeks, while the porosity was increased at all time points. Other important features such as osteophytes and subchondral bone cysts were evident. Histological analysis showed progressive cartilage degradation with total loss of cartilage and exposure of subchondral bone at the advanced stage of OA. Another key finding was that there was no change in serum C-reactive protein (CRP) level, a marker of systemic inflammation, in the MIA-injected rats compared to age matched control rats and over time.

After characterising the animal model, the hypothesis that subchondral bone remodelling inhibition had an effect on cartilage changes was tested (**Chapter 3**). This was achieved by investigating the effect of alendronate on OA subchondral bone, cartilage, bone and cartilage turnover and pain, with treatment initiated at various time points of the disease. This approach indicated that the time point of initiating bisphosphonate treatment for OA influences outcome and explains the discrepancies observed in clinical trials. In this study, pre-emptive ALN treatment was started on the day of OA induction. Two weeks of pre-emptive ALN treatment preserved the subchondral trabecular bone microarchitecture and inhibited increased bone turnover associated with the onset of OA. Pre-emptive treatment had a moderate effect on the

cartilage degradation. Both early and delayed ALN treatment prevented loss of trabeculae and decreased bone turnover, but did not have a significant effect on cartilage degradation.

Finally, the RANK/RANKL/OPG nexus, the regulator of bone remodelling responsible for increased subchondral bone remodelling in OA was characterised and the effect of alendronate was investigated using the low-dose MIA-induced OA rat model (**Chapter 4**). In the OA group, RANKL mRNA expression and RANKL/OPG mRNA ratio were significantly increased at 2 weeks in the distal femoral subchondral bone. OPG mRNA expression was significantly decreased at 2 and 6 weeks after MIA-injection. Pre-emptive and early ALN treatment significantly decreased the RANKL mRNA expression, RANKL/OPG mRNA ratio and non-significantly increased OPG mRNA expression. This shows that pre-emptive and early alendronate treatment significantly decreased osteoclast mediated bone resorption in this animal model.

5.2 Comparison to existing literature

Small animal models of OA are invaluable tools to investigate the pathophysiology of OA and they provide tissue samples at various stages of the disease. A single intra-articular injection of MIA into the rat's knee joint induced OA-like changes in both the cartilage and subchondral bone (Guingamp et al. 1997, Guzman et al. 2003, Kalbhen 1984). Other OA animal models have also been shown to mimic human OA (Bendele 2001). However, they are influenced by mechanical instability (surgical models), or are highly variable (genetically modified models) or have a reduced incidence or prolonged duration of OA development (spontaneous model). The MIA-induced OA rat model is a non-trauma model that reproduces key features of human OA such as cartilage

degradation, subchondral bone sclerosis, osteophyte formation, and cyst formation in an experimentally cost effective time frame. This animal model clearly demonstrates consistent progressive thickening of subchondral bone (sclerosis) and a close relationship between the subchondral bone changes and cartilage degradation in OA. Moreover, the use of high resolution *in vivo* micro-CT enabled a better understanding of OA-related changes in the 3D microarchitecture of subchondral bone which plays an important role in determining bone strength (Compston 2006, Dempster 2000).

The low-dose MIA-induced OA rat model showed disease progression from early, intermediate and late stages of OA and provides sufficient disease "dynamic range" to detect therapeutic effects. However, high-dose MIA (2 mg) induced severe cartilage degradation with aggressive bone erosion within 2 weeks comparable to advanced stages of OA (**appendix 1**). Previously, Guingamp et al. reported similar effects of high-dose MIA in a dose response study in rats (Guingamp et al. 1997). Hence, it is important to use appropriate concentrations of MIA depending on the aims of the OA study. The low-dose MIA suited this study as this dose clearly induced non-invasively detectable progressive and measurable changes in the cartilage and subchondral bone over a cost effective time frame. The MIA-induced OA rat model has also been previously characterised as a pain model which is discussed later. Thus, the low-dose MIA induced OA rat model reproduced key features of human OA such as increased subchondral bone remodelling, subchondral bone sclerosis, osteophyte formation and cyst formation.

Another important finding reported in **Chapter 2** was that the CRP level in this animal model did not differ between the OA group and control group of rats and between time

points in the MIA-injected rats. CRP is a marker of systemic inflammation and significantly increased serum CRP levels have been reported in animal models with systemic inflammation such as the adjuvant-induced arthritis in rats (Banerjee et al. 2003, Cai et al. 2006). This shows that low-dose (0.2 mg) MIA injection does not induce systemic inflammation in this animal model. Therefore, the dose of MIA injected is crucial in order to demonstrate non systemic inflammatory disease progression in this animal model of OA. In human clinical practice CRP plays an important role as a marker to diagnose a wide range of tissue-damaging, inflammatory, and infective conditions such as rheumatoid arthritis, cardiovascular disease, severe bacterial, fungal, and viral infections (Pepys and Hirschfield 2003). Measurement of CRP, an acute phase protein has emerged as a promising marker to diagnose human OA and predict disease progression (Spector et al. 1997). Increased serum CRP levels in OA patients have been reported previously. However, few studies that reported increased CRP levels in OA patients compared the CRP levels of OA patients to young healthy controls (Pearle et al. 2007, Sharif et al. 1997, Tetik et al. 2010). The results from an extremely large study that surveyed CRP levels in plasma of healthy individuals from 2291 males and 2203 females, ages 25–74 years, and from 604 males and 650 females, ages 25–64 years, showed a significant trend to higher CRP values with increasing age (Hutchinson et al. 2000).

Garnero et al. measured serum CRP levels in established knee OA patients using a highly sensitive assay and reported that there was no significant increase in CRP levels in OA patients compared to age matched controls (Garnero et al. 2001). CRP levels are also associated with body mass index (BMI) and CRP levels have been shown to increase with increases in BMI (Kao et al. 2009). The Rotterdam Study-I, the largest

cohort study to date reported an association between increased serum CRP level and prevalence of knee OA. However, in their study a systematic review of 18 studies showed no association between serum CRP levels and prevalence, incidence and severity of OA after adjusting for age and BMI (Kerkhof et al. 2010). This shows that the mild inflammatory response and associated increase in serum CRP levels observed in OA could be driven by BMI and/or age.

Chapter 3 of this thesis focused on bisphosphonate treatment effects on subchondral trabecular bone and cartilage in a low-dose MIA-induced OA rat model at various stages of OA progression. Previous pre-clinical studies (Hayami et al. 2004, Shirai et al. 2011, Zhang et al. 2011) have shown a positive effect of alendronate on both bone and cartilage; however, clinical studies have given mixed results (Saag 2008). While in the pre-clinical studies, treatment was initiated pre-emptively, in clinical studies the treatment was usually initiated at advanced stages of OA. This gives a strong indication that the efficacy of bisphosphonate treatment depends on the time of treatment initiation. A previous pre-clinical study determined the effect of zoledronic acid on subchondral bone mineral density using dual-emission X-ray absorptiometry (DXA) (Strassle et al. 2010). In this thesis the temporal changes in the subchondral trabecular microarchitecture and bisphosphonate treatment effects in OA have been clearly demonstrated using *in vivo* micro-CT. Moreover, this thesis focused on changes in 3D microarchitectural properties of subchondral bone which gives a better understanding of bone-related changes due to bisphosphonate treatment in OA.

Microarchitecture is an important determinant of bone quality (Cole and van der Meulen 2011, Dalle Carbonare and Giannini 2004, Dempster 2000) and deterioration in

bone microarchitecture diminishes bone quality (Brandi 2009). Advanced imaging technologies such as clinical micro-CT and MRI has been useful for evaluating bone architecture (Majumdar 2003) and to detect changes in bone architecture in response to bisphosphonate treatment in human osteoporosis (Burghardt et al. 2010). Improvement of bone architecture after bisphosphonate treatment has been reported in human osteoporosis (Jobke et al. 2006, Recker et al. 2005). Further research is warranted to determine the effects of long-term bisphosphonate treatment on bone as significant microdamage accumulation has been reported in canine trabecular bone due to high dose bisphosphonate treatment for up to one year (Mashiba et al. 2001). In this study, alendronate had a positive effect on bone architecture and remodelling but only had a moderate effect on cartilage condition. The pre-emptive effects of alendronate in this study are in line with a previous study (Hayami et al. 2004), which showed that two weeks of alendronate treatment(pre-emptive treatment started 3 days before OA induction) prevented bone loss and moderately improved cartilage.

Joint pain is an important symptom in OA, and the exact cause of joint pain in OA is unclear. If OA is primarily considered a cartilage disorder, cartilage damage could not be the source of pain as it is avascular and aneural (Becerra et al. 2010). On the other hand subchondral bone is highly innervated and both peripheral and central pain sensitisation is known to occur in human OA (Aspden 2008). Moreover, subchondral bone pathology such as bone osteophytes, and marrow lesions have been shown to be associated with human OA (Boegard et al. 1998, Felson et al. 2001). The MIA-induced OA rat model is an accepted model to assess OA-related pain (Combe et al. 2004, Pomonis et al. 2005). In **chapter 3**, MIA-induced OA pain was measured by the hind limb weight bearing (HLWB) in this animal model. There was a significant decrease in

HLWB of the MIA-injected knee in the OA group of rats from day 1 to 7 compared to the baseline value and on day 3 compared to the control group. Previously in this animal model, significantly increased activating transcription factor-3-immunoreactivity (a marker of nerve injury) following MIA-injection was measured in lumber (L)5 dorsal root ganglia of the knee on days 8 and 14 (Ivanavicius et al. 2007). This coincides with the findings of reduced weight bearing up to day 7 in the MIA-injected knee reported in **chapter 3**. Moreover, significantly increased calcitonin gene-related peptide (CGRP) positive cells was observed in the dorsal root ganglia that is involved in central and peripheral pain sensitisation in the MIA-injected rat knee (Ferreira-Gomes et al. 2010)

The decrease in HLWB of the MIA-injected knee reported in **chapter 3** could have contributed to the bone loss observed in this animal model at 2 weeks. Prevention of bone loss, bone pathology and preservation of bone microarchitecture by pre-emptive alendronate treatment coincides with the normalisation of weight bearing after pre-emptive ALN treatment in this animal model. This is consistent with a clinical trial in which alendronate treatment for knee OA was associated with decreased subchondral bone lesions and less severity of knee pain (Carbone et al. 2004). The investigations described in **chapter 3** of this thesis led to the conclusion that targeting subchondral bone remodelling could offer a potential treatment option for the management of OA.

Chapter 4 of this thesis reports RANK, RANKL, and OPG mRNA expression which controls bone remodelling (Khosla 2001, Kohli and Kohli 2011) and has an important role in OA (Fazzalari et al. 2001, Logar et al. 2007, Sakao et al. 2008, Tat et al. 2009). The results of this final study showed that the increased subchondral bone remodelling and the significant bone loss in OA observed in this animal model is associated with the

increased RANKL/OPG mRNA ratio at 2 weeks. Similar increased RANKL/OPG ratios have been reported in human OA studies (Kwan Tat et al. 2008, Pilichou et al. 2008). The structural data reported for the MIA-injected knee at 2, 6 and 10 weeks after OA induction in **chapters 2 and 3** coincides with gene expression data reported for the MIA-injected knee in **chapter 4**. The significantly increased RANKL mRNA expression and RANKL/OPG mRNA ratio in the subchondral bone of distal femur at 2 weeks in the MIA-injected knee reflects the significantly decreased subchondral BV and BV/TV observed in the tibia of the MIA-injected knee. Similarly at 10 weeks after OA induction, the RANKL mRNA expression and the RANKL/OPG mRNA ratio was significantly decreased compared to 2 weeks which suggested decreased osteoclastic activity. This reflects the significantly increased bone tibial subchondral BV and BV/TV in the MIA-injected knee reported in **chapter 2 and 3.**

The prevention of bone loss by alendronate treatment reported in **chapter 3** is explained by the decrease in RANKL/OPG mRNA ratio by alendronate at 2 weeks. In cell culture studies, human osteoblast-like cells with bisphosphonate treatment have shown decreased RANKL/OPG mRNA ratio (Eslami et al. 2011, Pan B. et al. 2004). In addition, the results from 6 and 10 week time points show that apart from the RANK/RANKL/OPG nexus other molecular mechanisms could come into play during the advanced stages of the disease (Beyer and Schett 2010, Funck-Brentano and Cohen-Solal 2011, Prasadam et al. 2010a, Wu et al. 2010). The investigation of the RANK, RANKL, and OPG nexus in this animal model has reinforced the important role of subchondral bone in OA and clearly indicates that subchondral bone is a potential target for OA drug intervention studies.

5.3 Strengths and limitations

The key strength of this thesis is the use of a longitudinal study design to assess microarchitectural changes in 3D using high resolution *in vivo* micro-CT. This study approach has reduced the number of animals required to detect OA-related changes in the subchondral bone. This approach has also strengthened the statistical power as each animal served as its own control. Moreover, very few studies have looked at the 3D microarchitectural changes in OA pre-clinical models. As mentioned earlier microarchitectural properties are important determinants of bone quality. This thesis has investigated temporal changes in bone microarchitecture with and without bisphosphonate treatment in OA progression. The choice of a minimally invasive, non-trauma rat model of OA is another strength of this thesis. The use of a low-dose MIA rat model eliminates the need for surgical interventions and is not influenced by mechanical instability of the knee joints. This OA rat model is highly reproducible and the severity and rate of progression of OA can be easily controlled by varying the dose of MIA injected into the rat's knee joint. Another advantage of the MIA-induced OA rat model is that pain has been validated as a clinical outcome in this model (Bove et al. 2003, Combe et al. 2004, Pomonis et al. 2005, Schuelert and McDougall 2009, Stevenson et al. 2011).

To the best of my knowledge, the study reported in **chapter 4** of this thesis is the first study to report temporal changes in gene expression of RANK, RANKL and OPG in OA. This is also the first study to report changes in the RANK, RANKL and OPG mRNA expression after alendronate treatment in a pre-clinical model of OA. Moreover, the structural changes in the proximal tibial subchondral bone coincide well with the gene expression analysis of distal femoral subchondral bone. These findings advance

the_understanding of the role of the RANK/RANKL/OPG nexus in OA subchondral bone remodelling.

The limitations of the studies reported in this thesis have already been discussed within the respective chapters. However, a few limitations are note worthy. Although the MIA rat model of OA reproduces important features of human OA, it does not fully represent the human disease condition. Differences between species, the time take for disease to develop, and tissue heterogeneity between rat and human need to be carefully considered. Hence, the results obtained from this thesis need to be interpreted with a caveat. In the alendronate treatment study, extension of the treatment regime for pre-emptive and early treatment groups out to 6 and 10 weeks (advanced stages of OA), would have given more information regarding alendronate efficacy. Finally, the RANK, RANKL and OPG mRNA expression could not be directly correlated with the subchondral bone histomorphometric parameters since gene expression analysis was performed in the distal femur whereas, histomorphometric parameters were determined for the proximal tibial. Further, immunohistochemical studies for the expression of RANK, RANKL and OPG protein in the proximal tibia were not undertaken which would have complemented the gene expression of RANK, RANKL and OPG in the femur.

5.4 Areas for further research and clinical implications

In this thesis a suitable animal model for OA was characterised and the temporal changes in the bone and cartilage in disease progression were clearly demonstrated. Moreover, bisphosphonate therapy has been shown to preserve the subchondral bone microarchitecture in this animal model of OA. This non-trauma animal model would

serve as an excellent model for further research to understand OA pathology and important molecular pathways involved in OA disease onset and progression. Moreover, it would serve as an excellent tool to test the efficacy of disease modifying OA drugs.

The large amount of data generated from *in vivo* micro-CT imaging reported in this thesis could be used in finite element (FE) analysis of tibial subchondral bone. Using FE analysis important information such as the stiffness of subchondral bone and its contribution to cartilage degradation and OA progression could be investigated (Brown and Vrahas 1984, Burr and Schaffler 1997, Burr and Radin 2003, Radin and Rose 1986). FE analysis could also be used to study the role of subchondral bone cysts in OA which have been shown to be associated with accelerated cartilage degeneration and OA progression (Crema et al. 2010b, Hayashi D. et al. 2011, Tanamas et al. 2010, Zhao et al. 2010). Furthermore, the changes in material properties of subchondral bone in the low-dose induced OA rat model have not yet been determined. Analysis of subchondral volumetric BMD and collagen content together with previously determined 3D microarchitectural properties of subchondral bone would provide us a picture of bone quality in this animal model during early, intermediate and late stages of OA.

As OA involves the whole joint, a number of tissues could be considered as targets for OA treatment. However, the subchondral bone and particularly the calcified cartilage layer are intricately involved in bone-cartilage cross talk and provide exciting opportunities to explore and target important pathways and key molecular regulators involved in OA pathogenesis. In the low-dose MIA-induced OA animal model, subchondral plate breach with reparative tissue was observed. This subchondral plate

breach associated with increased porosity could lead to increased communication between the joint tissues. This could subsequently provide pathways for the movement of factors such as IL-1, IL-17, TNFα or TGFβ that stimulate catabolic events in both the cartilage and bone and warrant investigation in this animal model.

RANK, RANKL, and OPG mRNA expression in the cartilage and detection of corresponding protein expression by immunohistochemical studies would provide further information regarding molecular cross talk between bone and cartilage. The role of other molecular pathways such as the Wnt signalling pathway have been shown to be involved in OA (Hopwood et al. 2007). The role of molecules involved in this pathway such as sclerostin and Dkk-1 could be another avenue to explored using this animal model. Recently the two aggrecanases ADAMTS-4 and ADAMTS-5 have been shown to have an important role in cartilage degradation and development of OA (Glasson et al. 2007, Kapoor et al. 2011). It has also come to light that these two aggrecanases are regulated not only at the transcriptional level but also at the level of their activation (Bertrand et al. 2010). These aggrecanages and associated molecules such as syndecans that are considered essential for the activity of ADAMTS-5 should also be investigated in this animal model.

Finally, this animal model provides an excellent opportunity to identify potential biomarkers to detect the onset and progression of OA, as it is easy to collect urine and blood samples from the rats. This has important clinical relevance as OA is mostly diagnosed at advanced stages by a patient presenting with OA symptoms and detecting joint space narrowing in radiographs. Hence, detection of OA at an early stage would

aid in signalling the need for early intervention to slow progression or use DMOAD to provide better treatment options for patients.

5.5 Conclusion

The studies reported in this thesis highlight the importance of subchondral bone remodelling and changes in trabecular microarchitecture in the initiation and progression of OA. *In vivo* micro-CT has enormous potential to track and accurately quantify subchondral bone changes in animal models of OA. The MIA-induced OA rat model mimics human OA progression and could be used to further explore cellular pathways involved in OA initiation and progression. It is also an excellent tool to explore the bone-cartilage cross talk in OA. The bisphosphonate study strongly suggests that targeting subchondral bone remodelling early in OA disease onset has the potential to slow the progression of OA. Further studies can determine the efficacy of bisphosphonate treatment to manage OA at different progressive stages of the disease.

APPENDICES

Appendix I

A dose response study in the monosodium iodoacetate rat model of osteoarthritis: *in vivo* micro-CT, histological and serological evaluation

Introduction

Osteoarthritis (OA) is a major cause of disability and a major socio economic burden to society. OA mainly affects the joints of knee, hip, spine, hand and foot. Knee and hip are the most commonly affected joints (Michael et al. 2010). The main characteristics of OA are cartilage loss, increased bone remodelling, osteophyte formation, subchondral sclerosis, and bone attrition. Although these changes are typical of end stage OA, recent studies have shown that bone changes occur early in the disease (Burr and Schaffler 1997, Calvo et al. 2001). OA develops progressively over several years, and in many patients it is asymptomatic. Mostly OA is diagnosed at advanced stages when the patients feel pain during movement of the joint and when narrowing of joint space width is visible in radiographs. For these reasons, study of early pathological changes in human OA is difficult.

Animal models have advanced our knowledge regarding the pathogenesis of OA and are useful to test suitable therapeutic drugs for OA. The choice of an OA animal model depends on the purpose of the study and the selected animal model should represent features of human OA as closely as possible. Some of the commonly used animal models of OA are spontaneous animal models, surgical models (anterior cruciate ligament transection, medial meniscectomy), genetically modified and chemically induced models (collagenase, monosodium iodoacetate) (Bendele 2001).

The monosodium iodoacetate (MIA) model was first introduced by Kalhben (Kalbhen 1987) in chicken and rats. MIA is a potent inhibitor of glucose-6-phosphate dehydrogenase and blocks glycolysis in chondrocytes (Kalbhen 1984). This leads to chondrocyte necrosis and cartilage matrix degradation. A single intraarticular injection of MIA into the rat's knee joint has been shown to induce features of human OA in both the cartilage and subchondral bone (Guingamp et al. 1997, van Osch et al. 1994). It is a highly reproducible and a non-trauma animal model. The MIA rat model of OA has been validated to study OA related pain (Bove et al. 2003, Fernihough et al. 2004, Pomonis et al. 2005)and to test suitable drugs for OA (Bar-Yehuda et al. 2009, Janusz et al. 2001, Kalff et al. 2010). In these pre-clinical studies, high doses of MIA (up to 3 mg) has been used which causes severe disease onset and rapid progression. However, a suitable MIA rat model is required to monitor gradual progression of OA that mimics human OA disease progression. In the present pilot study, the dose responsiveness of tibial cartilage and subchondral bone to a high-dose (2 mg) and a low-dose (0.2 mg) of MIA has been evaluated at 2, 6 and 10 weeks post OA induction.

Materials and Methods

Animals and OA induction

Eighteen 8-week-old young adult male Wistar rats ≈ 230 g (Animal Resource Centre, Canning Vale, WA, Australia), were used in the pilot study. Only two to three rats were group housed per cage, with solid bottom and paper beddings, in order to minimize any discomfort to the rats. The rats were kept in a sanitary ventilated animal room with controlled temperature (20 - 24°C), with a light-dark cycle (12h/12h), and they were fed with standard laboratory rodent chow (Specialty Feeds, Glen Forrest, WA, Australia) with water available *ad libitum*. The rats were randomly divided into two groups: high-

dose MIA group (n=9) and low-dose MIA group (n=9), and were acclimatised for one week before the start of the experiment. On day 0, all the rats were induced with OA under anaesthesia in strict aseptic conditions. The rats were anesthetised with isoflurane/O_2 mixture and were placed in supine position on the operating table. Both their knees were shaved using electrical clippers and disinfected using 70% alcohol. Each rat was given a single intra-articular injection of 2 mg MIA (high-dose group) or 0.2 mg MIA (low-dose group) through the infrapatellar ligament of the right knee (Fig. 1). MIA was dissolved in sterile physiologic saline and administered in a volume of 50 µl using a 26-gauge 0.5-inch needle. After injection, the knee joint was relaxed and then the needle was removed to make sure that MIA does not leak out and to prevent bleeding of the knee joints. Using the same technique, 50 µl of sterile saline was injected into the rat's left knee joint, which is used as the contralateral control.

Figure 1. OA induction by a single intraarticular injection of 0.2 mg MIA into the rat's knee joint under isoflurane anaesthesia.

Imaging

The hind limbs of all the rats were imaged with high-resolution *in vivo* micro-CT as described in the *in vivo* micro-CT analysis section of this appendix. The 2-week subgroup of rats from the high-dose group (n=3), and low-dose group (n=3) were scanned after 2 weeks of OA induction. The 6-week subgroup of rats from the high-dose group (n=3), and low-dose group (n=3) were scanned after 2 and 6 weeks of OA induction. The 10-week subgroup of rats from the high-dose group (n=3), and low-dose group (n=3) were scanned after 2, 6 and 10 weeks of OA induction. The rats from each subgroup were sacrificed after the final scans.

Rat urine and blood collection

Morning spot urine specimens were collected from each rat at 2, 6, and 10 weeks after overnight fasting for repeated measurement of cartilage turnover marker. Each rat was placed in an individual sterile, autoclavable cage with wire-mesh base for 3 – 5 minutes. After the rat urinated, the rat was removed from the cage and the urine was collected from the base of the cage using a sterile disposable pipette into a sterile eppendorf tube (Kurien et al. 2004). The urine specimens were transported to the lab on ice and immediately centrifuged at 3500 rpm for 5 minutes to remove any debris. Aliquots of urine specimen were stored at -80ºC until the assays were performed.

An overnight fasting blood specimen was collected from each rat at 2, 6, and 10 weeks after OA induction for repeated measurement of bone and cartilage turnover markers. After urine collection, the blood samples were collected under light anaesthesia (isoflurane/O2) from the rat's lateral tail vein by venipunture. To facilitate adequate blood flow the rat's tail was immersed in a warm water bath (40º C) for 10 seconds and

the tail was disinfected with 70% ethanol. A 21-gauge needle was inserted 4 – 5 mm into the lateral tail vein approximately one-third along the length of the tail from the tail tip at an angle of 45º (Furuhama and Onodera 1983). Blood flow occurs due to vessel pressure and 1 ml of blood was collected in a sterile eppendorf tube. After blood collection, the needle was gently withdrawn and pressure was applied on the site of puncture to stop bleeding. Just before sacrifice, blood sample was collected using cardiac puncture technique under isoflurane/O_2. The rats were laid on their back and 2 ml of blood was collected by inserting a 3 ml syringe with 21-gauge needle just underneath the sternum into the heart at an angle of 30º. The blood specimens were transported to the lab on ice and immediately centrifuged at 3500 rpm for 10 minutes to collect the serum. Aliquots of serum specimen were stored at -80ºC until the assays were performed.

Intraperitonial injection of fluorochrome labels

Double-fluorescent labelling of newly formed bone was achieved by intraperitonial injections (IP) of calcein (5 mg/kg body weight; Sigma-Aldrich, Sydney, NSW, Australia) and xylenol orange (90 mg/kg body weight; Sigma-Aldrich, Sydney, NSW, Australia), 7 and 2 days before sacrifice respectively. IP injections were given to the rats under light anaesthesia (isoflurane/O2) using a 1 ml syringe with 25-gauge, 1-inch needle with a short bevel. The injection was made in the lateral aspect of the lower left quadrant on the rat's right side and close to the midline. Inserting the short bevelled needle on the rat's right side avoids intestinal organs such as the cecum and small intestine. The needle was inserted at an angle of 30º to a depth of about 5 mm through the skin and musculature and immediately lifted against the abdominal wall, to avoid puncturing of the abdominal viscera. The syringe plunger was pulled back slightly

before injecting to ensure that the needle has not penetrated the bladder, blood vessels or intestines. The required volume of calcein or xylenol orange was injected gently and then the needle was removed.

The animal handling and experimental procedures outlined in this study were carried out in accordance with The University of Adelaide Animal Ethics Committee and The Institute of Medical and Veterinary Science Animal Ethics Committee. In addition, the rats were closely monitored and daily clinical data sheets were completed throughout the duration of the study by the members of the animal care facility.

***In vivo* micro-CT analysis**

In vivo micro-CT imaging was performed using a bench-top cone-beam type *in vivo* animal scanner (Skyscan model 1076, Skyscan, Kontich, Belgium). Each rat was anaesthetized with isofluroane/O2 and placed in the scanner bed in a supine position. The MIA-injected knees and the contralateral control knees were scanned together. During each scan only the knees were irradiated, while the rest of the body was lead-shielded from radiation. The hind limbs of the rats were positioned close to the central scanner axis, and were securely fixed to scanner bed with the help of masking tape (Fig. 2) to prevent any movement during scanning. The scans were performed using the following scanner settings: X-ray source voltage 74 kVp, current 100 μA, a 1-mm thick aluminum filter to reduce beam-hardening artefact, 1 frame averaging, pixel size 17.4 μm, exposure time 885 ms, rotation step was 0.5° over 180° rotation, with a scan width of 68 mm. Each acquisition comprised two adjacent laterally shifted consecutive scans (i.e. one shifted scan per leg, field of view 35 mm in width, 18 mm in length each), which were automatically combined to obtain a 68 mm-wide, 18 mm long image

(appendix II). The total acquisition time was 40 minutes for each animal (20 min per leg), during which the rat was under anaesthesia. The cross-sectional images were reconstructed using a filtered back-projection algorithm (NRecon, V 1.4.4, Skyscan, Kontich, Belgium).

Figure 2. *In vivo* micro-CT imaging of rat hind limbs with the rat on the scanner bed in supine position.

For each scan, a stack of 1800 cross-sections was reconstructed, centered over the knee-joint (total reconstructed height about 16 mm), with an interslice distance of 1 pixel (17.4 µm). The reconstructed images were of 2000×2000 pixels each, 17.4 µm pixel size, and were stored as 8-bit images (256 grey levels) (Perilli et al. 2010). On the stack of the reconstructed micro-CT cross-section images, manual regions of interest (ROI) of an irregular anatomical contour were drawn in the subchondral trabecular bone region for the medial and lateral tibial plateau (Fig. 3), for both the MIA-injected knee and the contralateral control knee (software CT Analyser, V 1.8.05, Skyscan, Kontich, Belgium). The volume of interest (VOI) consisted of a stack of ROIs drawn over 52 cross-sections, resulting in a height of 0.45 mm. The VOI included the subchondral

trabecular bone starting below the subchondral plate, and extending distally towards the growth plate, excluding both the cortical bone and growth plate interface. The VOI used was of the same size and shape for all the three time points (2, 6, and 10 weeks), for both the control and the MIA-injected tibia. For the calculation of the morphometric parameters, the images were segmented using a uniform threshold (Perilli et al. 2010). The following 3D morphometric parameters were calculated for the medial VOI, the lateral VOI and the total (=medial + lateral) VOI of subchondral trabecular bone (software CT Analyser, Skyscan): bone volume (BV, mm^3), bone volume fraction (BV/TV, %), trabecular thickness (Tb.Th, µm), trabecular separation (Tb.Sp, µm) and trabecular number (Tb.N, 1/mm). BV is the volume in 3D of the structure segmented as bone, and BV/TV is the ratio of the segmented bone volume to the total volume of the region of interest. Tb.Th is the mean thickness of the trabeculae, Tb.Sp is the mean distance between trabeculae, Tb.N is the average number of trabeculae present per unit length. Tb.Th and Tb.Sp were assessed using direct 3D methods, Tb.N was calculated using the formula Tb.N= (BV/TV)/Tb.Th (Bouxsein et al. 2010).

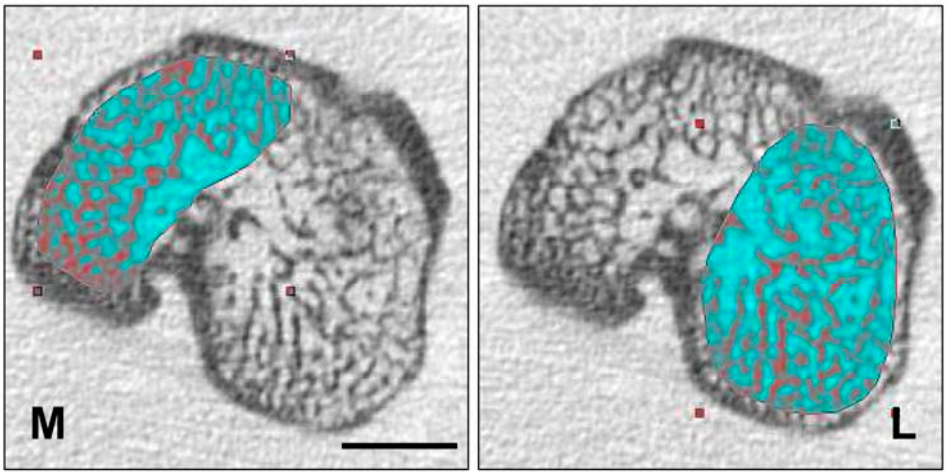

Figure 3. Manual region of interest (ROI) drawn in the medial (M) and lateral (L) compartment of tibial subchondral bone. Scale bar = 2 mm

Reproducibility study

A scavenged male Wistar rat was used for studying the reproducibility of the micro-CT analysis procedure. Both the right and left tibia were scanned five times in 1 day, repositioning the animal in the scanner each time for each scan, maintaining the same scanner settings. The morphometric parameters were calculated as described previously, and the coefficient of variation was determined. The reproducibility was high, with coefficient of variation (CV) values smaller than 5% for BV, BV/TV and Tb.N, smaller than 2% for Tb.Th and smaller than 3% for Tb.Sp (Table 1). These findings suggest that the *in vivo* micro-CT scanning procedure of the rat tibia had a good reproducibility and is similar to that of previous published studies on trabecular bone (Klinck et al. 2008, Perilli et al. 2010), as the effect due to MIA, to be measured, is expected to be larger than the CV reported here.

Table 1 Coefficient of variation (%) of subchondral trabecular bone determined from *in vivo* micro-CT reproducibility study

	BV		BV/TV		Tb.Th		Tb.N		Tb.Sp	
	Left	**Right**	**Left**	**Right**	**Left**	**Right**	**Left**	**Right**	**Left**	**Right**
Medial	4.2	5.1	5.4	4.3	1.5	2.0	4.6	2.8	2.7	2.1
Lateral	3.4	1.7	3.4	2.1	1.4	0.5	2.4	1.8	0.8	1.0
Total	3.2	3.2	4.2	2.3	0.8	1.2	3.5	1.2	1.3	0.6

Collection of bone specimens

At 10 weeks post-MIA injection the rats were euthanized with CO_2 overdose and both the right and left tibiae were dissected for macroscopic study. A set of sterile instruments were utilized to perform the dissection. A skin incision was made across the groin approximately at the level of the inguinal ligament. All the muscle groups were sharply divided with scissors and the femoral vessels were dissected free with scalpel.

The dissection was carried downward to expose the femur. As the dissection approached the hip joint, the hind limb was transected by incising the capsule using a scalpel so that the head of the femur dislodges from its socket form the pelvis. The removed hind limb was washed in sterile phosphate buffered saline and the knee joint was disarticulated using scalpel and sharp scissors to separate the femur and tibia.

Macroscopic analysis

Soft tissues surrounding the tibia and femur were carefully removed to prevent articular cartilage damage. The image of the tibial cartilage was recorded using a fluorescence stereomicroscope (SZX 10, Olympus). With the microscope, the fluorochrome labels calcein and xylenol orange were imaged and recorded. The macroscopic lesions were graded as follows: 0 = normal appearance, 1 = slight yellowish discoloration of the chondral surface, 2 = little cartilage erosions in load-bearing areas, 3 = large erosions extending down to the subchondral bone, and 4 = large erosion with large areas of subchondral bone exposure. The scores for the tibiae were combined and the average values were determined for the MIA-injected knee and the control knee (Guingamp et al. 1997).

Histological analysis

Paraffin sectioning: Safranin O/Fast Green staining

For histological analysis, the tibia and femur of one rat from each subgroup were fixed in freshly prepared 4% paraformaldehyde and left at 4°C for 24 hours. The bone samples were decalcified in freshly prepared 15% EDTA/0.5% paraformaldehyde solution, and left at 4°C for 4 weeks or until decalcified. Decalcification was monitored using a Faxitron radiography system (LX-60, Illinois, USA) at 60 KvP for 19 seconds.

The decalcified specimens were transferred to plastic cassettes (Sakura Tissue-Tek Uni-Cassette, California, USA) and processed in an automatic tissue processor (Sakura Tissue-Tek VIP 6, California, USA). The processed bone specimens were embedded in paraffin using the tissue embedding system (Sakura Tissue-Tek VIP 6, California, USA). From the paraffin embedded blocks, three sagittal sections (5 μm thick) 100 μm apart were obtained using a rotary microtome (Leica RM2235, Germany). The paraffin sections were stained with 1.5% Safranin O, and 0.02% fast green counter stain. Briefly, the sections were deparaffinised in xylene, rehydrated in decreasing concentrations of ethanol, and stained in 0.02% Fast Green FCF for 20 minutes. The sections were quickly rinsed in 1% acetic acid solution and stained in 1.5% alcoholic Safranin O solution for 5 minutes. Finally, the sections were dehydrated in increasing concentrations of ethanol, cleared in xylene and mounted permanently using DePex mounting medium. The stained sections were observed for OA-like features in the cartilage and subchondral bone.

Resin sectioning: Blank sections

The tibia and femur of another rat from each subgroup were fixed with 70% ethanol, dehydrated through a graded series of ethanol, and embedded in methyl methacrylate. For each sample, two sagittal sections were cut at 5μm thickness, spaced 100 μm apart using an automatic sliding microtome (Leica SM2500, Germany). Mineral apposition rate (MAR) was quantified for each sample at 20x objective from unstained sections. Three areas from either the medial or the lateral tibial plateau were assessed and then combined to obtain the total value. The amount of label incorporation in the tibial subchondral trabecular bone was measured under epi-fluorescence and the MAR was calculated as described by Frost et al. (Frost 1983):

$$\text{MAR } (\mu m/day) = \frac{\Sigma x(e)\,(\pi/4)}{nt}$$

where Σx is the sum of all the measurements between double labels, *e* is the micrometer calibration factor (μm), π/4 is the obliquity correction factor, *n* is the total number of measurements, and *t* is the time interval expressed (days).

Serum COMP, CTX-I and urine CTX-II analysis

The serum cartilage oligomeric matrix protein (COMP, cartilage turnover marker), serum C-terminal telopeptide of collagen type I (CTX-I, bone turnover marker) and C-terminal telopeptide of collagen type II (CTX-II, cartilage turnover marker) were measured at 2, 6 and 10 weeks after OA induction. Assays for serum COMP (Animal COMP ELISA, MD Bioproducts, St. Paul, MN, USA), serum CTX-I (IDS RatLaps ELISA, Fountain Hills, AZ, USA), and urine CTX-II (IDS Urine pre-clinical Cartilaps ELISA, Fountain Hills, AZ, USA) were performed according to the manufacturers instructions in duplicate which is given below.

Serum COMP

The serum samples were diluted (1:10) with sample buffer and the enzyme conjugate was diluted (1:10) with the conjugate buffer. Fifty μl of the standard solutions or diluted samples were incubated with 50 μl of polyclonal antibody in duplicate wells on a shaker at room temperature for 2 hours. The wells were washed 6 times manually with the wash buffer provided in the kit. The wells were completely emptied and incubated with 100 μl of enzyme conjugate on a slow shaker at room temperature for 1 hour. Again, the wells were washed 6 times manually with the wash buffer. The wells were completely emptied and incubated with 100 μl of enzyme substrate for 15 minutes at room

temperature. The reactions were arrested by adding 50 µl of stop solution (0.5 M H_2SO_4) into the wells placed on a shaker for 5 seconds to ensure complete mixing. Finally, the absorbance of the plate was read at 450 nm using an ultra microplate reader (Bio-Tek, Vermont, USA).

Serum CTX-I

The streptavidin-coated wells were incubated in 100 µl of biotinylated RatLaps antigen containing a biotinylated peptide, EKSQDGGR for 30 minutes at room temperature. The wells were washed 5 times manually with the 50X diluted washing solution. The wells were completely emptied and incubated with 20 µl standards (containing a synthetic peptide, EKSQDGGR), control (containing a synthetic peptide, EKSQDGGR) or the serum samples into the appropriate wells in duplicates followed by 100 µl of primary antibody (specific for a part of the C-telopeptide α1 chain of rat type I collagen) for 18 hours at 2-8°C. The wells were washed 5 times manually with the washing solution and the wells were incubated with 100 µl of peroxidase conjugated goat anti-rabbit IgG antibody for 1 hour at room temperature. The wells were washed 5 times manually with the washing solution and incubated with 100 µl of chromogenic substrate solution for 15 minutes at room temperature in darkness. The reaction was arrested by adding 100 µl of stopping solution (0.18 M H_2SO_4) into each well. Finally, the absorbance was measured within two hours at 450 nm with 650 nm as reference in an ultra microplate reader (Bio-Tek, Vermont, USA).

.

Urine CTX-II analysis

Standards covering the appropriate measuring range were prepared by diluting (1:2) Standard 1 provided in the kit. The wells were incubated with 100 µl of biotinylated

antigen for 30 minutes at room temperature. The wells were washed 5 times manually with 50X diluted wash buffer. The wells were emptied and incubated with 10 µl of either pre-diluted urine samples (1:3 in standard 0), controls or appropriate standards followed by 150 µl primary antibody for 21 hours at 2 – 8ºC. The wells were washed 5 times manually with the wash buffer and emptied completely. Then the wells were incubated with 100 µl peroxidase-conjugated antibody solution for 1 hour at room temperature. The wells were washed and incubated with 100 µl of the substrate solution for 15 minutes in darkness at room temperature. The reaction was arrested by adding 100 µl of the stopping solution (0.5 M H2SO4) into the wells. Finally, the absorbance was measure at 450 nm with 650 nm as reference within two hours in an ultra microplate reader (Bio-Tek, Vermont, USA).

For urine CTX-II, the values were corrected with urine creatinine (BioAssay Systems, California, USA) which was determined according to the manufactures instructions as given below: Five µl of 50 mg/100 ml standard solution and urine specimen was taken in duplicate into wells of a clear bottom 96-well plate. The working reagent was prepared by mixing 50 µl of reagent A, 50 µl of reagent, and 100 µl of distilled water. The plate was tapped briefly to mix the reagents well. Two hundred µl working reagent was quickly transferred to all wells, mixed briefly and the optical density was read at 510 nm.

Statistical analysis

For bone histomorphometric parameters repeated measures two-way ANOVA was applied to determine the “time effect” (indicates if there was any change over time within each group) and “time by group interaction effect” (indicates if the different

groups showed different patterns of changes over time). If F-values for a given variable were found to be significant, a paired Student's t-test was applied and the p-values were adjusted for repeated comparisons by Holm's Bonferroni stepdown procedure.

Results

In vivo micro-CT: changes in 3D microarchitecture of tibial subchondral bone

High-dose MIA group (2 mg MIA)

In the high-dose MIA group, there was a non-significant increase in BV, BV/TV, Tb.Th, and Tb.N and a non-significant decrease in Tb.Sp over time in both the MIA-injected (OA) and contralateral control knee (Fig. 4). The tibial subchondral BV of the high-dose MIA-injected knee was significantly lower than the contralateral control knee at 6 weeks (medial and total compartments). The tibial subchondral BV/TV was significantly lower at 6 weeks (all the compartments), and at 10 weeks (medial compartment). At 10 weeks, tibial subchondral Tb.Th was significantly increased in the MIA-injected knee compared to the contralateral control (medial and total compartments; Tb.Th in the lateral compartment showed a trend towards increase). The Tb.N was significantly decreased at 6 weeks (all the compartments), and at 10 weeks (medial and total compartments). Subchondral Tb.Sp of the MIA-injected knee was significantly increased at 6 weeks (all the compartments) and at 10 weeks (lateral and total compartments).

Low-dose MIA group (0.2 mg MIA)

In the low-dose MIA group, there was a significant increase in BV, BV/TV, Tb.Th, and Tb.N and a significant decrease in Tb.Sp over time in both the MIA-injected (OA) and contralateral control knee (Fig. 5). The tibial subchondral BV of the low-dose MIA-

injected knee was significantly higher than the contralateral control knee at 10 weeks post MIA injection in the medial compartment. There was a trend towards increased BV in the total compartment. The tibial subchondral BV/TV of the low-dose MIA-injected knee showed a trend towards increase at 10 weeks compared to the contralateral control knee (medial and total compartments). Tb.Th of the low-dose MIA injected knee was significantly increased at 6 weeks (total compartment) and at 10 weeks (all the compartments). Tb.N was significantly decreased at 6 weeks (total compartment) and there was no difference between the MIA-injected and the contralateral control at 10 weeks. There was no significant difference in Tb.Sp between the low-dose MIA-injected knee and the contralateral control knee at any time point.

Differences in histomorphometric parameters between the high-dose and the low-dose MIA-injected knee

The tibial subchondral BV and BV/TV of the high-dose MIA-injected knee was significantly lower compared to the low-dose MIA-injected knee at 6 weeks in all the compartments (Fig. 6). The BV of the high-dose MIA-injected knee was significantly decreased at 10 weeks (medial and total compartments), and BV/TV was significantly decreased at 10 weeks (medial compartment). There was no difference in Tb.Th between the low-dose and the high-dose MIA injected knee in any of the compartments. The Tb.N of the high-dose MIA-injected knee was significantly decreased at 6 weeks (all the compartments) and at 10 weeks (total compartment). Tb.Sp of the high-dose MIA-injected knee showed a trend towards decrease at 2 weeks, followed by a significant increase at 6 weeks (all the compartments), and a trend towards decrease at 10 weeks (all the compartments).

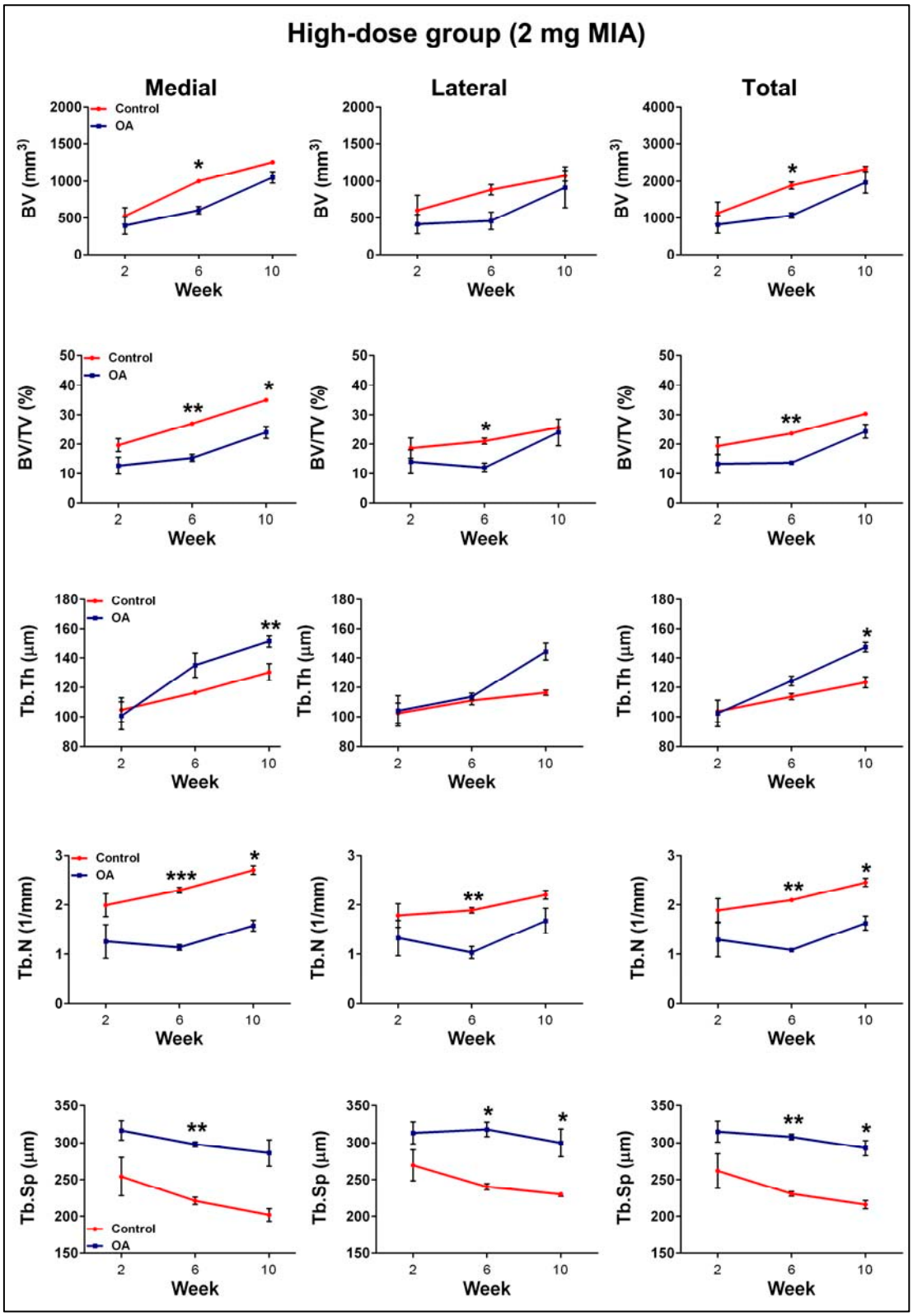

Figure 4. Subchondral trabecular bone histomorphometric parameters of the contralateral control tibiae and the high-dose MIA-injected tibiae determined by micro-CT, at 2, 6, and 10 weeks post-MIA injection. Error bars= SD. * p<0.05, ** p<0.01, *** p<0.001, between control tibiae and MIA-injected tibiae

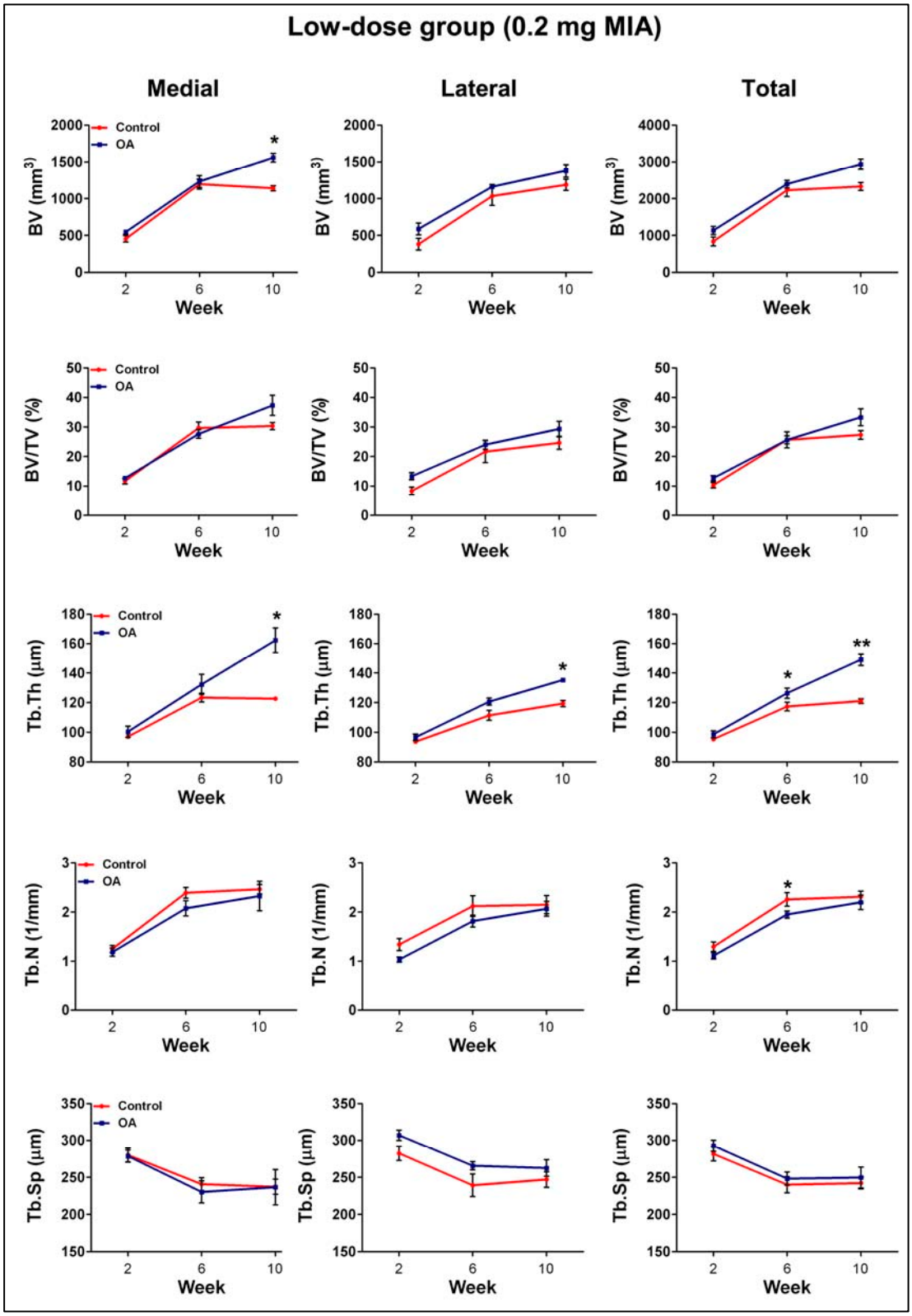

Figure 5. Subchondral trabecular bone histomorphometric parameters of the contralateral control tibiae and the low-dose MIA-injected tibiae determined by micro-CT, at 2, 6, and 10 weeks post-MIA injection. Error bars= SD. * p<0.05, ** p<0.01, *** p<0.001, between control tibiae and MIA-injected tibiae

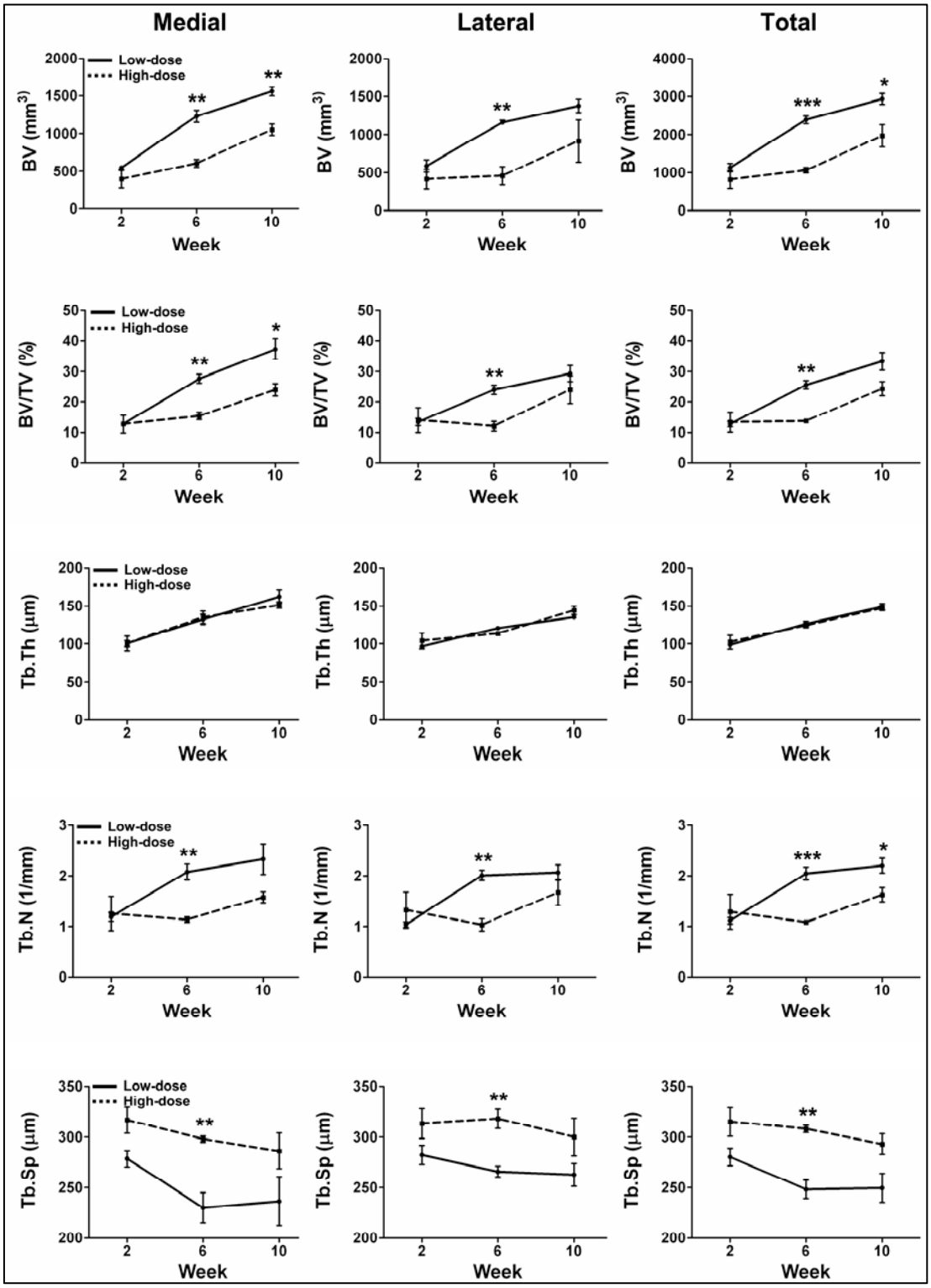

Figure 6. Comparison of subchondral trabecular bone histomorphometric parameters of the high-dose MIA-injected tibiae and the low-dose MIA-injected tibiae, at 2, 6, and 10 weeks post-MIA injection. Error bars= SD. * p<0.05, ** p<0.01, *** p<0.001, between the high-dose and the low-dose MIA-injected tibiae

Qualitative subchondral bone changes at 10 weeks after OA induction

At 10 weeks, two-dimensional (2D) coronal and axial micro-CT images of the contralateral control knee showed normal microarchitecture in the tibial subchondral bone (Fig. 7). The tibia of the low-dose MIA injected knee showed subchondral bone sclerosis in the medial tibial compartment. In contrast, the tibia of the high-dose MIA injected knee showed severe subchondral bone loss in both the medial and lateral tibial condyle, and the remaining trabecular structure showed thickening. These changes in the low-dose and the high-dose group were confirmed by the histology sections of the tibia (Fig. 10i).

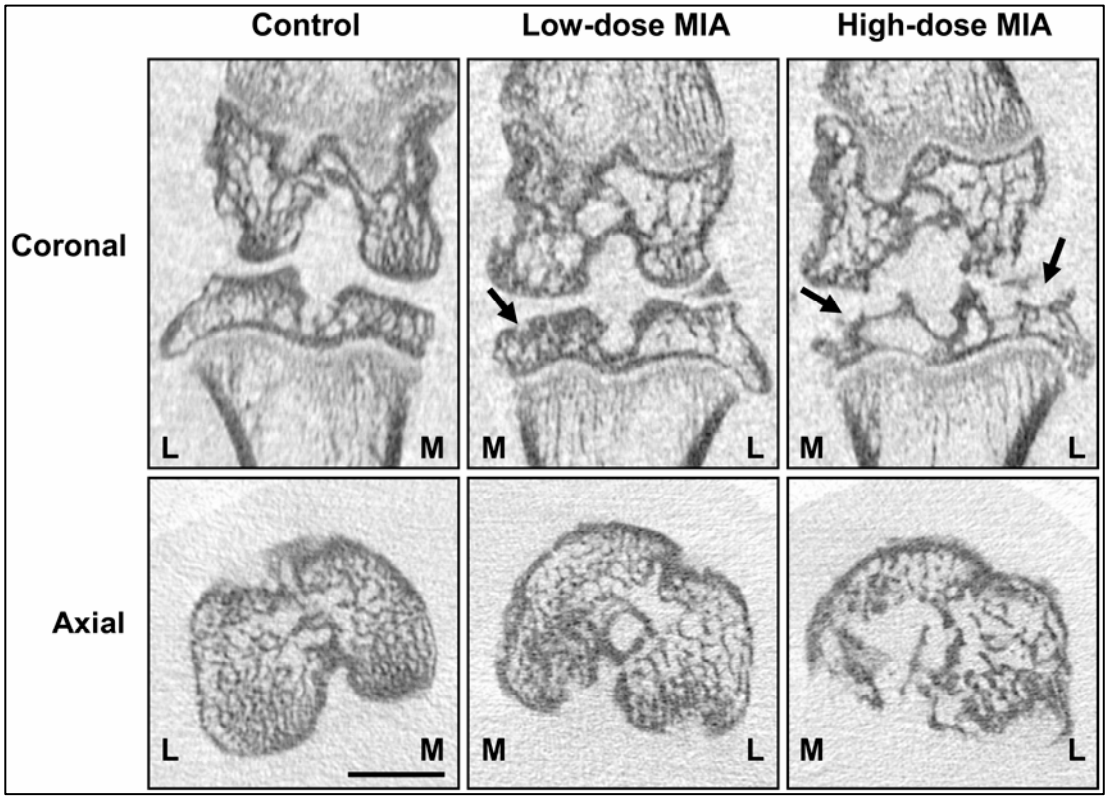

Figure 7. Coronal and axial micro-CT images of the control, the low-dose and the high-dose MIA-injected knee at 10 weeks after OA induction. Control knee (saline-injected) showed no OA-like changes. Low-dose MIA-injected knee showed subchondral plate breach (arrow) and sclerosis in the medial tibial compartment. High-dose MIA-injected knee showed sever bone erosion in the tibia (arrow) and femur in both the medial and lateral compartments. Scale bar = 2 mm

Three dimensional (3D) reconstructed micro-CT images of the contralateral control knee showed a smooth contour of the tibial plateau and femoral condyles (Fig. 8). The low-dose MIA-injected knee showed pitting of the tibial plateau and femoral condyles with marginal osteophytes. The tibial plateau and femoral condyles of the high-dose MIA-injected knee showed severe erosion of the subchondral bone and marginal osteophyte formation.

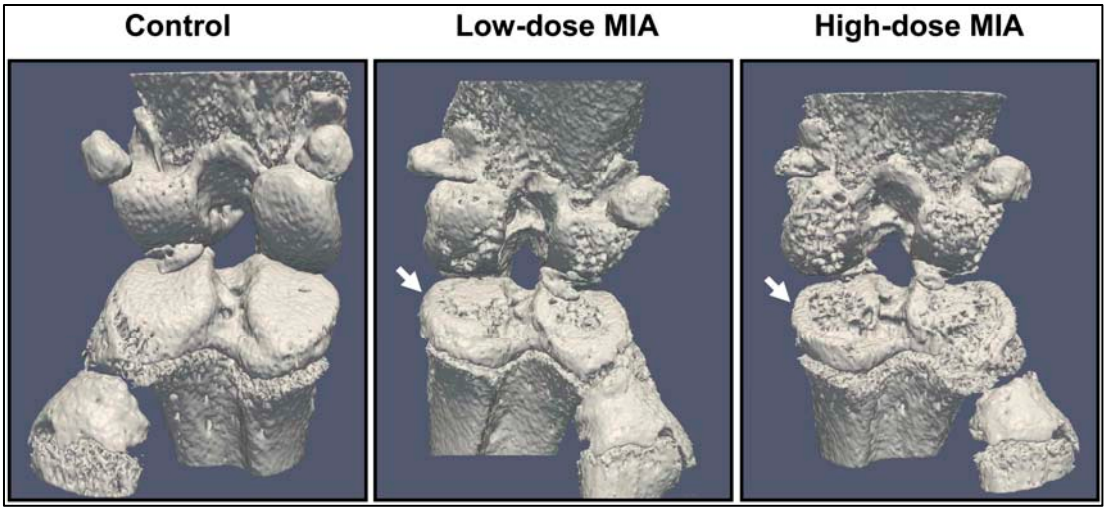

Figure 8. 3D reconstructed images of the control, the low-dose, and the high-dose MIA-injected knee at 10 weeks after OA induction. Control knee (saline-injected) showed smooth contoured surface of the tibia and femur. Low-dose MIA-injected knee showed pitting of surface in the tibial plateau and femoral condyles with osteophyte formation (arrow). High-dose MIA-injected tibia showed severe bone erosion and osteophyte formation (arrow).

Macroscopic changes

The tibia and the femur of the contralateral control knee (saline-injected) did not show any macroscopic lesions, at 2, 6 and 10 weeks after OA induction. Two weeks after OA induction, the tibia and femur of the low-dose MIA-injected knee showed mild cartilage changes, whereas the tibia and femur of the high-dose MIA-injected knee showed

prominent cartilage lesions (Fig. 9A, B). Six weeks after OA induction, the tibia and femur of the low-dose MIA-injected knee showed small cartilage lesions whereas, the tibia and femur of the high-dose MIA-injected knee showed sever cartilage lesions. Ten weeks after OA induction, the tibia and femur of the low-dose MIA-injected knee showed cartilage lesions on the medial and lateral condyle, while the tibia and femur of the high-dose MIA-injected knee showed severely remodelled cartilage surface.

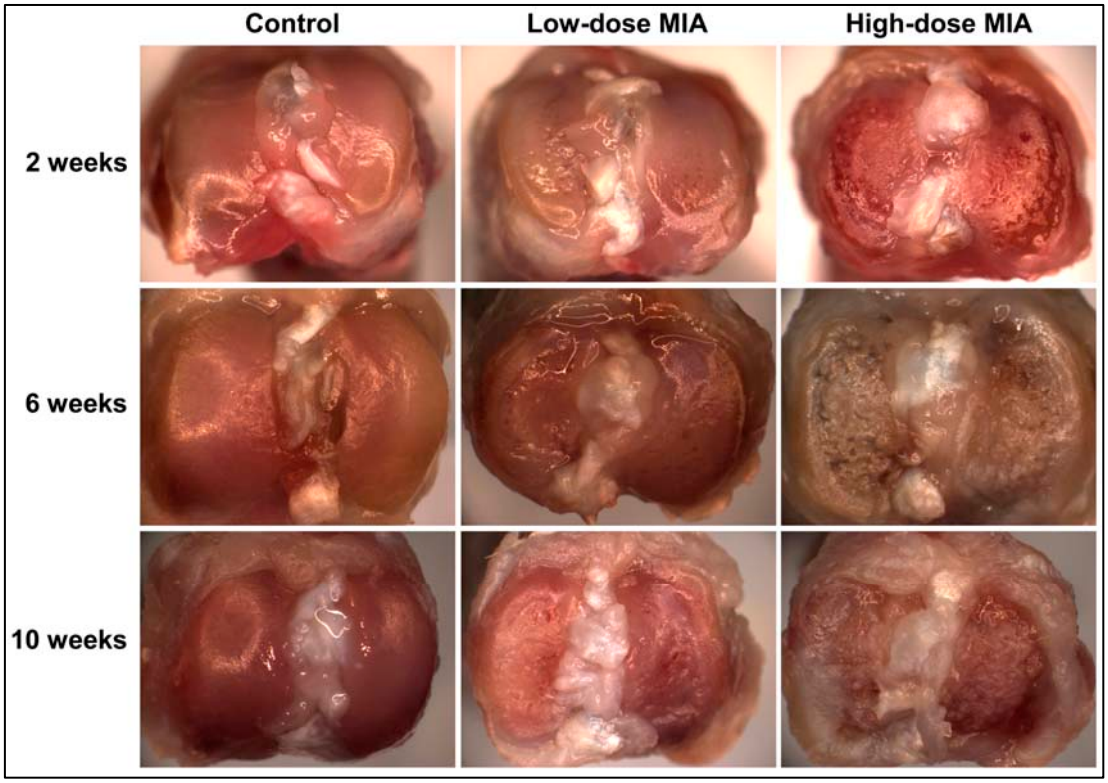

Figure 9A. Macroscopic changes in the tibia of the control (saline-injected), the low-dose MIA and the high-dose MIA-injected knee at 2, 6 and 10 weeks after OA induction. Tibia of the control knee did not show macroscopic lesions at any time point. Tibia of the low-dose MIA-injected knee showed progressive mild cartilage lesions while tibia of the high-dose MIA-injected knee showed severe macroscopic lesions.

Figure 9B. Macroscopic changes in the femur of the control (saline-injected), the low-dose MIA and the high-dose MIA-injected knee at 2, 6 and 10 weeks after OA induction. Femur of the control knee did not show macroscopic lesions at any time point. Femur of the low-dose MIA-injected knee showed progressive mild cartilage lesions. Femur of the high-dose MIA-injected knee showed severe macroscopic lesions.

Microscopic changes

The tibial articular cartilage of the contralateral control knee (saline-injected) did not show any OA-like changes 2, 6 and 10 weeks after OA induction (Fig. 10a-c). Two weeks after OA induction, the tibial articular cartilage of low-dose MIA-injected knee showed loss of proteoglycans from the weight bearing regions of the medial tibial plateau (Fig 10d). Whereas, the tibial articular cartilage of the high-dose MIA-injected

knee showed complete loss of cartilage, severe subchondral bone loss and exposure of subchondral bone at 2 weeks (Fig 10g, arrow). Six weeks after OA induction, the tibial articular cartilage of the low-dose MIA-injected knee showed loss of proteoglycans and fibrillation in the medial tibial plateau and sclerosis of subchondral bone (Fig. 10e). The low-dose MIA-injected knee showed loss of tibial articular cartilage, exposure of subchondral bone and sclerosis at 10 weeks after OA induction (Fig. 10f, arrow). On the other hand, the tibial articular cartilage of the high-dose MIA-injected knee showed complete loss of cartilage, subchondral bone sclerosis and exposure of subchondral bone at 6 and 10 weeks (Fig 10h, i, arrow) with bone erosion at 10 weeks. Progressive osteophyte formation was observed in both the low-dose and the high-dose MIA-injected knee from 2 weeks up to 10 weeks after OA induction. The OARSI score of the low-dose MIA injected knee was 5, 10 and 20 at 2, 6 and 10 weeks respectively. The OARSI score of the high-dose MIA injected knee was 18, 20 and 22 at 2, 6 and 10 weeks respectively.

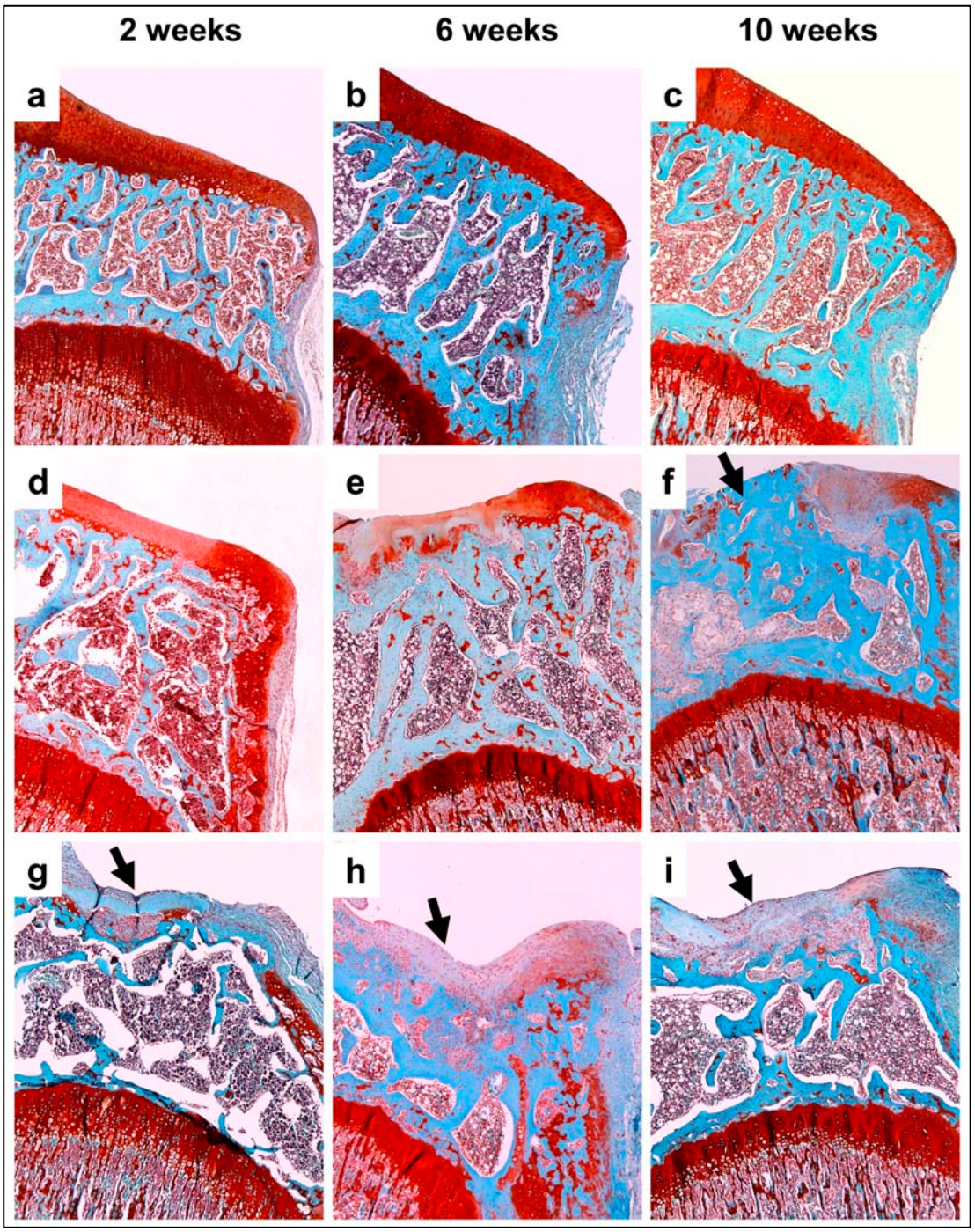

Figure 10. Safranin O/Fast green stained sections of rat tibia showing articular cartilage and subchondral bone of the contralateral control knee (a-c), the low-dose MIA-injected knee (d-f) and the high-dose MIA-injected knee (g-i) at 2, 6, and 10 weeks post injection. Note the gradual cartilage degradation in the tibia of the low-dose MIA-injected knee (d-f). Severe cartilage changes and reparative fibrocartilage formation was observed in the tibia of the high-dose MIA-injected knee (g-i).

OARSI score and MAR

The OARSI score of the contralateral control knee was zero for all time points. The fluorochrome double labels were significantly accumulated in regions of high bone resorption in the tibial subchondral bone of the high-dose MIA-injected knee. The tibial subchondral trabecular MAR of the low-dose MIA injected knee was 1.4 μg/day, 1.02 μg/day and 1.04 μg/day at 2, 6 and 10 weeks respectively. The MAR of the high-dose MIA injected knee was 1.8 μg/day, 1.05 μg/day and 1.06 μg/day at 2, 6 and 10 weeks respectively. The MAR of contralateral control knee was 1.23 μg/day, 0.82 μg/day and 0.81 μg/day at 2, 6 and 10 weeks respectively.

Serum COMP, CTX-I and urine CTX-II analysis

There was a non-significant decrease in serum COMP, CTX-I and urine CTX-II levels over time in both the high-dose MIA and the low-dose MIA group. The levels of serum COMP, CTX-I and urine CTX-II of the high-dose MIA group was non-significantly increased than the low-dose MIA group (Fig. 11).

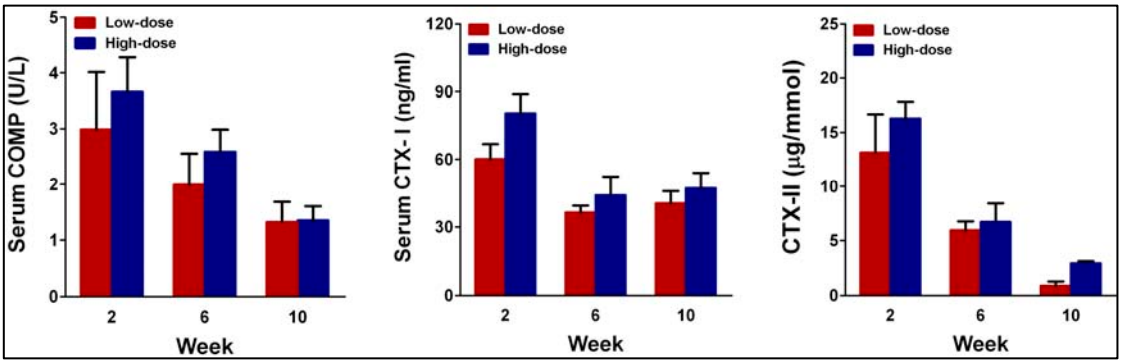

Figure 11. Serum COMP, serum CTX-I and urine CTX-II levels at 2, 6 and 10 weeks after OA induction in the low-dose and the high-dose MIA-injected rats.

Discussion

In this pilot study, the dose responsiveness of tibial cartilage and subchondral bone to monosodium iodoacetate (MIA) was evaluated in an experimental model of MIA-induced OA in rats. *In vivo* micro-CT analysis revealed that injection of high-dose MIA induced severe bone loss, with significantly reduced BV/TV, Tb.N and increased Tb.Sp at 6 and 10 weeks after OA induction. On the other hand, the low-dose MIA-injected knee at 10 weeks, showed significantly increased BV (medial compartment) due to subchondral bone sclerosis, which is similar to human OA. Histology revealed that high-dose MIA induced severe cartilage degradation (Fig. 10) and subchondral bone erosion (Fig. 7) in this animal model. Low-dose MIA induced progressive OA-like changes in both the cartilage (Fig 10) and subchondral bone in the rat tibia (Fig. 7). In the high-dose MIA group, severe articular cartilage degradation, subchondral bone erosion and exposure of subchondral bone was observed 2 weeks after OA induction whereas, these changes were observed only 10 weeks after OA induction in the low-dose MIA group. Thus, progressive joint degeneration was induced by low-dose MIA (0.2 mg), whereas high-dose MIA (2 mg) induced highly rapid joint degeneration.

Guingamp et al. reported similar observations in a dose-response study, in which sclerosed subchondral bone was exposed 15 days after OA induction using high doses of MIA (up to 3 mg) (Guingamp et al. 1997). The increased severity of joint degradation depends on the dose of MIA injected. The degree of joint pathology has been shown to correlate with a decrease in hind-paw weight bearing in this animal model (Bove et al. 2003, Kobayashi et al. 2003). Januz et al. reported that a dose of 0.25 mg MIA resulted in moderate cartilage damage without aggressive cartilage and bone changes three weeks after OA induction (Janusz et al. 2004, Janusz et al. 2001).

In both the low-dose and the high-dose MIA group, subchondral bone remodelling was observed to be increased, by monitoring MAR values. Though the levels of MAR could not be analysed statistically since we had only one rat for each time point, it served to develop the methodology for the subsequent study. Serum COMP, serum CTX-I and urine CTX-II levels indicated high bone and cartilage turnover rate at 2 weeks which gradually decreased over time due to the effect of aging. Similar age related decrease in COMP, CTX-I and CTX-II values have been reported previously in an anterior cruciate ligament transection model (ACLT) in rats (Hayami et al. 2004). As for MAR, the COMP, CTX-I and CTX-II levels were not significantly different between time points, since samples from only 3 rats were analysed. Nonetheless, these measurements served to develop the methodology and validate the use of these markers for subsequent studies.

In conclusion, the high-dose MIA rat model creates an acute model and is not suitable to track progressive changes in the cartilage and subchondral bone. The low-dose MIA rat model is less aggressive and provides a useful tool to study OA disease progression. Moreover, the low-dose MIA rat model of OA could be used to test OA-therapeutic drugs. *In vivo* micro-CT is a non destructive imaging technique that enables qualitative and quantitative tracking of subchondral bone changes in this animal model.

Appendix II

Development of an *in vivo* scanning protocol for tracking temporal changes in tibial subchondral bone in a low-dose MIA-induced OA rat model

Introduction

In vivo micro-CT is an invaluable tool that enables non-destructive imaging of small animals. Accurate quantification of bone changes and tracking of changes in individual trabeculae is now possible with this method (Waarsing et al. 2004b). This imaging modality has led to our improved understanding of changes in 3D bone histomorphometric parameters in rodent models of osteoporosis (Boyd et al. 2006, Perilli et al. 2010) and osteoarthritis (Botter et al. 2011, Jones M. D. et al. 2010, Mohan et al. 2011). However, scan resolution, scan time and radiation exposure are the limiting factors in micro-CT scanning *in vivo*. Scanning protocols need to be optimised for rat imaging in order to minimise radiation exposure and reduce scan time. The development of *in vivo* micro-CT protocol for the studies included in this thesis is discussed in detail in this appendix.

Development of *in vivo* micro-CT scanning in the pilot study

In the pilot study, *in vivo* micro-CT imaging was performed using a bench-top cone-beam type *in vivo* animal scanner (Skyscan model 1076, Skyscan, Kontich, Belgium). The recommended method for scanning the rat's hind limb is by positioning the hind limb using a centrally located plastic tube provided by the manufacturer (Fig. 1). This holder was likely developed for studies involving female rats, which are often used in osteoporosis related research, because of the commonly-used ovariectomized rat model (Brouwers et al. 2008, Perilli et al. 2010, Waarsing et al. 2006). However, for MIA-

induced OA animal models, male rats are commonly used (Guingamp et al. 1997, Guzman et al. 2003, Morenko et al. 2004, Strassle et al. 2010), as for the studies included in this thesis (male Wistar rats). Since the male rats are bigger in size compared to the female rats, it was very difficult to fit the rat's hind limb in the plastic tube provided by the manufacturer. Also when the hind limbs of the male rats were tried to fit into the plastic tube, the testicles of the rat tended to get trapped in the limb holder, with the consequence of being unnecessarily irradiated.

Initially in the pilot study (appendix I), both the hind limbs (MIA-injected and contralateral control) of the OA rats were scanned together during each acquisition (68 mm scan), with the rat placed in the scanner bed in a supine position (Fig. 2A). In the pilot study (appendix I), *in vivo* scanning was performed at 2, 6 and 10 weeks after OA induction using the following scanner settings: X-ray source voltage 74 kVp, current 100 μA, a 1-mm thick aluminum filter to reduce beam-hardening artefact, 1 frame averaging, pixel size 17.4 μm, exposure time 885 ms, rotation step 0.5° over 180 degrees rotation, with a scan width of 68 mm ("camera-shift" modality, Fig. 2B).

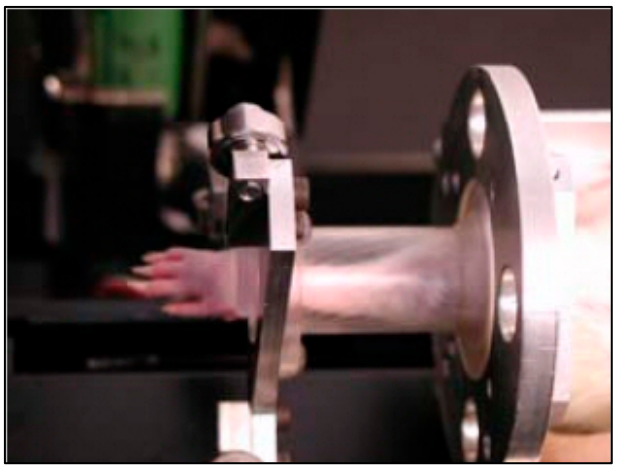

Figure 1. Hind limb of a rat fixed to a centrally located plastic tube provided by the manufacturer for *in vivo* scanning (Skyscan model 1076, Skyscan, Kontich, Belgium).

Figure 2A. *In vivo* micro-CT imaging of rat hind limbs with both hind limbs together. The rats were placed on the scanner bed in supine position, with the hind limb secured in place with masking tape.

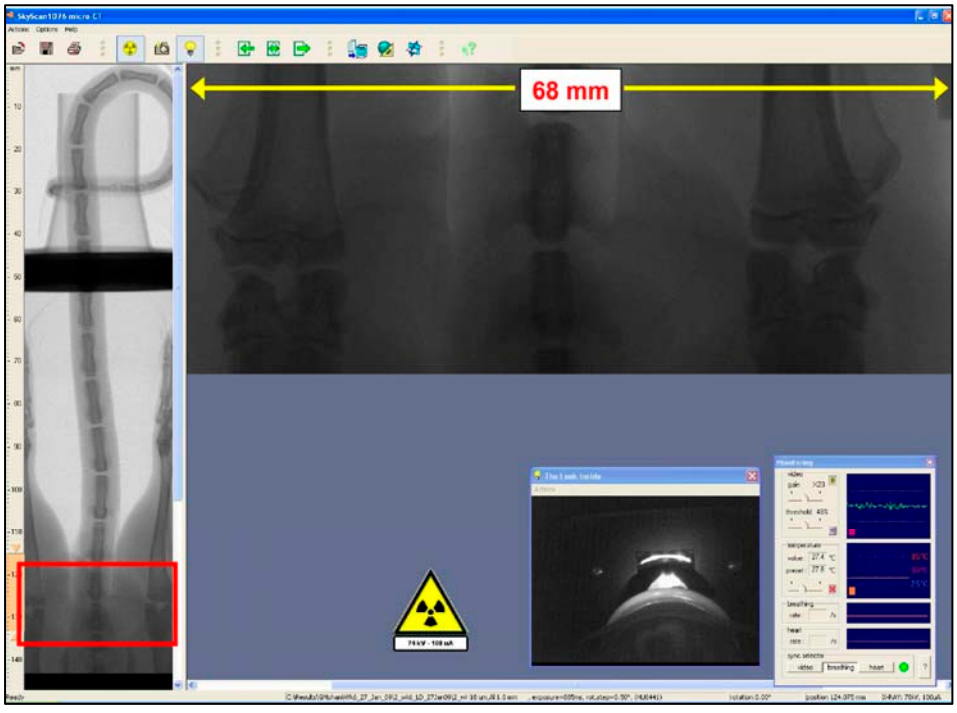

Figure 2B. Scout scan, with position of the knee joints highlighted (red rectangle), and X-ray image (center) of both hind limbs of the rat scanned simultaneously *in vivo* (17.4 mm pixel, 68 mm scan width obtained by combining two 35 mm-wide scans).

Improved *in vivo* micro-CT scanning protocol used in chapter 2 and 3

For the studies reported in chapter 2 and 3, a special hind limb holder was devised consisting of a cylindrical plastic holder fitted to a polystyrene tube (Fig. 3A). This enabled each hind limb to be scanned separately (field of view 35 mm), with the limb extended and placed at the center of the scanner axis (Fig. 3B). This involves manually repositioning the animal at each scan, and placing the limb to be scanned in the holder. During each scan only the knee for image data acquisition was irradiated, while the contralateral limb and the rest of the body were lead-shielded from radiation. The scanner settings were as follows: X-ray source voltage 60 kVp, current 100 μA, a 1-mm thick aluminum filter, 1 frame averaging, pixel size was 8.7 μm, exposure time 4.7 s, rotation step 0.8°, with a complete rotation over 197° (Perilli et al. 2010). The total scan time for each limb was 20 minutes during which the rat was under anaesthesia.

The use of the 9 μm pixel size protocol improved the image quality compared to the image of the 18 μm pixel size protocol, with reduced noise in the grey levels and increased spatial resolution. The time points (2, 6 and 10 weeks) for *in vivo* scans were selected in order to repeat the scans after a four weeks interval, to reduce radiation exposure (McErlain et al. 2008). Previous studies have shown that a radiation dose of 0.4 Gy for a single scan did not have adverse effects on bone cells (Dare et al. 1997). Repeated scanning of rat proximal tibia every two weeks at a dose of 0.6 Gy (Klinck et al. 2008) or weekly scan of proximal tibia at 0.9 Gy per scan showed no change in rat bone microarchitecture and bone marrow cells (Brouwers et al. 2007). In the present study, the effective radiation dose measured in air (Solidose 400, Sweden), for a single scan with the settings used with the 9 μm pixel size protocol is 1.6 Gy. The accumulated dose of 1.6 Gy per scan in one month is similar or inferior to the accumulated dose of

3.6 Gy in 1 month with 4 scans at 0.9 Gy per scan by others, where no changes in rat bone microarchitecture were observed (Brouwers et al. 2007) or the accumulated dose of 1.8 Gy in 1 month with 3 scans at 0.6 Gy per scan (Klinck et al. 2008). As such, effects on bone microarchitecture due to irradiation during micro-CT scanning can be excluded.

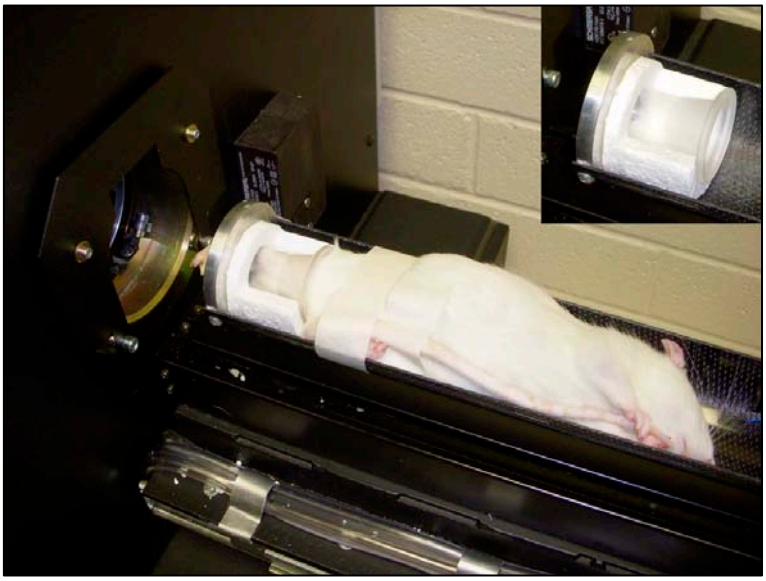

Figure 3A. *In vivo* micro-CT imaging of a rat hind limb with the rat placed on the scanner bed in supine position, with the hind limb secured in a customised leg fixative device (inset).

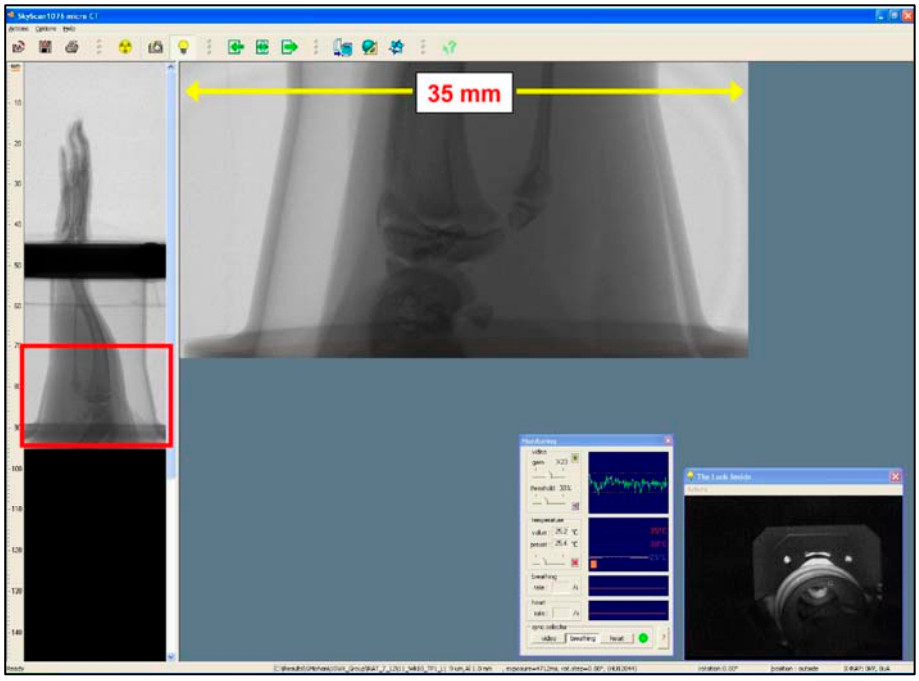

Figure 3B. Scout scan (red rectangle) and X-ray image (center) of single hind limb of the rat scanned *in vivo* (8.9 μm pixel, 35 mm scan width) with the hind limb fixed to the customised leg fixative device.

Image reconstruction and segmentation

The cross-sectional images were reconstructed from the projection data using a filtered back-projection algorithm (NRecon, V 1.4.4, Skyscan, Kontich, Belgium). For each 9 μm pixel size scan, a stack of 1800 cross-sections was reconstructed, centered over the knee-joint (total reconstructed height about 16 mm), with an interslice distance of 1 pixel (8.7 μm). The reconstructed images were of 1,500×1,500 pixels each, 8.7 μm pixel size, and were stored as 8-bit images (256 grey levels) (Perilli et al. 2010).

Segmentation is the process of separation of bone and non-bone in the grey level image. It is a crucial step for accurate quantification of bone microarchitectural properties. Commonly proposed segmentation techniques include the local thresholding and global

thresholding method. The local thresholding method is based on the gradients of the grey values of the pixels in a micro-CT cross-section image, in the transition between bone and non-bone (Waarsing et al. 2004a). The global threshold method is based on selecting a single grey level value from the grey level histogram, above (or below, depending on the look-up table) which all pixels are marked as bone and below (or above) which all remaining pixels are marked as non-bone (Ding et al. 1999, Hildebrand et al. 1999, Perilli et al. 2007b). In the studies included in this thesis, the images were segmented using the uniform global threshold method (Fig. 4). This segmentation value was based on comparisons with externally determined 3D quantities such as calibrated thickness measurements by scanning a specially designed micro-CT phantom (Perilli et al. 2006, Perilli et al. 2010).

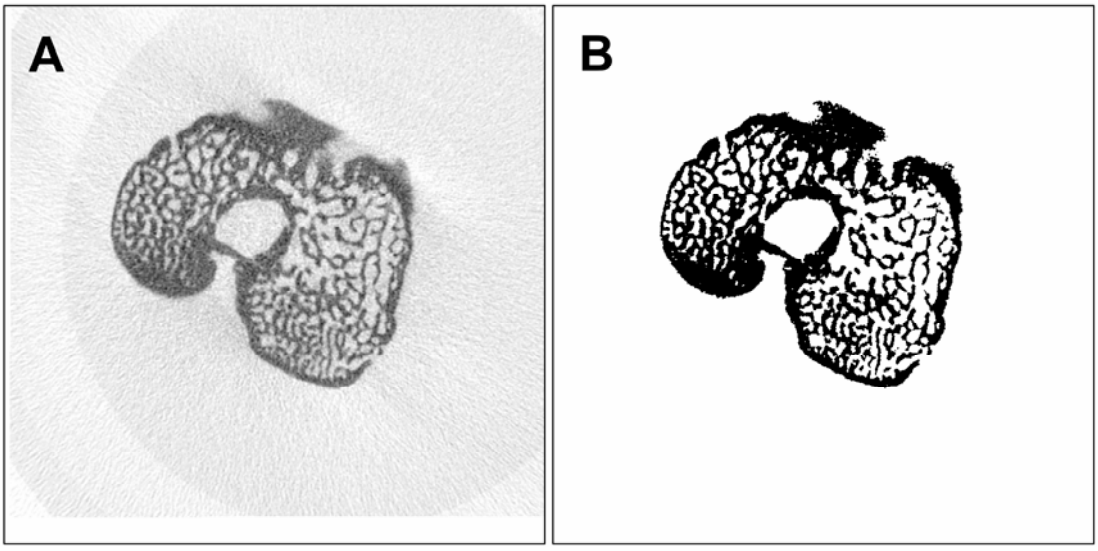

Figure 4. *In vivo* micro-CT scans with a pixel size of 9 μm (A) and the segmented micro-CT image using the global threshold method (B)

Comparison of grey level values between MIA-injected and contralateral control knee

To investigate whether the grey level values of the bone were different between OA and contralateral control knee, the grey level values of the tibial cortex, subchondral trabecular bone and subchondral plate was analysed for both the knees (n=12). There was no statistically significant difference between the average grey level value and standard deviation between the MIA-injected and contralateral control knee at 10 weeks (Table 1).

Table 1. Grey level values (out of 256 levels, stored in bitmap format) for subchondral bone and cortical bone in the saline-injected (contralateral control) knee and MIA-injected knee.

	Saline-injected knee	MIA-injected knee	p value
	Mean ± SD	Mean ± SD	
Subchondral trabecular bone	141 ± 18	146 ± 18	0.67
Cortical bone	171 ± 12	168 ± 8	0.45
Trabeculae	170 ± 10	165 ± 9	0.21
Tibial subchondral plate	163 ± 11	161 ± 7	0.61
Femoral subchondral plate	163 ± 6	159 ± 3	0.16

Significant difference (p-value) between the saline-injected and MIA-injected knee was determined by Student's paired t-test (n=12).

Selection of suitable ROI for measurement of subchondral trabecular bone histomorphometric parameters

An important step in the determination of bone histomorphometric parameters is the choice of the region of interest (ROI), its position, and the contouring method used, in order to capture the OA-related changes in the subchondral trabecular bone. One

approach reported in the literature is the use of cylindrical volumes of interest (VOI), which was used for bone mineral density measurements (Appleton et al. 2007, McErlain et al. 2008). In the present thesis, in order to select a suitable ROI to measure the tibial subchondral trabecular bone histomorphometric parameters, cylindrical VOIs were drawn in anterior and posterior regions of the proximal tibia, and the corresponding results were calculated and compared.

Bone histomorphometric parameters of tibial subchondral trabecular bone at 2, 6, and 10 weeks after OA induction were calculated as follows (n=12 rats at each time point). On the stack of the reconstructed micro-CT cross-section images, cylindrical VOIs were placed in the anterior and posterior regions of the tibial subchondral trabecular bone region for the medial and lateral tibial plateau (Fig. 5) for both the MIA-injected knee and the contralateral control knee (software CT Analyser, V 1.8.05, Skyscan, Kontich, Belgium). The volume of interest (VOI) consisted of a stack of circular ROIs (2 mm diameter) drawn over 52 cross-sections, resulting in a cylinder of 0.45 mm height. The VOI included the subchondral trabecular bone starting below the subchondral plate, and extending distally towards the growth plate, excluding both the cortical bone and growth plate interface (Fig. 6). The following 3D morphometric parameters were calculated for the medial VOI, the lateral VOI and the total (=medial + lateral) VOI of subchondral trabecular bone (software CT Analyser, Skyscan): bone volume (BV, mm3), bone volume fraction (BV/TV, %), trabecular thickness (Tb.Th, μm), trabecular separation (Tb.Sp, μm) and trabecular number (Tb.N, 1/mm) (Bouxsein et al. 2010, Parfitt et al. 1987).

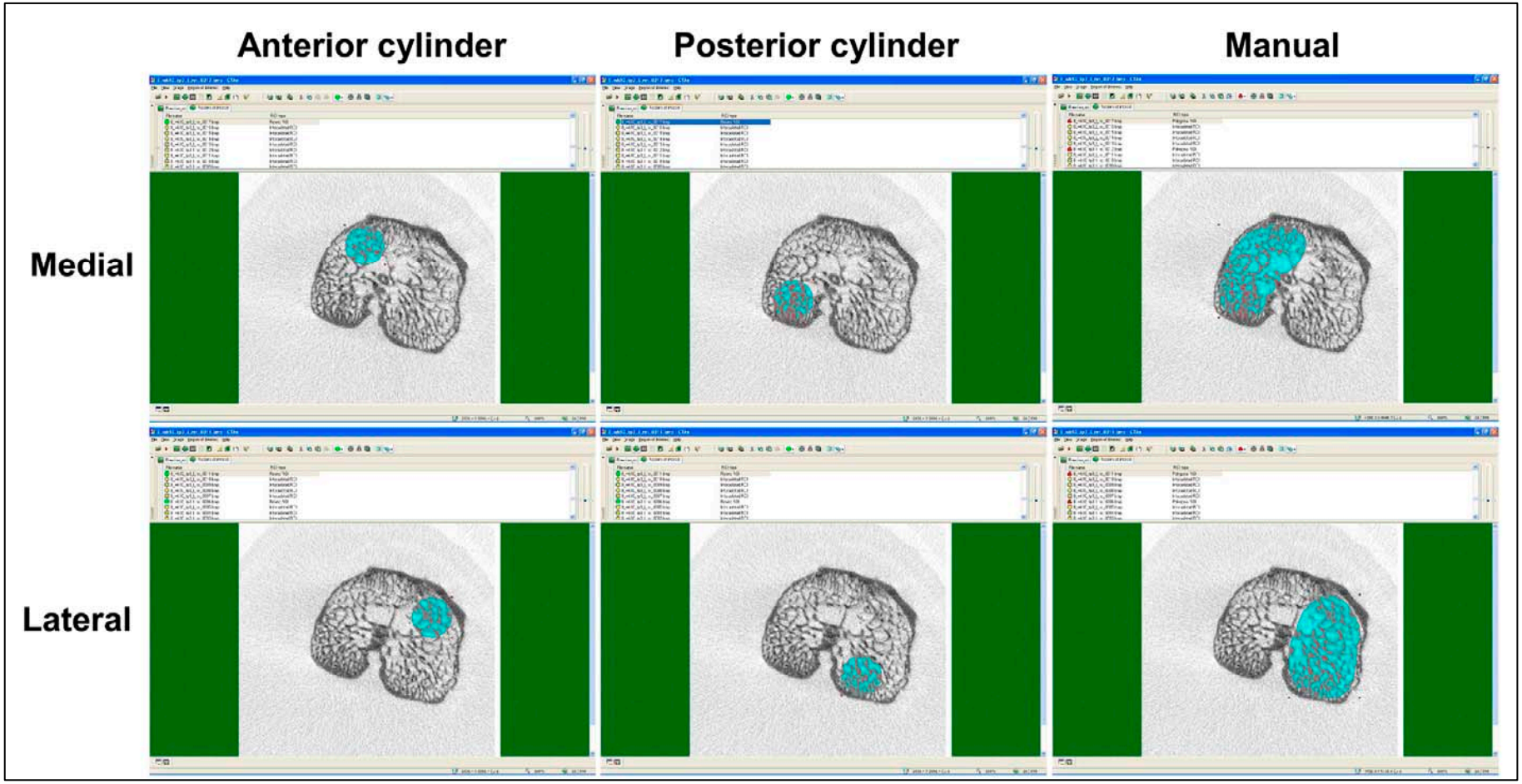

Figure 5. Circular ROIs (which, as a stack, builds a cylindrical VOI) placed in the anterior and posterior region, and manual ROI including the entire subchondral bone of the rat tibial subchondral bone, in the medial and lateral compartments.

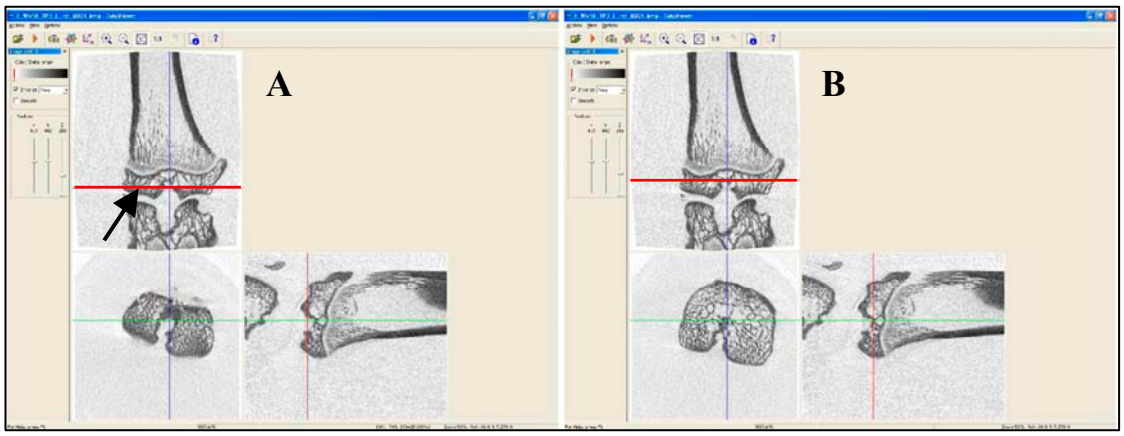

Figure 6. Selection of image slices of subchondral trabecular bone starting below the subchondral plate (A), and extending distally towards the growth plate (indicated by arrow); excluding both the cortical bone and growth plate (B).

Results:

The results of this sub analysis showed that all the bone histomorphometric parameters of the tibial subchondral bone differed significantly for anterior cylindrical ROI and posterior ROI at all time points for both the MIA-injected and the contralateral control knee (except Tb.Th in the contralateral control knee). Tables 2, 3 and 4 show the differences in bone histomorphometric parameters for both the MIA-injected and the contralateral control knee at 2, 6 and 10 weeks after OA induction respectively.

The results of this analysis indicate that subchondral bone sclerosis and trabecular thickening occurs mostly in the posterior region, whereas loss of trabeculae seems to occur in the anterior region of the tibia from the MIA-injected knee. In particular, analysis of bone histomorphometric parameters for anterior VOI (Fig. 7) showed significantly decreased BV, BV/TV, and Tb.N in the MIA-injected knee compared to the contralateral control knee in the medial (2, 6 weeks), lateral and total compartments (2, 6 and 10 weeks after OA induction). The Tb.Th was significantly increased at 2

weeks and there was no difference between the MIA-injected and the contralateral control knee at 6 and 10 weeks after OA induction. The Tb.Sp was significantly increased in the medial (2 weeks), lateral and total compartments (2, 6 and 10 weeks after OA induction). On the other hand, the posterior ROI (Fig. 8) showed significantly increased BV and BV/TV at 6 and 10 weeks after OA induction in the medial and total compartments. Tb.Th was significantly increased in the medial (6, 10 weeks), lateral and total compartments (2, 6 and 10 weeks after OA induction). The Tb.N was significantly decreased only in the lateral compartment at 10 weeks and Tb.Sp was significantly increased at 6 and 10 weeks in the lateral compartment. Similar regional differences (anterior and posterior) were observed in both medial and lateral compartment for tibial subchondral trabecular bone BV, BV/TV, Tb.N and Tb.Sp in the contralateral control knee at 2, 6 and 10 weeks (Table 2, 3, and 4 respectively). The regional differences in bone parameters in this study are in line with regional differences between anterior and posterior, and between medial and lateral condyles, previously reported in the literature for human OA (Bobinac et al. 2003).

In summary, the results indicate significant differences in bone histomorphometric parameters depending whether the ROI was chosen in the anterior or posterior regions of both the medial and lateral compartments of tibia. Thus, the results could be biased if the bone histomorphometric parameters are reported either from anterior ROI or posterior ROI alone. Therefore, to prevent this form of bias for the studies in this thesis, an ROI of irregular anatomical shape (Fig. 5) was manually drawn for each compartment (one ROI for the medial and one for the lateral, respectively), following the internal anatomical contours of the subchondral trabecular bone region, including the entire subchondral trabecular bone of the proximal tibia.

Table 2 Difference in tibial subchondral trabecular bone histomorphometric indices between anterior (n=12) and posterior (n=12) ROI in the control and the MIA-injected knee at 2 weeks. % diff is the difference in values between the anterior and posterior cylinder.

	2 Weeks									
	OA					Contralateral control				
	Anterior cylinder	Posterior cylinder	%diff	p-value		Anterior cylinder	Posterior cylinder	%diff	p-value	
	mean ± SD	mean ± SD				mean ± SD	mean ± SD			
BV (mm^3)										
Medial	127 ± 36	332 ± 61	-161	0.0000		202 ± 40	332 ± 53	-64	0.0000	
Lateral	113 ± 31	306 ± 65	-171	0.0000		170 ± 33	286 ± 56	-68	0.0001	
Total	240 ± 65	639 ± 111	-166	0.0000		372 ± 69	618 ± 106	-66	0.0000	
BV/TV (%)										
Medial	9.06 ± 2.57	23.70 ± 4.33	-162	0.0000		14.41 ± 2.85	23.68 ± 3.77	-64	0.0000	
Lateral	8.07 ± 2.19	21.85 ± 4.66	-171	0.0000		12.15 ± 2.38	20.38 ± 4.01	-68	0.0001	
Total	8.56 ± 2.32	22.77 ± 3.98	-166	0.0000		13.28 ± 2.47	22.03 ± 3.79	-66	0.0000	
Tb.N (1/mm)										
Medial	1.08 ± 0.28	2.44 ± 0.40	-126	0.0000		1.59 ± 0.28	2.53 ± 0.36	-59	0.0000	
Lateral	0.97 ± 0.24	2.35 ± 0.41	-141	0.0000		1.37 ± 0.25	2.32 ± 0.41	-70	0.0000	
Total	1.03 ± 0.26	2.39 ± 0.35	-133	0.0000		1.48 ± 1.48	2.43 ± 0.38	-64	0.0000	
Tb.Sp (μm)										
Medial	303 ± 27	211 ± 25	31	0.0001		275 ± 23	213 ± 23	22	0.0004	
Lateral	317 ± 22	222 ± 27	30	0.0000		296 ± 20	218 ± 21	26	0.0000	
Total	310 ± 23	216 ± 21	30	0.0000		286 ± 19	216 ± 20	25	0.0001	
Tb.Th (μm)										
Medial	84 ± 4	97 ± 5	-16	0.0005		90 ± 4	93 ± 3	-4	0.0723	
Lateral	82 ± 3	93 ± 6	-12	0.0002		89 ± 4	87 ± 3	2	0.2919	
Total	83 ± 3	95 ± 5	-14	0.0002		90 ± 3	90 ± 3	-1	0.4884	

Table 3 Difference in tibial subchondral trabecular bone histomorphometric indices between anterior (n=12) and posterior (n=12) ROI in the contralateral control and the MIA-injected knee at 6 weeks. % diff is the difference in values between the anterior and posterior cylinder.

	6 Weeks											
	OA						Contralateral Control					
	Anterior cylinder		Posterior cylinder		%diff	p-value	Anterior cylinder		Posterior cylinder		%diff	p-value
	mean ± SD		mean ± SD				mean ± SD		mean ± SD			
BV (mm^3)												
Medial	207 ± 86		602 ± 155		-191	0.0008	292 ± 72		402 ± 111		-38	0.0269
Lateral	171 ± 51		492 ± 75		-188	0.0001	236 ± 37		374 ± 87		-59	0.0042
Total	377 ± 132		1094 ± 193		-190	0.0002	527 ± 94		775 ± 189		-47	0.0101
BV/TV (%)												
Medial	14.67 ± 6.08		42.77 ± 10.94		-192	0.0008	20.77 ± 5.10		28.59 ± 7.87		-38	0.0264
Lateral	12.14 ± 3.62		35.02 ± 5.40		-188	0.0001	16.81 ± 2.64		26.65 ± 6.20		-59	0.0042
Total	13.40 ± 4.63		38.89 ± 6.75		-190	0.0001	18.79 ± 3.35		27.62 ± 6.70		-47	0.0100
Tb.N (1/mm)												
Medial	1.50 ± 0.53		3.23 ± 0.54		-116	0.0003	2.11 ± 0.40		2.88 ± 0.62		-37	0.0096
Lateral	1.31 ± 0.36		2.91 ± 0.25		-123	0.0001	1.73 ± 0.20		2.78 ± 0.53		-61	0.0007
Total	1.40 ± 0.42		3.07 ± 0.33		-119	0.0001	1.92 ± 0.25		2.83 ± 0.54		-48	0.0023
Tb.Sp (μm)												
Medial	280 ± 35		180 ± 19		36	0.0003	233 ± 30		186 ± 24		20	0.0031
Lateral	291 ± 35		201 ± 20		31	0.0005	259 ± 21		186 ± 23		28	0.0000
Total	286 ± 33		190 ± 10		33	0.0002	246 ± 22		186 ± 20		24	0.0002
Tb.Th (μm)												
Medial	96 ± 8		131 ± 16		-37	0.0042	98 ± 7		98 ± 10		0	0.9903
Lateral	93 ± 4		120 ± 10		-29	0.0009	97 ± 6		95 ± 7		2	0.5770
Total	94 ± 6		125 ± 11		-33	0.0013	97 ± 6		96 ± 8		1	0.7915

Table 4 Difference in tibial subchondral trabecular bone histomorphometric indices between anterior (n=12) and posterior (n=12) ROI in the contralateral control and the MIA-injected knee at 10 weeks. % diff is the difference in values between the anterior and posterior cylinder.

	10 Weeks													
	OA							Contralateral Control						
	Anterior cylinder			Posterior cylinder			%diff	p-value	Anterior cylinder			Posterior cylinder			%diff	p-value
	mean	±	SD	mean	±	SD			mean	±	SD	mean	±	SD		
BV (mm^3)																
Medial	318	±	157	780	±	133	-145	0.0002	366	±	102	529	±	113	-44	0.0010
Lateral	195	±	46	525	±	94	-169	0.0006	307	±	93	475	±	88	-55	0.0003
Total	513	±	191	1304	±	175	-154	0.0001	673	±	187	1004	±	192	-49	0.0004
BV/TV (%)																
Medial	22.71	±	11.20	55.62	±	9.47	-145	0.0002	26.07	±	7.34	37.66	±	8.06	-44	0.0010
Lateral	13.91	±	3.27	37.37	±	6.81	-169	0.0006	21.87	±	6.66	33.91	±	6.30	-55	0.0003
Total	18.31	±	6.81	46.49	±	6.24	-154	0.0001	23.97	±	6.69	35.79	±	6.89	-49	0.0004
Tb.N (1/mm)																
Medial	2.10	±	0.68	3.40	±	0.57	-62	0.0012	2.45	±	0.41	3.31	±	0.46	-35	0.0002
Lateral	1.47	±	0.27	2.94	±	0.21	-99	0.0000	2.09	±	0.41	3.21	±	0.37	-53	0.0000
Total	1.78	±	0.45	3.17	±	0.37	-78	0.0001	2.27	±	0.39	3.26	±	0.39	-44	0.0000
Tb.Sp (μm)																
Medial	255	±	41	174	±	33	32	0.0023	232	±	23	185	±	23	20	0.0027
Lateral	295	±	24	212	±	17	28	0.0004	251	±	18	186	±	15	26	0.0000
Total	275	±	29	193	±	17	30	0.0004	241	±	18	186	±	16	23	0.0001
Tb.Th (μm)																
Medial	104	±	20	166	±	31	-60	0.0096	105	±	13	113	±	14	-8	0.1599
Lateral	94	±	7	127	±	25	-36	0.0266	103	±	11	105	±	9	-2	0.5641
Total	99	±	13	147	±	27	-49	0.0128	104	±	12	109	±	11	-5	0.2602

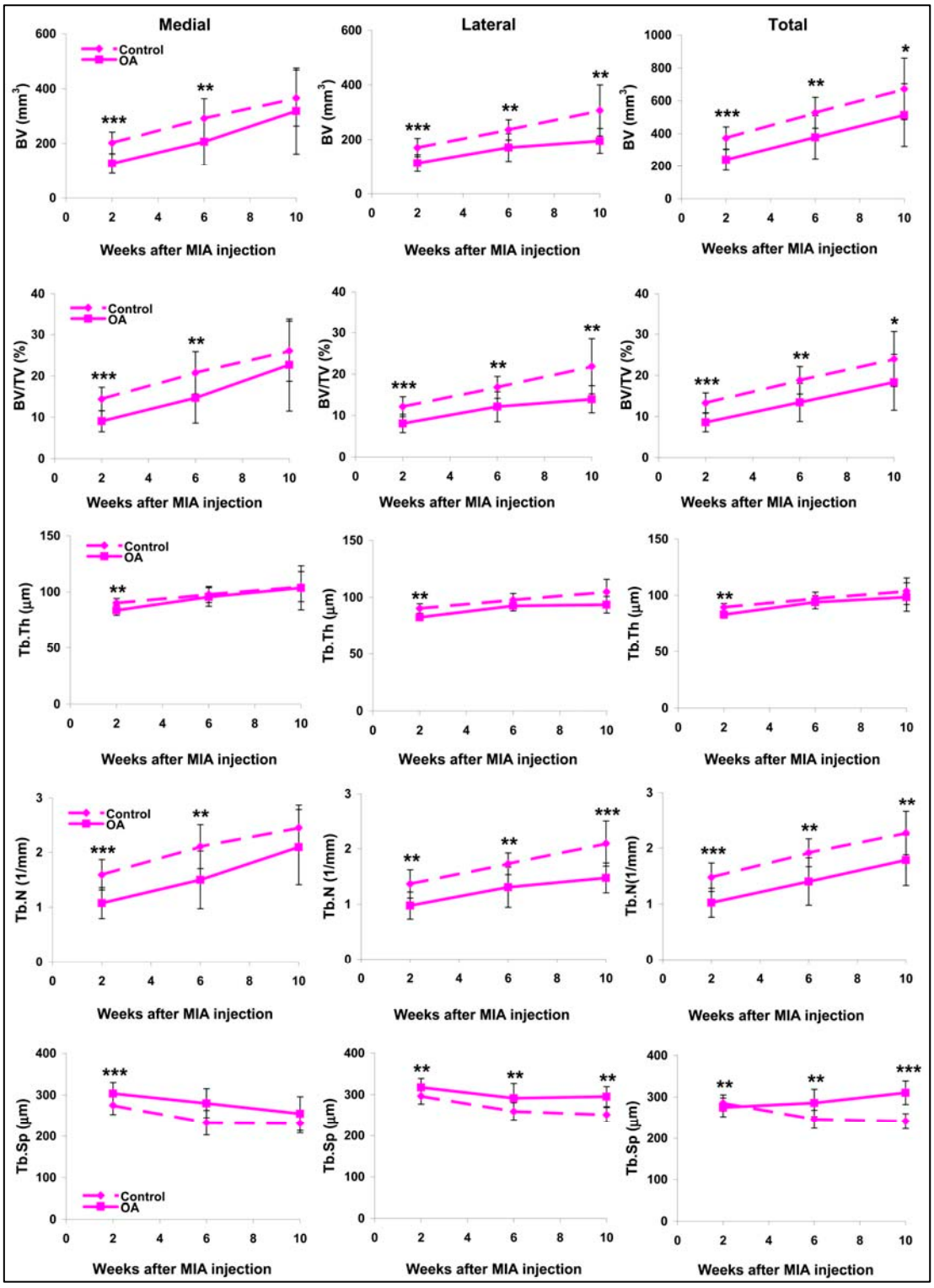

Figure 7. Tibial subchondral trabecular bone histomorphometric parameters calculated from anterior ROI (n=12) in the medial, lateral and total compartments at 2, 6, and 10 weeks for the contralateral control and the MIA-injected knee. Data represented as mean ± SD. * P <0.05, ** P <0.01, between the contralateral control and the MIA-injected tibiae.

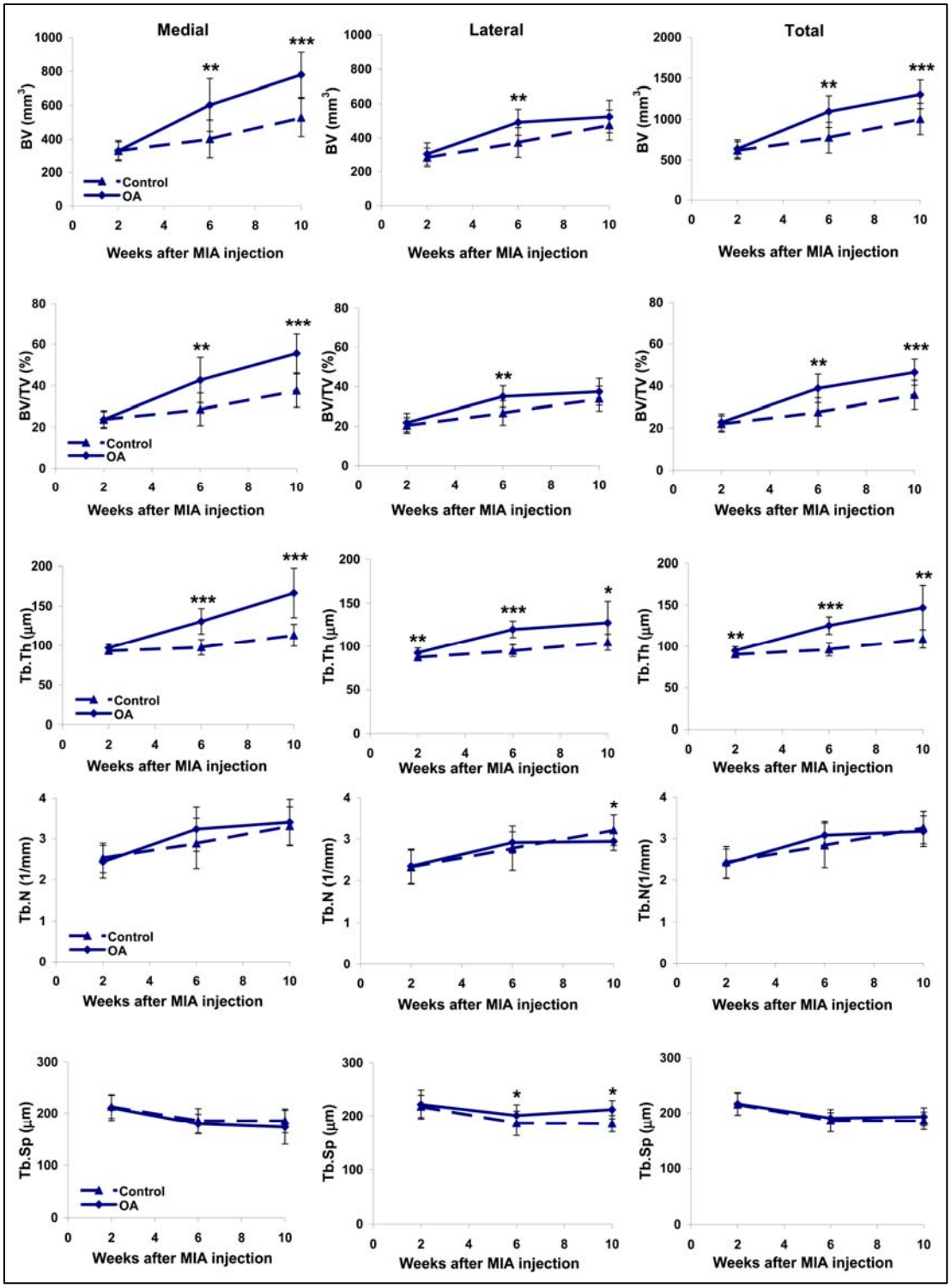

Figure 8. Tibial subchondral trabecular bone histomorphometric parameters calculated from posterior ROI (n=12) in the medial, lateral and total compartments at 2, 6, and 10 weeks for the contralateral control and the MIA-injected knee. Data represented as mean ± SD. * P <0.05, ** P <0.01, between the contralateral control and the MIA-injected tibiae.

Subchondral plate analysis

Subchondral plate thickening and increased subchondral plate porosity are important features of OA (Buckland-Wright 2004, Burr and Schaffler 1997, Dedrick et al. 1997, Intema et al. 2010). Recent studies show changes in subchondral plate thickness and porosity using micro-CT in mice and canine models of OA (Botter et al. 2011, Sniekers et al. 2008b). In the present thesis, changes in the tibial subchondral plate were determined in the MIA-injected knee and the contralateral control knee in a rat model of OA (Mohan et al. 2011). The 3D subchondral plate thickness (Pl.Th, μm) and porosity (volume of the pores in the plate over the total volume of the plate, Pl.Por, %) of the medial and lateral compartments of the tibial subchondral plate were calculated on regions, measuring 2.5 mm in length from the posterior side (Fig. 9), 1.5 mm mediolateral in width (Fig. 11).

The images were segmented using the same threshold used for subchondral trabecular bone analysis. The subchondral plate was separated from the trabecular bone of the tibia by using a software kindly provided by Botter et al (Botter et al. 2011). The separation of subchondral plate and trabecular bone was achieved by a second segmentation step after which, the cortex remains black, the trabeculae becomes dark grey, and bone marrow becomes light grey coloured (Fig. 10)

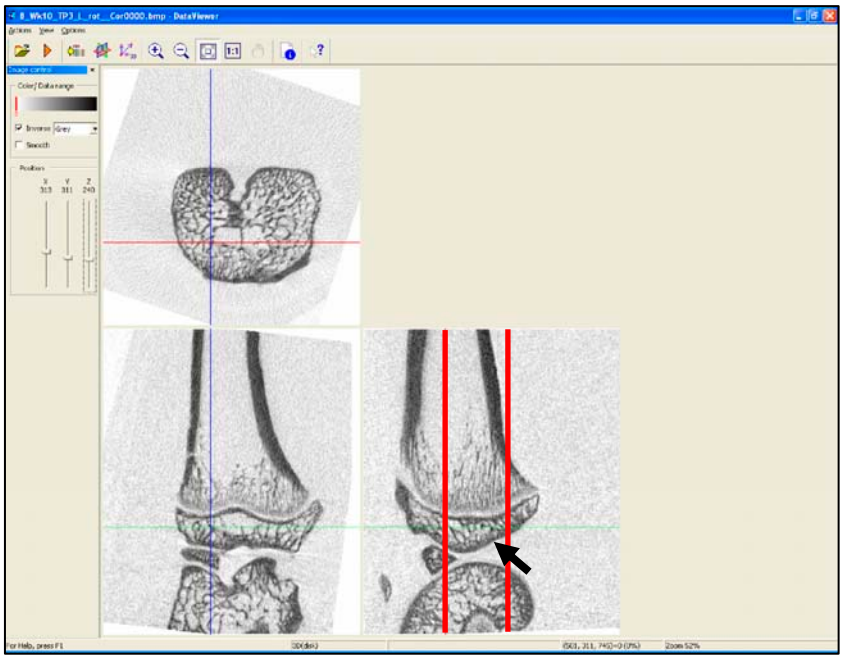

Figure 9. Image showing the selection of VOI for tibial subchondral plate analysis which included regions (between the red lines, indicated by arrow), measuring 2.5 mm in length from the posterior side.

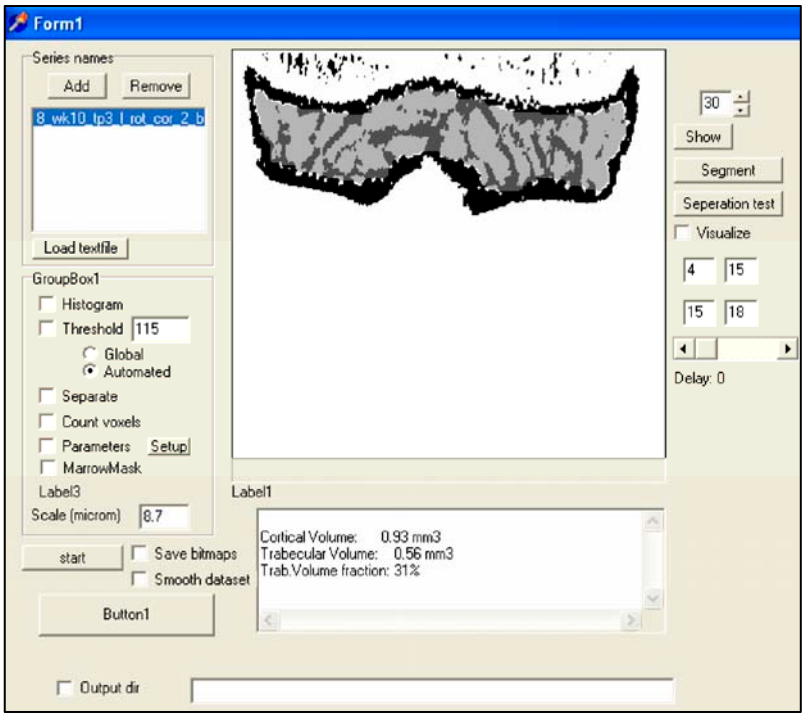

Figure 10. A software provided by Botter et al. was used to separate the subchondral plate and trabecular bone. After the second segmentation step the cortex, subchondral plate and growth plate remains black, the trabeculae becomes dark grey, and bone marrow becomes light grey coloured.

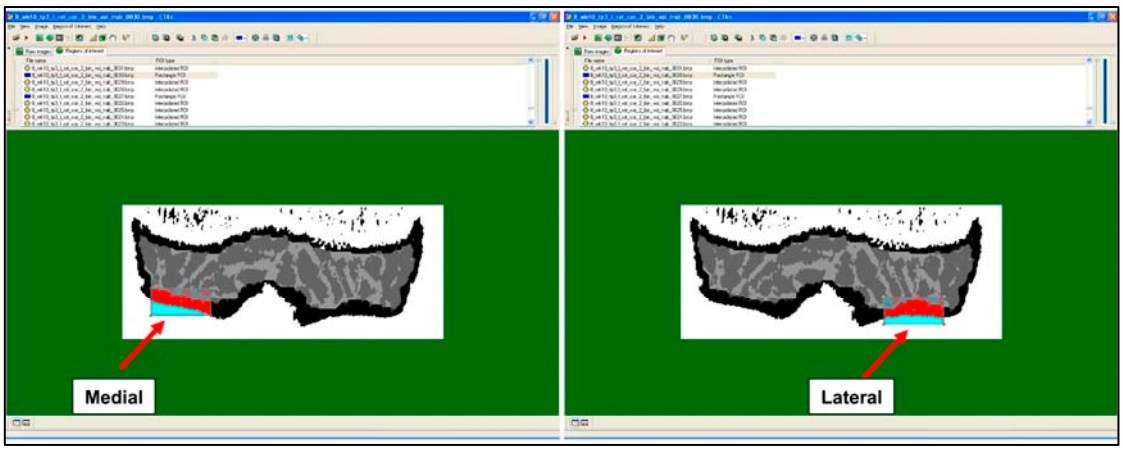

Figure 11. Calculation of tibial subchondral plate thickness and plate porosity in a region measuring 1.5 mm mediolateral in width (rectangular box indicated by arrow) in the medial and lateral compartments using CT Analyser, (V 1.8.05, Skyscan, Kontich, Belgium).

Conclusion

In vivo micro-CT scanning of rodents enables tracking of bone related changes over time. It is crucial to optimise the scanning protocol and data analysis to suit each study. The *in vivo* micro-CT protocols described in this section have been optimised to track changes in subchondral trabecular bone and subchondral bone plate, in a low-dose MIA-induced OA rat model. Reliable results obtained from *in vivo* scanning of rodent models depend on critical factors such as scanning protocol, image processing, segmentation and image analysis. All the above mentioned factors have been addressed in order to optimise scanning protocol and post processing steps to ensure that the results obtained are repeatable and accurate.

References (Chapter 1, 5 and appendices)

Agnello KA, Trumble TN, Chambers JN, Seewald W, Budsberg SC (2005) Effects of zoledronate on markers of bone metabolism and subchondral bone mineral density in dogs with experimentally induced cruciate-deficient osteoarthritis. *Am J Vet Res* 66:1487-1495.

Ahmed AM, Burke DL (1983) In-vitro measurement of static pressure distribution in synovial joints--Part I: Tibial surface of the knee. *J Biomech Eng* 105:216-225.

Aigner T, McKenna L (2002) Molecular pathology and pathobiology of osteoarthritic cartilage. *Cell Mol Life Sci* 59:5-18.

Altman RD (2010) Early management of osteoarthritis. *Am J Manag Care* 16 Suppl Management:S41-47.

Alvarez L, Peris P, Guanabens N, Vidal S, Ros I, Pons F, Filella X, Monegal A, Munoz-Gomez J, Ballesta AM (2003) Serum osteoprotegerin and its ligand in Paget's disease of bone: relationship to disease activity and effect of treatment with bisphosphonates. *Arthritis Rheum* 48:824-828.

Ameye LG, Young MF (2006) Animal models of osteoarthritis: lessons learned while seeking the "Holy Grail". *Curr Opin Rheumatol* 18:537-547.

Appleton CT, McErlain DD, Pitelka V, Schwartz N, Bernier SM, Henry JL, Holdsworth DW, Beier F (2007) Forced mobilization accelerates pathogenesis: characterization of a preclinical surgical model of osteoarthritis. *Arthritis Res Ther* 9:R13.

Arden N, Nevitt MC (2006) Osteoarthritis: epidemiology. *Best Pract Res Clin Rheumatol* 20:3-25.

Arkill KP, Winlove CP (2008) Solute transport in the deep and calcified zones of articular cartilage. *Osteoarthritis Cartilage* 16:708-714.

Aspden RM (2008) Osteoarthritis: a problem of growth not decay? *Rheumatology (Oxford)* 47:1452-1460.

Bailey AJ, Sims TJ, Knott L (2002) Phenotypic expression of osteoblast collagen in osteoarthritic bone: production of type I homotrimer. *Int J Biochem Cell Biol* 34:176-182.

Bancroft LW, Peterson JJ, Kransdorf MJ (2004) Cysts, geodes, and erosions. *Radiol Clin North Am* 42:73-87.

Banerjee M, Tripathi LM, Srivastava VM, Puri A, Shukla R (2003) Modulation of inflammatory mediators by ibuprofen and curcumin treatment during chronic inflammation in rat. *Immunopharmacol Immunotoxicol* 25:213-224.

Bar-Yehuda S, et al. (2009) Induction of an antiinflammatory effect and prevention of cartilage damage in rat knee osteoarthritis by CF101 treatment. *Arthritis Rheum* 60:3061-3071.

Bassiouni HM (2010) Bone marrow lesions in the knee: the clinical conundrum. *Int J Rheum Dis* 13:196-202.

Becerra J, Andrades JA, Guerado E, Zamora-Navas P, Lopez-Puertas JM, Reddi AH (2010) Articular cartilage: structure and regeneration. *Tissue Eng Part B Rev* 16:617-627.

Bendele AM (2001) Animal models of osteoarthritis. *J Musculoskelet Neuronal Interact* 1:363-376.

Bergstrom JD, Bostedor RG, Masarachia PJ, Reszka AA, Rodan G (2000) Alendronate is a specific, nanomolar inhibitor of farnesyl diphosphate synthase. *Arch Biochem Biophys* 373:231-241.

Berry JL, Thaeler-Oberdoerster DA, Greenwald AS (1986) Subchondral pathways to the superior surface of the human talus. *Foot Ankle* 7:2-9.

Bertrand J, Cromme C, Umlauf D, Frank S, Pap T (2010) Molecular mechanisms of cartilage remodelling in osteoarthritis. *Int J Biochem Cell Biol* 42:1594-1601.

Bettica P, Cline G, Hart DJ, Meyer J, Spector TD (2002) Evidence for increased bone resorption in patients with progressive knee osteoarthritis: longitudinal results from the Chingford study. *Arthritis Rheum* 46:3178-3184.

Beyer C, Schett G (2010) Pharmacotherapy: concepts of pathogenesis and emerging treatments. Novel targets in bone and cartilage. *Best Pract Res Clin Rheumatol* 24:489-496.

Bingham CO, 3rd, et al. (2006) Risedronate decreases biochemical markers of cartilage degradation but does not decrease symptoms or slow radiographic progression in patients with medial compartment osteoarthritis of the knee: results of the two-year multinational knee osteoarthritis structural arthritis study. *Arthritis Rheum* 54:3494-3507.

Blain EJ, Gilbert SJ, Wardale RJ, Capper SJ, Mason DJ, Duance VC (2001) Up-regulation of matrix metalloproteinase expression and activation following cyclical compressive loading of articular cartilage in vitro. *Arch Biochem Biophys* 396:49-55.

Blaney Davidson EN, van der Kraan PM, van den Berg WB (2007a) TGF-beta and osteoarthritis. *Osteoarthritis Cartilage* 15:597-604.

Blaney Davidson EN, Vitters EL, van der Kraan PM, van den Berg WB (2006) Expression of transforming growth factor-beta (TGFbeta) and the TGFbeta signalling molecule SMAD-2P in spontaneous and instability-induced osteoarthritis: role in cartilage degradation, chondrogenesis and osteophyte formation. *Ann Rheum Dis* 65:1414-1421.

Blaney Davidson EN, Vitters EL, van Beuningen HM, van de Loo FA, van den Berg WB, van der Kraan PM (2007b) Resemblance of osteophytes in experimental osteoarthritis to transforming growth factor beta-induced osteophytes: limited role of bone morphogenetic protein in early osteoarthritic osteophyte formation. *Arthritis Rheum* 56:4065-4073.

Blom AB, et al. (2009) Involvement of the Wnt signaling pathway in experimental and human osteoarthritis: prominent role of Wnt-induced signaling protein 1. *Arthritis Rheum* 60:501-512.

Bobinac D, Spanjol J, Zoricic S, Maric I (2003) Changes in articular cartilage and subchondral bone histomorphometry in osteoarthritic knee joints in humans. *Bone* 32:284-290.

Boegard T, Rudling O, Petersson IF, Jonsson K (1998) Correlation between radiographically diagnosed osteophytes and magnetic resonance detected cartilage defects in the tibiofemoral joint. *Ann Rheum Dis* 57:401-407.

Botter SM, van Osch GJ, Clockaerts S, Waarsing JH, Weinans H, van Leeuwen JP (2011) Osteoarthritis induction leads to early and temporal subchondral plate porosity in the tibial plateau of mice: an in vivo microfocal computed tomography study. *Arthritis Rheum* 63:2690-2699.

Botter SM, van Osch GJ, Waarsing JH, Day JS, Verhaar JA, Pols HA, van Leeuwen JP, Weinans H (2006) Quantification of subchondral bone changes in a murine osteoarthritis model using micro-CT. *Biorheology* 43:379-388.

Bouxsein ML, Boyd SK, Christiansen BA, Guldberg RE, Jepsen KJ, Muller R (2010) Guidelines for assessment of bone microstructure in rodents using micro-computed tomography. *J Bone Miner Res* 25:1468-1486.

Bove SE, Calcaterra SL, Brooker RM, Huber CM, Guzman RE, Juneau PL, Schrier DJ, Kilgore KS (2003) Weight bearing as a measure of disease progression and efficacy of anti-inflammatory compounds in a model of monosodium iodoacetate-induced osteoarthritis. *Osteoarthritis Cartilage* 11:821-830.

Boyce BF, Xing L (2008) Functions of RANKL/RANK/OPG in bone modeling and remodeling. *Arch Biochem Biophys* 473:139-146.

Boyd SK, Davison P, Muller R, Gasser JA (2006) Monitoring individual morphological changes over time in ovariectomized rats by in vivo micro-computed tomography. *Bone* 39:854-862.

Brandi ML (2009) Microarchitecture, the key to bone quality. *Rheumatology (Oxford)* 48 Suppl 4:iv3-8.

Brandt KD (2002) Animal models of osteoarthritis. *Biorheology* 39:221-235.

Brandt KD, Myers SL, Burr D, Albrecht M (1991) Osteoarthritic changes in canine articular cartilage, subchondral bone, and synovium fifty-four months after transection of the anterior cruciate ligament. *Arthritis Rheum* 34:1560-1570.

Breuil V, Cosman F, Stein L, Horbert W, Nieves J, Shen V, Lindsay R, Dempster DW (1998) Human osteoclast formation and activity in vitro: effects of alendronate. *J Bone Miner Res* 13:1721-1729.

Brouwers JE, van Rietbergen B, Huiskes R (2007) No effects of in vivo micro-CT radiation on structural parameters and bone marrow cells in proximal tibia of wistar rats detected after eight weekly scans. *J Orthop Res* 25:1325-1332.

Brouwers JE, Lambers FM, Gasser JA, van Rietbergen B, Huiskes R (2008) Bone degeneration and recovery after early and late bisphosphonate treatment of ovariectomized wistar rats assessed by in vivo micro-computed tomography. *Calcif Tissue Int* 82:202-211.

Brown TD, Vrahas MS (1984) The apparent elastic modulus of the juxtarticular subchondral bone of the femoral head. *J Orthop Res* 2:32-38.

Buckland-Wright C (2004) Subchondral bone changes in hand and knee osteoarthritis detected by radiography. *Osteoarthritis Cartilage* 12 Suppl A:S10-19.

Buckland-Wright C, Macfarlane D, Lynch J (1991a) Quantitative microfocal radiographic assessment of disease and progression in osteoarthritis of the hand. *J Rheumatol Suppl* 27:40-41.

Buckland-Wright JC, MacFarlane DG, Lynch JA (1992) Relationship between joint space width and subchondral sclerosis in the osteoarthritic hand: a quantitative microfocal radiographic study. *J Rheumatol* 19:788-795.

Buckland-Wright JC, Macfarlane DG, Jasani MK, Lynch JA (1994) Quantitative microfocal radiographic assessment of osteoarthritis of the knee from weight bearing tunnel and semiflexed standing views. *J Rheumatol* 21:1734-1741.

Buckland-Wright JC, Macfarlane DG, Fogelman I, Emery P, Lynch JA (1991b) Techetium 99m methylene diphosphonate bone scanning in osteoarthritic hands. *Eur J Nucl Med* 18:12-16.

Buckland-Wright JC, Messent EA, Bingham CO, 3rd, Ward RJ, Tonkin C (2007) A 2 yr longitudinal radiographic study examining the effect of a bisphosphonate (risedronate) upon subchondral bone loss in osteoarthritic knee patients. *Rheumatology (Oxford)* 46:257-264.

Buckwalter JA, Mankin HJ (1998) Articular cartilage: tissue design and chondrocyte-matrix interactions. *Instr Course Lect* 47:477-486.

Buckwalter JA, Saltzman C, Brown T (2004) The impact of osteoarthritis: implications for research. *Clin Orthop Relat Res*:S6-15.

Burghardt AJ, Kazakia GJ, Sode M, de Papp AE, Link TM, Majumdar S (2010) A longitudinal HR-pQCT study of alendronate treatment in postmenopausal women with low bone density: Relations among density, cortical and trabecular microarchitecture, biomechanics, and bone turnover. *J Bone Miner Res* 25:2558-2571.

Burr DB, Schaffler MB (1997) The involvement of subchondral mineralized tissues in osteoarthrosis: quantitative microscopic evidence. *Microsc Res Tech* 37:343-357.

Burr DB, Radin EL (2003) Microfractures and microcracks in subchondral bone: are they relevant to osteoarthrosis? *Rheum Dis Clin North Am* 29:675-685.

Cai X, Wong YF, Zhou H, Xie Y, Liu ZQ, Jiang ZH, Bian ZX, Xu HX, Liu L (2006) The comparative study of Sprague-Dawley and Lewis rats in adjuvant-induced arthritis. *Naunyn Schmiedebergs Arch Pharmacol* 373:140-147.

Calvo E, Palacios I, Delgado E, Ruiz-Cabello J, Hernandez P, Sanchez-Pernaute O, Egido J, Herrero-Beaumont G (2001) High-resolution MRI detects cartilage swelling at the early stages of experimental osteoarthritis. *Osteoarthritis Cartilage* 9:463-472.

Canalis E, Economides AN, Gazzerro E (2003) Bone morphogenetic proteins, their antagonists, and the skeleton. *Endocr Rev* 24:218-235.

Carbone LD, et al. (2004) The relationship of antiresorptive drug use to structural findings and symptoms of knee osteoarthritis. *Arthritis Rheum* 50:3516-3525.

Carlson CS, Loeser RF, Jayo MJ, Weaver DS, Adams MR, Jerome CP (1994) Osteoarthritis in cynomolgus macaques: a primate model of naturally occurring disease. *J Orthop Res* 12:331-339.

Carrino JA, Blum J, Parellada JA, Schweitzer ME, Morrison WB (2006) MRI of bone marrow edema-like signal in the pathogenesis of subchondral cysts. *Osteoarthritis Cartilage* 14:1081-1085.

Cawston TE, Wilson AJ (2006) Understanding the role of tissue degrading enzymes and their inhibitors in development and disease. *Best Pract Res Clin Rheumatol* 20:983-1002.

Chan TF, Couchourel D, Abed E, Delalandre A, Duval N, Lajeunesse D (2011) Elevated Dickkopf-2 levels contribute to the abnormal phenotype of human osteoarthritic osteoblasts. *J Bone Miner Res* 26:1399-1410.

Chappard C, Peyrin F, Bonnassie A, Lemineur G, Brunet-Imbault B, Lespessailles E, Benhamou CL (2006) Subchondral bone micro-architectural alterations in osteoarthritis: a synchrotron micro-computed tomography study. *Osteoarthritis Cartilage* 14:215-223.

Chowdhury TT, Salter DM, Bader DL, Lee DA (2008) Signal transduction pathways involving p38 MAPK, JNK, NFkappaB and AP-1 influences the response of chondrocytes cultured in agarose constructs to IL-1beta and dynamic compression. *Inflamm Res* 57:306-313.

Clark AL (2008) Osteoarthritis: what we have been missing in the patellofemoral joint. *Exerc Sport Sci Rev* 36:30-37.

Clark JM (1990) The structure of vascular channels in the subchondral plate. *J Anat* 171:105-115.

Clark JM, Huber JD (1990) The structure of the human subchondral plate. *J Bone Joint Surg Br* 72:866-873.

Clarke B (2008) Normal bone anatomy and physiology. *Clin J Am Soc Nephrol* 3 Suppl 3:S131-139.

Cole JH, van der Meulen MC (2011) Whole bone mechanics and bone quality. *Clin Orthop Relat Res* 469:2139-2149.

Combe R, Bramwell S, Field MJ (2004) The monosodium iodoacetate model of osteoarthritis: a model of chronic nociceptive pain in rats? *Neurosci Lett* 370:236-240.

Compston J (2006) Bone quality: what is it and how is it measured? *Arq Bras Endocrinol Metabol* 50:579-585.

Corrado A, Santoro N, Cantatore FP (2007) Extra-skeletal effects of bisphosphonates. *Joint Bone Spine* 74:32-38.

Couchourel D, Aubry I, Delalandre A, Lavigne M, Martel-Pelletier J, Pelletier JP, Lajeunesse D (2009) Altered mineralization of human osteoarthritic osteoblasts is attributable to abnormal type I collagen production. *Arthritis Rheum* 60:1438-1450.

Crema MD, Roemer FW, Marra MD, Guermazi A (2009) Magnetic resonance imaging assessment of subchondral bone and soft tissues in knee osteoarthritis. *Rheum Dis Clin North Am* 35:557-577.

Crema MD, Roemer FW, Marra MD, Niu J, Lynch JA, Felson DT, Guermazi A (2010a) Contrast-enhanced MRI of subchondral cysts in patients with or at risk for knee osteoarthritis: the MOST study. *Eur J Radiol* 75:e92-96.

Crema MD, et al. (2010b) Subchondral cystlike lesions develop longitudinally in areas of bone marrow edema-like lesions in patients with or at risk for knee osteoarthritis: detection with MR imaging--the MOST study. *Radiology* 256:855-862.

Dalle Carbonare L, Giannini S (2004) Bone microarchitecture as an important determinant of bone strength. *J Endocrinol Invest* 27:99-105.

Dare A, Hachisu R, Yamaguchi A, Yokose S, Yoshiki S, Okano T (1997) Effects of ionizing radiation on proliferation and differentiation of osteoblast-like cells. *J Dent Res* 76:658-664.

Day JS, Ding M, van der Linden JC, Hvid I, Sumner DR, Weinans H (2001) A decreased subchondral trabecular bone tissue elastic modulus is associated with pre-arthritic cartilage damage. *J Orthop Res* 19:914-918.

Day JS, Van Der Linden JC, Bank RA, Ding M, Hvid I, Sumner DR, Weinans H (2004) Adaptation of subchondral bone in osteoarthritis. *Biorheology* 41:359-368.

Dedrick DK, Goulet RW, O'Connor BL, Brandt KD (1997) Preliminary report: increased porosity of the subchondral plate in an accelerated canine model of osteoarthritis. *Osteoarthritis Cartilage* 5:71-74.

Del Carlo M, Jr., Loeser RF (2008) Cell death in osteoarthritis. *Curr Rheumatol Rep* 10:37-42.

Dempster DW (2000) The contribution of trabecular architecture to cancellous bone quality. *J Bone Miner Res* 15:20-23.

Devogelaer JP (2000) Treatment of bone diseases with bisphosphonates, excluding osteoporosis. *Curr Opin Rheumatol* 12:331-335.

Diarra D, et al. (2007) Dickkopf-1 is a master regulator of joint remodeling. *Nat Med* 13:156-163.

Dieppe P (1999) Subchondral bone should be the main target for the treatment of pain and disease progression in osteoarthritis. *Osteoarthritis Cartilage* 7:325-326.

Ding M, Odgaard A, Hvid I (1999) Accuracy of cancellous bone volume fraction measured by micro-CT scanning. *J Biomech* 32:323-326.

Dreier R (2010) Hypertrophic differentiation of chondrocytes in osteoarthritis: the developmental aspect of degenerative joint disorders. *Arthritis Res Ther* 12:216.

Duncan H, Jundt J, Riddle JM, Pitchford W, Christopherson T (1987) The tibial subchondral plate. A scanning electron microscopic study. *J Bone Joint Surg Am* 69:1212-1220.

Durr HD, Martin H, Pellengahr C, Schlemmer M, Maier M, Jansson V (2004) The cause of subchondral bone cysts in osteoarthrosis: a finite element analysis. *Acta Orthop Scand* 75:554-558.

Edwards JR, Mundy GR (2011) Advances in osteoclast biology: old findings and new insights from mouse models. *Nat Rev Rheumatol* 7:235-243.

Englund M (2010) The role of biomechanics in the initiation and progression of OA of the knee. *Best Pract Res Clin Rheumatol* 24:39-46.

Eriksen EF (2010) Cellular mechanisms of bone remodeling. *Rev Endocr Metab Disord* 11:219-227.

Eslami B, Zhou S, Van Eekeren I, LeBoff MS, Glowacki J (2011) Reduced osteoclastogenesis and RANKL expression in marrow from women taking alendronate. *Calcif Tissue Int* 88:272-280.

Fazzalari NL, Parkinson IH (1998) Femoral trabecular bone of osteoarthritic and normal subjects in an age and sex matched group. *Osteoarthritis Cartilage* 6:377-382.

Fazzalari NL, Vernon-Roberts B, Darracott J (1987) Osteoarthritis of the hip. Possible protective and causative roles of trabecular microfractures in the head of the femur. *Clin Orthop Relat Res*:224-233.

Fazzalari NL, Kuliwaba JS, Atkins GJ, Forwood MR, Findlay DM (2001) The ratio of messenger RNA levels of receptor activator of nuclear factor kappaB ligand to osteoprotegerin correlates with bone remodeling indices in normal human cancellous bone but not in osteoarthritis. *J Bone Miner Res* 16:1015-1027.

Felson DT, Zhang Y (1998) An update on the epidemiology of knee and hip osteoarthritis with a view to prevention. *Arthritis Rheum* 41:1343-1355.

Felson DT, Chaisson CE, Hill CL, Totterman SM, Gale ME, Skinner KM, Kazis L, Gale DR (2001) The association of bone marrow lesions with pain in knee osteoarthritis. *Ann Intern Med* 134:541-549.

Felson DT, et al. (2000) Osteoarthritis: new insights. Part 1: the disease and its risk factors. *Ann Intern Med* 133:635-646.

Fernihough J, Gentry C, Malcangio M, Fox A, Rediske J, Pellas T, Kidd B, Bevan S, Winter J (2004) Pain related behaviour in two models of osteoarthritis in the rat knee. *Pain* 112:83-93.

Ferreira-Gomes J, Adaes S, Sarkander J, Castro-Lopes JM (2010) Phenotypic alterations of neurons that innervate osteoarthritic joints in rats. *Arthritis Rheum* 62:3677-3685.

Fisher JE, Rodan GA, Reszka AA (2000) In vivo effects of bisphosphonates on the osteoclast mevalonate pathway. *Endocrinology* 141:4793-4796.

Frost HM, ed. 1983. Bone histomorphometry: Analysis of trabecular bone dynamics Florida: CRC Press, Inc.

Funck-Brentano T, Cohen-Solal M (2011) Crosstalk between cartilage and bone: when bone cytokines matter. *Cytokine Growth Factor Rev* 22:91-97.

Furuhama K, Onodera T (1983) A simple technique for repeated blood collection from the tail vein of the rat. *J Toxicol Sci* 8:161-163.

Garnero P, Piperno M, Gineyts E, Christgau S, Delmas PD, Vignon E (2001) Cross sectional evaluation of biochemical markers of bone, cartilage, and synovial tissue metabolism in patients with knee osteoarthritis: relations with disease activity and joint damage. *Ann Rheum Dis* 60:619-626.

Garnero P, Aronstein WS, Cohen SB, Conaghan PG, Cline GA, Christiansen C, Beary JF, Meyer JM, Bingham CO, 3rd (2008) Relationships between biochemical markers of bone and cartilage degradation with radiological progression in patients with knee

osteoarthritis receiving risedronate: the Knee Osteoarthritis Structural Arthritis randomized clinical trial. *Osteoarthritis Cartilage* 16:660-666.

Giuliani N, et al. (2002) Human myeloma cells stimulate the receptor activator of nuclear factor-kappa B ligand (RANKL) in T lymphocytes: a potential role in multiple myeloma bone disease. *Blood* 100:4615-4621.

Glasson SS, Blanchet TJ, Morris EA (2007) The surgical destabilization of the medial meniscus (DMM) model of osteoarthritis in the 129/SvEv mouse. *Osteoarthritis Cartilage* 15:1061-1069.

Goldring SR (2008) The role of bone in osteoarthritis pathogenesis. *Rheum Dis Clin North Am* 34:561-571.

Goldring SR (2009) Role of bone in osteoarthritis pathogenesis. *Med Clin North Am* 93:25-35, xv.

Guingamp C, Gegout-Pottie P, Philippe L, Terlain B, Netter P, Gillet P (1997) Mono-iodoacetate-induced experimental osteoarthritis: a dose-response study of loss of mobility, morphology, and biochemistry. *Arthritis Rheum* 40:1670-1679.

Guzman RE, Evans MG, Bove S, Morenko B, Kilgore K (2003) Mono-iodoacetate-induced histologic changes in subchondral bone and articular cartilage of rat femorotibial joints: an animal model of osteoarthritis. *Toxicol Pathol* 31:619-624.

Hardingham T (2008) Extracellular matrix and pathogenic mechanisms in osteoarthritis. *Curr Rheumatol Rep* 10:30-36.

Hayami T, Pickarski M, Zhuo Y, Wesolowski GA, Rodan GA, Duong le T (2006) Characterization of articular cartilage and subchondral bone changes in the rat anterior cruciate ligament transection and meniscectomized models of osteoarthritis. *Bone* 38:234-243.

Hayami T, Pickarski M, Wesolowski GA, McLane J, Bone A, Destefano J, Rodan GA, Duong le T (2004) The role of subchondral bone remodeling in osteoarthritis: reduction of cartilage degeneration and prevention of osteophyte formation by alendronate in the rat anterior cruciate ligament transection model. *Arthritis Rheum* 50:1193-1206.

Hayashi D, Guermazi A, Kwoh CK, Hannon MJ, Moore C, Jakicic JM, Green SM, Roemer FW (2011) Semiquantitative assessment of subchondral bone marrow edema-like lesions and subchondral cysts of the knee at 3T MRI: a comparison between intermediate-weighted fat-suppressed spin echo and Dual Echo Steady State sequences. *BMC Musculoskelet Disord* 12:198.

Hayashi M, Muneta T, Ju YJ, Mochizuki T, Sekiya I (2008) Weekly intra-articular injections of bone morphogenetic protein-7 inhibits osteoarthritis progression. *Arthritis Res Ther* 10:R118.

Haynes DR, Crotti TN, Loric M, Bain GI, Atkins GJ, Findlay DM (2001) Osteoprotegerin and receptor activator of nuclear factor kappaB ligand (RANKL)

regulate osteoclast formation by cells in the human rheumatoid arthritic joint. *Rheumatology (Oxford)* 40:623-630.

Heinegard D, Saxne T (2011) The role of the cartilage matrix in osteoarthritis. *Nat Rev Rheumatol* 7:50-56.

Herrero-Beaumont G, Roman-Blas JA, Castaneda S, Jimenez SA (2009) Primary osteoarthritis no longer primary: three subsets with distinct etiological, clinical, and therapeutic characteristics. *Semin Arthritis Rheum* 39:71-80.

Hilal G, Martel-Pelletier J, Pelletier JP, Ranger P, Lajeunesse D (1998) Osteoblast-like cells from human subchondral osteoarthritic bone demonstrate an altered phenotype in vitro: possible role in subchondral bone sclerosis. *Arthritis Rheum* 41:891-899.

Hildebrand T, Laib A, Muller R, Dequeker J, Ruegsegger P (1999) Direct three-dimensional morphometric analysis of human cancellous bone: microstructural data from spine, femur, iliac crest, and calcaneus. *J Bone Miner Res* 14:1167-1174.

Hildebrandt IJ, Su H, Weber WA (2008) Anesthesia and other considerations for in vivo imaging of small animals. *ILAR J* 49:17-26.

Hopwood B, Tsykin A, Findlay DM, Fazzalari NL (2007) Microarray gene expression profiling of osteoarthritic bone suggests altered bone remodelling, WNT and transforming growth factor-beta/bone morphogenic protein signalling. *Arthritis Res Ther* 9:R100.

Hopwood B, Gronthos S, Kuliwaba JS, Robey PG, Findlay DM, Fazzalari NL (2005) Identification of differentially expressed genes between osteoarthritic and normal trabecular bone from the intertrochanteric region of the proximal femur using cDNA microarray analysis. *Bone* 36:635-644.

Huebner JL, Hanes MA, Beekman B, TeKoppele JM, Kraus VB (2002) A comparative analysis of bone and cartilage metabolism in two strains of guinea-pig with varying degrees of naturally occurring osteoarthritis. *Osteoarthritis Cartilage* 10:758-767.

Hughes DE, Wright KR, Uy HL, Sasaki A, Yoneda T, Roodman GD, Mundy GR, Boyce BF (1995) Bisphosphonates promote apoptosis in murine osteoclasts in vitro and in vivo. *J Bone Miner Res* 10:1478-1487.

Hunter DJ, Hart D, Snieder H, Bettica P, Swaminathan R, Spector TD (2003) Evidence of altered bone turnover, vitamin D and calcium regulation with knee osteoarthritis in female twins. *Rheumatology (Oxford)* 42:1311-1316.

Hunziker EB, Quinn TM, Hauselmann HJ (2002) Quantitative structural organization of normal adult human articular cartilage. *Osteoarthritis Cartilage* 10:564-572.

Hutchinson WL, Koenig W, Frohlich M, Sund M, Lowe GD, Pepys MB (2000) Immunoradiometric assay of circulating C-reactive protein: age-related values in the adult general population. *Clin Chem* 46:934-938.

Hutton CW, Higgs ER, Jackson PC, Watt I, Dieppe PA (1986) 99mTc HMDP bone scanning in generalised nodal osteoarthritis. II. The four hour bone scan image predicts radiographic change. *Ann Rheum Dis* 45:622-626.

Ikeda T, Kasai M, Utsuyama M, Hirokawa K (2001) Determination of three isoforms of the receptor activator of nuclear factor-kappaB ligand and their differential expression in bone and thymus. *Endocrinology* 142:1419-1426.

Imhof H, Sulzbacher I, Grampp S, Czerny C, Youssefzadeh S, Kainberger F (2000) Subchondral bone and cartilage disease: a rediscovered functional unit. *Invest Radiol* 35:581-588.

Intema F, Hazewinkel HA, Gouwens D, Bijlsma JW, Weinans H, Lafeber FP, Mastbergen SC (2010) In early OA, thinning of the subchondral plate is directly related to cartilage damage: results from a canine ACLT-meniscectomy model. *Osteoarthritis Cartilage* 18:691-698.

Ivanavicius SP, Ball AD, Heapy CG, Westwood FR, Murray F, Read SJ (2007) Structural pathology in a rodent model of osteoarthritis is associated with neuropathic pain: increased expression of ATF-3 and pharmacological characterisation. *Pain* 128:272-282.

Jabbar S, Drury J, Fordham JN, Datta HK, Francis RM, Tuck SP (2011) Osteoprotegerin, RANKL and bone turnover in postmenopausal osteoporosis. *J Clin Pathol* 64:354-357.

Janusz MJ, Little CB, King LE, Hookfin EB, Brown KK, Heitmeyer SA, Caterson B, Poole AR, Taiwo YO (2004) Detection of aggrecanase- and MMP-generated catabolic neoepitopes in the rat iodoacetate model of cartilage degeneration. *Osteoarthritis Cartilage* 12:720-728.

Janusz MJ, et al. (2001) Moderation of iodoacetate-induced experimental osteoarthritis in rats by matrix metalloproteinase inhibitors. *Osteoarthritis Cartilage* 9:751-760.

Jobke B, Kulle B, Semler J, Delling G (2006) Bisphosphonates improve bone microarchitecture in middle-aged males with osteoporosis by reducing bone turnover: A paired biopsy micro-CT analysis over 38 months. *Journal of Bone and Mineral Research* 21:S87-S87.

Jones DH, Kong YY, Penninger JM (2002) Role of RANKL and RANK in bone loss and arthritis. *Ann Rheum Dis* 61 Suppl 2:ii32-39.

Jones MD, Tran CW, Li G, Maksymowych WP, Zernicke RF, Doschak MR (2010) In vivo microfocal computed tomography and micro-magnetic resonance imaging evaluation of antiresorptive and antiinflammatory drugs as preventive treatments of osteoarthritis in the rat. *Arthritis Rheum* 62:2726-2735.

Kalbhen DA 1984. Degenerative joint disease following chondrocyte injury: chemically induced osteoarthritis. Pages 299-309 in Verbruggen G, Veys EM, eds. Degenerative Joints. Ghent: Elsevier Science Publishers.

Kalbhen DA (1987) Chemical model of osteoarthritis--a pharmacological evaluation. *J Rheumatol* 14 Spec No:130-131.

Kalff KM, El Mouedden M, van Egmond J, Veening J, Joosten L, Scheffer GJ, Meert T, Vissers K (2010) Pre-treatment with capsaicin in a rat osteoarthritis model reduces the symptoms of pain and bone damage induced by monosodium iodoacetate. *Eur J Pharmacol* 641:108-113.

Kao TW, Lu IS, Liao KC, Lai HY, Loh CH, Kuo HK (2009) Associations between body mass index and serum levels of C-reactive protein. *S Afr Med J* 99:326-330.

Kapadia RD, Stroup GB, Badger AM, Koller B, Levin JM, Coatney RW, Dodds RA, Liang X, Lark MW, Gowen M (1998) Applications of micro-CT and MR microscopy to study pre-clinical models of osteoporosis and osteoarthritis. *Technol Health Care* 6:361-372.

Kapoor M, Martel-Pelletier J, Lajeunesse D, Pelletier JP, Fahmi H (2011) Role of proinflammatory cytokines in the pathophysiology of osteoarthritis. *Nat Rev Rheumatol* 7:33-42.

Kearns AE, Khosla S, Kostenuik PJ (2008) Receptor activator of nuclear factor kappaB ligand and osteoprotegerin regulation of bone remodeling in health and disease. *Endocr Rev* 29:155-192.

Kerkhof HJ, Bierma-Zeinstra SM, Castano-Betancourt MC, de Maat MP, Hofman A, Pols HA, Rivadeneira F, Witteman JC, Uitterlinden AG, van Meurs JB (2010) Serum C reactive protein levels and genetic variation in the CRP gene are not associated with the prevalence, incidence or progression of osteoarthritis independent of body mass index. *Ann Rheum Dis* 69:1976-1982.

Khosla S (2001) Minireview: the OPG/RANKL/RANK system. *Endocrinology* 142:5050-5055.

Kijowski R, Blankenbaker DG, Stanton PT, Fine JP, De Smet AA (2006) Radiographic findings of osteoarthritis versus arthroscopic findings of articular cartilage degeneration in the tibiofemoral joint. *Radiology* 239:818-824.

Kim HA, Blanco FJ (2007) Cell death and apoptosis in osteoarthritic cartilage. *Curr Drug Targets* 8:333-345.

Kimmel DB (2007) Mechanism of action, pharmacokinetic and pharmacodynamic profile, and clinical applications of nitrogen-containing bisphosphonates. *J Dent Res* 86:1022-1033.

Kirsch T, Swoboda B, Nah H (2000) Activation of annexin II and V expression, terminal differentiation, mineralization and apoptosis in human osteoarthritic cartilage. *Osteoarthritis Cartilage* 8:294-302.

Kleemann RU, Krocker D, Cedraro A, Tuischer J, Duda GN (2005) Altered cartilage mechanics and histology in knee osteoarthritis: relation to clinical assessment (ICRS Grade). *Osteoarthritis Cartilage* 13:958-963.

Klinck RJ, Campbell GM, Boyd SK (2008) Radiation effects on bone architecture in mice and rats resulting from in vivo micro-computed tomography scanning. *Med Eng Phys* 30:888-895.

Kobayashi K, Imaizumi R, Sumichika H, Tanaka H, Goda M, Fukunari A, Komatsu H (2003) Sodium iodoacetate-induced experimental osteoarthritis and associated pain model in rats. *J Vet Med Sci* 65:1195-1199.

Kohli SS, Kohli VS (2011) Role of RANKL-RANK/osteoprotegerin molecular complex in bone remodeling and its immunopathologic implications. *Indian J Endocrinol Metab* 15:175-181.

Komuro H, Olee T, Kuhn K, Quach J, Brinson DC, Shikhman A, Valbracht J, Creighton-Achermann L, Lotz M (2001) The osteoprotegerin/receptor activator of nuclear factor kappaB/receptor activator of nuclear factor kappaB ligand system in cartilage. *Arthritis Rheum* 44:2768-2776.

Kouri JB, Lavalle C (2006) Do chondrocytes undergo "activation" and "transdifferentiation" during the pathogenesis of osteoarthritis? A review of the ultrastructural and immunohistochemical evidence. *Histol Histopathol* 21:793-802.

Kouri JB, Jimenez SA, Quintero M, Chico A (1996a) Ultrastructural study of chondrocytes from fibrillated and non-fibrillated human osteoarthritic cartilage. *Osteoarthritis Cartilage* 4:111-125.

Kouri JB, Arguello C, Quintero M, Chico A, Ramos ME (1996b) Variability in the cell phenotype of aggregates or "clones" of human osteoarthritic cartilage. A case report. *Biocell* 20:191-200.

Krishnan V, Bryant HU, Macdougald OA (2006) Regulation of bone mass by Wnt signaling. *J Clin Invest* 116:1202-1209.

Kuliwaba JS, Findlay DM, Atkins GJ, Forwood MR, Fazzalari NL (2000) Enhanced expression of osteocalcin mRNA in human osteoarthritic trabecular bone of the proximal femur is associated with decreased expression of interleukin-6 and interleukin-11 mRNA. *J Bone Miner Res* 15:332-341.

Kumarasinghe DD, Hopwood B, Kuliwaba JS, Atkins GJ, Fazzalari NL (2011) An update on primary hip osteoarthritis including altered Wnt and TGF-beta associated gene expression from the bony component of the disease. *Rheumatology (Oxford)* 50:2166-2175.

Kumarasinghe DD, Perilli E, Tsangari H, Truong L, Kuliwaba JS, Hopwood B, Atkins GJ, Fazzalari NL (2010) Critical molecular regulators, histomorphometric indices and their correlations in the trabecular bone in primary hip osteoarthritis. *Osteoarthritis Cartilage* 18:1337-1344.

Kurien BT, Everds NE, Scofield RH (2004) Experimental animal urine collection: a review. *Lab Anim* 38:333-361.

Kwan Tat S, Lajeunesse D, Pelletier JP, Martel-Pelletier J (2010) Targeting subchondral bone for treating osteoarthritis: what is the evidence? *Best Pract Res Clin Rheumatol* 24:51-70.

Kwan Tat S, Pelletier JP, Lajeunesse D, Fahmi H, Lavigne M, Martel-Pelletier J (2008) The differential expression of osteoprotegerin (OPG) and receptor activator of nuclear factor kappaB ligand (RANKL) in human osteoarthritic subchondral bone osteoblasts is an indicator of the metabolic state of these disease cells. *Clin Exp Rheumatol* 26:295-304.

Lacey DL, et al. (1998) Osteoprotegerin ligand is a cytokine that regulates osteoclast differentiation and activation. *Cell* 93:165-176.

Lafont JE (2010) Lack of oxygen in articular cartilage: consequences for chondrocyte biology. *Int J Exp Pathol* 91:99-106.

Lajeunesse D, Reboul P (2003) Subchondral bone in osteoarthritis: a biologic link with articular cartilage leading to abnormal remodeling. *Curr Opin Rheumatol* 15:628-633.

Lammi MJ (2004) Current perspectives on cartilage and chondrocyte mechanobiology. *Biorheology* 41:593-596.

Lavigne P, Benderdour M, Lajeunesse D, Reboul P, Shi Q, Pelletier JP, Martel-Pelletier J, Fernandes JC (2005) Subchondral and trabecular bone metabolism regulation in canine experimental knee osteoarthritis. *Osteoarthritis Cartilage* 13:310-317.

Layton MW, Goldstein SA, Goulet RW, Feldkamp LA, Kubinski DJ, Bole GG (1988) Examination of subchondral bone architecture in experimental osteoarthritis by microscopic computed axial tomography. *Arthritis Rheum* 31:1400-1405.

Lehmann HJ, Mouritzen U, Christgau S, Cloos PA, Christiansen C (2002) Effect of bisphosphonates on cartilage turnover assessed with a newly developed assay for collagen type II degradation products. *Ann Rheum Dis* 61:530-533.

Li B, Aspden RM (1997a) Composition and mechanical properties of cancellous bone from the femoral head of patients with osteoporosis or osteoarthritis. *J Bone Miner Res* 12:641-651.

Li B, Aspden RM (1997b) Mechanical and material properties of the subchondral bone plate from the femoral head of patients with osteoarthritis or osteoporosis. *Ann Rheum Dis* 56:247-254.

Li X, et al. (2008) Targeted deletion of the sclerostin gene in mice results in increased bone formation and bone strength. *J Bone Miner Res* 23:860-869.

Lisignoli G, Toneguzzi S, Pozzi C, Piacentini A, Riccio M, Ferruzzi A, Gualtieri G, Facchini A (1999) Proinflammatory cytokines and chemokine production and

expression by human osteoblasts isolated from patients with rheumatoid arthritis and osteoarthritis. *J Rheumatol* 26:791-799.

Little CB, Barai A, Burkhardt D, Smith SM, Fosang AJ, Werb Z, Shah M, Thompson EW (2009) Matrix metalloproteinase 13-deficient mice are resistant to osteoarthritic cartilage erosion but not chondrocyte hypertrophy or osteophyte development. *Arthritis Rheum* 60:3723-3733.

Logar DB, Komadina R, Prezelj J, Ostanek B, Trost Z, Marc J (2007) Expression of bone resorption genes in osteoarthritis and in osteoporosis. *J Bone Miner Metab* 25:219-225.

Lories RJ, Luyten FP (2011) The bone-cartilage unit in osteoarthritis. *Nat Rev Rheumatol* 7:43-49.

Luckman SP, Hughes DE, Coxon FP, Graham R, Russell G, Rogers MJ (1998) Nitrogen-containing bisphosphonates inhibit the mevalonate pathway and prevent post-translational prenylation of GTP-binding proteins, including Ras. *J Bone Miner Res* 13:581-589.

Luyten FP, Tylzanowski P, Lories RJ (2009) Wnt signaling and osteoarthritis. *Bone* 44:522-527.

Lyons TJ, Stoddart RW, McClure SF, McClure J (2005) The tidemark of the chondro-osseous junction of the normal human knee joint. *J Mol Histol* 36:207-215.

Lyons TJ, McClure SF, Stoddart RW, McClure J (2006) The normal human chondro-osseous junctional region: evidence for contact of uncalcified cartilage with subchondral bone and marrow spaces. *BMC Musculoskelet Disord* 7:52.

Lyons TJ, Stoddart RW, McClure SF, McClure J (2007) Lectin and other histochemical studies of the articular cartilage and the chondro-osseous junction of the normal human knee joint. *J Mol Histol* 38:13-23.

MacNeil JA, Doschak MR, Zernicke RF, Boyd SK (2008) Preservation of periarticular cancellous morphology and mechanical stiffness in post-traumatic experimental osteoarthritis by antiresorptive therapy. *Clin Biomech (Bristol, Avon)* 23:365-371.

Madry H, van Dijk CN, Mueller-Gerbl M (2010) The basic science of the subchondral bone. *Knee Surg Sports Traumatol Arthrosc* 18:419-433.

Majumdar S (2003) Current technologies in the evaluation of bone architecture. *Curr Osteoporos Rep* 1:105-109.

Mansell JP, Bailey AJ (1998) Abnormal cancellous bone collagen metabolism in osteoarthritis. *J Clin Invest* 101:1596-1603.

Mansell JP, Tarlton JF, Bailey AJ (1997) Biochemical evidence for altered subchondral bone collagen metabolism in osteoarthritis of the hip. *Br J Rheumatol* 36:16-19.

Martel-Pelletier J, Pelletier JP (2010) Is osteoarthritis a disease involving only cartilage or other articular tissues? *Eklem Hastalik Cerrahisi* 21:2-14.

Martel-Pelletier J, Boileau C, Pelletier JP, Roughley PJ (2008) Cartilage in normal and osteoarthritis conditions. *Best Pract Res Clin Rheumatol* 22:351-384.

Mashiba T, Turner CH, Hirano T, Forwood MR, Johnston CC, Burr DB (2001) Effects of suppressed bone turnover by bisphosphonates on microdamage accumulation and biomechanical properties in clinically relevant skeletal sites in beagles. *Bone* 28:524-531.

Matsui H, Shimizu M, Tsuji H (1997) Cartilage and subchondral bone interaction in osteoarthrosis of human knee joint: a histological and histomorphometric study. *Microsc Res Tech* 37:333-342.

Matsuo M, Nishida K, Yoshida A, Murakami T, Inoue H (2001) Expression of caspase-3 and -9 relevant to cartilage destruction and chondrocyte apoptosis in human osteoarthritic cartilage. *Acta Med Okayama* 55:333-340.

McErlain DD, Milner JS, Ivanov TG, Jencikova-Celerin L, Pollmann SI, Holdsworth DW (2011) Subchondral cysts create increased intra-osseous stress in early knee OA: A finite element analysis using simulated lesions. *Bone* 48:639-646.

McErlain DD, Appleton CT, Litchfield RB, Pitelka V, Henry JL, Bernier SM, Beier F, Holdsworth DW (2008) Study of subchondral bone adaptations in a rodent surgical model of OA using in vivo micro-computed tomography. *Osteoarthritis Cartilage* 16:458-469.

Michael JW, Schluter-Brust KU, Eysel P (2010) The epidemiology, etiology, diagnosis, and treatment of osteoarthritis of the knee. *Dtsch Arztebl Int* 107:152-162.

Milz S, Eckstein F, Putz R (1995) The thickness of the subchondral plate and its correlation with the thickness of the uncalcified articular cartilage in the human patella. *Anat Embryol (Berl)* 192:437-444.

Mohan G, Perilli E, Kuliwaba JS, Humphries JM, Parkinson IH, Fazzalari NL (2011) Application of in vivo micro-computed tomography in the temporal characterisation of subchondral bone architecture in a rat model of low-dose monosodium iodoacetate-induced osteoarthritis. *Arthritis Res Ther* 13:R210.

Moreau M, et al. (2011) Tiludronate treatment improves structural changes and symptoms of osteoarthritis in the canine anterior cruciate ligament model. *Arthritis Res Ther* 13:R98.

Morenko BJ, Bove SE, Chen L, Guzman RE, Juneau P, Bocan TM, Peter GK, Arora R, Kilgore KS (2004) In vivo micro computed tomography of subchondral bone in the rat after intra-articular administration of monosodium iodoacetate. *Contemp Top Lab Anim Sci* 43:39-43.

Moreno-Rubio J, Herrero-Beaumont G, Tardio L, Alvarez-Soria MA, Largo R (2010) Nonsteroidal antiinflammatory drugs and prostaglandin E(2) modulate the synthesis of osteoprotegerin and RANKL in the cartilage of patients with severe knee osteoarthritis. *Arthritis Rheum* 62:478-488.

Moskowitz RW (1999) Bone remodeling in osteoarthritis: subchondral and osteophytic responses. *Osteoarthritis Cartilage* 7:323-324.

Moskowitz RW, Goldberg VM (1987) Osteophyte evolution: studies in an experimental partial meniscectomy model. *J Rheumatol* 14 Spec No:116-118.

Moskowitz RW, Altman RD, Howell DS, Buckwlater JA, Goldberg VM, eds. 2001. Osteoarthritis: Diagnosis and Medical/Surgical Management. 3rd ed. Pennsylvania: W.B. Saunders Company.

Muehleman C, Green J, Williams JM, Kuettner KE, Thonar EJ, Sumner DR (2002) The effect of bone remodeling inhibition by zoledronic acid in an animal model of cartilage matrix damage. *Osteoarthritis Cartilage* 10:226-233.

Myers SL, Brandt KD, Burr DB, O'Connor BL, Albrecht M (1999) Effects of a bisphosphonate on bone histomorphometry and dynamics in the canine cruciate deficiency model of osteoarthritis. *J Rheumatol* 26:2645-2653.

Nancollas GH, Tang R, Phipps RJ, Henneman Z, Gulde S, Wu W, Mangood A, Russell RG, Ebetino FH (2006) Novel insights into actions of bisphosphonates on bone: differences in interactions with hydroxyapatite. *Bone* 38:617-627.

Neogi T, Nevitt MC, Ensrud KE, Bauer D, Felson DT (2008) The effect of alendronate on progression of spinal osteophytes and disc-space narrowing. *Ann Rheum Dis* 67:1427-1430.

Noble J, Alexander K (1985) Studies of tibial subchondral bone density and its significance. *J Bone Joint Surg Am* 67:295-302.

Nolte-Ernsting CC, Adam G, Buhne M, Prescher A, Gunther RW (1996) MRI of degenerative bone marrow lesions in experimental osteoarthritis of canine knee joints. *Skeletal Radiol* 25:413-420.

Odgaard A, Pedersen CM, Bentzen SM, Jorgensen J, Hvid I (1989) Density changes at the proximal tibia after medial meniscectomy. *J Orthop Res* 7:744-753.

Oliveria SA, Felson DT, Reed JI, Cirillo PA, Walker AM (1995) Incidence of symptomatic hand, hip, and knee osteoarthritis among patients in a health maintenance organization. *Arthritis Rheum* 38:1134-1141.

Pacifici M, Koyama E, Iwamoto M, Gentili C (2000) Development of articular cartilage: what do we know about it and how may it occur? *Connect Tissue Res* 41:175-184.

Pan B, Farrugia AN, To LB, Findlay DM, Green J, Lynch K, Zannettino AC (2004) The nitrogen-containing bisphosphonate, zoledronic acid, influences RANKL expression in human osteoblast-like cells by activating TNF-alpha converting enzyme (TACE). *J Bone Miner Res* 19:147-154.

Pan J, Zhou X, Li W, Novotny JE, Doty SB, Wang L (2009) In situ measurement of transport between subchondral bone and articular cartilage. *J Orthop Res* 27:1347-1352.

Pan J, Wang B, Li W, Zhou X, Scherr T, Yang Y, Price C, Wang L (2011) Elevated cross-talk between subchondral bone and cartilage in osteoarthritic joints. *Bone*.

Panula HE, Nieminen J, Parkkinen JJ, Arnala I, Kroger H, Alhava E (1998) Subchondral bone remodeling increases in early experimental osteoarthrosis in young beagle dogs. *Acta Orthop Scand* 69:627-632.

Parfitt AM, Drezner MK, Glorieux FH, Kanis JA, Malluche H, Meunier PJ, Ott SM, Recker RR (1987) Bone histomorphometry: standardization of nomenclature, symbols, and units. Report of the ASBMR Histomorphometry Nomenclature Committee. *J Bone Miner Res* 2:595-610.

Pastoureau P, Leduc S, Chomel A, De Ceuninck F (2003) Quantitative assessment of articular cartilage and subchondral bone histology in the meniscectomized guinea pig model of osteoarthritis. *Osteoarthritis Cartilage* 11:412-423.

Pastoureau PC, Chomel AC, Bonnet J (1999) Evidence of early subchondral bone changes in the meniscectomized guinea pig. A densitometric study using dual-energy X-ray absorptiometry subregional analysis. *Osteoarthritis Cartilage* 7:466-473.

Pearle AD, Scanzello CR, George S, Mandl LA, DiCarlo EF, Peterson M, Sculco TP, Crow MK (2007) Elevated high-sensitivity C-reactive protein levels are associated with local inflammatory findings in patients with osteoarthritis. *Osteoarthritis Cartilage* 15:516-523.

Pepys MB, Hirschfield GM (2003) C-reactive protein: a critical update. *J Clin Invest* 111:1805-1812.

Perilli E, Baruffaldi F, Bisi MC, Cristofolini L, Cappello A (2006) A physical phantom for the calibration of three-dimensional X-ray microtomography examination. *Journal of Microscopy* 222:124-134.

Perilli E, Baleani M, Ohman C, Baruffaldi F, Viceconti M (2007a) Structural parameters and mechanical strength of cancellous bone in the femoral head in osteoarthritis do not depend on age. *Bone* 41:760-768.

Perilli E, Le V, Ma B, Salmon P, Reynolds K, Fazzalari NL (2010) Detecting early bone changes using in vivo micro-CT in ovariectomized, zoledronic acid-treated, and sham-operated rats. *Osteoporos Int* 21:1371-1382.

Perilli E, Baruffaldi F, Visentin M, Bordini B, Traina F, Cappello A, Viceconti M (2007b) MicroCT examination of human bone specimens: effects of polymethylmethacrylate embedding on structural parameters. *J Microsc* 225:192-200.

Pesesse L, Sanchez C, Henrotin Y (2011) Osteochondral plate angiogenesis: a new treatment target in osteoarthritis. *Joint Bone Spine* 78:144-149.

Pfeilschifter J, Wolf O, Naumann A, Minne HW, Mundy GR, Ziegler R (1990) Chemotactic response of osteoblastlike cells to transforming growth factor beta. *J Bone Miner Res* 5:825-830.

Pilichou A, Papassotiriou I, Michalakakou K, Fessatou S, Fandridis E, Papachristou G, Terpos E (2008) High levels of synovial fluid osteoprotegerin (OPG) and increased serum ratio of receptor activator of nuclear factor-kappaB ligand (RANKL) to OPG correlate with disease severity in patients with primary knee osteoarthritis. *Clin Biochem* 8:8.

Piscaer TM, van Osch GJ, Verhaar JA, Weinans H (2008a) Imaging of experimental osteoarthritis in small animal models. *Biorheology* 45:355-364.

Piscaer TM, Waarsing JH, Kops N, Pavljasevic P, Verhaar JA, van Osch GJ, Weinans H (2008b) In vivo imaging of cartilage degeneration using microCT-arthrography. *Osteoarthritis Cartilage* 16:1011-1017.

Piscaer TM, Muller C, Mindt TL, Lubberts E, Verhaar JA, Krenning EP, Schibli R, De Jong M, Weinans H (2011) Imaging of activated macrophages in experimental osteoarthritis using folate-targeted animal single-photon-emission computed tomography/computed tomography. *Arthritis Rheum* 63:1898-1907.

Pomonis JD, Boulet JM, Gottshall SL, Phillips S, Sellers R, Bunton T, Walker K (2005) Development and pharmacological characterization of a rat model of osteoarthritis pain. *Pain* 114:339-346.

Poole AR, Kojima T, Yasuda T, Mwale F, Kobayashi M, Laverty S (2001) Composition and structure of articular cartilage: a template for tissue repair. *Clin Orthop Relat Res*:S26-33.

Poole AR, et al. (2002) Type II collagen degradation and its regulation in articular cartilage in osteoarthritis. *Ann Rheum Dis* 61 Suppl 2:ii78-81.

Poole R, et al. (2010) Recommendations for the use of preclinical models in the study and treatment of osteoarthritis. *Osteoarthritis Cartilage* 18 Suppl 3:S10-16.

Pottenger LA, Phillips FM, Draganich LF (1990) The effect of marginal osteophytes on reduction of varus-valgus instability in osteoarthritic knees. *Arthritis Rheum* 33:853-858.

Pouders C, De Maeseneer M, Van Roy P, Gielen J, Goossens A, Shahabpour M (2008) Prevalence and MRI-anatomic correlation of bone cysts in osteoarthritic knees. *AJR Am J Roentgenol* 190:17-21.

Prasadam I, van Gennip S, Friis T, Shi W, Crawford R, Xiao Y (2010a) ERK-1/2 and p38 in the regulation of hypertrophic changes of normal articular cartilage chondrocytes induced by osteoarthritic subchondral osteoblasts. *Arthritis Rheum* 62:1349-1360.

Prasadam I, Friis T, Shi W, van Gennip S, Crawford R, Xiao Y (2010b) Osteoarthritic cartilage chondrocytes alter subchondral bone osteoblast differentiation via MAPK signalling pathway involving ERK1/2. *Bone* 46:226-235.

Pufe T, Petersen W, Tillmann B, Mentlein R (2001) The splice variants VEGF121 and VEGF189 of the angiogenic peptide vascular endothelial growth factor are expressed in osteoarthritic cartilage. *Arthritis Rheum* 44:1082-1088.

Radin EL, Rose RM (1986) Role of subchondral bone in the initiation and progression of cartilage damage. *Clin Orthop Relat Res*:34-40.

Radin EL, Abernethy PJ, Townsend PM, Rose RM (1978a) The role of bone changes in the degeneration of articular cartilage in osteoarthrosis. *Acta Orthop Belg* 44:55-63.

Radin EL, Ehrlich MG, Chernack R, Abernethy P, Paul IL, Rose RM (1978b) Effect of repetitive impulsive loading on the knee joints of rabbits. *Clin Orthop Relat Res*:288-293.

Radin EL, Paul IL, Lowy M (1970) A comparison of the dynamic force transmitting properties of subchondral bone and articular cartilage. *J Bone Joint Surg Am* 52:444-456.

Reboul P, Pelletier JP, Tardif G, Cloutier JM, Martel-Pelletier J (1996) The new collagenase, collagenase-3, is expressed and synthesized by human chondrocytes but not by synoviocytes. A role in osteoarthritis. *J Clin Invest* 97:2011-2019.

Recker R, Masarachia P, Santora A, Howard T, Chavassieux P, Arlot M, Rodan G, Wehren L, Kimmel D (2005) Trabecular bone microarchitecture after alendronate treatment of osteoporotic women. *Curr Med Res Opin* 21:185-194.

Reszka AA, Rodan GA (2004) Nitrogen-containing bisphosphonate mechanism of action. *Mini Rev Med Chem* 4:711-719.

Russell RG (2007) Bisphosphonates: mode of action and pharmacology. *Pediatrics* 119 Suppl 2:S150-162.

Russell RG, Rogers MJ (1999) Bisphosphonates: from the laboratory to the clinic and back again. *Bone* 25:97-106.

Russell RG, Croucher PI, Rogers MJ (1999) Bisphosphonates: pharmacology, mechanisms of action and clinical uses. *Osteoporos Int* 9 Suppl 2:S66-80.

Russell RG, Watts NB, Ebetino FH, Rogers MJ (2008) Mechanisms of action of bisphosphonates: similarities and differences and their potential influence on clinical efficacy. *Osteoporos Int* 19:733-759.

Saag KG (2008) Bisphosphonates for osteoarthritis prevention: "Holy Grail" or not? *Ann Rheum Dis* 67:1358-1359.

Sabokbar A, Crawford R, Murray DW, Athanasou NA (2000) Macrophage-osteoclast differentiation and bone resorption in osteoarthrotic subchondral acetabular cysts. *Acta Orthop Scand* 71:255-261.

Sahni M, Guenther HL, Fleisch H, Collin P, Martin TJ (1993) Bisphosphonates act on rat bone resorption through the mediation of osteoblasts. *J Clin Invest* 91:2004-2011.

Sakao K, et al. (2008) Enhanced expression of interleukin-6, matrix metalloproteinase-13, and receptor activator of NF-kappaB ligand in cells derived from osteoarthritic subchondral bone. *J Orthop Sci* 13:202-210.

Saklatvala J (2007) Inflammatory signaling in cartilage: MAPK and NF-kappaB pathways in chondrocytes and the use of inhibitors for research into pathogenesis and therapy of osteoarthritis. *Curr Drug Targets* 8:305-313.

Salminen HJ, Saamanen AM, Vankemmelbeke MN, Auho PK, Perala MP, Vuorio EI (2002) Differential expression patterns of matrix metalloproteinases and their inhibitors during development of osteoarthritis in a transgenic mouse model. *Ann Rheum Dis* 61:591-597.

Sanchez C, Deberg MA, Piccardi N, Msika P, Reginster JY, Henrotin YE (2005a) Osteoblasts from the sclerotic subchondral bone downregulate aggrecan but upregulate metalloproteinases expression by chondrocytes. This effect is mimicked by interleukin-6, -1beta and oncostatin M pre-treated non-sclerotic osteoblasts. *Osteoarthritis Cartilage* 13:979-987.

Sanchez C, Deberg MA, Piccardi N, Msika P, Reginster JY, Henrotin YE (2005b) Subchondral bone osteoblasts induce phenotypic changes in human osteoarthritic chondrocytes. *Osteoarthritis Cartilage* 13:988-997.

Sanchez C, Deberg MA, Bellahcene A, Castronovo V, Msika P, Delcour JP, Crielaard JM, Henrotin YE (2008) Phenotypic characterization of osteoblasts from the sclerotic zones of osteoarthritic subchondral bone. *Arthritis Rheum* 58:442-455.

Sato M, Grasser W (1990) Effects of bisphosphonates on isolated rat osteoclasts as examined by reflected light microscopy. *J Bone Miner Res* 5:31-40.

Sato M, Grasser W, Endo N, Akins R, Simmons H, Thompson DD, Golub E, Rodan GA (1991) Bisphosphonate action. Alendronate localization in rat bone and effects on osteoclast ultrastructure. *J Clin Invest* 88:2095-2105.

Scharstuhl A, Glansbeek HL, van Beuningen HM, Vitters EL, van der Kraan PM, van den Berg WB (2002) Inhibition of endogenous TGF-beta during experimental osteoarthritis prevents osteophyte formation and impairs cartilage repair. *J Immunol* 169:507-514.

Schenk R, Eggli P, Fleisch H, Rosini S (1986) Quantitative morphometric evaluation of the inhibitory activity of new aminobisphosphonates on bone resorption in the rat. *Calcif Tissue Int* 38:342-349.

Schuelert N, McDougall JJ (2009) Grading of monosodium iodoacetate-induced osteoarthritis reveals a concentration-dependent sensitization of nociceptors in the knee joint of the rat. *Neurosci Lett* 465:184-188.

Schumacher BL, Block JA, Schmid TM, Aydelotte MB, Kuettner KE (1994) A novel proteoglycan synthesized and secreted by chondrocytes of the superficial zone of articular cartilage. *Arch Biochem Biophys* 311:144-152.

Seeman E (2008) Bone quality: the material and structural basis of bone strength. *J Bone Miner Metab* 26:1-8.

Sharif M, Elson CJ, Dieppe PA, Kirwan JR (1997) Elevated serum C-reactive protein levels in osteoarthritis. *Br J Rheumatol* 36:140-141.

Sharma L, Eckstein F, Song J, Guermazi A, Prasad P, Kapoor D, Cahue S, Marshall M, Hudelmaier M, Dunlop D (2008) Relationship of meniscal damage, meniscal extrusion, malalignment, and joint laxity to subsequent cartilage loss in osteoarthritic knees. *Arthritis Rheum* 58:1716-1726.

Shirai T, Kobayashi M, Nishitani K, Satake T, Kuroki H, Nakagawa Y, Nakamura T (2011) Chondroprotective effect of alendronate in a rabbit model of osteoarthritis. *J Orthop Res* 29:1572-1577.

Siebelt M, Waarsing JH, Kops N, Piscaer TM, Verhaar JA, Oei EH, Weinans H (2011a) Quantifying osteoarthritic cartilage changes accurately using in vivo microCT arthrography in three etiologically distinct rat models. *J Orthop Res* 29:1788-1794.

Siebelt M, et al. (2011b) Clinically applied CT arthrography to measure the sulphated glycosaminoglycan content of cartilage. *Osteoarthritis Cartilage* 19:1183-1189.

Skoumal M, Kolarz G, Haberhauer G, Woloszczuk W, Hawa G, Klingler A (2005) Osteoprotegerin and the receptor activator of NF-kappa B ligand in the serum and synovial fluid. A comparison of patients with longstanding rheumatoid arthritis and osteoarthritis. *Rheumatol Int* 26:63-69.

Sniekers YH, Weinans H, Bierma-Zeinstra SM, van Leeuwen JP, van Osch GJ (2008a) Animal models for osteoarthritis: the effect of ovariectomy and estrogen treatment - a systematic approach. *Osteoarthritis Cartilage* 16:533-541.

Sniekers YH, Intema F, Lafeber FP, van Osch GJ, van Leeuwen JP, Weinans H, Mastbergen SC (2008b) A role for subchondral bone changes in the process of osteoarthritis; a micro-CT study of two canine models. *BMC Musculoskelet Disord* 9:20.

Spector TD, Hart DJ, Nandra D, Doyle DV, Mackillop N, Gallimore JR, Pepys MB (1997) Low-level increases in serum C-reactive protein are present in early osteoarthritis of the knee and predict progressive disease. *Arthritis Rheum* 40:723-727.

Spector TD, Conaghan PG, Buckland-Wright JC, Garnero P, Cline GA, Beary JF, Valent DJ, Meyer JM (2005) Effect of risedronate on joint structure and symptoms of knee osteoarthritis: results of the BRISK randomized, controlled trial [ISRCTN01928173]. *Arthritis Res Ther* 7:R625-633.

Stevenson GW, Mercer H, Cormier J, Dunbar C, Benoit L, Adams C, Jezierski J, Luginbuhl A, Bilsky EJ (2011) Monosodium iodoacetate-induced osteoarthritis produces pain-depressed wheel running in rats: implications for preclinical behavioral assessment of chronic pain. *Pharmacol Biochem Behav* 98:35-42.

Stewart A, Black A, Robins SP, Reid DM (1999) Bone density and bone turnover in patients with osteoarthritis and osteoporosis. *J Rheumatol* 26:622-626.

Stoop R, van der Kraan PM, Buma P, Hollander AP, Billinghurst RC, Poole AR, van den Berg WB (1999) Type II collagen degradation in spontaneous osteoarthritis in C57Bl/6 and BALB/c mice. *Arthritis Rheum* 42:2381-2389.

Strassle BW, Mark L, Leventhal L, Piesla MJ, Jian Li X, Kennedy JD, Glasson SS, Whiteside GT (2010) Inhibition of osteoclasts prevents cartilage loss and pain in a rat model of degenerative joint disease. *Osteoarthritis Cartilage* 18:1319-1328.

Suri S, Walsh DA (2011) Osteochondral alterations in osteoarthritis. *Bone*.

Takahashi M, Kushida K, Ohishi T, Kawana K, Hoshino H, Uchiyama A, Inoue T (1994) Quantitative analysis of crosslinks pyridinoline and pentosidine in articular cartilage of patients with bone and joint disorders. *Arthritis Rheum* 37:724-728.

Tanaka H, Mine T, Ogasa H, Taguchi T, Liang CT (2011) Expression of RANKL/OPG during bone remodeling in vivo. *Biochem Biophys Res Commun* 411:690-694.

Tanamas SK, Wluka AE, Pelletier JP, Martel-Pelletier J, Abram F, Wang Y, Cicuttini FM (2010) The association between subchondral bone cysts and tibial cartilage volume and risk of joint replacement in people with knee osteoarthritis: a longitudinal study. *Arthritis Res Ther* 12:R58.

Tat SK, Pelletier JP, Velasco CR, Padrines M, Martel-Pelletier J (2009) New perspective in osteoarthritis: the OPG and RANKL system as a potential therapeutic target? *Keio J Med* 58:29-40.

Tessier JJ, Bowyer J, Brownrigg NJ, Peers IS, Westwood FR, Waterton JC, Maciewicz RA (2003) Characterisation of the guinea pig model of osteoarthritis by in vivo three-dimensional magnetic resonance imaging. *Osteoarthritis Cartilage* 11:845-853.

Tetik S, Ahmad S, Alturfan AA, Fresko I, Disbudak M, Sahin Y, Aksoy H, Yardimci KT (2010) Determination of oxidant stress in plasma of rheumatoid arthritis and primary osteoarthritis patients. *Indian J Biochem Biophys* 47:353-358.

Thompson RC, Jr., Oegema TR, Jr., Lewis JL, Wallace L (1991) Osteoarthrotic changes after acute transarticular load. An animal model. *J Bone Joint Surg Am* 73:990-1001.

Truong LH, Kuliwaba JS, Tsangari H, Fazzalari NL (2006) Differential gene expression of bone anabolic factors and trabecular bone architectural changes in the proximal femoral shaft of primary hip osteoarthritis patients. *Arthritis Res Ther* 8:R188.

Umlauf D, Frank S, Pap T, Bertrand J (2010) Cartilage biology, pathology, and repair. *Cell Mol Life Sci* 67:4197-4211.

Upton AR, Holding CA, Dharmapatni AA, Haynes DR (2012) The expression of RANKL and OPG in the various grades of osteoarthritic cartilage. *Rheumatol Int* 32:535-540.

van den Berg WB (1995) Growth factors in experimental osteoarthritis: transforming growth factor beta pathogenic? *J Rheumatol Suppl* 43:143-145.

van den Berg WB, van Osch GJ, van der Kraan PM, van Beuningen HM (1993) Cartilage destruction and osteophytes in instability-induced murine osteoarthritis: role of TGF beta in osteophyte formation? *Agents Actions* 40:215-219.

van denBerg WB (1999) Osteophyte formation in osteoarthritis. *Osteoarthritis Cartilage* 7:333.

van der Kraan PM, van den Berg WB (2007) Osteophytes: relevance and biology. *Osteoarthritis Cartilage* 15:237-244.

van der Kraan PM, van den Berg WB (2012) Chondrocyte hypertrophy and osteoarthritis: role in initiation and progression of cartilage degeneration? *Osteoarthritis Cartilage* 20:223-232.

van der Kraan PM, Blaney Davidson EN, van den Berg WB (2010) Bone morphogenetic proteins and articular cartilage: To serve and protect or a wolf in sheep clothing's? *Osteoarthritis Cartilage* 18:735-741.

van der Kraan PM, Vitters EL, van de Putte LB, van den Berg WB (1989) Development of osteoarthritic lesions in mice by "metabolic" and "mechanical" alterations in the knee joints. *Am J Pathol* 135:1001-1014.

van der Kraan PM, Buma P, van Kuppevelt T, van den Berg WB (2002) Interaction of chondrocytes, extracellular matrix and growth factors: relevance for articular cartilage tissue engineering. *Osteoarthritis Cartilage* 10:631-637.

van der Kraan PM, Blaney Davidson EN, Blom A, van den Berg WB (2009) TGF-beta signaling in chondrocyte terminal differentiation and osteoarthritis: modulation and integration of signaling pathways through receptor-Smads. *Osteoarthritis Cartilage* 17:1539-1545.

van der Kraan PM, Vitters EL, van Beuningen HM, van de Putte LB, van den Berg WB (1990) Degenerative knee joint lesions in mice after a single intra-articular collagenase injection. A new model of osteoarthritis. *J Exp Pathol (Oxford)* 71:19-31.

van Osch GJ, van der Kraan PM, van den Berg WB (1994) Site-specific cartilage changes in murine degenerative knee joint disease induced by iodoacetate and collagenase. *J Orthop Res* 12:168-175.

van Osch GJ, van der Kraan PM, van Valburg AA, van den Berg WB (1996) The relation between cartilage damage and osteophyte size in a murine model for osteoarthritis in the knee. *Rheumatol Int* 16:115-119.

Viguet-Carrin S, Garnero P, Delmas PD (2006) The role of collagen in bone strength. *Osteoporos Int* 17:319-336.

Waarsing JH, Day JS, Weinans H (2004a) An improved segmentation method for in vivo microCT imaging. *J Bone Miner Res* 19:1640-1650.

Waarsing JH, Day JS, Weinans H (2005) Longitudinal micro-CT scans to evaluate bone architecture. *J Musculoskelet Neuronal Interact* 5:310-312.

Waarsing JH, Day JS, Verhaar JA, Ederveen AG, Weinans H (2006) Bone loss dynamics result in trabecular alignment in aging and ovariectomized rats. *J Orthop Res* 24:926-935.

Waarsing JH, Day JS, van der Linden JC, Ederveen AG, Spanjers C, De Clerck N, Sasov A, Verhaar JA, Weinans H (2004b) Detecting and tracking local changes in the tibiae of individual rats: a novel method to analyse longitudinal in vivo micro-CT data. *Bone* 34:163-169.

Wachsmuth L, Engelke K (2004) High-resolution imaging of osteoarthritis using microcomputed tomography. *Methods Mol Med* 101:231-248.

Walsh DA (2004) Angiogenesis in osteoarthritis and spondylosis: successful repair with undesirable outcomes. *Curr Opin Rheumatol* 16:609-615.

Walsh DA, Bonnet CS, Turner EL, Wilson D, Situ M, McWilliams DF (2007) Angiogenesis in the synovium and at the osteochondral junction in osteoarthritis. *Osteoarthritis Cartilage* 15:743-751.

Wang F, Ying Z, Duan X, Tan H, Yang B, Guo L, Chen G, Dai G, Ma Z, Yang L (2009) Histomorphometric analysis of adult articular calcified cartilage zone. *J Struct Biol* 168:359-365.

Watts NB, Becker P (1999) Alendronate increases spine and hip bone mineral density in women with postmenopausal osteoporosis who failed to respond to intermittent cyclical etidronate. *Bone* 24:65-68.

Winkler DG, et al. (2003) Osteocyte control of bone formation via sclerostin, a novel BMP antagonist. *EMBO J* 22:6267-6276.

Wu Q, Zhu M, Rosier RN, Zuscik MJ, O'Keefe RJ, Chen D (2010) Beta-catenin, cartilage, and osteoarthritis. *Ann N Y Acad Sci* 1192:344-350.

Yasuda H, et al. (1998) Osteoclast differentiation factor is a ligand for osteoprotegerin/osteoclastogenesis-inhibitory factor and is identical to TRANCE/RANKL. *Proc Natl Acad Sci U S A* 95:3597-3602.

Zamli Z, Sharif M (2011) Chondrocyte apoptosis: a cause or consequence of osteoarthritis? *Int J Rheum Dis* 14:159-166.

Zhang L, Hu H, Tian F, Song H, Zhang Y (2011) Enhancement of subchondral bone quality by alendronate administration for the reduction of cartilage degeneration in the early phase of experimental osteoarthritis. *Clin Exp Med* 11:235-243.

Zhao J, Li X, Bolbos RI, Link TM, Majumdar S (2010) Longitudinal assessment of bone marrow edema-like lesions and cartilage degeneration in osteoarthritis using 3 T MR T1rho quantification. *Skeletal Radiol* 39:523-531.